MICROSTRUCTURAL EFFECTS IN RELATION TO THE LEACHING OF GLASSES

by

Ronald Maddison B.Sc.

Thesis for the Degree of Doctor of Philosophy
of the University of Warwick.

Physics Department, University of Warwick. April 1980

DECLARATION

The work reported in this thesis is the author's own, except where it is specifically stated as otherwise. This work was carried out in the Physics Department of the University of Warwick during the period October 1975 to September 1978.

Ronald Maddison

ACKNOWLEDGEMENTS

The author wishes to express his appreciation to Professor P.W. McMillan for his guidance throughout this programme of work, and to Professor A.J. Forty who, as Chairman of the Department of Physics at the University of Warwick, made the research facilities available . He wishes also to thank the Procurement Executive of the Ministry of Defence for the financial support of the programme and their representatives, Dr. N.S. Corney and Mr. I.McC. Taylor, who made valuable contributions as external advisers.

The author would also like to express his gratitude to all the members of the Glass Ceramics research group, in particular to Mr. S.M. Tran and Dr. D. Armitage for many interesting discussions on the work. He also wishes to thank Mr. J. Lau and Ms. L. Heath for their help. Finally, he wishes to thank his wife, for typing the manuscript, but primarily for her understanding during the work and the preparation of this thesis.

ABSTRACT

A study of the acid leaching of a series of glasses has been made. This was undertaken to provide information concerning the production of microporous glass membranes with reverse osmosis desalination potential.

The chemical compositions of the glasses investigated were developed from a commercial glass composition known as 'E-glass'. This glass, phase separates into mutually interconnecting acid soluble and acid insoluble phases, during cooling from the molten state. Treating the glass with mineral acid solutions removes the soluble phase, yielding a porous glass skeleton. The amount of SiO_2 in the original composition was varied, and it was found possible to produce microporous glass skeletons from glasses having a range of SiO_2 contents. These glasses also phase separated into mutually interconnecting phases during cooling.

The parent glasses were studied by viscosity and electrical conductivity measurements. The results of those investigations were consistent with the rapid phase separation of the glasses.

The leaching rates of the glasses were studied by weight loss measurements and those measurements indicated that the leaching rate was controlled by the durability of the acid soluble phase.

The leached glasses were characterised by some electron microscopy, but primarily by inert gas adsorption measurements. The porous glasses contained pores of about 2 nm radius although there was also evidence of the presence of even finer pores.

The reverse osmosis performance of several of the glasses was investigated using single hollow fibre membranes and salt rejections of up to 50% were recorded.

CONTENTS

CHAPTER 5

CHAPTER 6

CHAPTER 7

APPENDICES

LIST OF FIGURES

CHAPTER 1

LIST OF TABLES

CHAPTER 1

Introduction

1.1 Preamble

Glasses are often regarded as homogeneous materials in which the local atomic arrangements are randomly repeated throughout their bulk. In many glasses it is possible however, to induce a separation into two or more glassy phases differing in chemical composition. In certain glasses, this separation can result in the formation of mutually interconnecting phases of widely differing chemical durabilities. These glasses can be treated in acid solutions to remove one of the phases, and porous glass skeletons can be produced from them.

As the kinetics of phase separation are controlled by the same transport properties that limit crystallisation, the scale of the phase separation in glass is characteristically small. The glass skeletons produced from glasses can, therefore, contain very fine pores of the order of a few nanometers in diameter. One possible application of this microporous glass is as a semi-permeable membrane for use in reverse osmosis desalination and it was an objective of this investigation to develop and characterise a porous glass suitable for that purpose.

1.2 The development of an interconnected microstructure in glass

"A glass is an inorganic product of fusion which has cooled to a rigid condition without crystallisation" (A.S.T.M. (1945)) . Below the liquidus temperature, glass is metastable with respect to some crystalline phase and so can be considered as an extension of the liquid state. As a consequence of this, the simple models of the stable immiscibility of a liquid can be extended into the metastable-glass forming region. If the two phase region is below the liquidus then the whole process may be metastable, but is still subject to the same analysis. These two cases are illustrated in figure 1.1.

1.2.1 The thermodynamics of liquid-liquid immiscibility

The free energy of an ideal binary solution (Gi) is given by

$$Gi = Go - T\,\Delta Sm \qquad 1.1$$

where ΔSm is the entropy of mixing, T is absolute temperature and Go is the free energy of a 'mechanical mixture' defined as

$$Go = X_a G_b + X_a G_b \qquad 1.2$$

Where X_a and X_b are the fractions of components a and b. G_a and G_b are the free energies of pure components a and b. The entropy of mixing for an ideal solution is given by

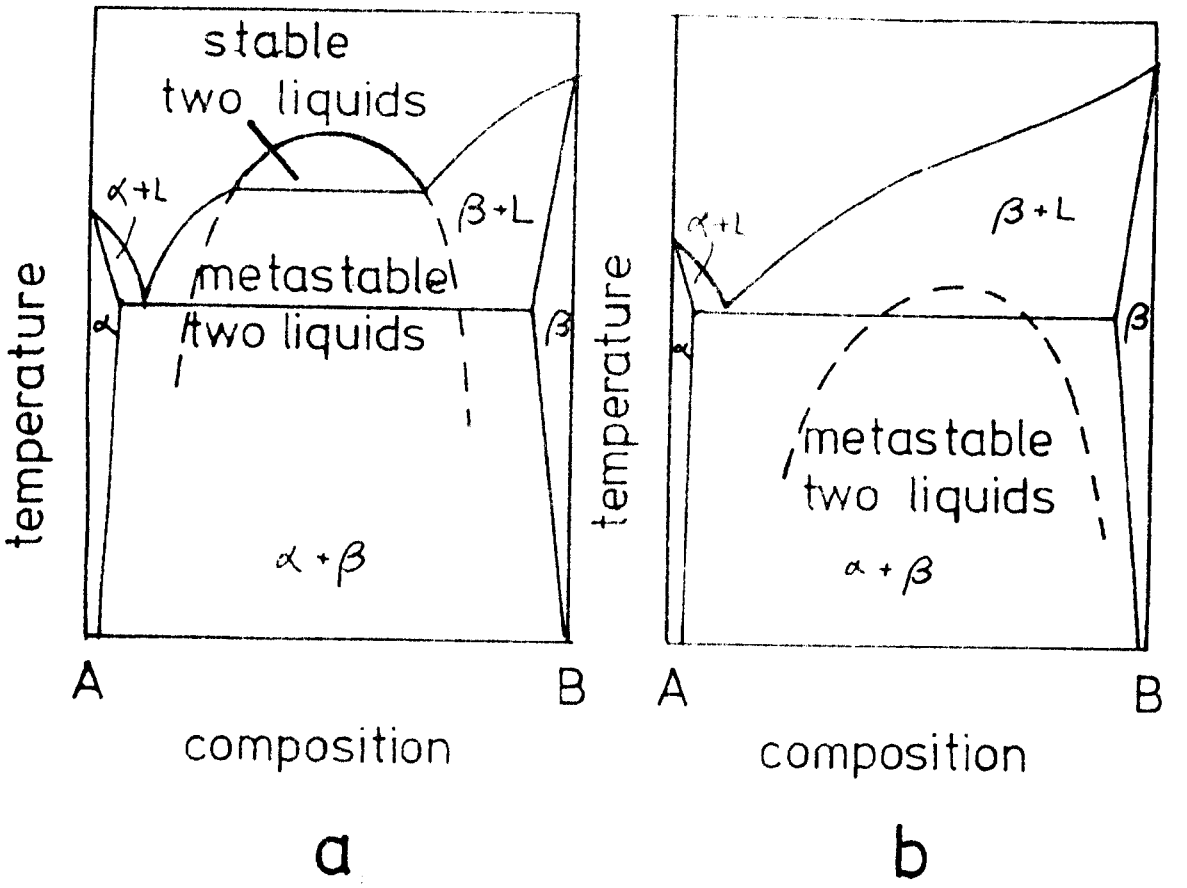

Figure 1.1 Schematic phase diagrams showing two liquid immiscibility. In a) the stable region has a sub-liquidus extension and in b) the immiscible region is entirely sub-liquidus

$$\Delta Sm = R(X_a \ln X_a + X_b \ln X_b) \qquad 1.3$$

where R is the gas constant.

The composition dependence of Go, $T\Delta Sm$ and Gi are shown in figure 1.2, and as Gi is 'concave down', a single phase solution is thermodynamically stable.

Generally, the free energies of the components in the solution are not those of the pure components and for real solutions this departure can be included as an extra term in equation 1.1. The free energy of a real binary solution (Gr) is then

$$Gr = Go - T\Delta Sm + \Delta Gx \qquad 1.4$$

At sufficiently low temperatures, the entropy contribution (ΔSx) to ΔGx is negligible compared with the enthalpy contribution (ΔHx) as $\Delta Gx = \Delta Hx - T\Delta Sx$. It can easily be shown that the enthalpy of a binary liquid can be approximated by

$$\Delta Hx = ZNX_aX_b(E_{ab} - \tfrac{1}{2}(E_{aa} + E_{bb})) \qquad 1.5$$

where E_{ab} represents the energy of the interaction between the unlike components (a and b), E_{aa} that between a and a components and E_{bb} that of the b components. Z is the average co-ordination number.

If the interaction between dissimilar components is less than the average of the like component interactions, then ΔHx is negative and Gr is made even more concave than shown

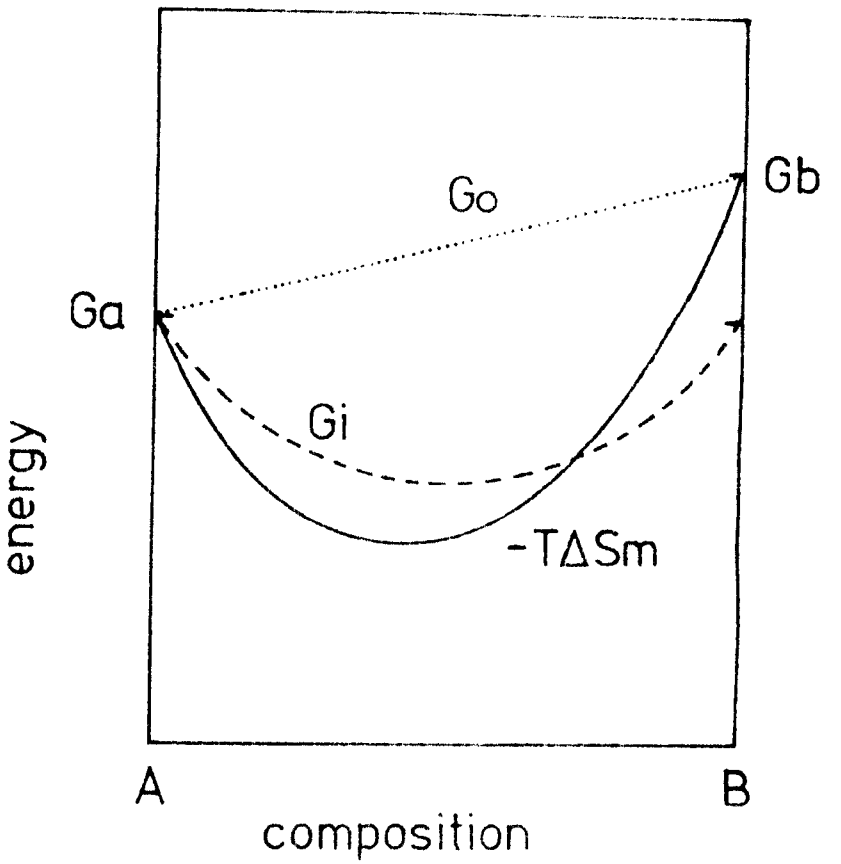

Figure 1.2 Schematic representation of the compositional dependence of the free energy of an ideal binary solution (Gi). The two contributions to this, Go(the free energy of a mechanical mixture) and -T Sm (the free entropy of mixing) are also shown

in figure 1.2. However, if $2E_{ab} > E_{aa} + E_{bb}$, ΔHx is positive and Gr can show inflections in its compositional dependence. Such a case is illustrated in figure 1.3 which shows the free energy at three temperatures: T_1, above the two phase region, T_2 at the critical temperature, and T_3 well into the two phase region. In figure 1.3 the phase diagram predicted by this mixing model is shown. Three regions are apparent, the spinodal region in which the single phase composition is unstable, the metastable region and the single phase region.

In certain liquids, regular type mixing is closely approximated, but in glass this is not so. Charles (1969) has pointed out that the calculation of the entropy of mixing of a glass is entirely dependent on the structural model adopted and has proposed that in a binary silicate the entropy is primarily due to the exchange of bridging and non-bridging oxygen ions. The concept of bridging and non-bridging oxygen ions is a consequence of the random network of glass. Oxygen ions which are shared by two silicon ions are considered to be bridging and those bonded only to one, non-bridging. In pure amorphous silica it is generally believed that all oxygen ions are shared, but the addition of metal oxide introduces extra oxygens, and some oxygens then become only singly bonded. Stevels (1954), and others, have shown the significance of the ratio of non-bridging to bridging oxygens and have developed a

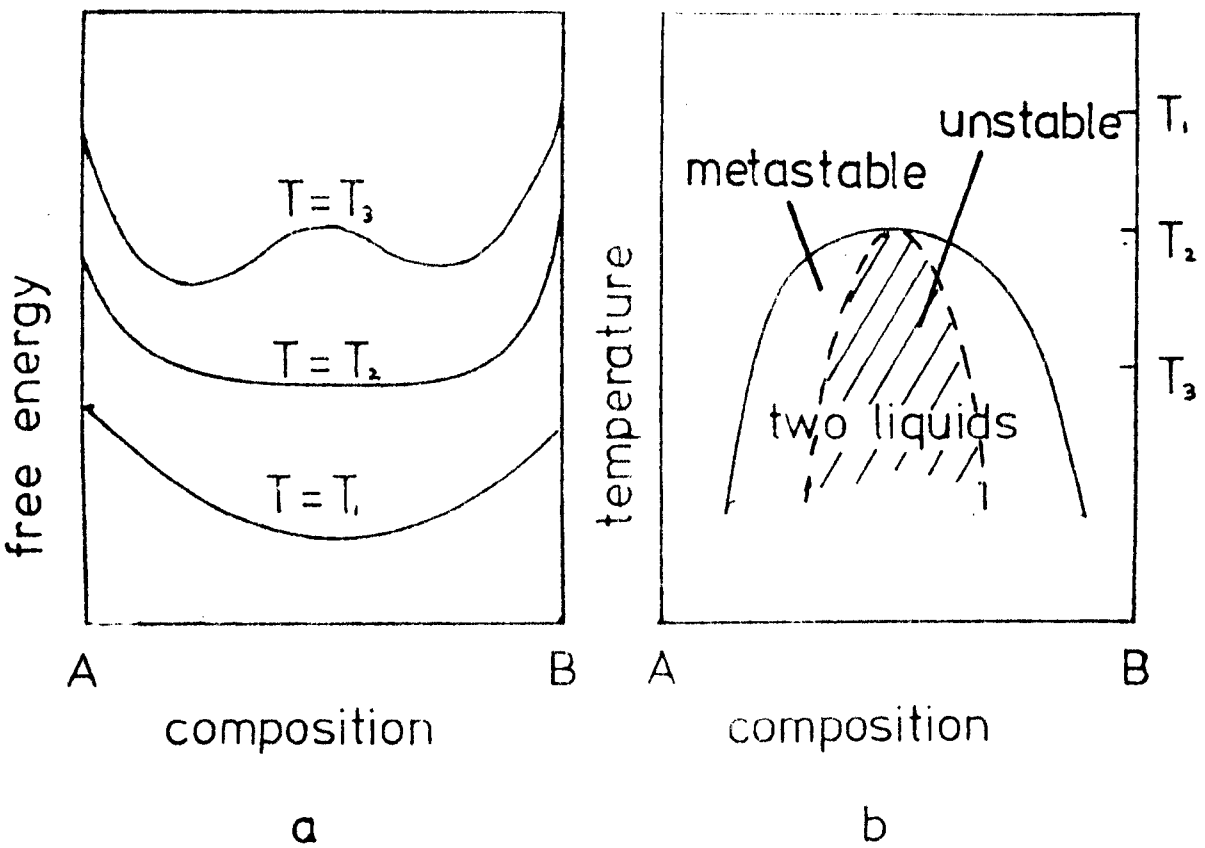

Figure 1.3 A schematic representation of the free energy of an immiscible solution at three temperatures is shown in (a). The phase diagram corresponding to the free energy curves are shown in (b).

polymer model of glass from it.

For 1 mole of binary solution containing Xm and Xs molar fractions of metal oxide and silica, the number of non-bridging pairs is Xm. The fraction of bridging oxygens is 2-3Xm (=2Xs-Xm). As these are exchanged over 2(1-Xm) sites, the entropy of mixing is

$$Sm = -R\left[\frac{Xm}{2(1-Xm)}.\ln\frac{Xm}{2(1-Xm)} + \frac{2-3Xm}{2(1-Xm)}.\ln\frac{2-3Xm}{2(1-Xm)}\right] \quad 1.6$$

Figure 1.4 compares the form of entropy of mixing calculated from equation 1.4 with that calculated from equation 1.6 (after Charles (1969)). For a ternary glass there exists the possibility of separation into three phases (by analogy with the Gibbs phase rule) and there is experimental evidence of this (e.g. Vogel (1966) and Porai-Koshits and Averjanov (1968)). For multicomponent glasses even more phases are possible.

1.2.2 Mechanisms of decomposition

There are two proposed mechanisms by which an interconnected microstructure in glass may develop. Isolated droplets may grow to touch each other, provided that the volume fraction of both phases is similar i.e. the homogeneous composition is near the centre of the immiscibility dome. In this central region, however, spinodal

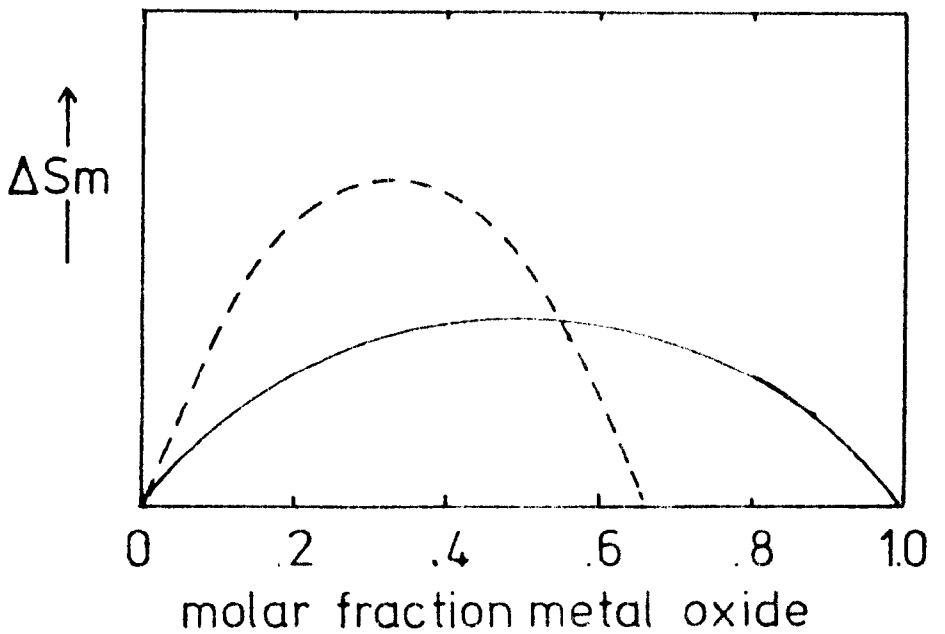

Figure 1.4 Schematic diagram showing the entropy of mixing. The solid line corresponds to regular mixing, and the broken line to that calculated using equation 1.6(after Charles(1969))

decomposition may operate and this produces a strongly interconnecting microstructure directly.

The theory of spinodal decomposition is well advanced as the process can be modelled mathematically but the intersecting growth process involves three distinct stages and cannot easily be modelled. These two mechanisms of decomposition are discussed below and a comparision of the predicted morphologies made.

Spinodal decomposition

If the local Helmholtz free energy (f(r))* is dependent only on composition and its spatial derivatives, then it can be expressed as a Maclaurin series about the free energy of the uniform composition (f(c)) i.e.

$$f(r) = f(c) + K_1 \nabla c^2 + K_2 (\nabla c)^2 + K_3 \nabla c^4 + K_4 (\nabla c^2)^2 + \ldots \quad 1.7$$

Cahn and Hilliard (1958) proposed that a good approximation could be made by retaining only the first three terms in equation 1.7.This is known as the diffuse interface expansion.

* Note

Following Cahn and co-workers, the Helmholtz free energy is used in the discussion of spinodal decomposition. As far as the work presented here is concerned,the difference between it and the more familiar Gibbs energy is negligible.

The free energy of the inhomogeneous solution is then

$$F = \int \left[(f(c) + K_1 \nabla c^2 + K_2 (\nabla c)^2) \right] dv \qquad 1.8$$

The free energy of the uniform solution can be expanded as a Taylor series about the average composition (c_o) i.e.

$$f(c) = (c-c_o)\frac{\partial f}{\partial c} + \frac{1}{2}(c-c_o)^2 \frac{\partial^2 f}{\partial c^2} + \frac{1}{6}(c-c_o)^3 \frac{\partial^3 f}{\partial c^3} + \ldots \qquad 1.9$$

Neglecting terms higher than second order and noting that $\int (c-c_o)dv = 0$, the change in free energy due to compositional fluctuations is

$$\Delta F = \int (\tfrac{1}{2}(c-c_o)^2 \partial^2 f/\partial c^2 + K_1 \nabla c^2 + K_2 (\nabla c)^2) dv \qquad 1.10$$

For some $\partial^2 f / \partial c^2$, ΔF can be negative.

So compositional fluctuations lower the free energy and are stable. The loci of the $\partial^2 f/\partial c^2 = 0$ points on the phase diagram is known as the spinodal and this defines the limit of the unstable region. This is shown in figure 1.3b.

Infinitesimal compositional fluctuations of the form $C = A\cos\beta x$ lower the free energy if $\beta < \beta_c$ where

$$\beta_c = (-\partial^2 f/\partial c^2 . 1/2K)^{\frac{1}{2}} \qquad 1.11$$

and

$$K = K_2 - dK_1/dc \qquad 1.12$$

To determine the kinetics of the transformation it is necessary to solve the diffusion equation inside the spinodal region. To do this a mobility (M) is defined as

$$J_b = -J_a = M \nabla (\mu_a - \mu_b) \qquad 1.13$$

where J_b and J_a are the fluxes of components a and b; μ_a and μ_b are the chemical potentials of a and b. The variational derivative of equation 1.8 is

$$\delta F/\delta c_a = \mu_a - \mu_b = \partial F/\partial c_a - 2K \nabla^2 c_a + \ldots \qquad 1.14$$

where the subscript a refers to component a and the subscript b to component b. K_γ has replaced the original two coefficients K_1 and K_2 (using equation 1.12). Neglecting all terms higher than shown in equation 1.14, substituting into equation 1.13 and taking the divergence

$$\nabla J_a = \partial c/\partial t = \nabla(M \nabla(\partial f/\partial c_a - 2K_\gamma \nabla^2 c_a)) \qquad 1.15$$

$$\text{i.e. } \partial c/\partial t = M(\partial^2 f/\partial c^2) \nabla^2 c - 2MK_\gamma \nabla^4 c + \ldots\ldots \qquad 1.16$$

For the early stages, the higher terms in equation 1.16 are not important as they are not linear in C. This simplifies the solutions of equation 1.16, which are now

$$(c-c_o) = \sum_\beta \exp(R_\beta t).(A_\beta \cos(\beta.r) + B_\beta \sin(\beta.r)) \qquad 1.17$$

where

$$R_\beta = -M\beta^2(\partial^2 f/\partial c^2) - 2MK_\gamma \beta^4 \qquad 1.18$$

R_β has the form shown in figure 1.5 and is an amplification factor. As R_β appears as an exponent and has a fairly sharp maximum, all Fourier components in equation 1.17 other than those for which R_β is a maximum (Rm) can be neglected. From the differential of equation 1.18

$$Rm = ((M\beta m/2K_\gamma)(-\partial^2 f/\partial c^2))^{\frac{1}{2}} \qquad 1.19$$

$$= 2MK_\gamma \beta_m^4 \qquad 1.20$$

$$= M(\partial^2 f/\partial c^2)(1/8K_\gamma) \qquad 1.21$$

where βm is the wavenumber of maximum amplification. equation 1.16 simplifies to

$$(c-c_o) = \exp(Rmt) \sum (A_\beta \cos(\beta.r) + B_\beta \sin(\beta.r)) \qquad 1.22$$

After some finite time the composition will be represented

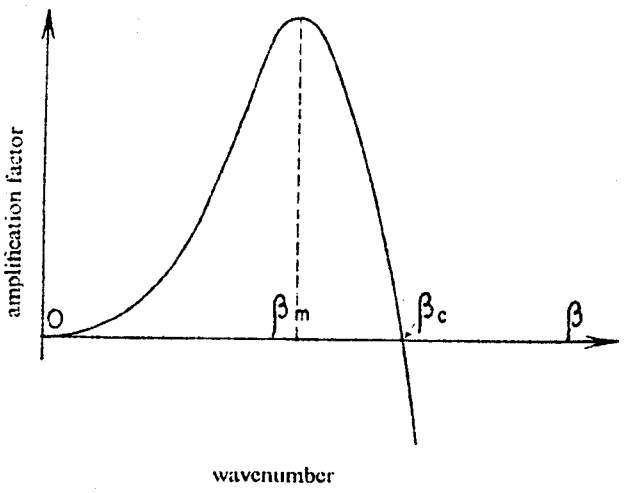

Figure 1.5 The form of the amplification factor in the linearised spinodal decomposition theory (after Cahn (1965))

by a superposition of sine waves of fixed wavelength, but random in orientation and phase. Cahn (1967) has shown by numerical simulation that in an isotropic solid this leads to a strongly interconnected two phase structure.

Spinodal decomposition during isothermal holding

From equation1.19

$$\lambda_m = 2\pi/\beta_m = 4\pi(K_V V_m/(\partial^2 F/\partial c^2))^{\frac{1}{2}} \qquad 1.23$$

where the molar volume (Vm) has been included so that $\partial^2 F/\partial C^2$ is the second derivative of the molar free energy

i.e.

$$\lambda_m = 4\pi(K_V V_m/(\partial^2 S/\partial c^2))^{\frac{1}{2}}(1/\Delta T_s)^{\frac{1}{2}} \qquad 1.24$$

here ΔT_s is the undercooling (below the spinodal boundary) and S is the molar entropy.

Equation1.24 is shown in figure1.6 (after Cahn (1968)).

A time constant that is representative of the process can be derived from equation1.20, and Cahn has shown that as the maximum growth occurs at undercoolings of about 10% the minimum time required for the process is approximately

$$(\lambda^2 V_m)/(2\pi M T_m^2(\partial^2 S/\partial c^2)) \qquad 1.25$$

where Tm is the maximum growth temperature.

Cahn and Charles (1965) have simplified equation1.25 by approximating $\partial^2 S/\partial C^2$ as 4R and M= VmD/RT. For λ of 10 nm and T of 2,000K

$$t(\text{min}) \simeq (10^{-14}/D) \qquad 1.26$$

where D is the limiting diffusion coefficient (ms^{-1})

For a glass forming material D can have a very wide

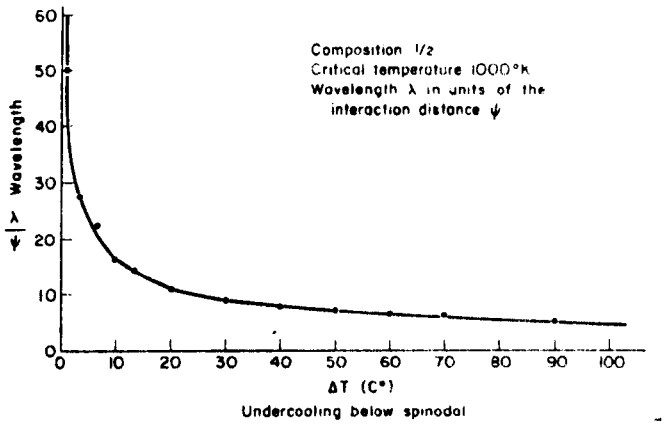

Figure 1.6 The relationship between the maximum amplified wave number and undercooling into the spinodal region (after Cahn(1968)). The interaction distance (ψ) will depend on the exact species and the type of bonding, but to a first approximation can be regarded as being the interatomic distance.

range e.g. $D = 10^{-10} m^2 s^{-1}$, well above the glass transition and $D = 10^{-20} m^2 s^{-1}$ well below it. The minimum time may therefore be anything from a few hundred seconds to microseconds.

Once the spinodal structure has developed it will start to lower its interfacial energy by coarsening and will start to lose connectivity. These later stages have been considered by Cahn (1966).

Spinodal decomposition during continuous cooling

In some glasses there is considerable decomposition during the cooling to and from the isothermal treatment temperature. It has been suggested that this may explain the disagreement between the theory and the experimental evidence concerning the phase separation of some glass compositions. It is important, therefore, to establish the kinetics of the process during continuous cooling.

This has been considered by Husten, Cahn and Hilliard (1966) who found that the resultant structure should be qualitatively similar to the isothermal case, but since λ_m is temperature dependent (equation 1.23) a range of wavelengths undergoes maximum amplification. Initially the average wavelength of the transformation increases as 1/6 power of the quench, but eventually this weak dependence is lost. Figure 1.7 shows the results of Husten, Cahn and Hilliard, and in figure 1.8 linear quench rates are superimposed on the isothermal T-T-T diagram (after Husten, Cahn and Hilliard (1966)) to show the relationship between the two extreme cases of isothermal and continuous cooling.

Intersecting growth theory

In the metastable region of the two-phase area (figure 1.3b)

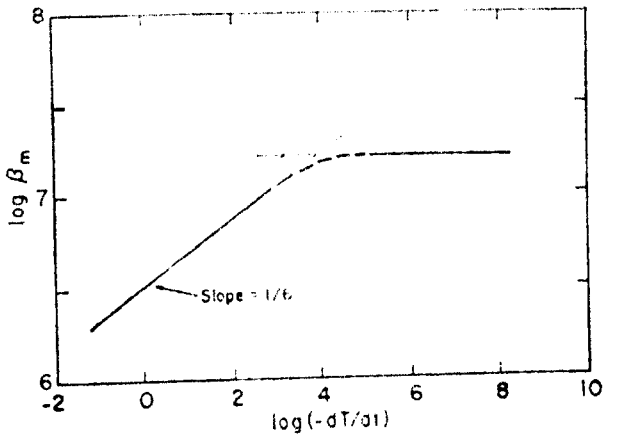

Figure 1.7 The relationship between the maximum amplified wave number and the linear cooling rate (after Husten, Cahn and Hilliard (1966))

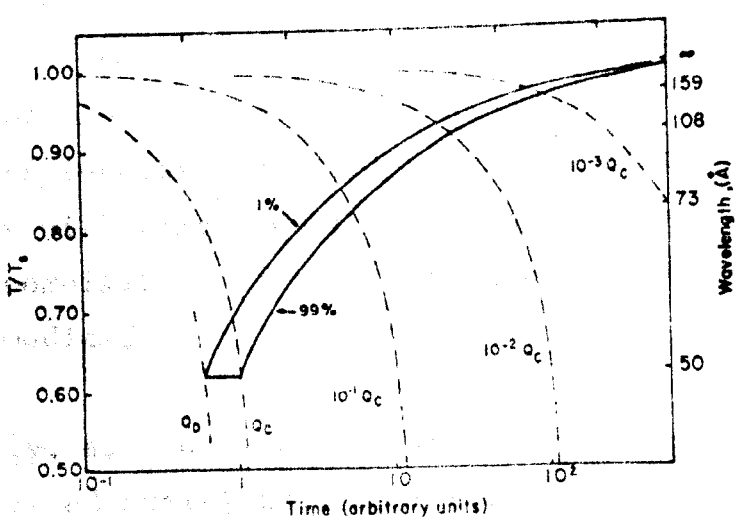

Figure 1.8 The time-temperature-transformation for spinodal decomposition. Superimposed on this are thermal histories representing linear quench rates (broken lines)(after Husten, Cahn and Hilliard (1966))

compositional changes initially increase the free energy so spontaneous decomposition cannot take place. However, once nuclei have formed they can grow to lower the net energy. The rate of formation of nuclei (I) will be proportional to the probability of the formation of the nuclei i.e.

$$I = K\exp - \left(\frac{\Delta Gc + \Delta Gd}{kT}\right) \qquad 1.27$$

where K is a proportionality constant, ΔGc is the energy required to form a critical nucleus, and ΔGd is the energy associated with the limiting process i.e. the diffusion to the interface or the viscous flow through the interface.

Figure 1.9 shows the temperature dependence of I; this first increases with undercooling (due to the decrease in Gc) but then decreases as transport becomes more difficult.

The growth rate/temperature relationship is subject to the same driving force and limitations, and so has a similar temperature dependence. The kinetics of the growth stage depend on the controlling mechanism. If the growth is diffusion limited, the precipitated phase grows at a rate proportional to $(\text{time})^{\frac{1}{2}}$; if interface controlled, the precipitated phase grows linearly with time. Generally, the process will be limited by a combination of these two factors and the growth rate is intermediate.

Eventually, according to the intersecting growth theory the randomly sited nuclei grow to touch one another and so form a continuous phase microstructure. Haller (1965) has shown that a highly interconnecting microstructure could develop by this method using a geometrical analysis. The degree of connectivity will be a maximum for 50-50% phase volumes, but

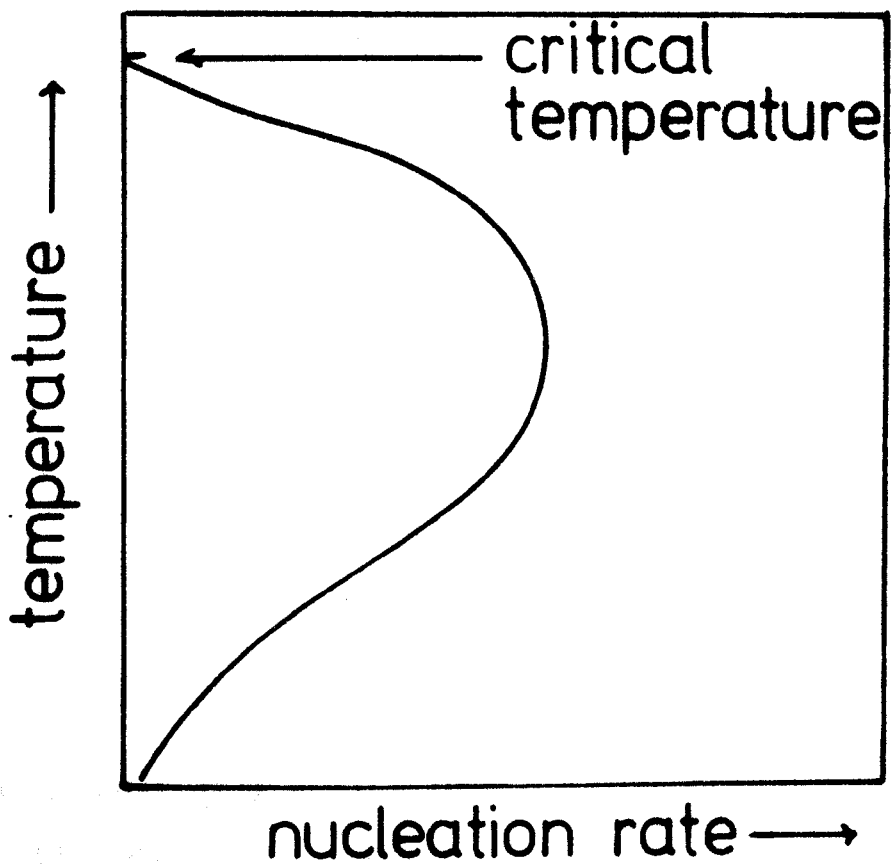

Figure 1.9 The temperature dependence of the nucleation rate

Haller showed that even for a 30-70% (which corresponds to the spinodal limit for a symmetrical metastability boundary) less than 5% of the droplets are isolated.

Haller's simple statistical model cannot be directly applied to the classical nucleation and growth model, since there is no mechanism by which diffusional growth alone can lead to interparticle contact. Goldstein (1968) has observed that because of the depleted zone around each particle the two interfaces will only grow parallel to one another. Haller and Macedo (1968) have proposed several mechanisms to overcome this difficulty including the introduction of a diffuse interface rather than the classical sharp interface. This modification has also received support from Hopper and Uhlmann (1970).

A comparison of the two mechanisms

The morphologies developed by the two models are compared in figure 1.10. Figure 1.10a is after Cahn (1965) showing the structure predicted by spinodal decomposition and figure 1.10b shows the morphology produced by the intersecting growth model after Haller (1965). The similarities between the two have led Tomozowa (1978) to suggest that it is not possible to differentiate between the two by a morphological analysis alone.

One unambiguous difference between the two is that during classical nucleation and growth the composition of the second phase is constant, but during spinodal decomposition the compositions of both phases change continuously. This is illustrated in figure 1.11. (after Cahn (1968)). This suggests that it may be possible to differentiate between the two processes by the measurement of composition dependent properties such as viscosity, electrical conductivity and

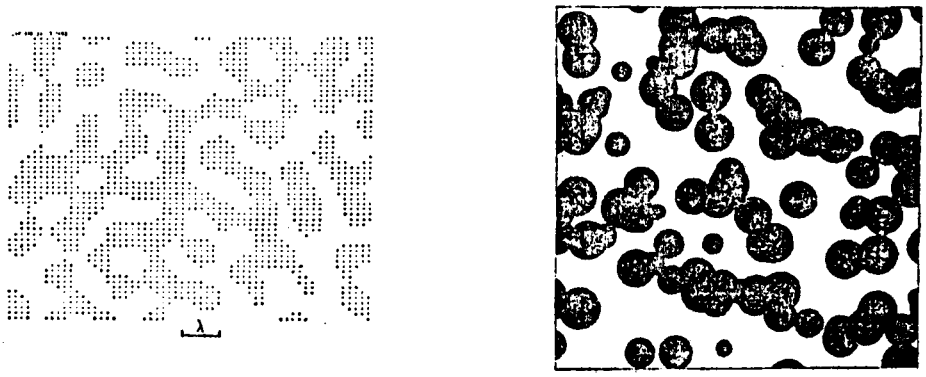

Figure 1.10 The structure predicted by spinodal decomposition (a) and by intersecting growth (b) (after Cahn (1965) and Haller (1965)).

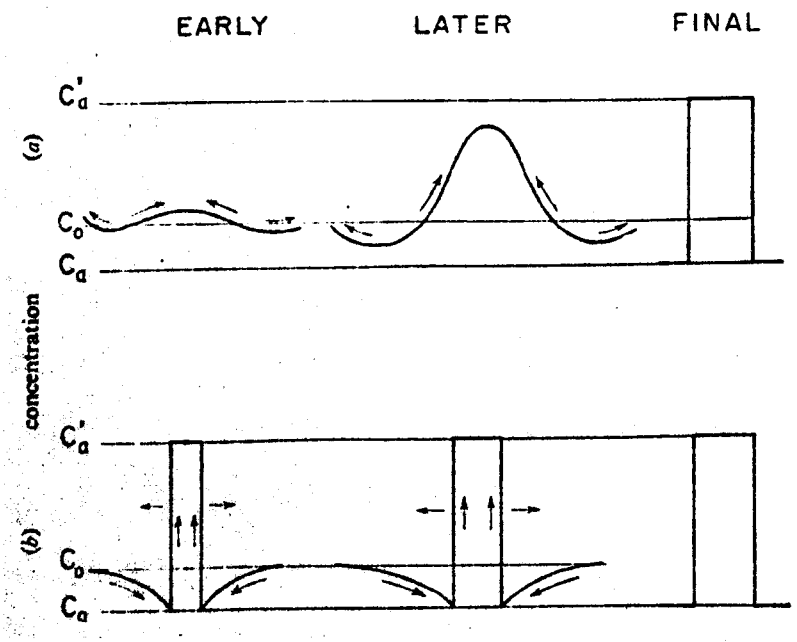

Figure 1.11 Concentration profiles as a function of time for spinodal decomposition (a) and for nucleation and growth (b)

leaching rate.

1.3 The leaching of glass to produce a porous skeleton

When an alkali silicate glass is exposed to water, protons are exchanged for the monovalent ions which then form alkali hydroxides e.g.

$$\left(\equiv Si - O^-\right) + \left(H_2O\right) \rightleftharpoons \left(\equiv Si - OH\right) + \left(OH^-\right) \qquad 1.29$$

The hydroxyl ion produced by this reaction can then attack the silicon-oxygen network e.g.

$$\left(\equiv Si - O - Si \equiv\right) + \left(OH^-\right) \rightleftharpoons \left(\equiv Si - OH\right) + \left(\equiv Si - O^-\right) \qquad 1.30$$

If the glass is in contact with acid instead of water, the alkali reaction product is neutralised and unless the acid actually attacks the Si − O − Si linkages (as with H·F and H_3PO_3) this network is left intact. Further, if the glass is separated into interconnecting phases, one of silica and the other of an alkali-borate or a similarly soluble glass, then that phase can be removed leaving a skeleton of silica.

Nordberg and Hood (1940) found a range of alkali-borosilicates that could be leached free of virtually all non-silicate constituents after suitable heat treatment. The porous material produced is known as Vycor and its production and properties have been reviewed extensively by Wolf (1961a). The composition of the parent glass is critical for several reasons. Firstly, the glass must lie in the centre of the immiscibility region so that the two phases may be continuous. Secondly, it was found that stresses are built up in the leached glass (due to hydration) during to the leaching stage. Glasses having compositions near an empirically determined line

on the ternary phases diagram (Wolf (1961b)) are not as subject to this effect. This effect can also be reduced by including ammonium chloride in the leaching solution (Eguchi, Tasaka and Tarumi (1969)) although the reason for this is unclear.

The leaching rate of alkali-borosilicates has been studied by Charles (1964), Shimbo (1972) and Eguchi, Tasaka and Tarumi (1969), who concluded that it was determined by the size of the microstructure. However, Takamori and Tomozawa (1978) reported that it was the composition of the chemically less durable phases, which controlled the rate.

As well as alkali borosilicates; alkaline earth-alkali boro silicates containing zirconia can be leached in acid to produce an integral porous skeleton (Nordberg (1950)). E-glass, a multicomponent alkali free glass can be leached to yield a porous skeleton (Nordberg and Hood (1950)). and barium-borosilicate glass is also known to retain integrity during leaching (Kusnetsov (1974)).

1.4 Desalination

Sodium chloride dissolves in water releasing an amount of energy known as the heat of solution. This, therefore, represents the minimum energy requirement to reverse the process i.e. to desalinate the solution. This is demonstrated in the following section and then the requirements of real desalination processes are estimated.

1.4.1 The heat of solution

The dissolution of an ionic crystal can be modelled in two steps, first the ions are removed from the crystal surface into a vacuum, and then they are plunged

into the solvent. The energy required to remove a pair of ions is given by the Born theory

$$(Ae^2/a)(1 - 1/n) \qquad 1.31$$

where A is the Madelung constant, a is the interionic spacing, e is the elemental charge and n is the Born exponent.

The energy released on submerging the pair into the solvent of dielectric constant ϵ is

$$(e^2/2)(1/r_1 + 1/r_2) - (e^2/2\epsilon)(1/r_1 + 1/r_2) \qquad 1.32$$

where r_1 and r_2 are the ionic radii.
The net change in energy is then

$$E = (e^2/a)(A(1-1/n) - (1-1/\epsilon)) \qquad 1.33$$

for $r_1 \simeq r_2 \simeq a/2$.
For water ϵ is of the order of 80 and $n \simeq 9$ for NaCl so E is negative and the process is spontaneous.

Thermodynamically, the energy released can be described as

$$RT \ln a_o \qquad 1.34$$

where R is the gas constant, T is the absolute temperature and a_o is the activity of the solution relative to that of pure water.

1.4.2 A nearly ideal desalination process

Rather than finding the minimum energy for desalination by just using the tabulated data for heat of solution (e.g. Handbook of Chemistry and Physics (1975)), it can be calculated in the context of a desalination process. Howe (1966) has illustrated this limit by devising the nearly ideal desalting process shown schematically in figure 1.12. This consists of two isothermal containers connected by a frictionless pump. One chamber (A) contains pure water

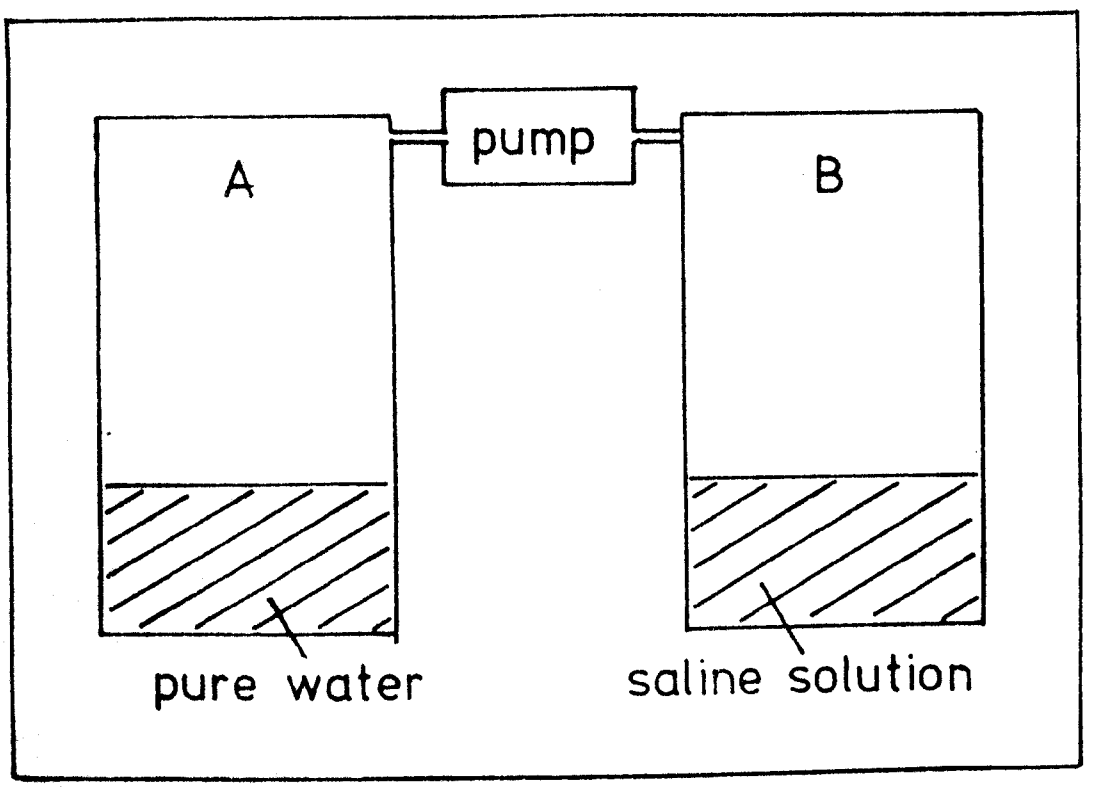

Figure 1.12 A "nearly" ideal desalination process (after Howe (1966))

and the other (B) a saline solution. Without the pump, the lower vapour pressure in B would induce water to condense into the saline solution. To reverse the process the pump has to overcome this pressure difference. As the process is purely mechanical the energy required is simply

$$W = \int_{Pb}^{Pa} Pdv \qquad 1.35$$

If the process is performed reversibly and the salt concentration of chamber B does not change, then

$$W = Pa\ Va\ \ln(Pa/Pb) \qquad 1.36$$

where Pa is the vapour pressure of pure water

Pb is the vapour pressure of the saline solution

and Va is the specific volume of the pure water vapour

At $20^{o}C$ and for 1 molar salt solution

$Pa = 2.34$ KPa
$Va = 57.8 m^{2} Kg^{-1}$ } Obtained from steam tables (Mayhew and Rogers (1972))

and $Pb = 2.27$ KPa ..... Obtained from International critical tables of numerical data (1928)

This gives W as 4.2 MJm^{-3} which is in approximate agreement with the minimum calculated from heat of solution data.

1.4.3 Real desalination processes

Commercial desalination processes have been the subject of many reviews (e.g. Diamont (1974), U.K.E.A. (1967) and Howe (1966) and may be divided into two categories - athermal and isothermal. Athermal techniques include the most common process, that of distillation, which relies on the low vapour.

pressure of NaCl to effect the separation. Other athermal processes include freeze separation, hydrate separation and liquid-liquid separation.

Isothermal techniques are primarily electrodialysis, ion exchange and reverse osmosis. In ion exchange the two ionic species are replaced by acid and basic radicals, and these are allowed to react to form more water. In electrodialysis, an electric field is used to deplete the solution of ions by forcing them through cation and anion permeable membranes. In reverse osmosis, mechanical work is used to force the solvent through a semi-permeable membrane.

1.3.4 An estimate of the energy requirements of real desalination processes

Real desalination processes use more than the minimum energy to effect the separation. To indicate the potential advantage of isothermal techniques, the practical energy requirements of three representative processes will be estimated in this section. To simplify this estimate, it is assumed that all the stages in the process are equally efficient, and that the ideal (reversible) work required to perform the separation is negligible compared to that of the inefficiences of the processes.

Thermal distillation

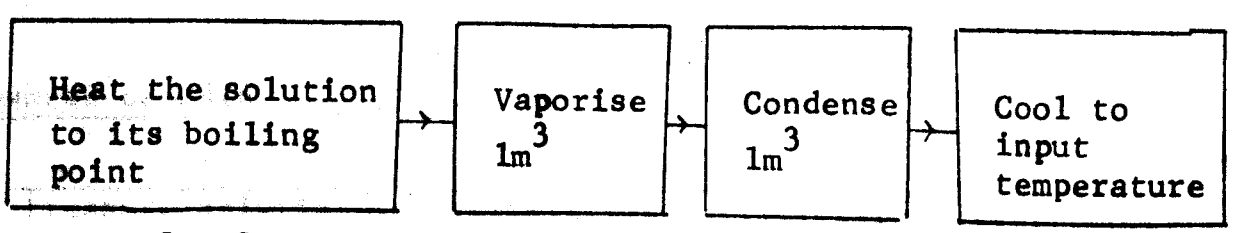

$$H = - C_p^s \Delta T^s \quad - Lv \quad + Lv \quad + C_p^w \Delta T^w$$

where C_p^s and C_p^w are the specific heats of the saline solution and water, ΔT^s and ΔT^w are the temperature differences

between the input/output temperature and the boiling points of the saline solution and water respectively. Lv is the latent heat of vaporisation. For 1 molar NaCl solution at $20^{o}C$ and approximating $C_p^s = C_p^w$

$$H = -4.2 \times 10^6 \times 84 \quad -2{,}000 \times 10^6 + 2{,}000 + 10^6 + 4.2 \times 10^6 \times 80$$

so for an efficiency of (1-a), the total energy cost is $4.6a\ GJm^{-3}$.

Freeze separation

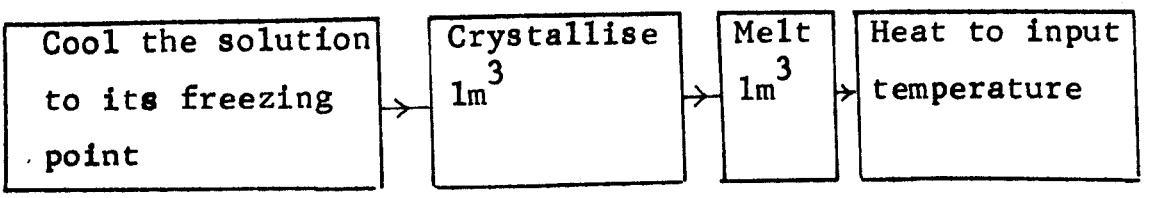

$$H = + C_p^s \Delta T^s \quad + Lf \quad - Lf \quad - C_p^s \Delta T^w$$

where ΔT^s and ΔT^w are now the temperature differences between the input temperature and the two freezing points. Lf is the latent heat of freezing.

For 1 molar solution at $20^{o}C$ and approximating C_p^s as C_p^w

$$H = 4.2 \times 10^6 \times 23 + 330 \times 10^6 - 330 \times 10^6 - 4.2 \times 10^6 \times 20$$

If at each step the efficiency is (1-b), the energy cost is $.8b\ GJm^{-3}$.

Reverse osmosis

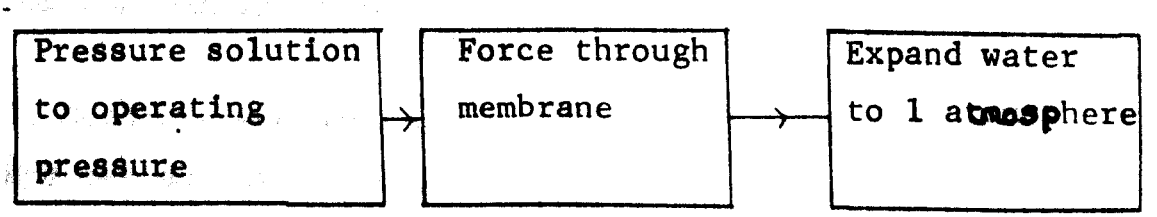

$$W = - v\Delta p \quad - v\Delta\pi \quad + v\Delta(p-\pi)$$

where p is operating pressure, π is osmotic pressure and v is volume compressivity.

For a 1 molar salt solution $\pi \sim 20$ bars. For an operating pressure of 100 bars.

$$W = -100 \times 10^5 \times 1 - 20 \times 10^5 \times 1 + 80 \times 10^5 \times 1$$

With an efficiency of (1-c) the energy requirement is $.02c\ GJm^{-3}$. In table 1.1 the energy requirements of these three processes are compared with the ideal limit. It is clear, from table 1.1 that reverse osmosis and other isothermal processes have a potential energy advantage over athermal techniques providing that the efficiency parameters a,b and c do not differ by more than an order of magnitude.

1.5 Porous glass for reverse osmosis desalination: A reveiw

In this section the scale of the membrane microstructure required for desalting applications is established by reviewing published data on reverse osmosis desalination using porous glass. The performance of the membranes is characterised by two phenomenological parameters. The flux rate defined as the product in cubic meters from one square meter of external surface area in one hour which has the units mhr^{-1} and the rejection coefficient defined by

$$\text{rejection } \% = \frac{Cf - Cp}{Cf} \times 100$$

where Cf is the feed concentration in weight % NaCl and Cp is the product concentration also in weight % NaCl.

Nordberg and Hood (1938) first suggested that porous glass may act as a semipermeable membrane and later Kraus et al (1966) reported measurable salt rejections from porous Vycor membranes. The preparation and performance

Table 1.1 A comparison of the estimated energy requirements of several desalination processes

PROCESS	ENERGY / $1m^3$
DISTILLATION*	4 600a MJ
FREEZE SEP.*	800b MJ
R.O.*	20c MJ
IDEAL	4.2MJ

* These estimates are of the excess energy requirement i.e. above that of the ideal limit.

of membranes produced from Vycor and Vycor-like glass compositions has been discussed by Phillips et al (1974), McMillan and Matthews (1976), Elmer (1978) and reviewed by Schnabel and Vaulont (1978). Schnabel and Vaulont in describing the engineering aspects of reverse osmosis desalination, emphasised the importance of having turbulent flow at the solution/membrane interface to reduce concentration polarisation. Most investigators have used a recirculating feed solution to achieve this, but Elmer used an essentially static system which was stirred at some distance from the membrane. Probably, because of this he could not correlate the rejection of the membrane with its pore size and instead considered that the rejection mechanism was due to a secondary precipitate in the pores of the glass. With the exception of Elmer, all workers have found that as the pore size is decreased, the salt rejection tends to increase.

Phillips et al found that the salt rejection of porous Vycor membranes could be improved by partially collapsing the pores by thermal treatments near the sintering temperature. They achieved rejection coefficients of up to 88% (using a 3.5 wt% Na Cl) with a product flux of .2 mhr^{-1} for membranes with 2nm radius pores. McMillan and Matthews tried to minimise the pore size by including Al_2O_3 in the parent glass to slow the phase separation reaction. They found that this was more controllable and reported rejections of the order of 60% at a flux of .002$m.hr^{-1}$ for membranes with pores of 2.6nm radius.

The performance of porous Vycor membranes supplied by the Corning Glass Company has been investigated by Belfort (1972), Ballou and Wyderal (1972) and Littman and Guter (1968). All used a glass known as Corning Code 7930 which has a nominal pore radius of 2 nm. The rejections reported are

all of the order of 60% (using a 0.1 weight % NaCl feed) but Ballou and Wydevæn found evidence that the rejection increased dramatically if the pore size was reduced below 2nm radius. They reported a rejection of 92% for membrane having a pore size distribution peaked at 1.9nm.

Membranes based on glasses of the Vycor composition but containing nucleating agents to modify the microstructure have been prepared at the Stanford Institute (Littman and co-workers (1968-71). Amongst these membranes, one produced from a parent glass containing zirconia has been evaluated as an osmosis desalting membrane by Belfort (1972) and Littman, Kleist and Croopnick (1971). With this membrane (designated AG-39)salt rejections of over 70% have been reported.

Schnabel and Vaulont (1978) have made desalination measurements using a porous Vycor membrane which has been modified by organic treatments. Rejections as high as 97% have been reported by them with 0.5 weight % NaCl feed solutions at product fluxes of 0.001 mhr^{-1}. In figure 1.13 the data of Ballou et al (1971), McMillan and Matthews (1976), Kraus et al (1966) and Littman and Guter (1968) are shown. It is clear from this figure that salt rejection improves rapidly if the pore size of the glass can be reduced below 2nm.

1.6 Objectives of investigation

The aims of this programme were:

i to investigate the interconnected microstructure and its relationship with thermal history

ii to establish the role of the parent glass in determining the microstructure of the porous glass skeleton

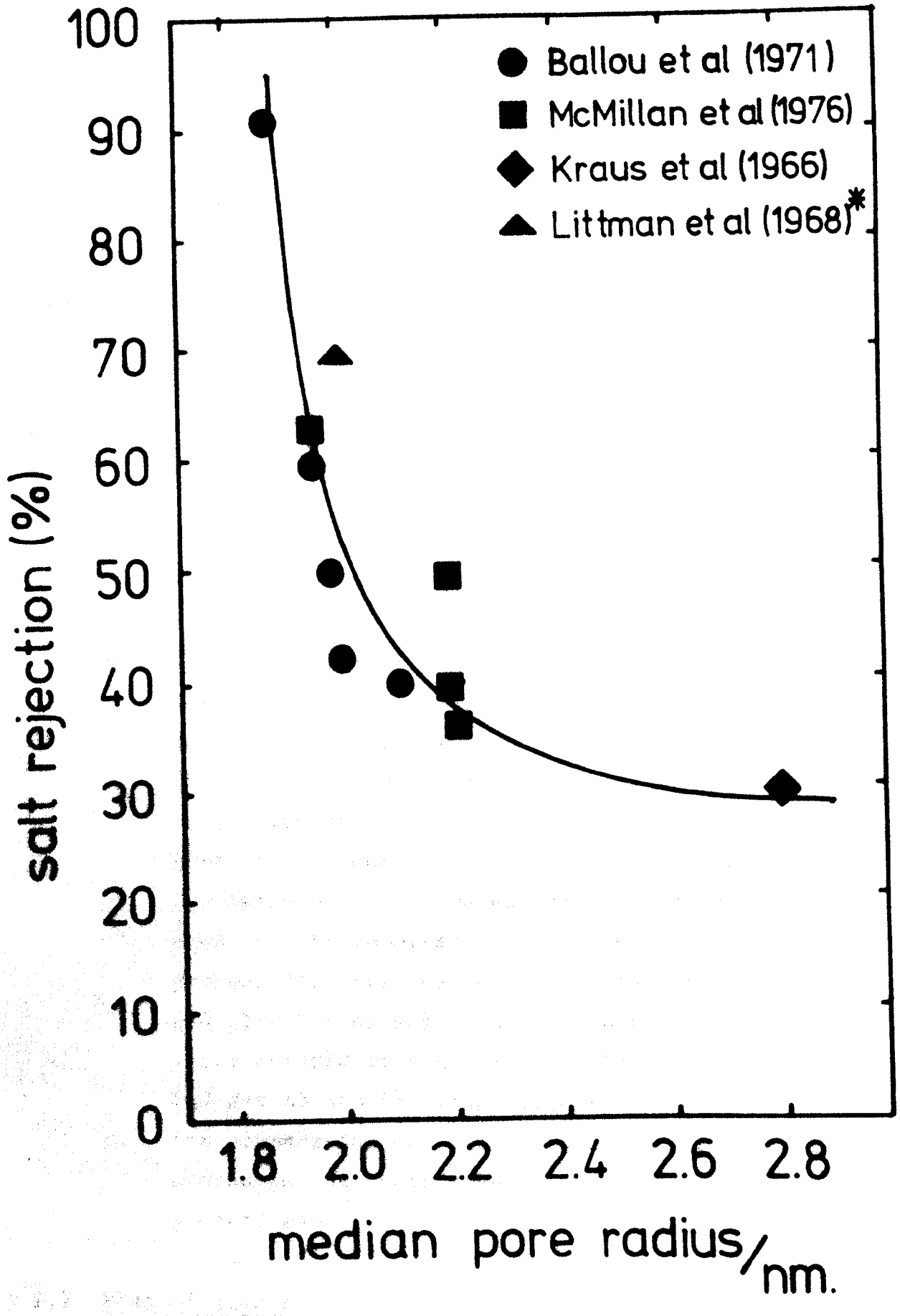

Figure 1.13 The salt rejection of porous glass membranes as a function of the median pore size. A compilation of the data of Ballou et al (1971), McMillan and Matthews (1976) and Littman and Gutter (1968)

iii. to develop and characterise a microporous glass membrane for reverse osmosis desalting applications.

1.7 The research programme

As practical 'isothermal' treatments to induce phase separation in glass involve athermal cooling and/or heating stages, there is always some ambiguity in relating the resulting microstructure with the treatment. For that reason it was decided to restrict this investigation to glasses which have received no isothermal treatments i.e. which were continuously cooled from the molten state.

The experimental investigation was divided into three parts:

a. the production of phase separated glass and an investigation of its microstructure by two composition dependent properties: electrical conductivity and viscosity. These measurements were correlated with the thermal history of the glass by the measurement of its cooling rate.

b. the leaching of the parent glass, including a study of the important parameters in the leaching process i.e. acid concentration, leachant temperature and time in the solution. The porous product was characterised by transmission electron microscopy and gas adsorption measurements.

c. the preparation of hollow fibre membranes and an evaluation of their reverse osmosis desalting properties.

1.7 Plan of Thesis

In Chapter 2 the selection of the glass systems to be

investigated is described together with a description of the glass preparation. The experimental techniques used to study the microstructure are also described.

The leaching of the glass is fully described in Chapter 3, together with the experimental details of the techniques used to characterise the porous product. As the gas adsorption measurements are central to the argument presented, the theory is treated in detail.

Chapter 4 contains the results of the analysis of the parent glass and a brief discussion of the implications of the results.

The results of the investigation of the porous glass are presented in Chapter 5 and the optimum leaching conditions for the production of an integral porous skeleton are discussed.

All work concerning reverse osmosis desalination is contained in Chapter 6. The experimental arrangement used is described, the characterisation of the porous membranes and the results of the measurements are presented together with a discussion of the operational performance in terms of membrane pore size.

In Chapter 7 the results of all the investigations are drawn together and further conclusions are made. Recommendations for future work are also included in this section.

CHAPTER 2

The production of the parent glasses and experimental details of the measurements on these glasses

2.1 Introduction

In this chapter the reasons for the selection of the basic glass composition investigated are presented. The logic of the subsequent generation of a series of compositions from the basic composition is also outlined together with a description of the preparation of the glasses. An account of the experimental techniques employed to characterise them is also given.

The experimental techniques selected to characterise the glasses were: the measurement of critical opalescence, viscosity and d.c. resistivity. Electron microscopy was also evaluated, but it was found not to be suitable for this part of the research programme.

The observation of critical opalescence is the most commonly used technique to estimate the metastability limit in glass. This involves determining the highest temperature at which opalescence can be induced, and the lowest temperature at which opalescence clears. To cause opalescence, the scale of the phase separation must be of the order the wavelength of visible light. The clearing temperature may then only indicate the temperature at which submicron phase separation is present, and so underestimate the metastability limit. D.c resistivity measurements were made to complement the critical opalescence measurements. This is a strongly

compositionally dependent property and should be sensitive to the compositional changes occuring at and below the metastability limit.

Viscosity measurements have also been used to determine the metastability limit in several glasses (Haller, Simmons and Napolitano (1971)), and as the viscosity/temperature relationship controls transport processes in the glass, the measurement of viscosity was of special interest.

2.2 The selection of the glass compositions

Although many glass compositions yield phase separated glass, only a few produce the interconnected phase microstructure necessary for the production of a porous material. As it was one of the primary aims of this investigation to produce such materials, it was clearly important to base this study on a glass composition known to be suitable for the production of porous glass. This restricted the potentially applicable glass compositions to those described in section 1.3 .

Most of the previous work on the reverse osmosis desalting performance of porous glass has centered on the use of hollow fibre membranes. This form of membrane is mechanically suited to withstand the large hydrostatic pressures applied during the desalting process and produces a large product flux because of its great external surface to volume ratio. The hollow fibre membranes previously investigated were manufactured from parent glass hollow fibres, themselves produced by 'drawing down' larger glass tubes. As a consequence of this, they have a complex thermal history. Since it is possible to produce hollow fibres directly from the glass melt and to produce porous

glass skeletons from certain glasses which have undergone no isothermal treatment, it was decided to investigate the microstructure and its relationship to the leaching of fibres drawn directly from the glass melt. The thermal history of such fibres is relatively simple, being that of continuous cooling.

The two theories of decomposition in glass predict optimum connectivity for glasses having two phases of equal volume fraction. If the volume fraction of the two phases is dissimilar then the microstructure of the glass will show only limited connectivity according to Haller's intersecting growth model; and only tenuous connectivity according to the theory of spinodal decomposition. In a three or more component glass there may be more than two phases induced (by analogy with the Gibbs phase rule) but as far as the leaching properties are concerned the glass may be considered as having two phases: acid soluble and acid insoluble (silica phase). For a systematic study of the interconnectivity of these two phases it is important, therefore, to be able to vary the relative proportions of these phases.

Glass formation in multicomponent glasses like E-glass is generally insensitive to the concentration of any particular constituent. Stevels (1954) and Huggins (1954) have shown that in some multicomponent glass compositions it is possible to vary the SiO_2 content over a wide range and still produce glasses. The relative insensitivity to the SiO_2 content of glass formation in compositions of the E-glass family was confirmed in preliminary experiments and this material was selected as a starting point for this investigation.

To summarise E-glass was selected as the basic glass composition for this investigation because:

i it is known to phase separate and form an interconnected microstructure, suitable for the production of porous glass,

ii it is suitable for the production of hollow fibre membranes with a simple thermal history

iii glass formation is relatively insensitive to the SiO_2 content.

That E-glass could be leached free of virtually all non-silicate constituents was first recognised by Nordberg and Hood (1950) and this forms the basis of the production of a commercial high silica fibre known as Refrasil. The composition of commercial E-glass varies within the limits shown in table 2.1. Table 2.2 shows the composition of the leached glass after drying at 100°C.

The material is designated E-glass because of its high Electrical resistivity which is primarily the result of its low alkali content. It is used as a general purpose glass fibre in many applications (Lowrie (1967)). The composition of E-glass is based on the eutectic at 1170°C in the Al_2O_3-CaO-SiO_2 system but it contains B_2O_3 (replacing SiO_2) to improve its fibre forming properties and MgO (replacing CaO) to facilitate melting.

E-glass fibres were used extensively by investigators studying the mechanical properties of glass fibres (e.g. Holloway (1960), Bartenev and Ismailova (1962) and Thomas (1960)) but phase separation in this glass has been studied only by Hammel and Ohlberg (1965), Ohlberg

Table 2.1 The composition limits of commercial E-glass

SiO_2	Al_2O_3	CaO	MgO	B_2O_3	Na_2O $+K_2O3$	TiO_2	FeO_3	Fe_2
52	12	16	0	8	0	0	.05	0
56	16	25	6	13	3	.4	.4	5

Table 2.2 The composition of leached E-glass*

SiO_2	Al_2O_3	CaO	MgO	B_2O_3	Na_2O	TiO_2	FeO_3
99.3	0.15	0.08	0.1	0.02	0.01	0.17	0.07

*Reference: Chemical and Insulating Co. Ltd. Darlington, Publication 2/1.

Hammel and Golob (1965) and Haller, Simmons and Napolitano (1971).

To a good approximation (>99%) the acid insoluble phase is pure silica. To investigate the interconnectivity of the phase microstructure, a series of glasses was prepared by varying the SiO_2 content, but maintaining the relative proportions of the balance: (.38 CaO, .30 Al_2O_3, .22 B_2O_3 and .1 MgO by weight). It was found that glasses could be produced from compositions having from 10% (by weight) to at least 70% (by weight) of SiO_2. Further, it was possible to produce glass fibres from a melt representing only the acid soluble phase in the original glass i.e. a magnesia - calcia - aluminoborate.

In table 2.3 the compositions of the glasses investigated in this programme are given in both weight and molecular percentages. These glasses were designated according to their SiO_2 content. For example, the glass selected as the basic E-glass composition and lying near the centre of the E-glass compositional limits shown in table 2.1, of the composition 54% SiO_2, 17.5% CaO, 14% Al_2O_3, 10% B_2O_3, and 4.5% MgO (by weight), was designated E-54.

2.3 Glass preparation

All of the glasses used in this investigation were made from Analar grade aluminium oxide, calcium carbonate magnesium oxide, boric acid and precipitated silica. Batches of 300g were tumble mixed for three hours and then melted in platinum/rhodium crucibles. The electric furnaces used for the melting were open to the atmosphere. To ensure homogeneity, when bubble free the melts were quenched onto pyrolytic graphite sheets, crushed and remelted.

Table 2.3 The glass compositions

The glass compositions investigated

DES'N	SiO_2	WT%					MOL %				
		CaO	Al_2O_3	B_2O_3	MgO		SiO_2	CaO	Al_2O_3	B_2O_3	MgO
E-70	70.00	11.41	9.13	6.52	2.93		71.47	12.63	5.58	5.83	4.51
E-67	67.00	12.56	10.04	7.17	3.28		68.48	13.91	6.12	6.41	5.06
E-65	65.00	13.31	10.65	7.61	3.42		66.50	14.78	6.51	6.83	5.28
E-60	60.00	15.22	12.17	8.69	3.91		61.68	16.96	7.46	7.82	6.06
E-58	58.00	15.98	12.78	9.13	4.11		59.70	17.83	7.84	8.23	6.38
E-56.5	56.5	16.58	13.27	9.43	4.26		57.79	18.51	8.14	8.54	6.61
E-54	54.00	17.50	14.00	10.00	4.50		55.76	19.59	8.62	9.06	7.01
E-51	51.00	18.64	14.91	10.65	4.79		52.77	20.90	9.20	9.65	7.47
E-50	50.00	19.02	15.22	10.87	4.89		51.76	21.35	9.40	9.85	7.64
E-45	45.00	20.92	16.92	11.92	5.38		46.75	23.50	10.37	10.88	8.43
E-40	40.00	22.83	18.26	13.04	5.87		41.70	25.81	11.35	11.90	9.23
E-30	30.00	26.63	21.30	15.22	6.85		31.50	30.31	13.34	14.00	10.85
E-10	10.00	34.24	27.39	19.56	8.80		10.65	39.55	17.40	18.25	14.14
E-0	0.10	38.05	30.43	21.79	9.78		0	44.29	19.48	20.39	15.84

The temperatures and times required, to complete the fusion of the raw materials and for the 'fining' of the melt, were dependent on the silica content of the original batch. The melting schedules are shown in table 2.4. The raw material for glass E-70 could not be fused at the maximum available temperature, so an extra step was included to produce this glass.

For glass E-70, deionised water was added to the raw materials to form a slurry of the insoluble refractory components and the water soluble boric acid. On drying, the boric acid coated the refractory particles, and this more intimate mixture reduced the temperature required for the fusion reactions. Although Tomlinson (1956), and Scholtze (1959) reported that the equilibrium water content of glass melts is dependent only on the partial pressure of water above the melt, one batch of glass E-65 was prepared as glass E-70, so that any effects due to a different water content could be isolated. The melting schedules for these two glasses are given in table 2.5.

After 'fining', glass fibres and hollow fibres were produced and the remainder of the glass cast into a block.

2.3 Glass fibre production

The glass fibres used in this investigation were drawn directly from the glass melt. To do this, the crucible was first removed from the furnace and a platinum-rhodium alloy rod was dipped into the surface of the cooling melt. Once wetted this was pulled vertically upwards at a nominal velocity of $1 ms^{-1}$. A range of glass fibres was achieved by drawing the fibres over a range of melt viscosities (estimated at from 10^2 to 10^3 poise).

Table 2.4 The melting schedules

GLASS	FUSION		FINING		HOLDING
	T/°C	t/hr.	T/°C	t/hr	T/°C
E-67	1700	5	1450	36	1600
E-65	1650	5	1450	20	1450
E-62	1600	5	1450	20	1420
E-62	1600	5	1450	20	1420
E-60	1600	3	1450	20	1350
E-58	1450	10	1400	20	1280
E-56	1450	5	1350	20	1250
E-54	1400	5	1250	20	1250
E-51	1400	3	1200	20	1250
E-50	1400	3	1200	20	1250
E-45	1400	3	1150	10	1200
E-40	1350	3	1150	8	1150
E-30	1300	3	1100	5	1000
E-20	1300	3	1100	5	1000
E-10	1200	2	1000	2	900
E-0	1200	2	1000	2	900

All temperatures are accurate to $\pm$ 20°C

Table 2.5 The melting schedules of the glasses prepared from water saturated chemicals

GLASS	FUSION		FINING		HOLDING
	T/°C	t/hr	T/°C	t/hr	T/°C
E-70	1600	10	1500	36	1650
E-65	1550	10	1450	20	1450

All temperatures are accurate to $\pm$20°C.

Between each drawing operation, the crucible and contents were returned to the furnace and heated to the holding temperature indicated in table 2.4. From each drawing operation approximately 2m of fibre was produced. To produce sufficient fibre for the investigation programme (about 50m) the glass melt was maintained at the holding temperature for a total of approximately 10 hours. During this time, volatilisation losses from each melt amounted to less than 0.5% of the melt weight. This was established by weighing the contents of duplicate melts as a function of time.

2.3.2 Hollow fibre production

The drawing process outlined above was modified to manufacture hollow fibres. The metal rod was replaced by a short length of silica tube connected to about 1m of plastic tubing. The silica tube was dipped into the surface of the cooling melt and a bubble was blown near the glass surface. The tube was then pulled vertically upwards at a nominal $1ms^{-1}$ drawing the bubble into a fine capillary. A range of capillary dimensions was obtained by varying the bubble size and pulling it out over a range of melt viscosities.

2.4 The measurement of critical opalescence

2.4.1 Introduction

If the scale of the phase separation in a glass is similar to the wavelength of light, Mie scattering will cause the glass to appear opalescent. The limiting temperature at which opalescence occurs has been taken to define the metastability limit in several glass forming systems e.g. Na_2O - SiO_2 (Rawson (1967)). In practice,

for each glass the critical temperature is bracketed between the highest temperature at which opalescence can be induced and the lowest temperature at which the opalescence clears.

If the scale of the phase separation is less than the wavelength of light, the glass does not appear opalescent . However, providing it is greater than about 50nm it will still cause some scattering of light. Hammel and Ohlberg (1965) have made light scattering measurements on an E-glass (54% SiO_2, 22% CaO, 14% Al_2O_3 and 10% B_2O_3) and determined a critical temperature of 878°C. They determined, also, that the scattering was due to an isolated droplet phase and that this represented only 5% of the total volume of the glass. As a 5% - 95% phase separation volume ratio cannot account for the ability of the glass to yield a porous skeleton, the phase separation phenomenon they reported must represent some later stage in the decomposition process.

Whilst phase separation on a fine scale was the major interest in this programme it was decided to use the technique of observing critical opalescence to tentatively establish the critical temperatures of the glasses under investigation.

2.4.2 Apparatus and procedure

The arrangement used to observe the appearance and disappearance of opalescence in the glass is shown schematically in figure 2.1. The glass, in the form of(10x10x10mm) cubes , was placed in contact with a type R thermocouple (Pt vs. Pt/13%Rh) in a horizontal tube furnace. A Pye portable potentiometer was used to determine the thermocouple e.m.f and opalescence was observed by the scattering of a strong light source through the glass block. Each glass

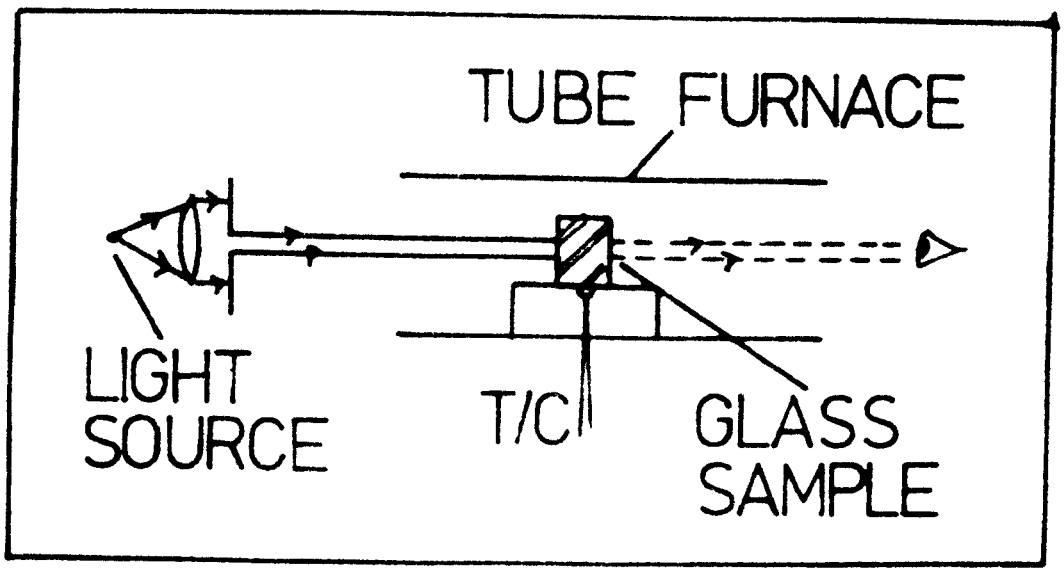

Figure 2.1 Schematic diagram of the apparatus used to determine the critical temperature of the glass by observing opalescence

was subject to a series of 3 hour isothermal treatment from its annealing temperature, the treatment temperature being increased by about 50°C until either opalescence occurred or the glass block started to deform under its own weight. If opalescence was detected, the temperature was increased in 20°C steps until the glass cleared or softened. For the glasses which became opalescence, the process was repeated using new samples but incrementing the treatment temperature in 10°C steps to define the highest temperature at which opalescence occurred and the lowest temperature at which it cleared.

2.5 D.c. resistivity

2.5.1 Introduction

The electrical conductivity of the oxide glasses is usually due to ionic diffusion and is described by an Arrhenius type rate equation i.e.

$$\sigma = \sigma_0 \exp-(E/kT) \qquad 2.1$$

where σ is the specific conductivity, k is the Boltzmann constant and T is the absolute temperature. E and σ_0 are respectively an activation energy and a constant both of which are dependent on the composition of the glass.

The electrical properties of a phase separated glass will depend, therefore, on the composition as well as the morphology of the phases. For an isolated droplet microstructure the matrix phase provides the only continuous path for the current. In such a glass the electrical properties will be similar to those of a homogeneous glass of the matrix phase composition.

If both phases are continuous and one phase has a much lower resistivity, the electrical properties will be controlled by the low resistivity phase.

In phase separated alkali silcate glasses the conductivities of the two phases are very different and several investigators have confirmed that the occurrence and extent of phase separation has a large effect on the electrical properties (e.g. Redwine and Field (1969), Charles (1963 and 1964) and Hakim and Uhlmann (1971)). Charles in particular has used the activation energy of the conduction mechanism as evidence of the presence of an alkali-rich or alkali deficient continuous phase.

In binary alkaline earth silicates it is generally accepted that the divalent ions are responsible for conduction at moderate temperatures. As these ions are much larger than alkali ions, their mobility is less and consequently the conductivity of alkaline earth silicates is much less than that of alkali-silicates. At higher temperatures, oxygen ions have a larger diffusion coefficient and there is evidence that they are the carriers in several molten glasses (Terai and Hayama (1975)).

Electrical resistivity measurements were undertaken here to complement the critical opalescence measurements i.e. in determining the onset of phase separation. As conductivity is a composition dependent property it was expected to be sensitive to the precipitation of a second phase. Both the pre-exponential constant and the activation energy in the Arrhenius expression describing the conduction process in glass are sensitive to composition (Owen (1963)) but as the physical interpretation of the pre-exponential constant is not clear, the activation energy was of more interest.

2.5.2 Apparatus and procedure

A cell was devised for the resistivity measurement, with which it was possible to measure the change in resistivity of the glass melt as it cooled from the molten state. This is shown schematically in figure 2.2. The outer electrode of the cell was a small (20ml) platinum/5% rhodium alloy crucible. This was charged with 40g of glass cullet. The inner electrode was a platinum/ 5% rhodium alloy rod which was a friction fit into an alumina lid made for the crucible. This rod penetrated the molten glass to approximately half its depth in the crucible. Electrical contact to the electrodes was by thin platinum/ 5% rhodium wires, spot welded into position. These wires were then wrapped onto 2mm diameter nickel wires. The platinum/nickel junctions were positioned as close together as possible to minimise thermoelectrical e.m.f.'s due to the dissimilar temperatures of the junctions.

This cell was placed in a furnace with the electrical leads fed through holes to the measuring apparatus. The temperature of the cell was measured with a Comark 1652 thermometer and a type R thermocouple which was situated near to the cell.

A Marconi universal bridge (model TF 2700) was used to directly measure the resistance of the cell. This was operated with an external adjustable power supply of 1.5 to 200 volts. An ammeter measuring the current passing through the glass and a current reversing switch were also included in the measuring circuit which is shown in figure 2.3.

The cell was calibrated at room temperature using a 1N KCl solution with the bridge operating at 10 kHz.

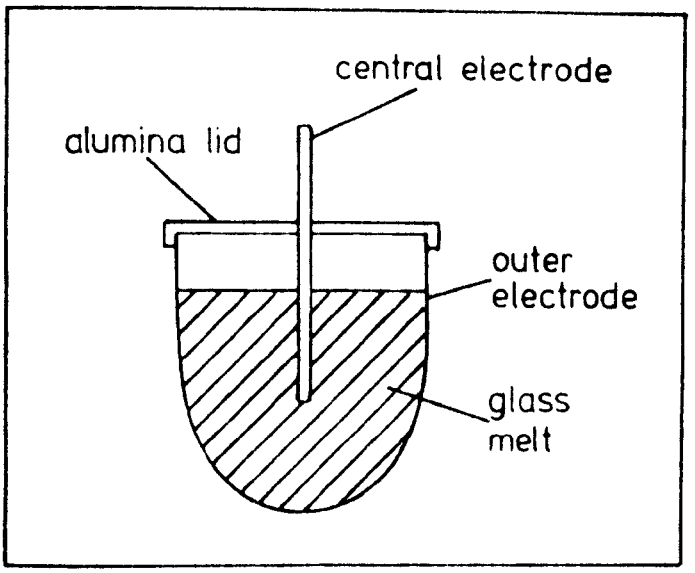

Figure 2.2 Schematic diagram of the conductivity cell

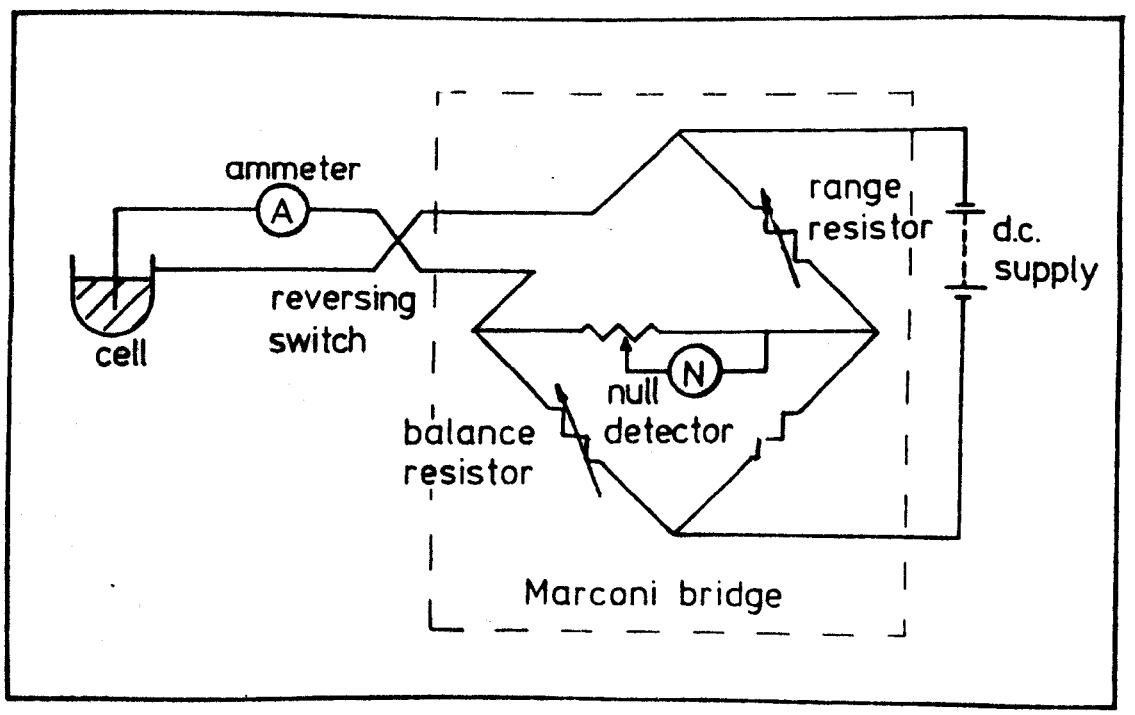

Figure 2.3 The electrical circuit used to measure the resistivity of the molten glass

These measurements confirmed that the position of the central electrode was not reproducible. As a result of this, the measured specific resistivity was only accurate to ±30%. The activation energy of the conduction process, however, is not affected by this as it is determined from relative measurements. The effect of thermal expansion on the height of the glass in the crucible and on the separation of the electrodes was neglected as these changes are small and have opposing effects on the geometry of the cell. The cell constant was found to be 1.2 ±0.4 (95% confidence level).

Prior to making the measurements, the cell was heated to the 'holding temperature' used for fibre production with the particular glass being evaluated (table 2.2). At that temperature it was known that the melt would be bubble free in less than 20 minutes. After 20 minutes at that temperature, the furnace was switched off and allowed to cool. The measurements were made as the furnace cooled. To establish the resistance of the cell with the current flowing in both directions required approximately 20 seconds, during which time the melt temperature changed by a maximum of 2°C.

As the resistivity of the cell increased the operating voltage to the bridge was increased to maintain a measuring current of 50μA. Between measurements the measuring current was removed.

2.6 Viscosity measurements

2.6.1 Introduction

The viscosity of a molecular liquid changes with

the temperature following Arrhenius type behaviour i.e.

$$\eta = A\exp(E/RT) \qquad 2.2$$

where η is viscosity, A and E are constants and R is the universal gas constant.

Such behaviour is only observed in few glasses e.g GeO_2, the majority showing more complex behaviour with temperature. Because of the great technological importance of the viscosity/temperature relationship for glasses, several empirical formulae describing the behaviour have been developed. These have been reviewed by Weyl and Marboe (1964 a).

In a phase separating glass, viscosity may also be a function of time and Haller, Simmons and Napolitano (1971) have determined the metastability limit of several glasses by exploiting this. They proposed that the changing morphology (e.g. the growth of droplets or the coarsening of the structure) was the major cause of the time dependent behaviour . More recently, however, Tomozowa (1978) has suggested that the phenomenon is primarily due to compositional changes in the phases.

If the phase separated morphology of the glass is that of isolated droplets then the matrix phase determines the viscous behaviour i.e. the viscosity of the phase separated glass will be similar to that of a homogeneous glass of the matrix phase composition. If the morphology is that of interconnecting phases then the viscous properties will be similar to that of a homogeneous glass composed of the most viscous phase.

Viscosity measurements were undertaken in this investigation for three reasons. Firstly, to determine

the viscosity/temperature behaviour so that hollow fibres could be produced and the conductivity measurements made. Secondly, to establish the metastability limit in the glasses following the procedure of Haller, Simmons and Napolitano. Thirdly, to observe the change in viscosity with time during the phase separation process.

2.6.2 Apparatus and procedure

Viscosity measurements were made using the fibre elongation technique which is described in detail by Napolitano and Hawkins (1964). This involves measuring the rate of elongation of a fibre under an applied stress. The glass is assumed to behave as a Newtonian fluid, for which the viscosity is defined by

$$\sigma = \eta \nabla v \qquad 2.3$$

where σ is the stress tensor, η is viscosity and ∇v is the rate of change of the fluid velocity with a distance.

Under the uniaxial loading of the fibre elongation technique the velocity gradient is

$$v = e\hat{i} + (-e/2)\hat{j} + (-e/2)\hat{k} \qquad 2.4$$

wnere $\hat{i},\hat{j},\hat{k}$ are orthogonal direction vectors and e is the rate of change (w.r.t)time of a unit length of fluid in the direction of the applied load ($\hat{i}$). For uniaxial loading the stress tensor reduces to a scalar given by

$$\sigma = 3\eta e \qquad 2.5$$

i.e

$$\eta = \sigma/3e \qquad 2.6$$

Rewriting equation 2.6 in terms of the experimentally measured quantities

$$\eta = mgl \,/\, 3\pi r^2 \, dl/dt \qquad 2.7$$

where m is applied load, g is the acceleration due to gravity, l is the fibre length and dl/dt the extension rate.

With the particular apparatus used, the change in length with time was detected with a linear voltage-displacement transducer (L.V.D.T.) and displayed on a y/t chart recorder. With this arrangement it was possible to measure the change in length of the fibre due to viscous flow and thermal expansion. It was also possible to estimate the change in the fibre radius due to viscous flow by assuming a constant fibre volume. These changes were compensated for in the calculation of viscosity from equation 2.7. The extension rate could be determined to an accuracy of $\pm$1% and the dimensions of the fibre to better than 1%. The accuracy of the viscosity calculated is, therefore, approximately $\pm$ 2%. The temperature of the fibre could be measured to better than $\pm$ 4^{o}C.

The arrangement used to measure the viscosity of the glass fibres is shown schematically in figure 2.4. The viscosity/temperature relationship for fibres which show no time dependent viscous behaviour was established by measuring the rate of extension at several (typically 10) temperatures.

Time dependent viscous behaviour was studied by the continuous recording of fibre elongation at one temperature for periods of up to several days. Since thermal history effects the viscosity, a new fibre was used at each temperature except for the measurements to establish the critical temperature (the temperature at which time dependent behaviour ceases). For that measurement the procedure of Haller, Simmons and Napolitano (1971) was followed.

Haller, Simmons and Napolitano investigated nine

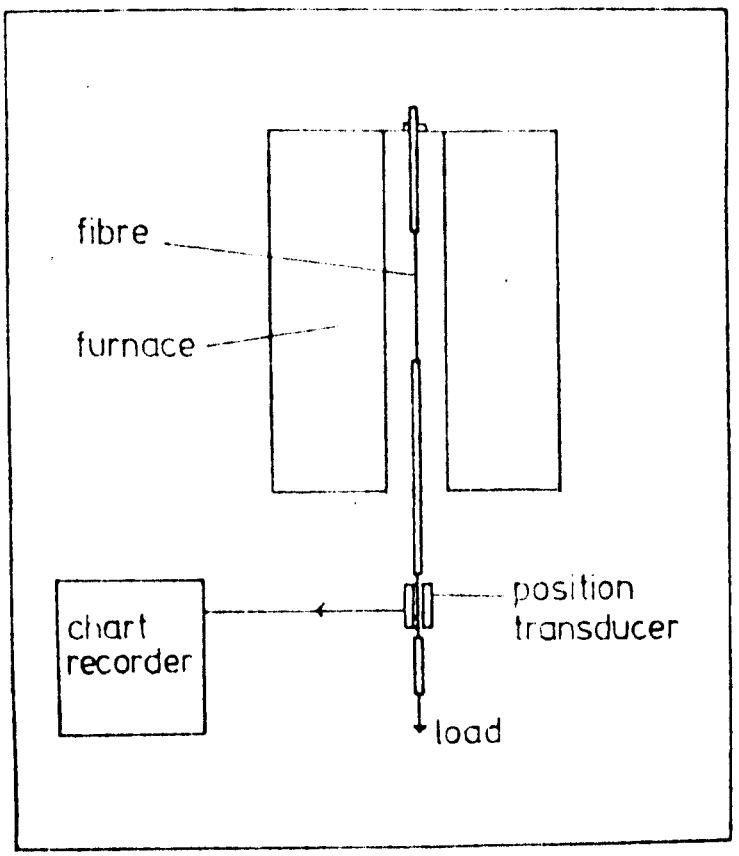

Figure 2.4 Schematic diagram of the fibre elongation apparatus used to measure the viscosity of glass

glasses some of which were known to phase separate, and found that there was a critical temperature below which drift in the viscosity did not occur. This temperature, which they found by progressively decreasing the temperature of the fibre and measuring the rate of extension, coincided with the temperature at which opalescence occurs. For the viscosity drift measurements, the viscometer was preheated to the required temperature and then the fibre was inserted into it. This caused the furnace temperature to change, and it required approximately 4 minutes to be reestablished. For this reason, it was not possible to measure the viscosity of the glass for very short times.

To identify any stress dependent behaviour two loads were used ($2 \times 10^{4} Nm^{-2}$ and $2 \times 10^{5} Nm^{-2}$) for some of the measurements. Delayed elastic effects were investigated by increasing the load after significant drift had occured.

2.7 The cooling rate of thick glass fibres

2.7.1 Introduction

For spinodal decomposition during continuous cooling, Husten, Cahn and Hilliard (1966) have shown that the cooling rate can affect the scale of the phase microstructure (section 1.2). If the separation proceeds by the nucleation and growth of a second phase, then this too will be dependent on the cooling rate since this limits the time available for the process to occur. The glasses produced for this investigation have a thermal history of continuous cooling and it was clearly important to establish the rate of this.

There have been three previous estimates of the cooling rate of glass fibres. Anderson (1958) and Glicksman (1968) made theoretical estimates and Arridge and Prior (1964) made experimental measurements of it. Anderson's theoretical estimates for thin fibres (10 to 50 μm diameter) predicted times of the order of milliseconds for cooling from 1,700°C to nearly room temperature, but Arridge and Prior measured rates some 30 times slower than this. Glicksman modified Anderson's theory and found much closer agreement with the experimental values but he (and Anderson) predicted that the cooling rate should be proportional to the drawing velocity disagreeing with the data of Arridge and Prior.

The purpose of the measurements presented here was to determine the cooling rate of thick glass fibres as a function of drawing velocity and fibre diameter.

An account of these measurements was published in Glass Technology 19, 5, (1978) and is included as Appendix 1.

2.7.2 Apparatus and Procedure

The technique used to measure the cooling rate of glass fibres was a modification of that used by Arridge and Prior (1964) which itself was a modification of an idea first suggested by Culpin and Madoc-Jones (1959). Arridge and Prior mounted a thermocouple near a heating element and used it as a null detector to determine the temperature gradient along a fibre drawn from a heat source at a steady rate.

In this investigation the thermocouple was heated directly with a Griffin-Telin hot stage microscope power supply. This provided a heating current at mains

frequency through a half wave silicon rectifier. During alternate half cycles, when the current was off, the thermocouple e.m.f.(via a phased synchronous chopper) could be measured.

A type K thermocouple (Chromel-Alumel) was used to obtain high temperature sensitivity. To obtain a symmetrical hot junction, differing gauge wires were used for the junction arms to compensate for the differing resistivities of the two alloys. The thermocouple output was measured across a 50k resistor with a digital multimeter

To obtain the steady state drawing conditions required for the measurements, a motor driven drum was mounted 1m above a furnace. The drum was marked around the circumference, so that its velocity could be determined with a stroboscopic lamp. Figure 2.5 is a schematic diagram of the apparatus, and figure 2.6 shows the temperature measuring circuit. Due to temperature limitations it was not possible to make these measurements using any of the glasses produced for this investigation. Instead a low melting temperature glass of the composition 53.5%SiO_2, 19%BaN, 8%NaO_2, 7.5%B_2O_3, 5%Al_2O_3, 3%CaO, 2%MgO and 2%ZnO was used. This composition has previously been exploited for commercial continuous filament production (Wolf(1961c)).

To start the drawing process, a wire was connected to the drum above the glass melt, and the free end dipped into the melt. When the wire was wetted it was pulled up by starting the motor driven drum This drew up a glass filament which then wound around the drum. When steady drawing conditions were

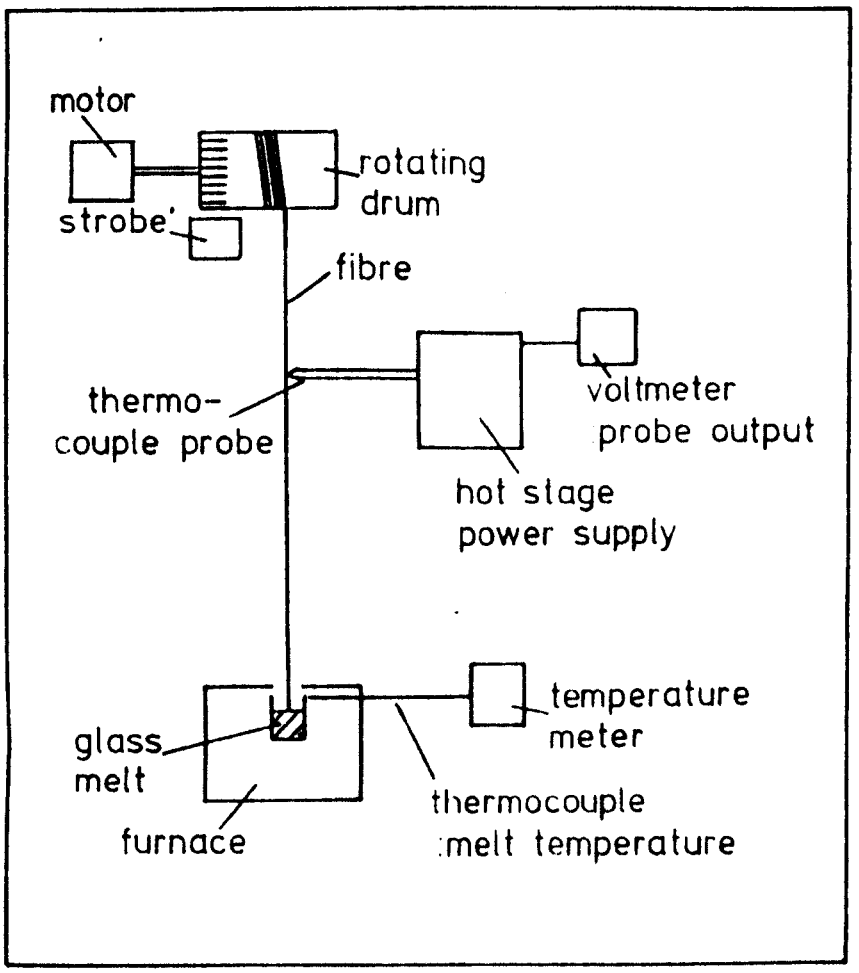

Figure 2.5 Schematic diagram of the apparatus used to determine the cooling rate of glass fibres

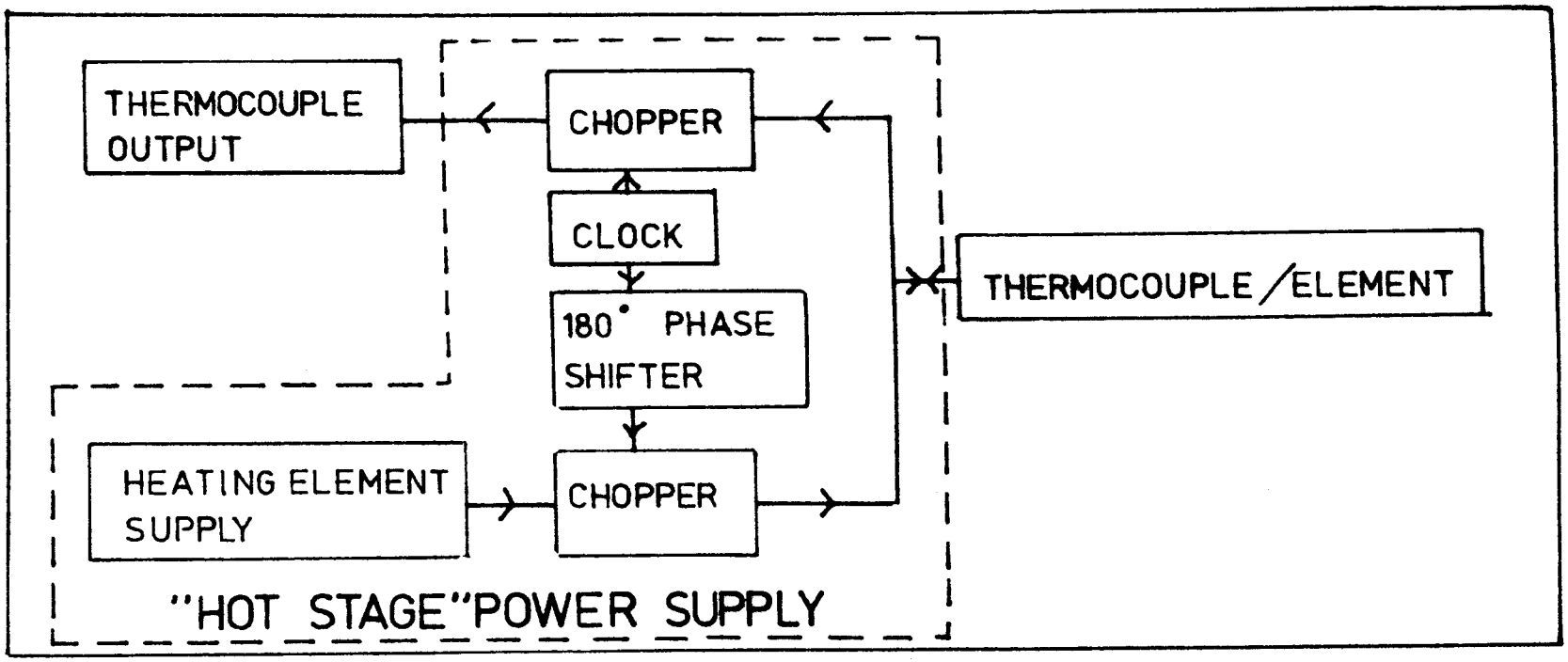

Figure 2.6 Schematic diagram of the temperature measuring circuit used to determine the cooling rate of glass fibres.

were attained, the heated thermocouple was touched onto the moving fibre. If the thermocouple was hotter than the fibre at the point of contact heat flowed from it to the fibre, if it was cooler then the heat flowed to it from the fibre. The change in temperature of the thermocouple was detected by the multimeter, and by moving the thermocouple up or down the wire, the position at which the two temperatures were identical could be established to within 1cm. The thermocouple temperature was then altered, and the process repeated several times to determine the temperature gradient along the fibre. These measurements were undertaken for two drawing velocities $1ms^{-1}$ and $1.5ms^{-1}$.

Measurements on cold running threads (of metal wire) indicated that the effect of frictional heating was negligible at the contact pressures applied.

CHAPTER 3

Experimental details of the leaching of the glasses and the characterisation of the porous products

3.1 Introduction

This chapter details the leaching procedure and the experimental techniques used to evaluate the leaching and to characterise the porous structures produced. Water displacement and weight loss measurements were made to determine the extent of the leaching. Quantitative measurements of the porous structures were made by gas adsorption and electron microscopy.

A detailed description of the gas adsorption apparatus, procedure and data analysis is presented as this was found to be a very sensitive technique to characterise porous glass. The sample preparation for microscopy and the analysis technique applied to the micrographs is also discussed.

3.2 The leaching of the glass

Hydrochloric acid solutions were employed for all the leaching operations. Sufficient acid solution was used to provide a volume ratio of acid to glass of at least 500 to 1. Freshly prepared solutions were used for each leaching operation and except for the operations to evaluate the effect of temperature, these were maintained at $(90\pm2)^{\circ}C$ under reflux conditions. To evaluate the effect of leachant temperature, three solution temperatures were used; these were $25^{\circ}C$, $60^{\circ}C$ and $90^{\circ}C$.

To establish the effect of acid concentration on the

leaching process, three solution concentrations were used. These were 30 v/v%, 18 v/v%, and 5 v/v% (i.e. 8.6N, 5.7N and 1.5N solutions respectively). As a strong acid solution was found desirable for the leaching of glass E-54, solutions of 30 v/v% were used for all other leaching operations.

During the leaching, the glass fibres were periodically removed, washed in running water for 4 hours and the extent of the leaching estimated by the measurement of the weight loss and the porous volume of the glass. These measurements indicated when a more quantitative measurement was required or when the leaching was complete.

The leaching operations were continued until either the fibres lost structural integrity or the weight loss measurements indicated that the leaching process was completed. Samples removed from the solutions for the weight loss and water displacement measurements were replaced in the solution after these measurements, as they had only undergone reversible drying. Samples removed for electron microscopy and gas adsorption measurements were not replaced as they were considered to have become contaminated as a consequence of the vacuum drying of the surface.

The leaching solutions were contained in Pyrex glass ware as this is known to be relatively inert to mineral acid solutions (Wolf (1961c)). Throughout the leaching processes and during the washing and subsequent drying operations, care was taken to avoid contamination of the leached glass. In particular, sources of organic materials e.g. plastics, were avoided and, as far as possible, the leached glass specimens were subjected to the characterisation techniques as soon as they were produced. Where a

delay was unavoidable, the glass was stored under doubly distilled water to minimise contamination from atmospherically borne materials (e.g. Hydrocarbons).

Some leaching operations were undertaken using leaching solutions saturated with ammonium chloride. Euguchi et al (1965) reported that the presence of these materials reduced the damage to the porous skeletons produced from the alkali-borosilicate glasses. The gas adsorption measurements indicated that these materials were not fully removed from the porous glass by the washing step and for that reason these materials were not included in the majority of the solutions. It was noted, however, that the presence of these materials had a favourable effect on the integrity of the porous skeletons produced.

After acid leaching, fibres of glass E-54 were further leached in an alkali solution of 1N sodium hydroxide. This was undertaken to investigate the presence of reaction precipitate in the pores of the glass. Such precipitate has been reported in leached alkali-borosilicate glasses and treatment of those glasses in alkaline solutions is known to remove it (Elmer and Nordberg (1970)).

In this investigation the effects of fibre cooling rate (i.e. fibre diameter) and fibre composition on the leaching process were evaluated, as well as the effects of the leaching conditions on several glass compositions.

3.3 Weight loss measurements and estimates of the porous volume

To determine the extent of the leaching, the glass was periodically removed from the leachant and weighed after drying the external surface. The glass was then dried at 80°C above cold silica gel, and reweighed. The chemical balance used to measure the weight of the glass (Oertling R20) had a resolution of 10μg. As the samples typically weighed 100mg, the exact weight could be determined to better than 0.1%. However, the amount of water present in the pores and on the surface of the glass, before and after drying, would be dependent on the efficiencies of the two drying steps. As these were not precisely controlled the accuracy of the weights probably varied by up to 10%.

The difference between the original sample weight and the weight of the dried (at 80°C) leached sample was due to the removal of the soluble component in the glass. This was used to determine the extent of the leaching. The difference between the weight of the superficially dried glass and the weight after drying at 80°C was due to water in the pores of the glass. This was used to estimate the porous volume of the glass. This volume was estimated by assuming the pore water had the density of bulk water ($1x10^{-3}Kg.m^{-3}$) and that the porous skeleton had the density of amorphous silica ($2.5x10^{-3}Kg.m^{-3}$). This estimate of the pore volume was relatively inaccurate and was used only to establish when a more quantitative measurement was required i.e. gas adsorption measurements.

3.4 Electron microscopy

3.4.1 Introduction

Both transmitted electron microscopy (T.E.M.) and scanning electron microscopy (S.E.M.) were used to characterise the porous glass. The T.E.M. equipment available had a theoretical resolution of 0.3nm, which exceeds the resolution of quantitative adsorption measurements.

S.E.M. was used to investigate the structure between 50nm and 1μm as this range is also beyond that for which gas adsorption measurements are suitable.

3.4.2 Sample preparation

Several preparation techniques for the production of T.E.M. samples were evaluated, these including chemical thinning, air abrading, ion beam machining and fragmentation. The fragmentation procedure outlined below was found to yield the most reproducible results and this was used to prepare all the samples for this investigation.

For T.E.M. the leached or partially leached glass fibres were ground with an agate mortar and pestle under 'Analar' chloroform. A dilute suspension of the fine particles from the porous glass was then prepared by the ultrasonic excitation of the ground powder in the

chloroform. The unleached glass remained as large particles compared to the brittle leached glass and so constituted only a fraction of the suspended particles. A drop of this suspension was then allowed to evaporate on the carbon film covering a microscope grid. The smallest particles adhered to the film and they were examined with J.E.M. 100c and J.E.M. 200 transmission electron microscopes.

Scanning electron microscopy specimens were prepared by attaching leached or partially leached fibres to microscope stubs with a proprietary silver suspension ('Silverdag'). These were then coated with evaporated films of carbon or gold. The silver suspension relies on the evaporation of an organic solvent (amyl acetate) to achieve solidification and this may have contaminated the surface of the glass. As S.E.M. was used only to investigate relatively coarse structure the effect of this contamination was not considered to be important.

3.4.3 Analysis of the micrographs

The interconnected microstructure of porous glass is the result of the interconnected phase microstructure of the parent glass. The phase microstructure may develop either by nucleation and growth (to intersection) or by spinodal decomposition. Classical morphological analysis techniques can characterise the microstructure of interconnected systems, but provides no representative length which has meaning in terms of spinodal decomposition. So that a length characteristic of spinodal decomposition (λ - the spinodal wavelength) could be obtained as well as a length characteristic of the actual morphology, lineal analysis was applied

to all of the micrographs, and to the computer simulated structures developed by Cahn (1967).

Lineal Analysis

This analytical technique assumes that the fractional length of a line, drawn on a micrograph, inside a particular phase is equal to the volume fraction of that phase i.e.

$$V_\alpha / V = \ell_\alpha / \ell \qquad 3.1$$

where V_α is the volume fraction of the α phase, V is the total volume, ℓ_α is the length of the line inside the α phase and ℓ is the length of the line.

Gladman (1963) has considered the statistical accuracy of equation 3.1, and has shown that the standard deviation (σ) of the volume fraction is approximated by

$$\sigma = V_\alpha (1-V_\alpha)(2/n)^{\frac{1}{2}} \qquad 3.2$$

where n is the number of phase boundaries traversed by the line.

In this investigation the statistical deviation in the analysis of the micrographs was maintained below 5% by ensuring that n was at least 200.

Lineal analysis can be extended to yield several characteristic lengths for the microstructure. The length adopted in this investigation was the average distance between phase boundaries ($\bar{r}$) and is defined by

$$\bar{r} = 1/(n-1) \qquad 3.3$$

This length has been used by several investigators (e.g. Mahoney et al (1974)) to characterise the interconnected microstructure of glass.

The practical accuracy of all microscopic techniques is dependent on the interaction between the preparation procedure and the sample morphology (e.g. sectioning errors) and on the resolution of the microscope. The latter results in diffuseness of the phase boundaries and dominates if the scale of the structure under investigation is similar to the resolution of the microscope. The volume attributable to the phase boundary is proportional to the ratio of the resolution to the average partical size (Pickering (1975)). This results in an error in $\bar{r}$ of the order of 25% for $\bar{r}$ 5nm with a resolution of 0.5nm.

As the mechanism of the decomposition is uncertain in the glass, to obtain a relationship between $\bar{r}$ and λ (the spinodal wavelength), equation 3.3 was applied to the numerical simulations of Cahn (1970) in which the spinodal wavelength is known exactly. It was found that at the 95% confidence level

$$\lambda/r = (1.15 \pm .08) \qquad 3.4$$

3.5 Gas adsorption

3.5.1 Introduction

Adsorption phenomena can be divided into two categories, chemical adsorption (chemisorption) or physical adsorption (Van der Waals adsorption). The dividing line between the two is not precise, but generally chemisorption involves valence bonding with

energies of usually greater than 5Kcal/mole and physical adsorption is a weak interaction of less than a few Kcals/mole. As physical adsorption is weak, it is reversible at the same temperature, and the adsorbate can be removed by evacuation.

At present, inert gas adsorption at low temperatures provides the best means of establishing the surface area of porous solids and once certain assumptions have been made as to the shape of the pores in a porous material it can provide detailed information as to the distribution of pores in the material.

In this section the gas adsorption measurements undertaken to characterise the leached glass are described and the theory of the pore size analysis of the data is presented.

3.5.2 Apparatus

Gas adsorption measurements were made using a low temperature gravimetric nitrogen adsorption/desorption apparatus constructed by C. Matthews (McMillan and Matthews (1976)) and improved by S.M. Tran (Tran (1976)). This apparatus is shown schematically in figure 3.1, and consists of a current balance, with a sensitivity of 5μg inside an evacuable glass container. The porous material (absorbent) was hung from one arm of the balance and counterbalanced with a non-porous solid (platinum wire). A removable heating cell was used to outgas the absorbent at a temperature of 200°C prior to the measurements. For the adsorption measurements the sample was cooled to 70K by immersing the sample limb in liquid nitrogen.

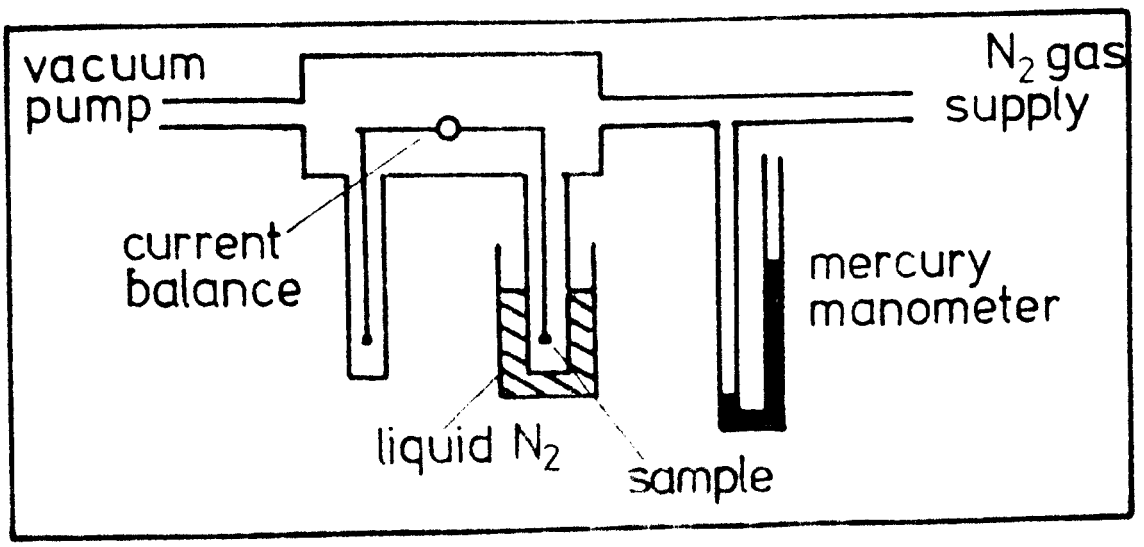

Figure 3.1 Schematic diagram of the gas adsorption /desorption apparatus

Industrial grade nitrogen was used as the adsorbate and water was removed from this with a nitrogen cold trap. The internal pressure (p) in the glass body, due to the presence of N_2 gas, was measured using a mercury barometer and a cathetometer. The external pressure (p_o-nitrogen saturation pressure) was measured with an aneroid barometer calibrated against a mercury barometer.

The glass body could be evacuated to better than 10^{-5} torr and was itself periodically outgassed at 200°C (about every five runs). High temperature vacuum grease (Apeizon T) was used for all the seals in the system to minimise the contamination of the adsorbate by organic vapours.

3.5.3 Procedure

Prior to making the adsorption measurements, the adsorbent was outgassed at 200°C and 10^{-5} torr for 16 hours. The adsorbent was then cooled to 77K by immersing the sample limb in liquid nitrogen. Nitrogen gas was then admitted into the system in steps of 10 torr. Once equilibrium was established, or after 20 minutes, the internal pressure (p) and external pressure (p_0) were recorded together with the new weight of the sample. When within a few torr of atmospheric pressure (p_0), adsorption measurements were ceased and desorption measurements started. For the desorption measurements, a mechanical vacuum pump was used to decrease the internal pressure in steps of 10 torr. These measurements were continued until the internal pressure was less than 1 torr.

Vapour phase adsorption techniques, like N_2

adsorption, ideally require an atomically clean surface, but to remove all hydroxyl groups from a silica surface requires thermal treatment in excess of 850°C (Young (1958)). Porous alkali-borosilicate glasses start to compact at temperatures below this (Nordberg (1944)) and preliminary measurements on leached E-54 glass indicated that this underwent similar shrinkage at such temperatures. The outgassing procedure adopted here (200°C for 16 hours) while satisfying the empirical equation for outgassing prior to making adsorption measurements, developed by Dalla Valle, Orr and Blocker (1959), can only remove physically adsorbed water. It has however been used successfully to characterise silicates by several investigators (e.g. Haller (1965), Huang, Demirel and McGee (1972) and Cranston and Inkley (1959)). More importantly, it does not induce any measurable compaction of the skeleton.

3.5.4 Data analysis

Surface area measurements

The surface of an adsorbent can be estimated from gas adsorption data, using an expression originally developed by Langmuir (1915) and later, generalised by Brunauer, Emmett and Teller (1938) in a unified theory of physical adsorption phenomena known as B.E.T. theory.

Langmuir considered monomolecular adsorption phenomena and proposed that the equilibrium amount of adsorption would occur when the rate of adsorption of the monolayer was equal to the rate of desorption from the monolayer. If the fraction of the adsorbent surface

covered is θ, then the rate of desorption (R(des)) will be proportional to this i.e.

$$R(des) = K'\theta \qquad 3.5$$

The rate of adsorption (R(ads)) will be proportional to the uncovered area $(1-\theta)$ and the rate at which molecules are hitting the surface and adhering to it. If the rate at which the adsorbate is hitting the surface is u, and the fraction staying on the surface for some finite time (i.e. adsorbing) is α, then

$$R(ads) = (1-\theta)\, u\alpha \qquad 3.6$$

At equilibrium R(des)=R(ads) i.e.

$$K'\theta = (1-\theta)\, u\alpha \qquad 3.7$$

therefore

$$\theta = 1/(1+k'/u\alpha) \qquad 3.8$$

The rate of arrival of molecules will be proportional to the pressure of adsorbing gas (p), i.e.

$$u = k''p \qquad 3.9$$

so

$$\theta = kp/(1+kp) \text{ where } k = \frac{k''\alpha}{k'} \qquad 3.10$$

If Vm is the volume of a monolayer and V is the volume adsorbed at pressure p then from equation 3.10

$$V = Vmkp/(1+kp) \qquad 3.11$$

this can be written in linear form

$$p/V = 1/(Vmk) + p/Vm \qquad 3.12$$

from which it is clear that a plot of p/V vs. p will have a gradient of 1/Vm.

The surface area of the adsorbent can then be calculated providing that the area occupied by 1 molecule (a) is known, i.e.

$$s = VmaN/M \qquad 3.13$$

where N is Avogadro's number and M is the molar volume of the adsorbate.

After an extensive survey of adsorption data, Joy (1953) recommended a best value of the area occupied by 1 nitrogen molecule of $(15.8 \pm 0.4)\ \text{Å}^2$.

Monomolecular adsorption is only one of the five common adsorption processes, the other four concern multimolecular adsorption. The five common adsorption isotherms (plots of volume adsorbed vs. relative pressure) are shown in figure 3.2 and are classified following Brunauer et al (1940). Brunauer, Emmett and Teller (1938) extended Langmuir's concept to describe all five types by assuming that at equilibrium, the rate of evaporation from the n^{th} layer was equal to rate of condensation of the (n-1)th layer. They derived the B.E.T. equation

$$V = VmCp/((po-p)(1+(C-1)p/po)) \qquad 3.14$$

where C is a constant and is approximated by

$$\exp \frac{(E_1 - E_2)}{RT} \qquad 3.15$$

E_1 is the heat of adsorption of the gas forming

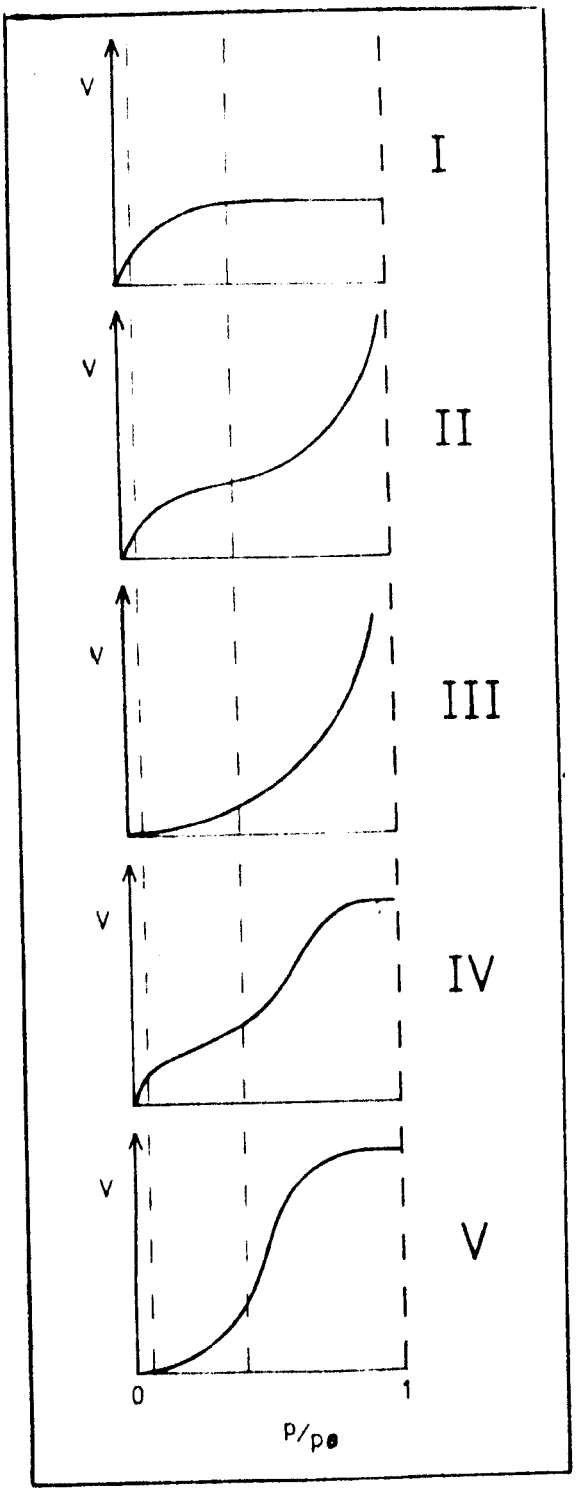

Figure 3.2 The five common adsorption isotherms classified following Brunauer et al (1940). Relative pressures of 0.05 and 0.35 are indicated

a monolayer, E_L is the heat of liquifaction of the gas (i.e. the heat of adsorption of subsequent layers) and R,T are the gas constant and absolute temperature, respectively.

Equation 3.14 can be used to describe all five isotherms and qualitatively the B.E.T. explanations are:

Type 1: Monomolecular adsorption,

" 11: Multimolecular adsorption where $E_1 > E_L$ (i.e.C is large). The adsorbent-adsorbate interaction is stronger than the adsorbate-adsorbate interaction,

" 111: Multimolecular adsoption where $E_1 < E_L$ (i.e. C is small),

" 1V: As type 11, but with a finite number of layers possible because of the geometry of the adsorbent,

" V: As type 111, but with a finite number of layers possible.

The B.E.T. equation can be written in linear form i.e.

$$p/(V(p_o-p))=1/VmC + (C-1)p/(VmCp_o) \qquad 3.16$$

From which it is clear that a plot of $p/(V(p_o-p))$ vs. p/p_o will have a slope of (C-1)/VmC and an intercept on the ordinate axis at 1/VmC. From such a plot Vm and C can be calculated and then the surface area estimated using equation 3.13.

In practice, C is very small for nitrogen and, providing only data for relative pressures between .05 and .35 are used, the similarity of the five.

isotherms over this region (figure 3.2) allows the surface area to be estimated from equations 3.12 and 3.13. This procedure was adopted for the surface areas measured ~~for the surface areas measured~~ in this investigation.

Average pore size

For a porous adsorbent, the number of molecular layers possible is limited, which gives rise to the saturation effects in the Type 1V and V isotherms. For such adsorbents it is possible, therefore, to determine the porous volume directly from the isotherm.

As the surface area and pore volume are related by the geometry of the pores, once a particular model of the pore geometry is adopted the average pore size can be estimated. The simplest model applicable to porous glass is that of uniform non-intersecting cylindrical pores. The surface area (A) and the pore volume of such pores are related by

$$A = 2\pi rL \qquad 3.17$$

and

$$V = \pi r^2 L \qquad 3.18$$

i.e.

$$r = 2V/A \qquad 3.19$$

where r is the average pore size (radius) and L is the total length of the pores

A more realistic model is that of uniform intersecting pores which modifies equation 3.19 to

$$r = (5d / (5d + 3r)).(2V / A) \qquad 3.20$$

where d is the the distance between the pores. For a 50:50 volume fraction $d \simeq 2r$ so equation 3.20 reduces to

$$r = (.8)\ 2V/A \qquad 3.21$$

The accuracy of the pore size estimated by this treatment of gas adsorption data is difficult to estimate because of the many assumptions made, but for monomodel pore distributions Everett (1958) has concluded that the estimate is unlikely to be in error by more than 10%.

Pore size distribution

Types 1V and V isotherms contain information on the pore size distribution of the adsorbent and in theory, this can be extracted from either the adsorption or desorption isotherm. In practice, however, the desorption branch is almost universally used for this (Orr (1977)).

Figure 3.3 shows the adsorption and desorption isotherms for one of the porous glasses evaluated. The isotherms are both of the Type 1V and are not co-linear because of the effective lowering of the vapour pressure during the desorption measurements caused by the presence of a meniscus in the pores. During adsorption, a meniscus does not form until the adsorption process in a pore is complete, and no longer taking part in the adsorption process. During desorption, however, the meniscus is initially present and this causes the liquid below it to be stable to

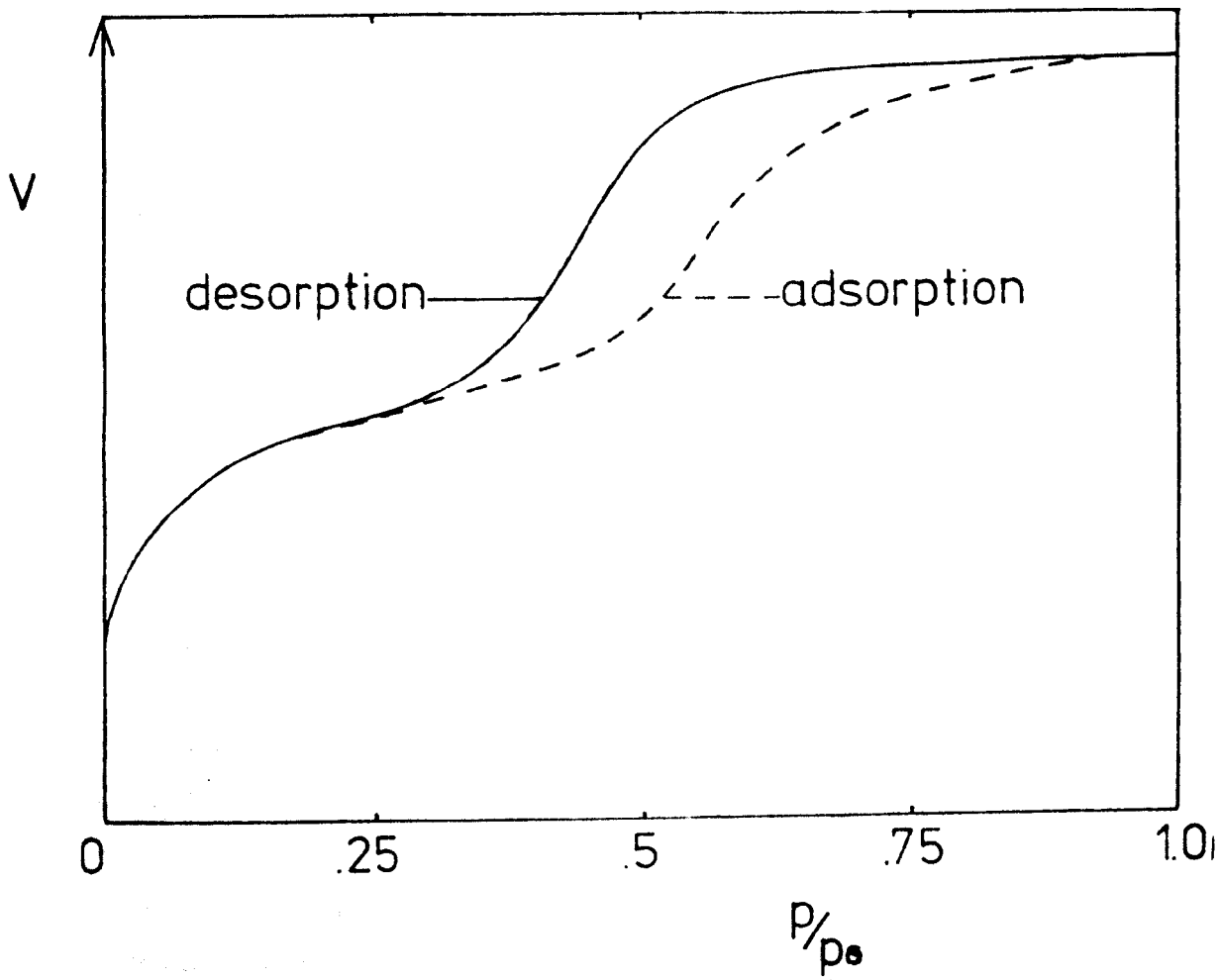

Figure 3.3 Adsoption and desorption isotherms for one of the porous glasses evaluated (E-54)

pressures lower than described by the B.E.T. theory.

The relative pressure around a spherical droplet is described by the Kelvin equation (Thompson (1871))

$$\ln (p/p_o) = 2V\gamma/rRT \qquad 3.22$$

where V is the molar volume of the liquid, γ is its surface tension and r is the radius of the droplet. For a concave meniscus in a cylindrical capillary, the Kelvin equation can be written as

$$\ln(p/p_o) = -2V\gamma\cos\theta/rRT \qquad 3.23$$

where r is now the radius of curvature of the meniscus and θ is the contact angle.

The Kelvin equation can, therefore, be used to determine the pore size distribution in the porous adsorbent by modelling the pores on cylinders. At any pressure there exists a critical meniscus radius (rc) which defines the limit of filled pores and this is given by the Kelvin equation. As the surface of the adsorbent will also be coated with a blanket of adsorbate of thickness t, the critical meniscus radius corresponds to a critical pore radius (R_c) given by

$$R_c = r_c + t \qquad 3.24$$

This is illustrated in figure 3.4.

Using the Kelvin equation (equation 3.23)

$$R_c = ((2v\gamma\cos\theta)/RT\ln(p_o/p)) + t \qquad 3.25$$

From figure 3.4, the contact angle can be seen to refer to the angle between the liquid adsorbate in the pore and the equilibrium adsorbate on the surface of the adsorbent. It is reasonable, therefore, to assume that this is very close to 90° (i.e. complete wetting). Equation 3.25 can then be simplified to

$$R_c = ((2V\gamma)/(RT\ln(p_o/p))) + t \qquad 3.26$$

The Kelvin equation was derived from thermodynamic arguments, and so can only be applied unambiguously to macroscopic systems. The bulk surface tension and bulk density of the adsorbate liquid can, therefore, be used in equation 3.26 without any further loss in generality. Equation 3.26 can now be written in a form suitable for gas adsorption pore size measurements.

$$R_c = ((2\gamma M)/(RT\rho \ln(P_s/p))) + t \qquad 3.27$$

where ρ is the bulk density, γ is the surface tension and M the molecular weight of the adsorbate liquid.

The thickness of the adsorbed layer (t) with relative pressure could be obtained from the adsorption isotherm, but it is more usually estimated from adsorption measurements on non-porous solids. The thickness has been evaluated by many investigators (e.g. Blachere(1974) and Cranston and Inkley (1959)). Figure 3.5 is taken from Cranston and Inkley (1959) and is a compilation of the results of several investigations.

In a material having cylindrical pores all of one

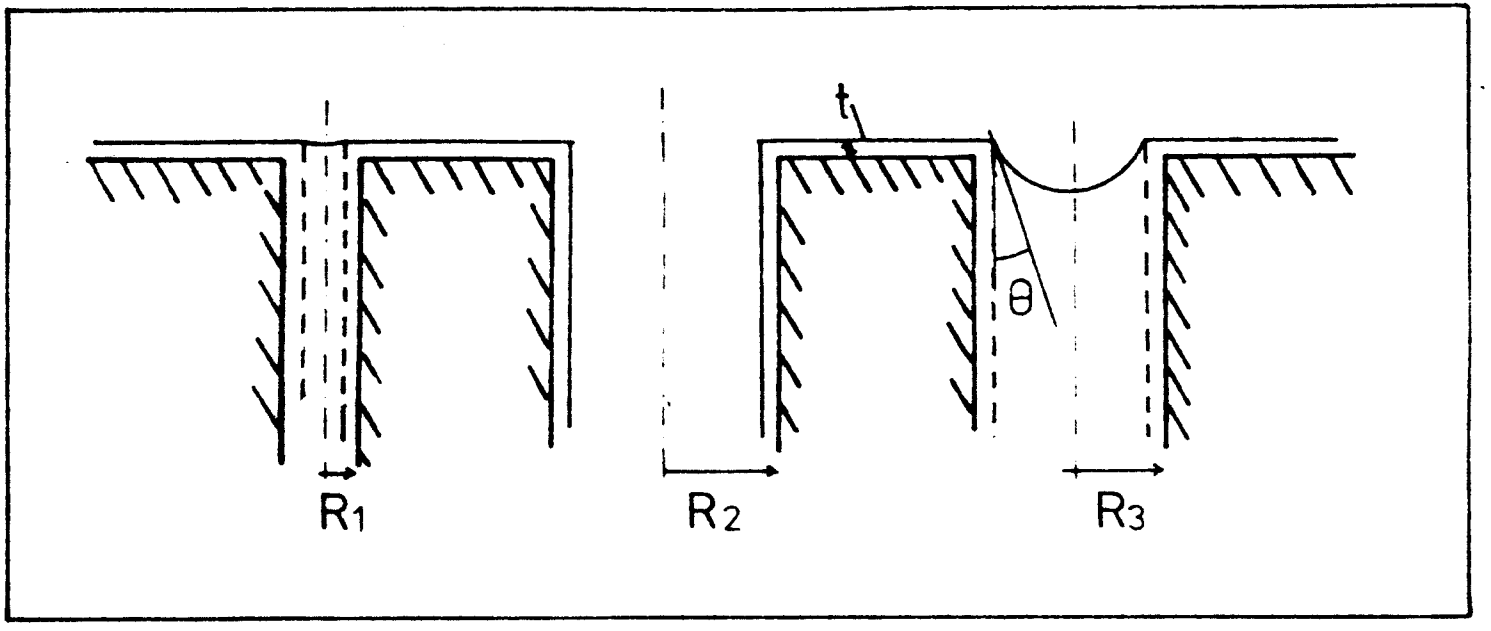

Figure 3.4 Schematic diagram of adsorption in a porous material. The pore on the L.H.S. is filled (as $R_1 < R_c$), the central pore is empty (as $R_2 = R_c$), the pore on the R.H.S. is of the critical radius ($R_3 > R_c$)

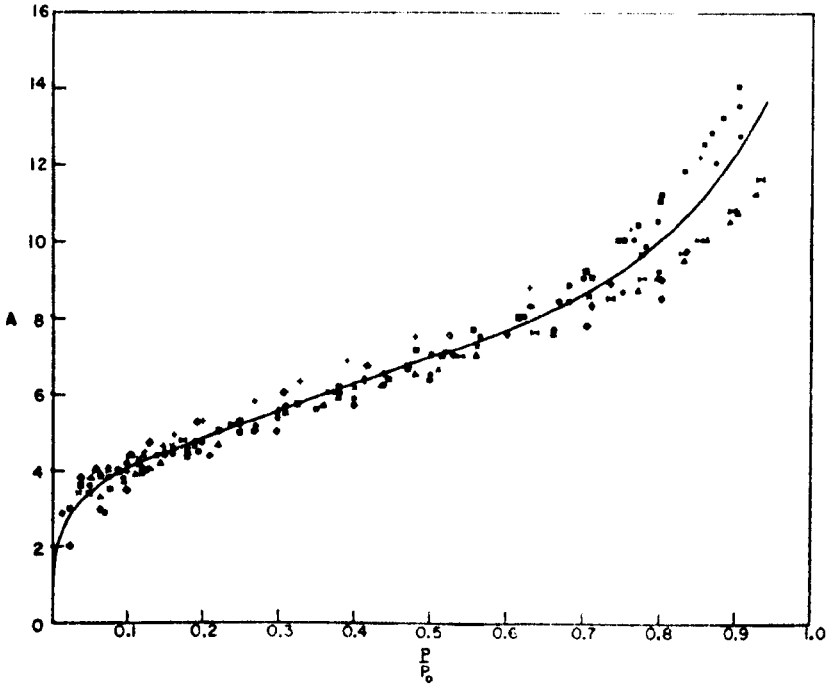

FIG. 1. Graph of thickness of adsorbed layer vs. relative pressure for several nonporous materials. ⊙, precipitated silver (*6*); △, 200-mesh glass spheres (*7*); ×, tungsten powder (*8*); ⊡, zinc oxide (*9*); ◇, 7-μ glass spheres (*10*); +, glass spheres. Average 3 μ (*11*); ⊗, zinc oxide. Sample K1602 (*12*); ◆, zinc oxide. Sample F1601 (*12*); ⊞, zinc oxide. Sample G1603 (*12*); ◊, zinc oxide. Sample KH1604 (*12*); ○, $ZrSiO_4$ [2.76 sq.m./g.] (*13*); ▷◁, $BaSO_4$ [4.30 sq m./g.] (*13*); ▲, TiO_2 [9.88 sq.m./g.] (*13*); ■, TiO_2 [13.90 sq.m./g.] (*14*); ●, TiO_2 surface treated [9.60 sq.m./g.] (*14*).

Figure 3.5 The thickness of the adsorbed gas as a function of relative pressure.(after Cranston and Inkley (1959)

6 Harris,E.L. and Emmett,P.H. (1949). J.Phys.& Colloid Chem. 53,819, fig. 5.

7 Davis,R.T.,DeWitt,T.W. and Emmett,P.H. (1947). J.Phys. & Colloid Chem. 51,1238, fig. 3.

8 Davis,R.T.,DeWitt,T.W. and Emmett,P.H. (1947). J.Phys. & Colloid Chem. 51,1241, fig. 4.

9 Davis,R.T.,DeWitt,T.W. and Emmett,P.H. (1947). J.Phys. & Colloid Chem. 51,1241, fig. 6.

10 Davis,R.T.,DeWitt,T.W. and Emmett,P.H. (1947). J.Phys. & Colloid Chem. 51,1241, fig. 4.

11 Davis,R.T. and DeWitt,T.W. (1948). J.Am.Chem.Soc. 70, 1138, fig.1.

12 Emmett,P.H. and DeWitt,T.W. (1941). Ind.Eng.Chem.Anal.Ed. 13,31, fig.4.

13 Emmett,P.H. and DeWitt,T.W. (1941). Ind.Eng.Chem.Anal.Ed. 13,30, fig.3.

14 Harkins,W.D. and Jura,G.J. (1944). J.AM.Chem.Soc. 66, 1367, fig.2.

radius the total pore volume is

$$\pi r^2 L \qquad 3.28$$

Where L is the total pore length. The desorption isotherm of such a material would be as shown in figure 3.6. In a real porous material there will be a range of pore radii and a corresponding distribution in pore length (L(r)). The total pore volume will then be

$$\pi \int_0^\infty rL(r).dr \qquad 3.29$$

At any pressure below p_o the volume of pores filled will be

$$\pi \int_{R_c}^\infty (Rc-t)L(r).dr \qquad 3.30$$

where R_c is given by the Kelvin equation.

As the Kelvin equation is the result of a thermodynamic analysis its validity is questionable for microscopic systems. This places a limit on the pore sizes which can be characterised by the above analysis. Several investigators have applied similar analysis to pores of less than 1 nm (Barrett, Joyner and Halenda (1951)), but others have questioned the accuracy of the results (Spencer and Fereday (1968)). It is more general practice to restrict the analysis to pores of more than 2nm and this limit was adopted here. Before discussing the method by which equation 3.30 was solved in this investigation, it must be pointed out that there is one other possible cause of hysteresis in the isotherms (figure 3.3). If the pores have a narrow entry neck (illustrated in figure 3.7) then

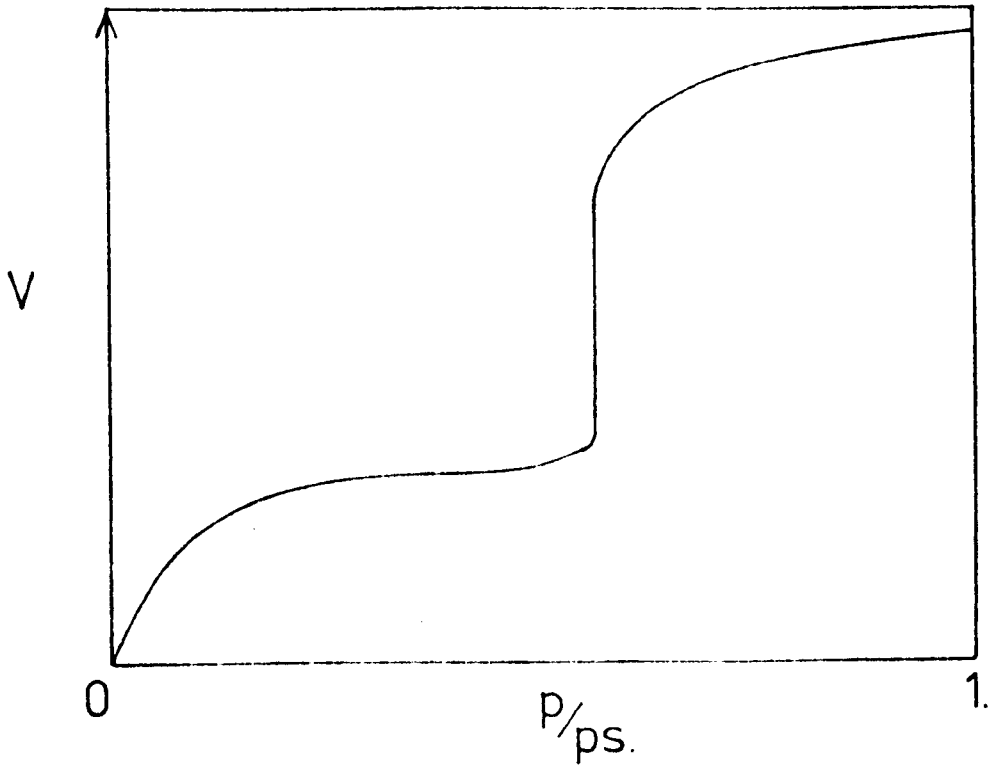

Figure 3.6 The desorption isotherm of a porous material having pores of one radius only

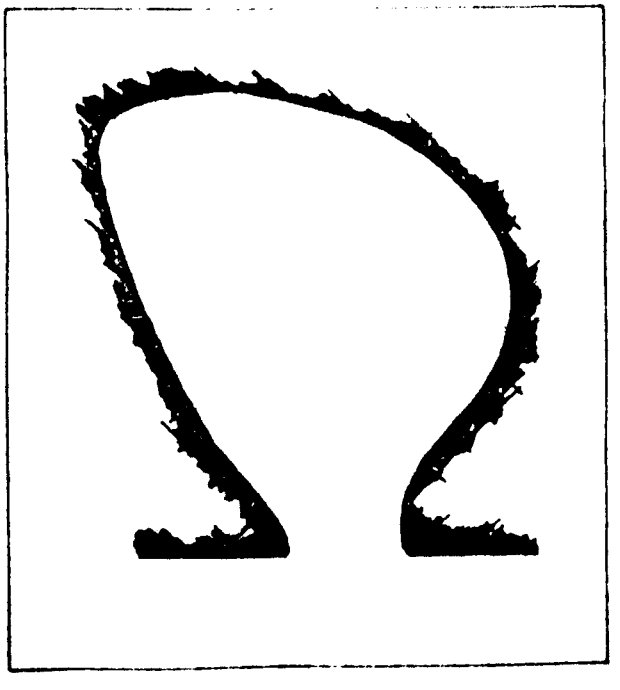

Figure 3.7 An 'ink bottle' pore. Such pores represent one other possible cause of hysteresis in the adsorption/desorption isotherms

the evaporation of the liquid from the bulk of the pore is controlled by the radius of the pore neck. There is little evidence for the presence of such pores in leached glass and the presence of such pores was neglected in the analysis of the gas adsorption data obtained in this investigation.

Numerical solution of the pore size distribution

As the form of the pore size distribution (L(r) in equation 3.30) was unknown, a numerical method of solving equation 3.30 was adopted here. The procedure employed was based on the modified Pierce analysis described by Orr and Dalla-Valle (1959). The solution described by Orr and Dalla-Valle used an arithmetic expression to determine the thickness of the adsorbed layer t. They used the Halsey equation for this (Halsey (1948)).

$$t=4.3\left(\frac{-5}{\ln(p/p_o)}\right)^{1/3} \qquad 3.31$$

The form of this equation is shown in figure 3.8 together with the experimental t measurements compiled by Cranston and Inkley (1959). Also shown in figure 3.8 is the form of the phenomenological equation developed by Hauser (1940) which shows far better agreement with the experimental data. For that reason, the Hauser equation

$$t=3.54\left(\frac{-5}{\ln(p/p_o)}\right)^{1/3} \qquad 3.32$$

was used instead of the Halsey equation in the 'modified Pierce analysis'.

In the Pierce analysis, the volume change of the

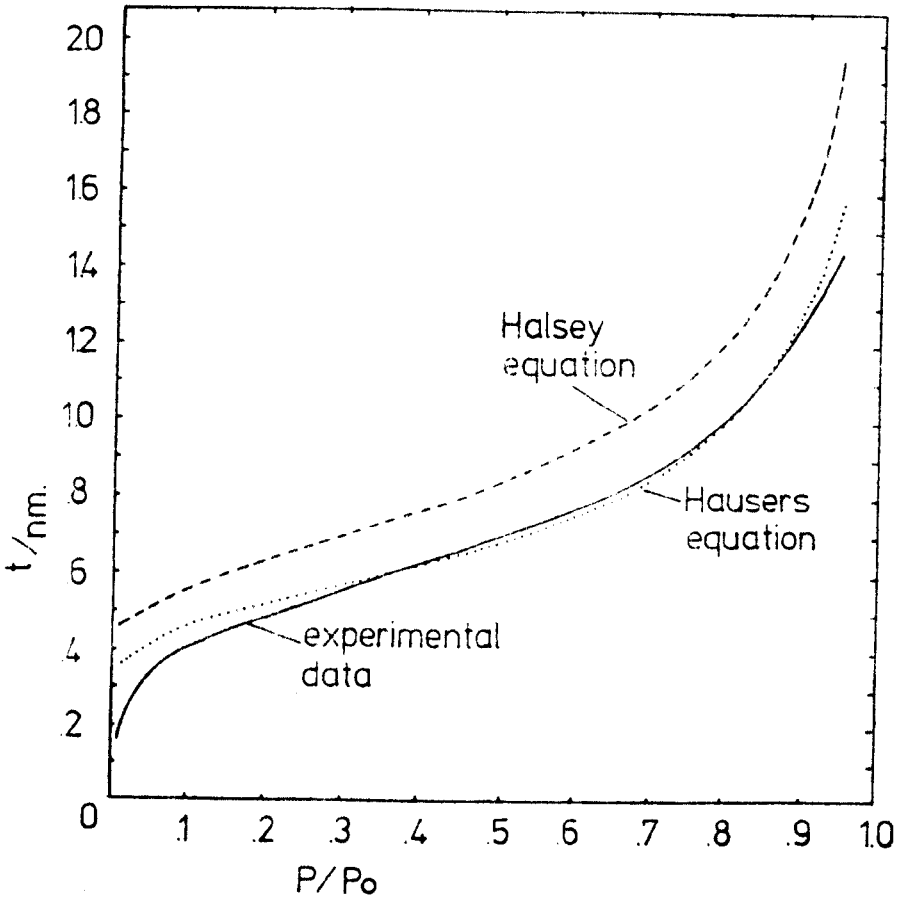

Figure 3.8 Halsey's and Hauser's equations describing the thickness of the adsorbed layer as a function of relative pressure. The experimentally derived curve of Cranston and Inkley is also shown

adsorbent is considered to be due to two distinct sources. These are surface desorption and evaporation from the pores. The amount desorbed from the surface can be calculated from Hausers equation (equation 3.32) and knowledge of the surface area from which it leaves ie

$$\Delta V_t = \Delta t A \qquad 3.33$$

where ΔV_t is the volume desorbed from the surface, Δt is the change in the equilibrium thickness of the adsorbed layer and A is the surface area available for the desorption. Near a relative pressure of 1, A is virtually zero and increases as liquid evaporates from the largest pores.

The remaining volume (ΔVp) is due to evaporation from the pores, the radii of which are given by equation 3.27. The length of the pores can therefore be calculated (assuming cylindrical pores) and the new area revealed, calculated and added to the previous area for the calculation of the following desorption decrement.

The length of the pores as a function of pore radius is thus obtained from the desorption isotherm. In this investigation, the pore volume as a function of pore radius is used to characterise the pore size distribution. There are two reasons for this, firstly, the pore lengths obtained from microporous materials are extremely large (e.g. 10^6 m/g) and are consequently difficult to visualise. Secondly, the contribution of very small pores (< 2.0nm radius) is small in terms of volume, but significant in terms of length.

As a gravimetric technique was used in this investigation, the volume of adsorbate liberated

at each decrement was calculated from the weight change of the sample.

The numerical analysis was performed on a Burroughs 6700 computer using a program written by S.M. Tran. The program, which provided a graphical pore size distribution is included as Appendix 3. This particular analysis was found to be extremely sensitive to scatter in the data, and it was found necessary to first plot the data, as a desorption isotherm, and then pick new data from the smooth curve fitted to the experimental data.

CHAPTER 4

The results of the measurements on the parent glass

4.1 Introduction

The critical opalescence measurements determined the critical temperatures for three of the glasses under investigation. For one of these glasses this critical temperature was also confirmed by the measurement of viscosity drift. The other glasses did not show viscosity drift or opalescence and so the critical temperatures could not be established by these techniques.

The resistivity measurements, however, revealed a transition by all of the glasses evaluated. In the one glass for which opalescence and resistivity measurements were both made, the electrical transition temperature was close to the critical temperature as determined by opalescence. Because of this, and as the likely conduction mechanism would be extremely sensitive to the onset of phase separation, the electrical transitions are tentatively assumed to define the metastability limit.

The cooling rate measurements indicate that the rate of heat transfer from the surface of the fibres controls the quench rate, and because of this the measured rate can be extrapolated to higher temperatures.

These data are given in this chapter, together with a preliminary discussion of results. A more complete discussion of the results is deferred until the data concerning the porous glass have been presented.

4.1 Results of the critical opalescence measurements

Opalescence could be induced only in glasses E-65, E-67 and E-70. The critical temperatures for these glass were determined to be $(905 \pm 10)^{o}C$ for E-70 and $(885 \pm 10)^{o}C$ for E-67 and $(895 \pm 10)^{o}C$ for E-65.

4.2 Results of the d.c. resistivity measurements

As all of the glasses for which resistivity measurements were made exhibited polarisation, the conductivity mechanism is largely ionic. The glasses were all found to have the high resistivity characteristic of alkali free glasses and in table 4.1 the measured specific resistivities at $1000^{o}C$ are compared to that of silica at the same temperature.

The results of the resistivity measurements are shown in figures 4.1a, 4.2a, 4.3a, 4.4a, 4.5a and 4.6a as plots of the logarithm of specific resistance vs. reciprocal absolute temperature. These sets of data could be more accurately fitted to two straight lines than to one, and the two line fits are shown in figures 4.1 to 4.6. Two measures of the 'goodness' of fit' of data to a given equation are the standard deviation and the randomness of departures. The randomness of departures is illustrated in figures 4.1b to 4.6b for the two line fit. In figure 4.7 as an example of the non-random scatter to one line, the departures from a single line fit to the data for glass E-60 are shown. In table 4.2 the standard deviations of the data from a single line fit and a two line fit are compared for all of the glasses evaluated. It is clear from this that the fit to two lines is between

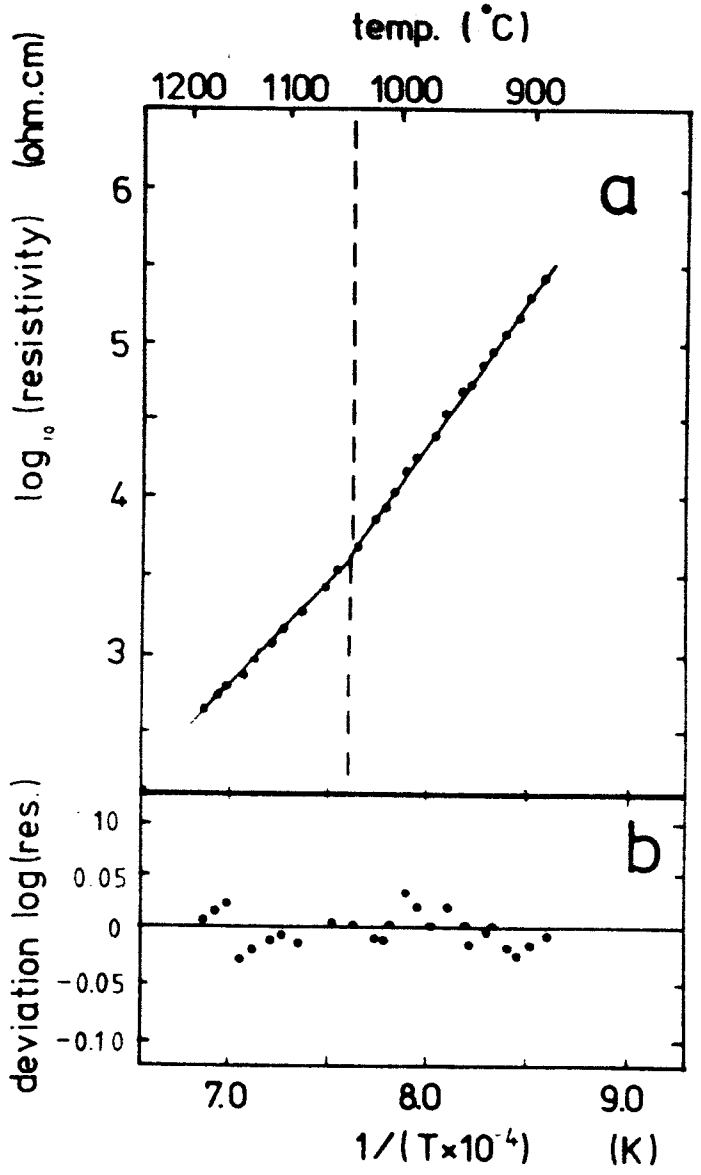

Figure 4.3 The resistivity as a function of temperature for glass E-54 (a). The deviations from the two line fit to the data (b)

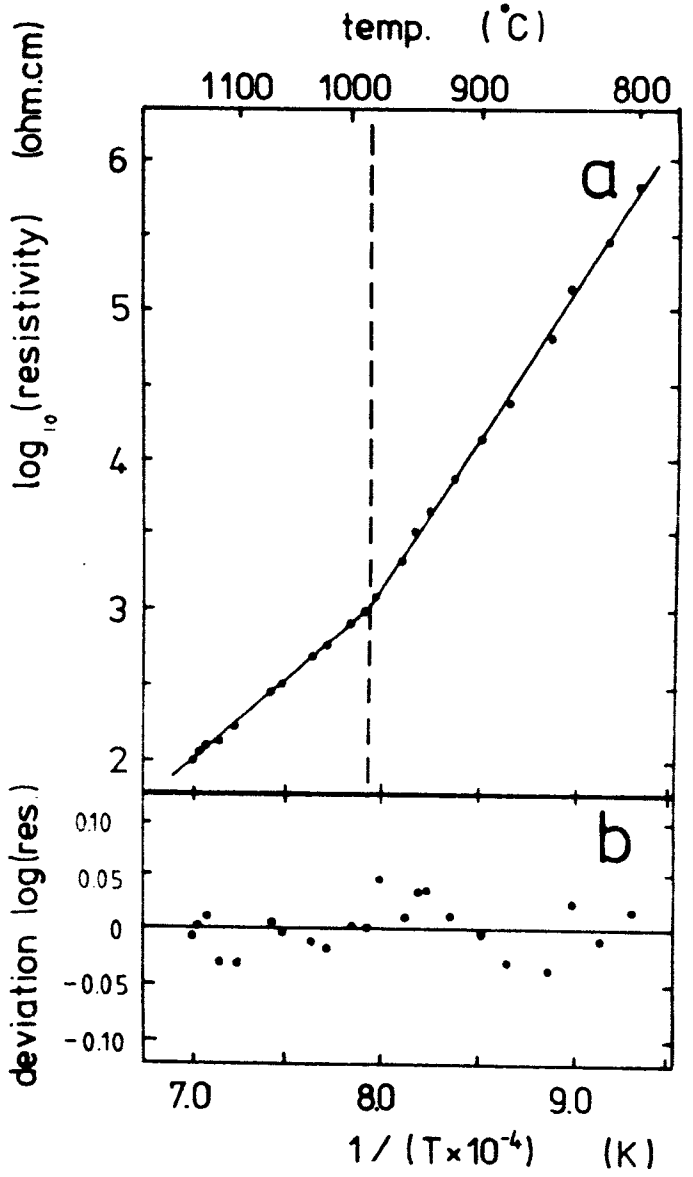

Figure 4.4 The resistivity as a function of temperature for glass E-45 (a). The deviations from the two line data fit (b)

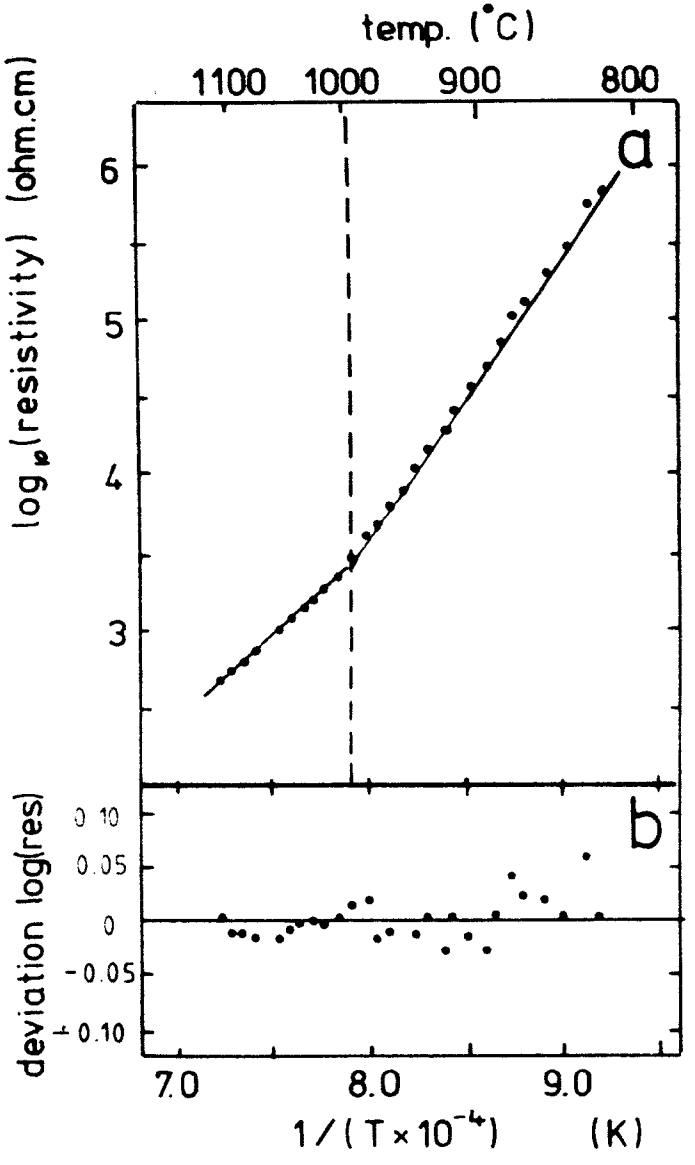

Figure 4.5 The resistivity as a function of temperature for glass E-40 (a). The deviations from the two line fit to the data (b)

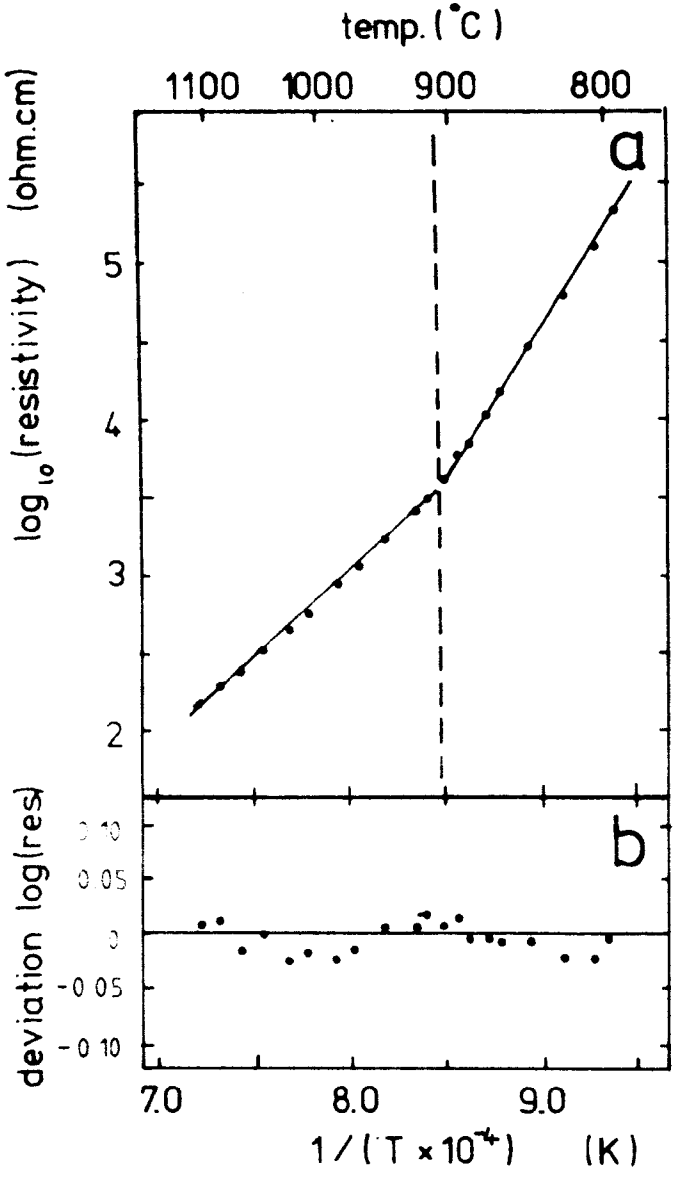

Figure 4.6 The resistivity as a function of temperature for glass E-30(a). The deviations from the two line fit to the data (b)

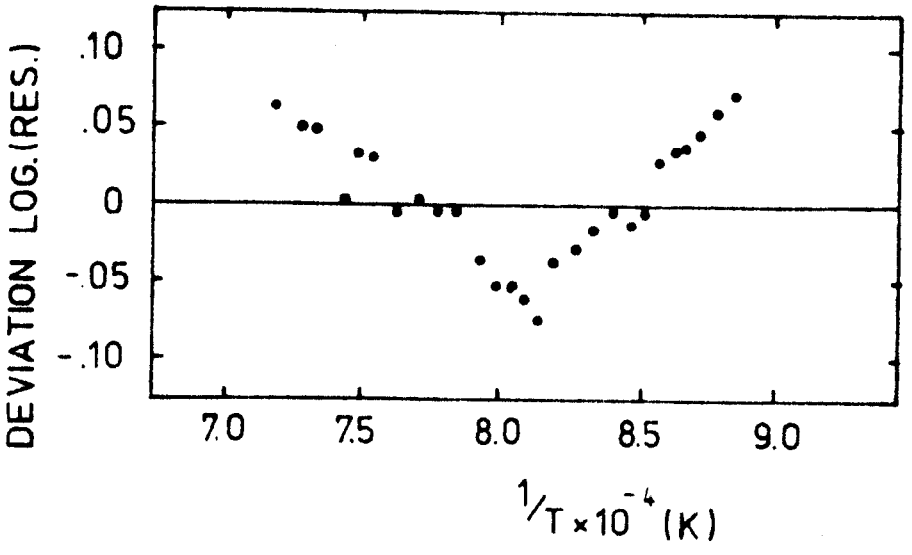

Figure 4.7 The deviations from the single line fit to the resistivity data of glass E-60

Table 4.1 The resistivities of the glasses at 1000°C

GLASS	CONDUCTIVITY AT 1000°C OHM.CM
Silica*	300.0×10^3
E-20	1.0×10^3
E-40	2.5×10^3
E-45	0.8×10^3
E-54	12.0×10^3
E-60	5.7×10^3
E-65	3.1×10^3

*Velti (1963)

Table 4.2 The standard deviations of the conductivity data fit to a straight line, and to two straight lines

GLASS	STANDARD DEVIATIONS (%)	
	1 line	2 lines
E-30	30.0	6.4
E-40	20.2	9.5
E-45	32.8	10.7
E-54	17.0	8.4
E-60	12.1	6.8
E-65	18.2	9.4

2 and 4 times more accurate than the fit to a single line in all cases, and that the departure from a single straight line is least for glass E-60.

While it is, of course, possible to fit n data points perfectly to n-1 straight line sections, the division of the data shown in figures 4.1 to 4.6 separates the data into groups of at least 10 points. As this division results in a much improved fit, it indicates that two Arrhenius type expressions are required to describe the conductivity of each glass over the temperature region measured.

In table 4.3 the activation energies of the conduction mechanisms over each of the two regions are shown together with the temperature at which the transition occurs.

4.3 Results of the viscosity measurements .

Of the glasses evaluated, only glass E-70 exhibited a time dependent viscosity region. For glass E-70 above the time dependent region, and for all of the other glasses investigated, the results of the viscosity measurements are shown as plots of the logarithm of viscosity against reciprocal temperature in figure 4.8. The best straight line fit to the data for each glass is also shown in figure 4.8. The straight line fits to the viscosity data were good (less than 5% error at 95% confidence level) for all glasses except E-70 for which there were few data points recorded, and E-54. E-54 showed evidence of curvature on the $\log \eta$ vs $1/T$ plot, and because of this the straight line fit had an error of 8%. Departure from linearity is common for multicomponent glasses and has been attributed to

Table 4.3 The activation energies of conduction

GLASS	ACT.ENERGY/ev (ABOVE INFLECT'N)	ACT.ENERGY/ev (BELOW INFLECT'N)	INFLECTION TEMP^{o}C
E-30	2.24±0.06	3.8 ±0.1	910±10
E-40	2.6 ±0.1	3.7 ±0.1	990±10
E-45	2.2 ±0.1	3.75±0.1	985±10
E-54	2.59±0.08	3.42±0.08	1040±10
E-60	2.3 ±0.1	2.76±0.04	960±10
E-65	2.6 ±0.1	1.77±0.06	910±10

(Accuracies stated are to the 95% confidence level)

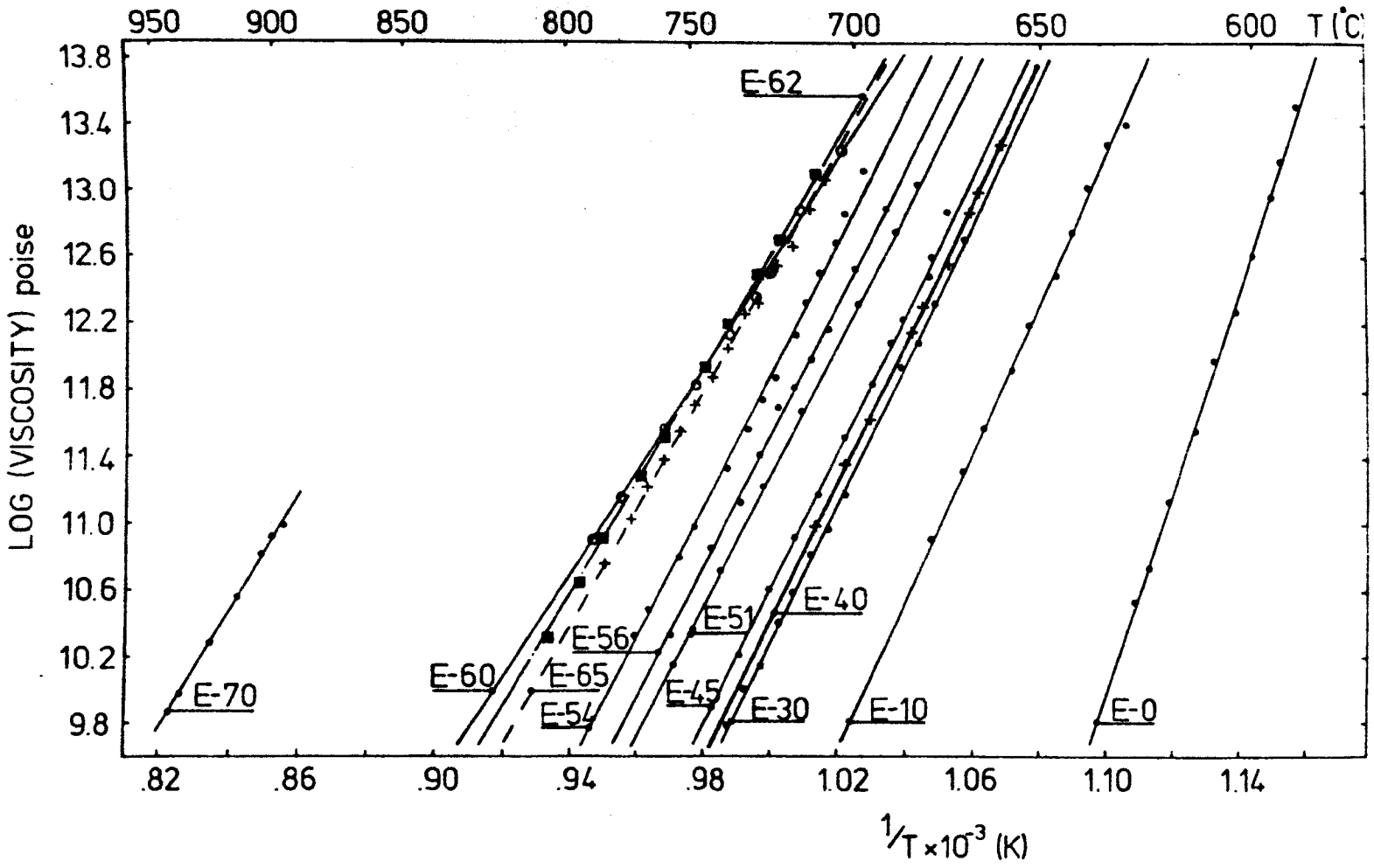

Figure 4.8 The viscosity data

several phenomena e.g. a change in the free volume or a change in the size of the polymeric flow unit (Weyl and Marboe (1964)). Several phenomenological equations have been proposed to describe this type of viscosity/temperature behaviour, but the parameters in these have no obvious physical interpretation. Because of this, and in order that that the behaviour of glass E-54 could be compared to that of the other glasses, the viscosity/temperature behaviour was approximated to the simple Arrhenius type expression even though a more accurate description of the behaviour would be given by one of several phenomenological expressions e.g. Fulcher equation (Fulcher (1925)).

The activation energies of viscous flow for the glasses evaluated are shown in table 4.4; these values were calculated using equation 2.2 . The activation energy initially decreases as the SiO_2 content increases from 0 to 60%. Above 60% wt SiO_2 the trend reverses and the activation energy of viscous flow increases as the SiO_2 content is increased. Increasing the SiO_2 content generally caused an increase in the viscosity of the glass. This is apparent in figure 4.8 but is further illustrated in figure 4.9, in which lines of constant viscosity are shown as functions of temperature and SiO_2 content. The viscosity values indicated in figure 4.9 refer to the best straight line fits to the data and not discrete measurements. Although the viscosity does increase with SiO_2 from 0% SiO_2 to about 60% SiO_2 it does not do so very strongly, being almost constant over the range 30% to 50%. Above 60% SiO_2 the behaviour becomes more complex; the viscosity of E-65 at 800°C being less than that of E-60, at the same temperature.

Table 4.4 The activation energies of viscous flow

GLASS	ACTIVATION ENERGY/kcals/mole
E-0	273 ± 9
E-10	201 ± 5
E-30	187 ± 5
E-40	187 ± 7
E-45	186 ± 7
E-51	178 ± 5
E-54	178 ± 14
E-56	178 ± 7
E-60	141 ± 7
E-62	150 ± 5
E-65	161 ± 7
E-70	157 ± 11

(Accuracies stated are to the 95% confidence level)

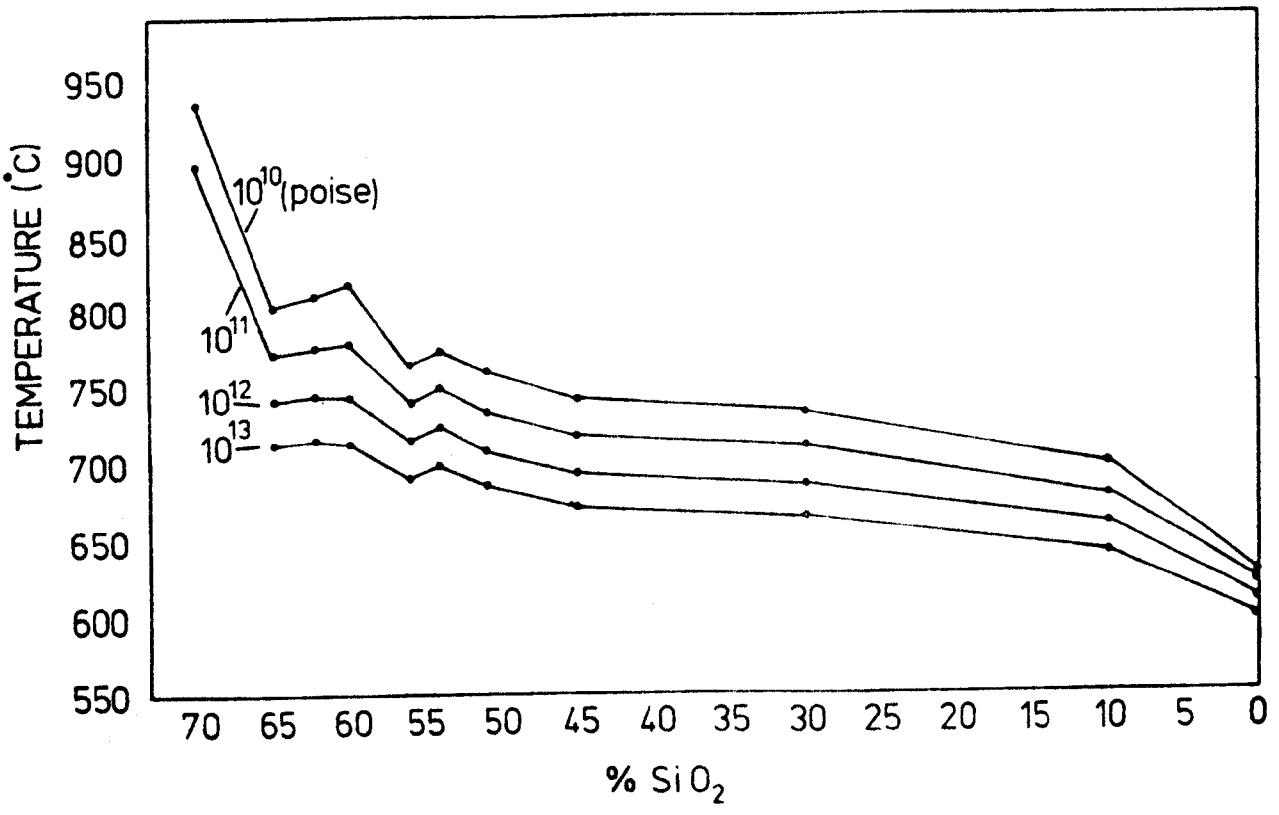

Figure 4.9 Viscosity as a function of temperature and composition.

Below a temperature of (870 ± 4)°C, glass E-70 exhibited an increase in viscosity with time. This is illustrated in figure 4.10 which shows 3 viscosity isotherms as functions of time. Glass E-70 was prepared from water saturated raw materials unlike all the other glasses. To determine if this was the cause of the viscosity drift, another glass (E-65) which showed no time dependent behaviour when prepared from dry chemicals, was prepared as glass E-70. This glass also exhibited no time dependent viscosity behaviour from which it was concluded that the preparation technique was not responsible for the viscosity drift in glass E-70.

The time dependent viscosity behaviour was not dependent on the level of stress applied to the glass. This is illustrated in figure 4.11 which shows the viscosity drift of three fibres at 770°C. Two of these were subjected to the measuring stress of 2×10^5 Pa after significant drift had occurred. Immediately after the increase in stress, delayed elastic effects operate, but after approximately 10 minutes these have no further effect.

The prolonged thermal treatments during the isothermal viscosity measurements eventually caused devitrification. For example, after 40 hours at 850°C faint lines were found in the X-ray powder patterns of the glass. While the measurements shown in figure 4.11 concern treatments which resulted in no evidence of devitrification (i.e. no sharp lines on the powder picture) it is possible that the amount of crystallised material was small and simply not detected.

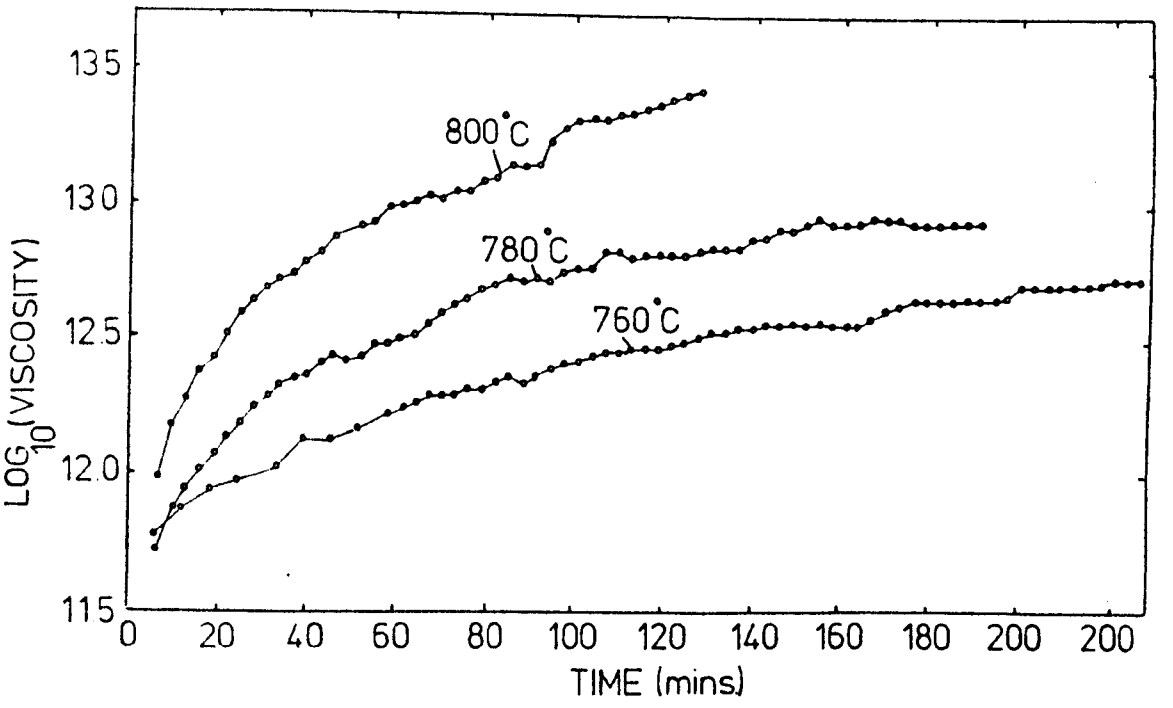

Figure 4.10 The isothermal viscosity drift of glass E-70

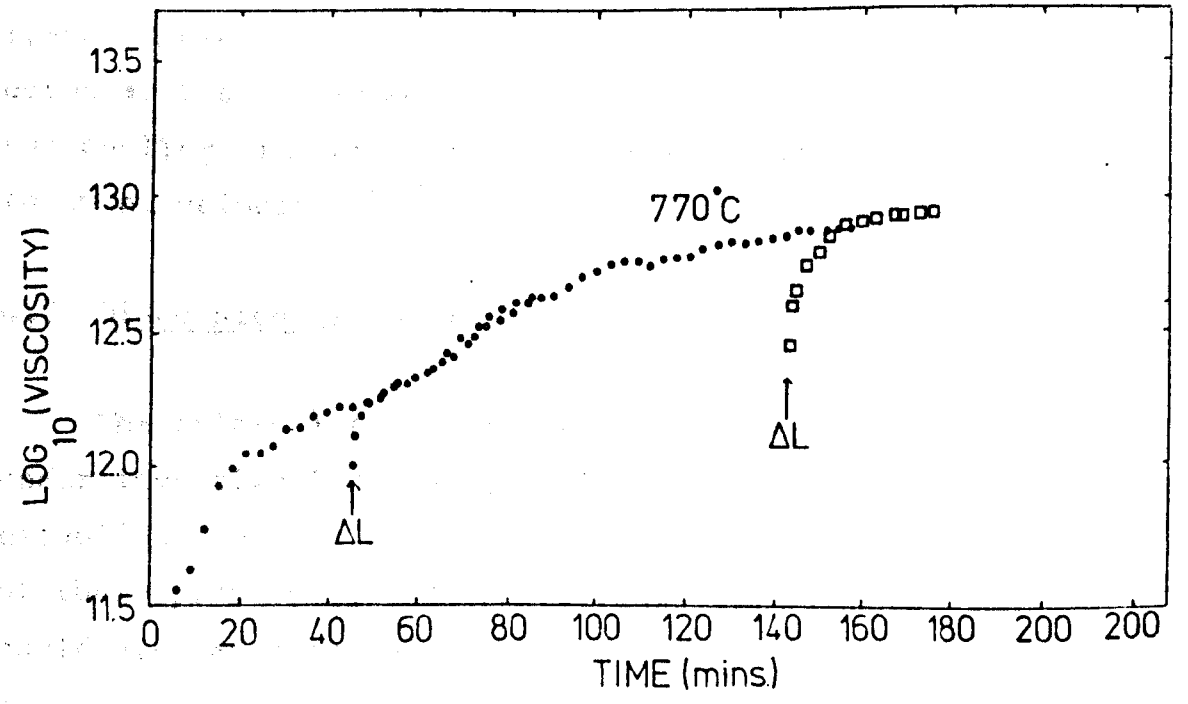

Figure 4.11 The isothermal viscosity drift of glass E-70. Three samples, subjected to the measuring stress at different periods during heat treatment

4.4 Results of the cooling rate measurements

The cooling time data for fibres having four different diameters drawn at $1ms^{-1}$ and two diameters drawn at $1.5ms^{-1}$ are shown on a log/temperature-time basis in figures 4.12 and 4.13 respectively. Within experimental error, these are straight lines confirming that over the measured temperature range, Newton's law of cooling is obeyed i.e. the rate of heat loss is proportional to the excess temperature.

Figure 4.14 shows the time taken for the fibres to cool from $800^{o}C$ to $400^{o}C$ as a function of fibre diameter. For the $1ms^{-1}$ drawing velocity this plot has a slope of 1.5 ± 0.3 (95% confidence limits). Thus, the time required for a fibre to cool through a given temperature range is proportional to the $(\text{fibre radius})^{1.5}$.

From figure 4.14, it can be seen that the two fibres drawn at $1.5ms^{-1}$ cooled more rapidly than those drawn at $1ms^{-1}$. From the two drawing velocities evaluated, the cooling time appears to be proportional to the $(\text{drawing velocity})^{-0.7}$.

4.5 Discussion of the results

The critical temperatures of three of the glasses under investigation (E-70, E-65 and E-62) were established by the opalescence measurements. For one of these glasses (E-70) the critical temperature could also be obtained from the viscosity drift measurements. However, as no drift was detected for glasses E-65 and E-62, this absence of drift

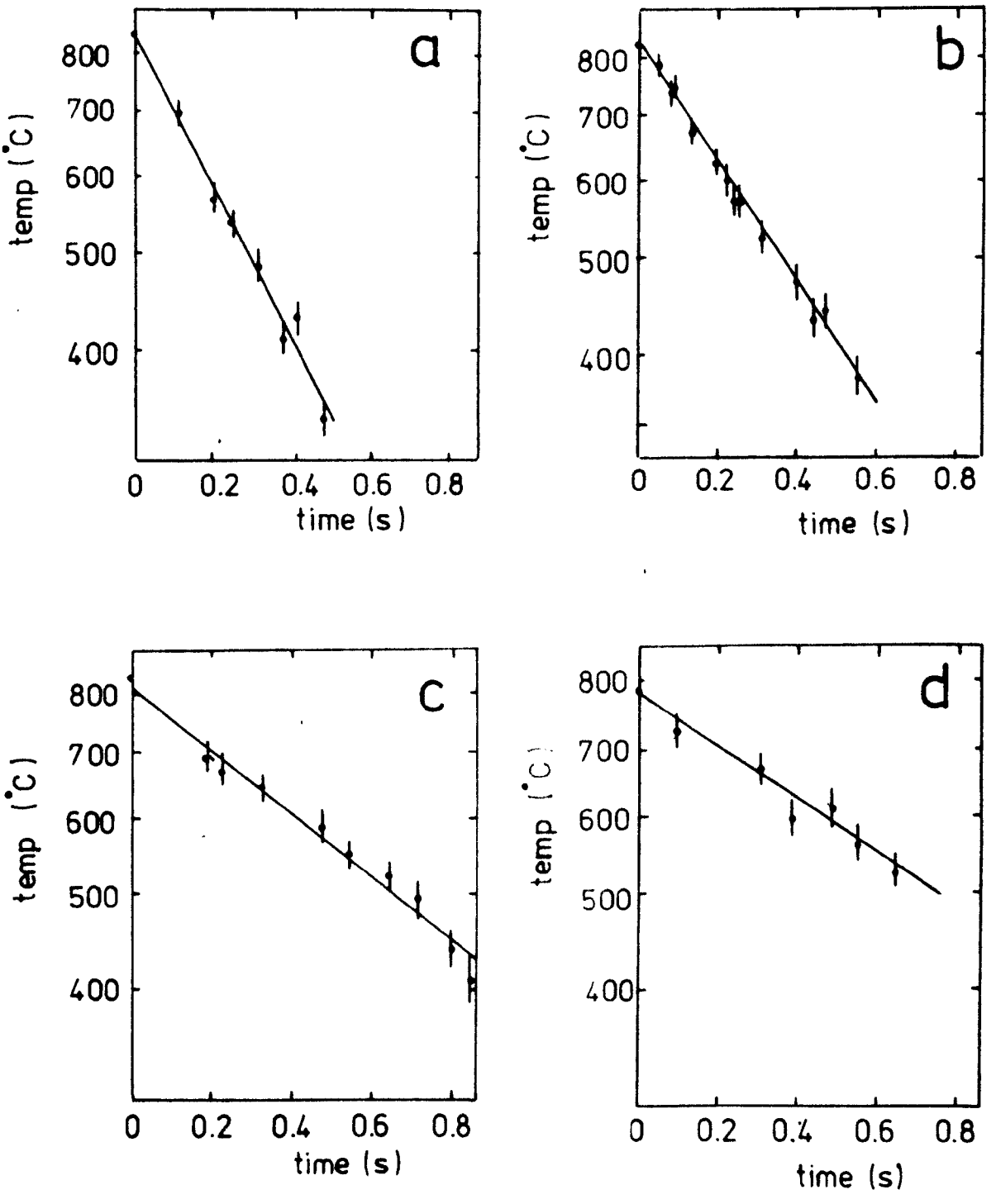

Figure 4.12 The temperature of the fibre as a function of time after leaving the glass, drawing velocity 1ms^{-1}. 0.09mm dia.(a). 0.12mm dia.(b). 0.18mm dia.(c). 0.20mm dia.(d).

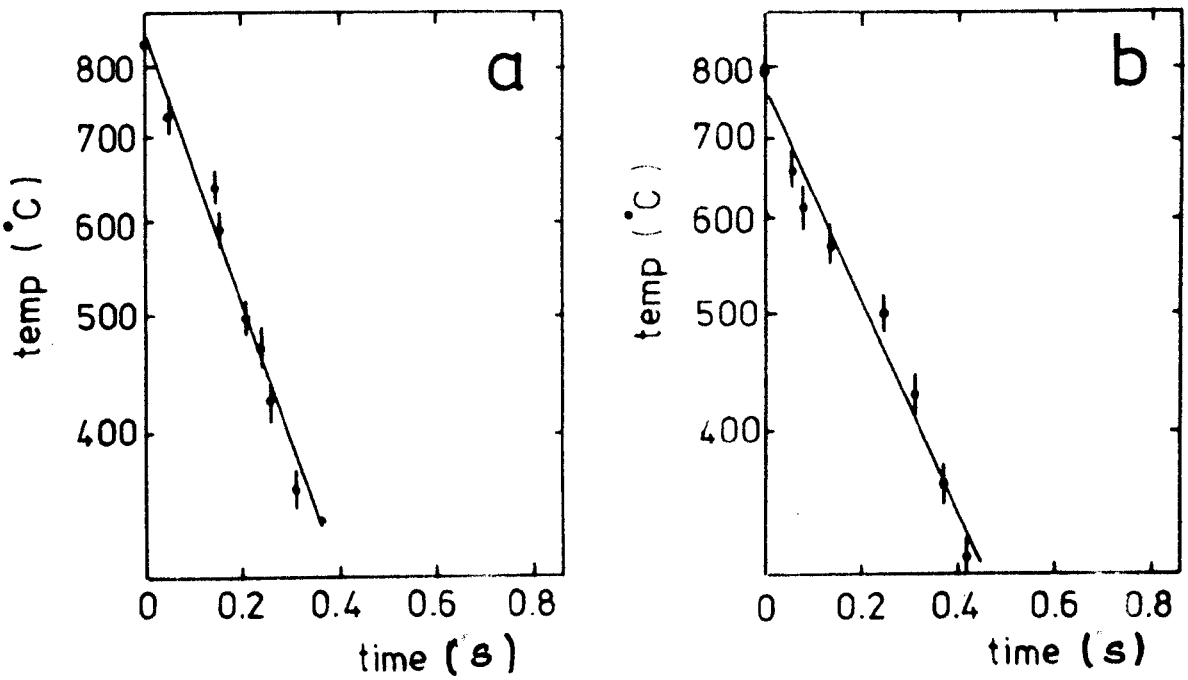

Figure 4.13 The temperature of the fibre as a function of time after leaving the glass melt, drawing velocity 1.5ms^{-1}. 0.09mm dia.(a). 0.20mm dia.(b).

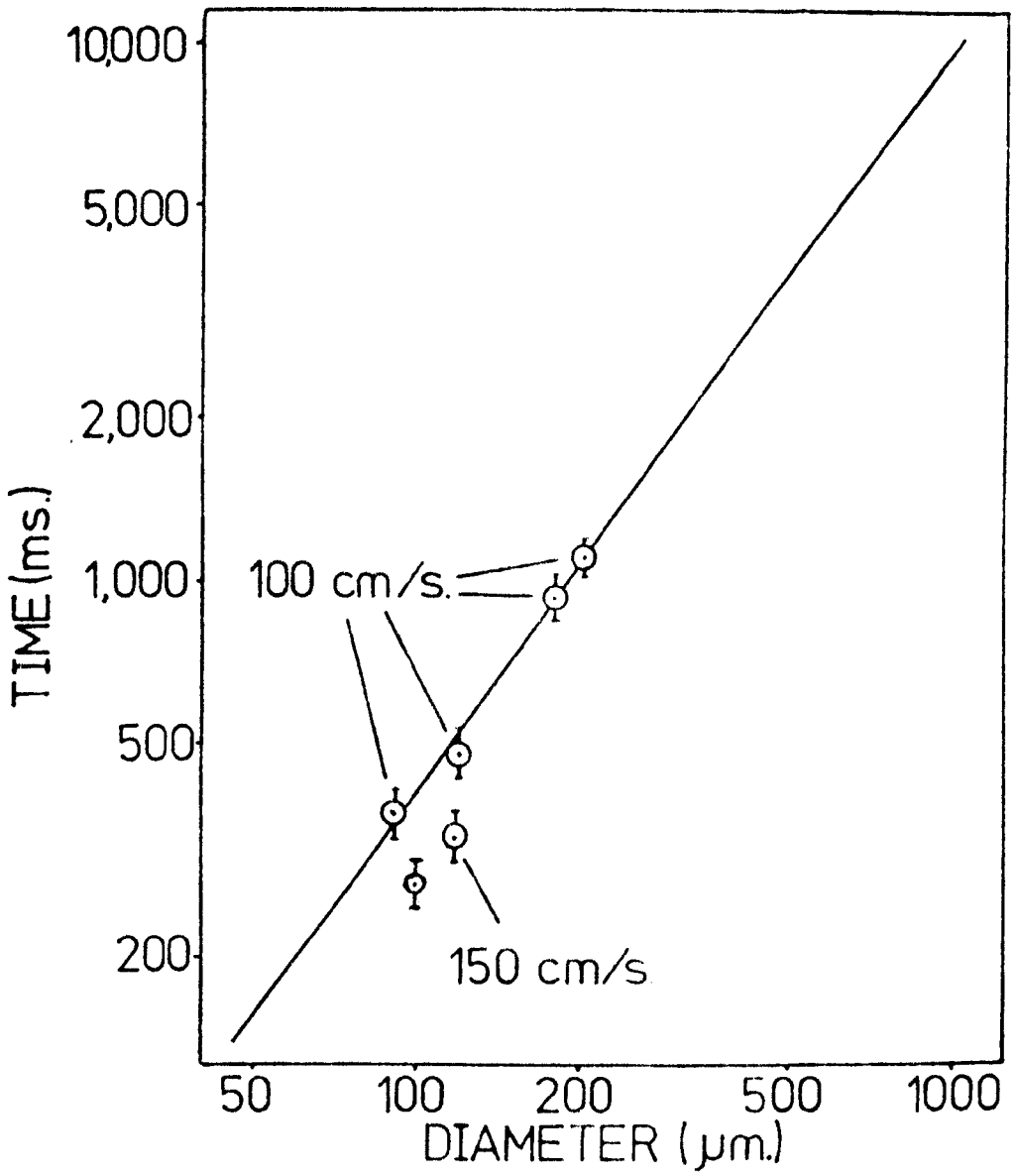

Figure 4.14 The time to cool from 800°C to 400°C as a function of fibre diameter

clearly does not indicate the absence of phase separation. The critical temperature for E-70 found by these two techniques are in reasonable agreement. These critical temperatures are shown in figure 4.15 as a function of the SiO_2 content of the glasses. Also shown in figure 4.15 are the inflection temperatures at which the activation energy of electrical conductivity changed (for the glasses for which resistivity measurements were made). These temperatures exhibit a progression which suggests that the onset of phase separation may be related to this transition. In particular, for glass E-65 the critical opalescence temperature is very close to the electrical inflection temperature.

The log resistivity vs. 1/T plot for glass E-65 is somewhat different in character to that of the other glasses. For glass E-65, the activation energy of conduction decreases below the inflection temperature. This is typical of materials for which two parallel conduction mechanisms exist e.g. intrinsic and extrinsic conduction in ionic crystals and doped semi-conductors. In these materials the total conductivity is given by the sum of that of the individual processes. At low temperatures the process with the lowest activation energy predominates, but as the temperature increases the activation energy becomes less of a restriction and processes described by a lower pre-exponential constant become dominant.

While two parallel conduction mechanisms may describe the behaviour of glass E-65, it does not describe the behaviour of the other glasses. For the other glasses the activation energy increases below the inflection temperature. For these glasses

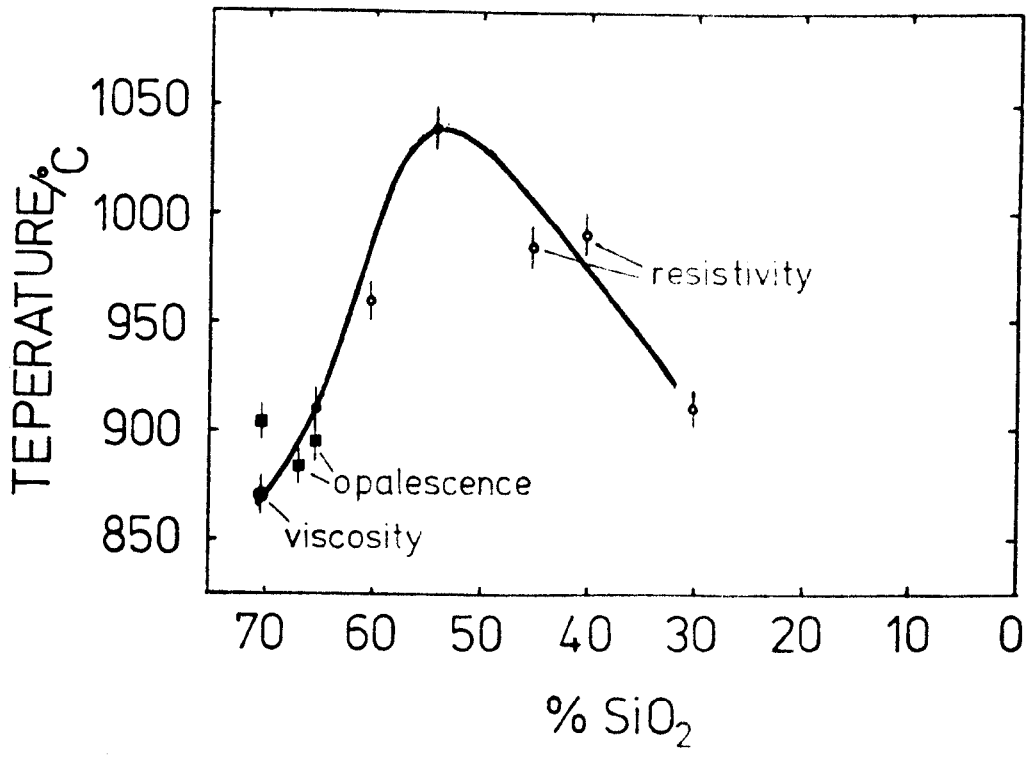

Figure 4.15 The critical temperatures as determined by opalescence and viscosity drift measurements. Also shown are the inflection temperatures found in the electrical behaviour of each glass

the high temperature conduction mechanism cannot be available below the inflection temperature. The activation energies above and below the inflection are shown as a function of the SiO_2 content of the glass in figure 4.16. While the activation energy above the inflection is approximately constant, the activation energy below the inflection temperature decreases with increasing SiO_2 content. Therefore, the differing behaviour of glass E-65 is consistent with the trend apparent in the other glasses.

The activation energies above the inflection for all of the glasses are similar, the mean value being 2.4 ev (55 kcal/mole). This value and the insensitivity of it to composition are characteristic of oxygen ion diffusion in glass. Hagel and MacKenzie (1964) reported a value of 53 kcal/mole for oxygen diffusion in $CaO-Al_2O_3-SiO_2$ glasses. As oxygen ions have the largest diffusion coefficient of the ions present in molten glass (Terai and Hayama (1975)) the available evidence suggests that these are the primary carriers in these glasses above the inflection temperature.

The transition from the high temperature conduction mechanism to the lower temperature mechanism does not appear to occur at any particular viscosity. As evidence for this, in table 4.5, the viscosities of the glasses at the inflection temperature are compared. These viscosity values were obtained by extrapolation of the linear fit to the data shown in figure 4.8. As this may not be valid, then the viscosities shown in table 4.5 are only intended to indicate the order of magnitude of the viscosities. However as these vary greatly, ranging from 10^1 poise to

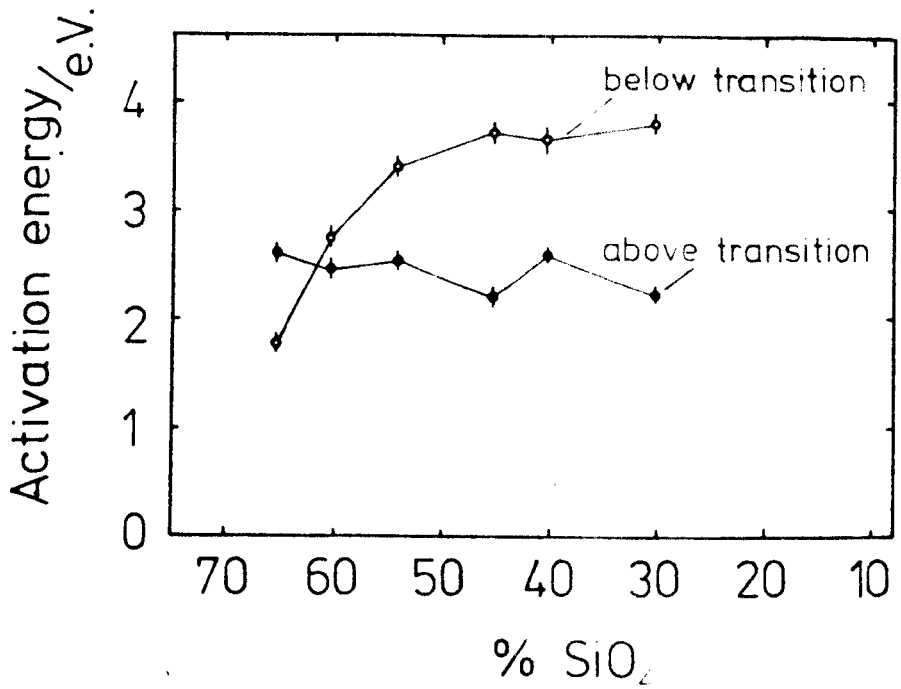

Figure 4.16 The activation energies of conduction above and below the inflection temperature as a function of the wt.% SiO_2

Table 4.5 The estimated viscosity of the glasses at the electrical inflection temperature

GLASS	VISCOSITY poise
E-30	$10^{3.8 \pm 10^{0.2}}$
E-40	$10^{1.8 \pm 10^{0.6}}$
E-45	$10^{2.2 \pm 10^{0.5}}$
E-54	$10^{2.6 \pm 10^{1.4}}$
E-60	$10^{6.8 \pm 10^{0.2}}$
E-65	$10^{5.5 \pm 10^{0.2}}$

10^7 poise, it is unlikely that the inflection does occur at a particular viscosity for all of the glasses. If the conduction above the inflection is due to oxygen ion diffusion then this would be sensitive to phase separation. Glasses phase separate because the oxygen ion concentration is below that required to satisfy the various cations present unless the cations congregate non-randomly. The process of phase separation has been described as a 'struggle for oxygen' (Wolf (1961e)) and once this starts to take place, the ions become less available for the conduction process. The conduction must then either proceed by some modified mechanism e.g. another carrier type or with an increased activation energy related to the stronger oxygen-cation bonding.

The activation energy of viscous flow shows a similar compositional trend to that of the activation energy of conduction below the inflection. This is not surprising, since both refer to the same temperature region, and both are transport properties. The two activation energies are compared in figure 4.17 as a function of the SiO_2 content of the glasses. At this stage, little can be concluded from these data except for noting that the relative insensitivity of the activation energies to composition from about 55% SiO_2 to 30% SiO_2 is consistent with the presence of a continuous phase or phases of virtually constant composition. The more rapid change in both, for SiO_2 contents greater than about 55 to 60%, may then indicate a change in the character of the phase separation e.g. a loss of connectivity of one of the phases.

The measurements on the fibre cooling rate prove that Newton's law of cooling is obeyed. This has important consequences as far as this investigation

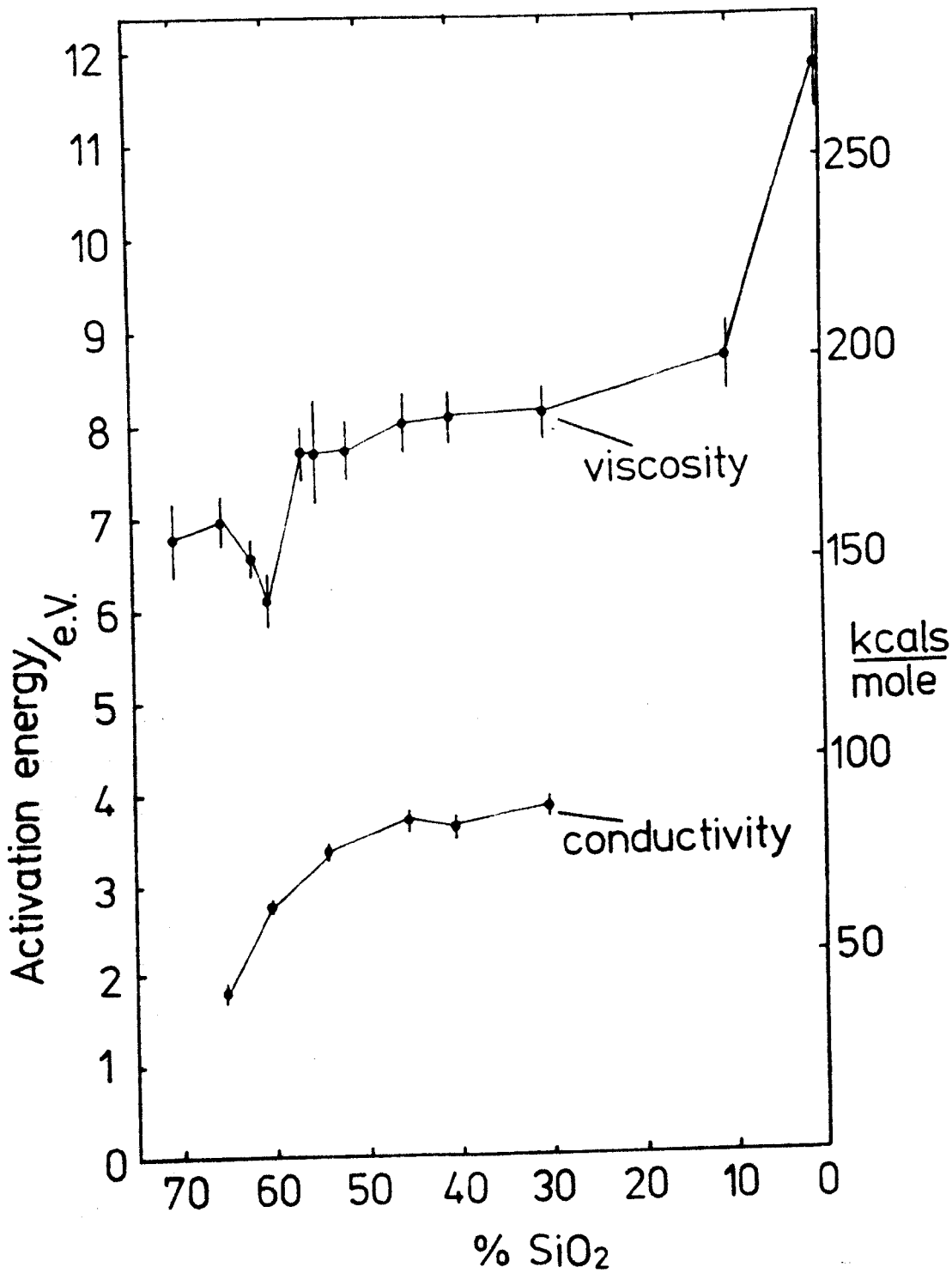

Figure 4.17 The activation energies of conductivity below the transition temperature and those of viscous flow

is concerned. Firstly, the thermal conductivity of the glass has a negligible effect on the rate of cooling, as this is controlled by the rate of heat transfer from the surface. The temperature profile of the glass will therefore be flat, and this precludes any radial anisotropy effects as there is no differential cooling. Secondly, as the thermal conductivities of all glasses are similar and increase with temperature, the rates measured can be applied to the glasses under investigation and can be extrapolated to higher temperatures.

The weak dependence of cooling rate on the drawing velocity indicates that any departures from the nominal drawing velocity of $1m^{-1}$, used in the fibre production, will have a minimal effect on the thermal history, and hence on the phase morphology of the fibres.

CHAPTER 5

The results of the leaching measurements and of the characterisation of the porous glasses

5.1 Introduction

The results of the acid leaching measurements on the glasses are presented in this chapter. Glass E-54, the original E-glass composition from which all the other glass compositions were developed, was studied in detail to establish the role of the leachant concentration and temperature on the leaching process. This glass was also used to evaluate the effect that the thermal history (i.e. the fibre cooling rate) had on the leaching and on the porous product.

The leaching conditions found to be most suitable for the leaching of glass E-54 were used to leach all the other glasses investigated. The optimum leaching condition: for glass E-54 was found to be a hot concentrated HCl solution and with this leachant it was possible to prepare integral porous skeletons from parent glasses containing between 45 and 60% (by weight) SiO_2. Typically the measured pore size was of the order of 2nm radius but there was also evidence of an even finer level of structure in the leached glass.

To establish the validity of the trends apparent in the data, a rigorous statistical analysis was applied in several cases. This often resulted in determining parameters such as correlation coefficients and

significance levels. As these are not commonly encountered, reference to them has been kept to a minimium.

5.2 The effect of the leachant temperature

Increasing the leachant temperature increased the leaching rate of 0.3mm E-54 glass fibres. This can be seen in figure 5.1 in which the weight loss is shown as a function of time for three leachant temperatures. The time required to establish a constant weight was of the order of 16 hours 90°C, 60 hours at 60°C and several hundred hours at 25°C (using 30 v/v% HCl solutions).

The soluble phase in glass E-54 is similar to the composition of glass E-0, the weight loss of 0.3mm fibres of glass E-0 under the same conditions is shown in figure 5.2. This glass (E-0) lost weight at about twice the rate that glass E-54 did. As the final porous volume of glass E-54 was approximately 50%, (section 5.4) these results suggest that the leaching rate of glass E-54 is controlled by the rate of dissolution of the acid soluble phase present and is not restricted by some other mechanism e.g. diffusion through the porous layer to the unreacted glass.

5.3 The effect of the leachant concentration

Increasing the leachant acid concentration from 5v/v% to 30v/v% marginally increases the leaching of glass E-54. This is shown in figure 5.3 in which the weight loss of 0.3mm diameter E-54 glass fibres is shown as a function of time in three acid solutions. Figure 5.4

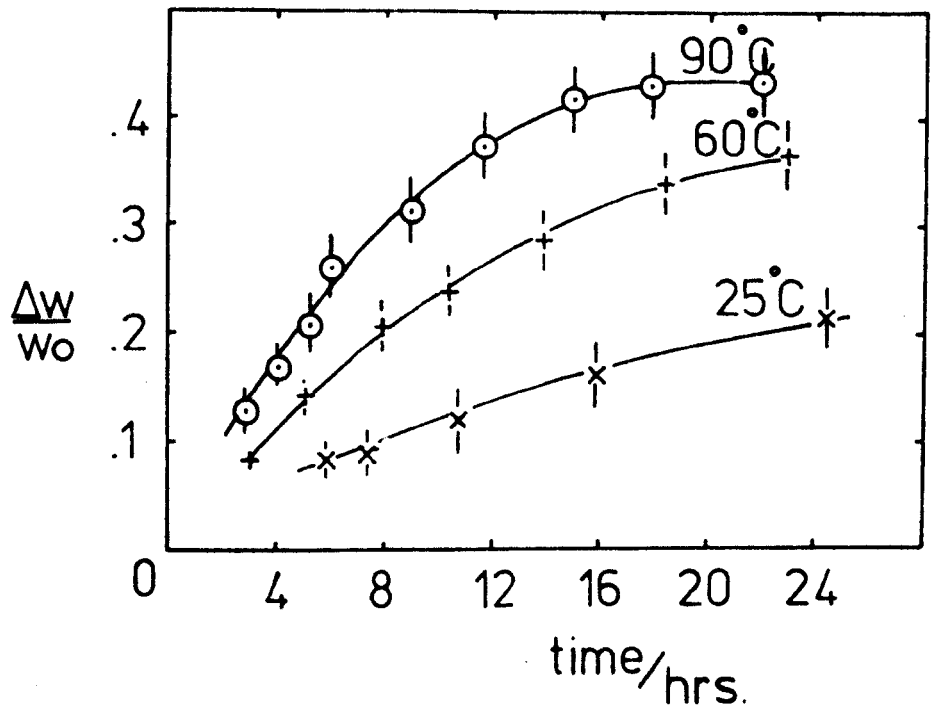

Figure 5.1 Weight loss as a function of time in the leaching solution. 0.3mm dia. E-54 glass fibres; 30v/v% HCl solutions

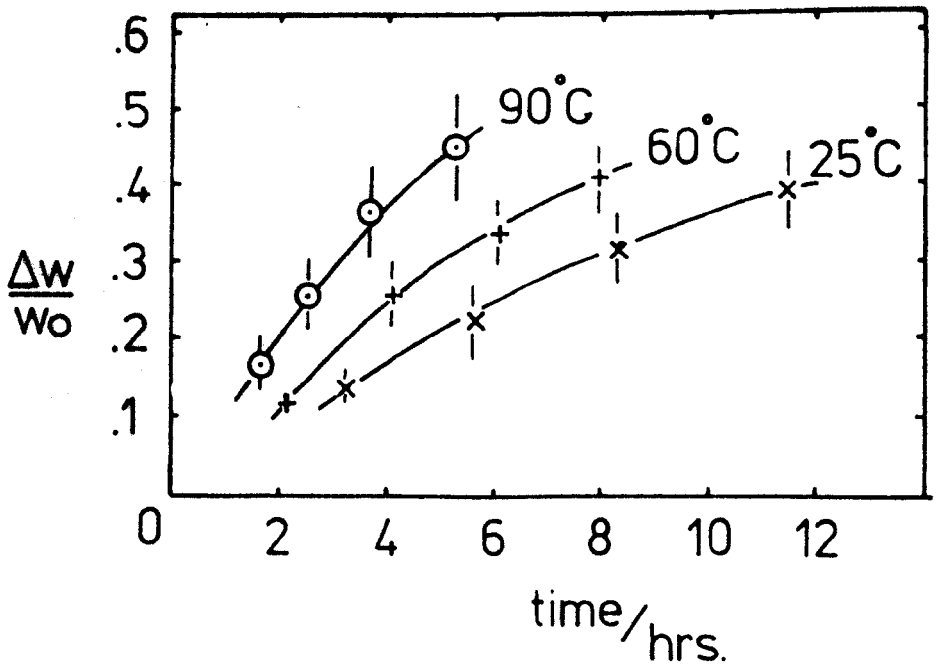

Figure 5.2 Weight loss as a function of time in the leaching solution. 0.3mm dia. E-0 glass fibres 30v/v% HCl solutions

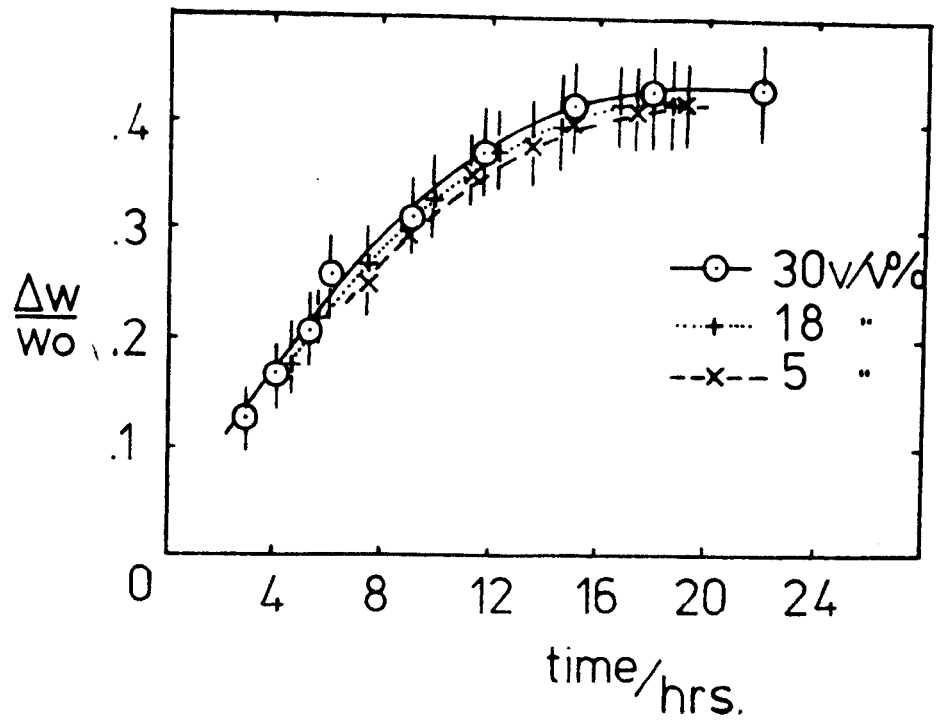

Figure 5.3 Weight loss as a function of time in the leaching solution. 0.3mm dia. E-54 glass fibres HCl solutions at 90°C

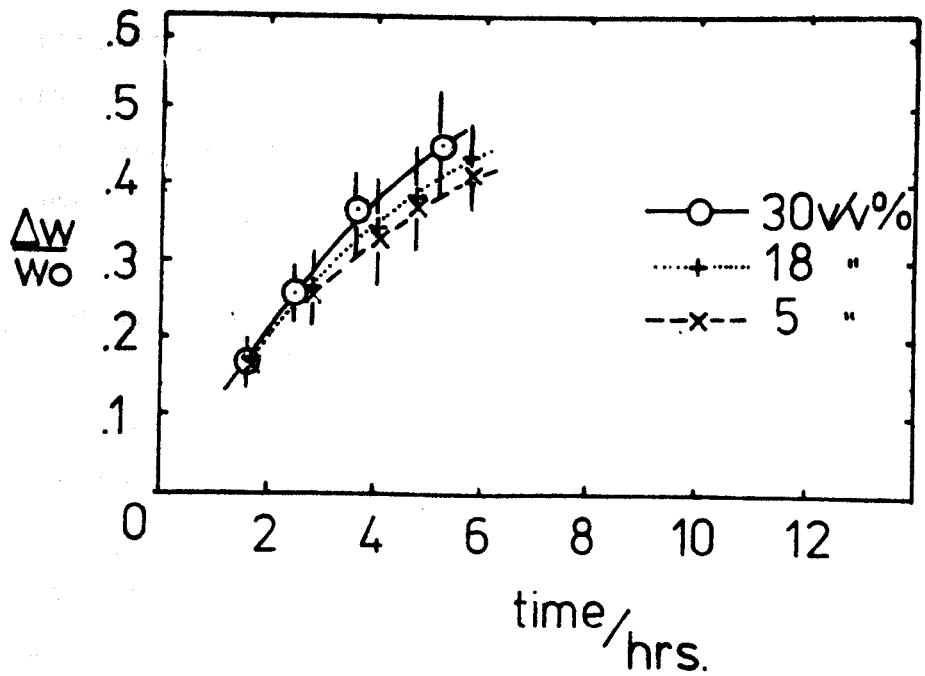

Figure 5.4 Weight loss as a function of time in the leaching solution. 0.3mm dia. E-0 glass fibres HCl solutions at 90°C

shows the weight loss of glass E-0 under the same conditions and this shows a similar trend with acid concentration.

This behaviour was not confirmed by the more quantitative gas adsorption measurements. In figure 5.5 the pore volume is shown as a function of time in the leaching solutions. These data suggest the moderate solution (18v/v%) resulted in the most rapid leaching.

The ultimate specific surface area of the leached glass was dependent on the acid concentration used for the leaching. Figure 5.6 shows the surface area as a function of time for the 0.3mm E-54 glass fibres. The surface area in all cases shows a maximum before stabilising. This maximum in the surface area is most likely to be due to debris as well as reaction products present in the pores. These would slowly be dissolved or diffuse out of the skeleton during longer acid treatments. As the largest surface areas were obtained by leaching the glass in 30v/v% HCl solutions at 90°C, these conditions were employed in all subsequent leaching operations

5.4 The effect of thermal history

The weight losses after 5 hours leaching of fibres of E-54 glass as a function of (fibre diameter)^2 are shown in figure 5.7. The departure from linearity indicates that the weight loss is not simply related to the surface area and that the cooling rate of the glass fibres affects the leaching rate.

The pore volumes of the fully leached fibres as a function of fibre diameter are shown in figure 5.8.

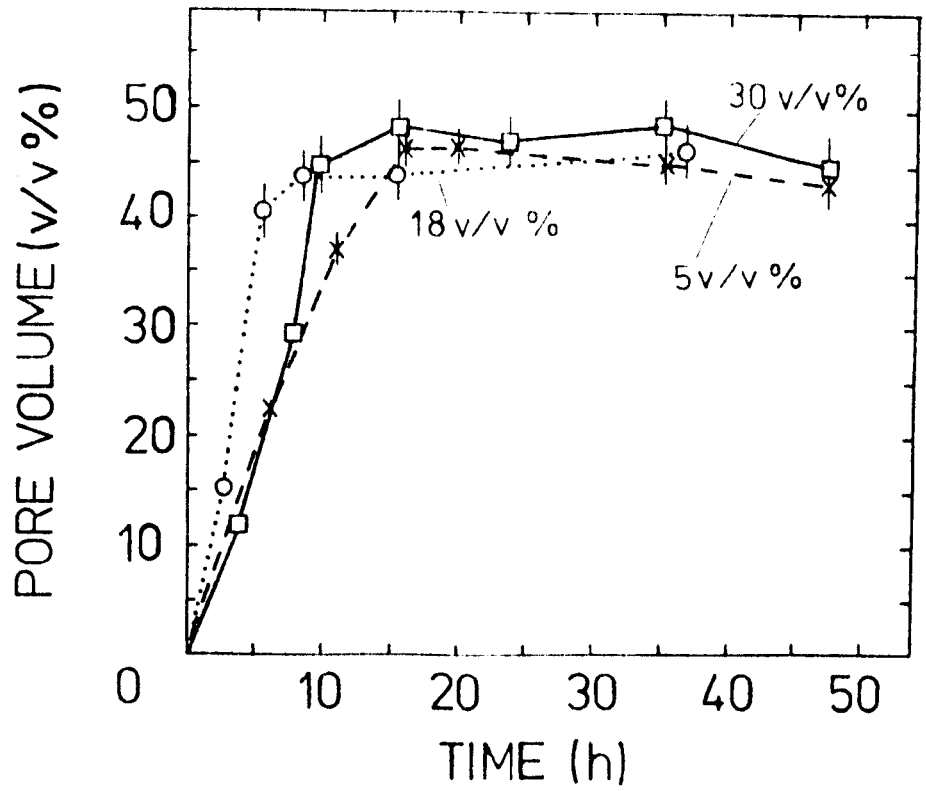

Figure 5.5 Pore volume as a function of time in the leaching solution. 0.3mm dia. E-54 glass fibres in HCl solutions at 90°C

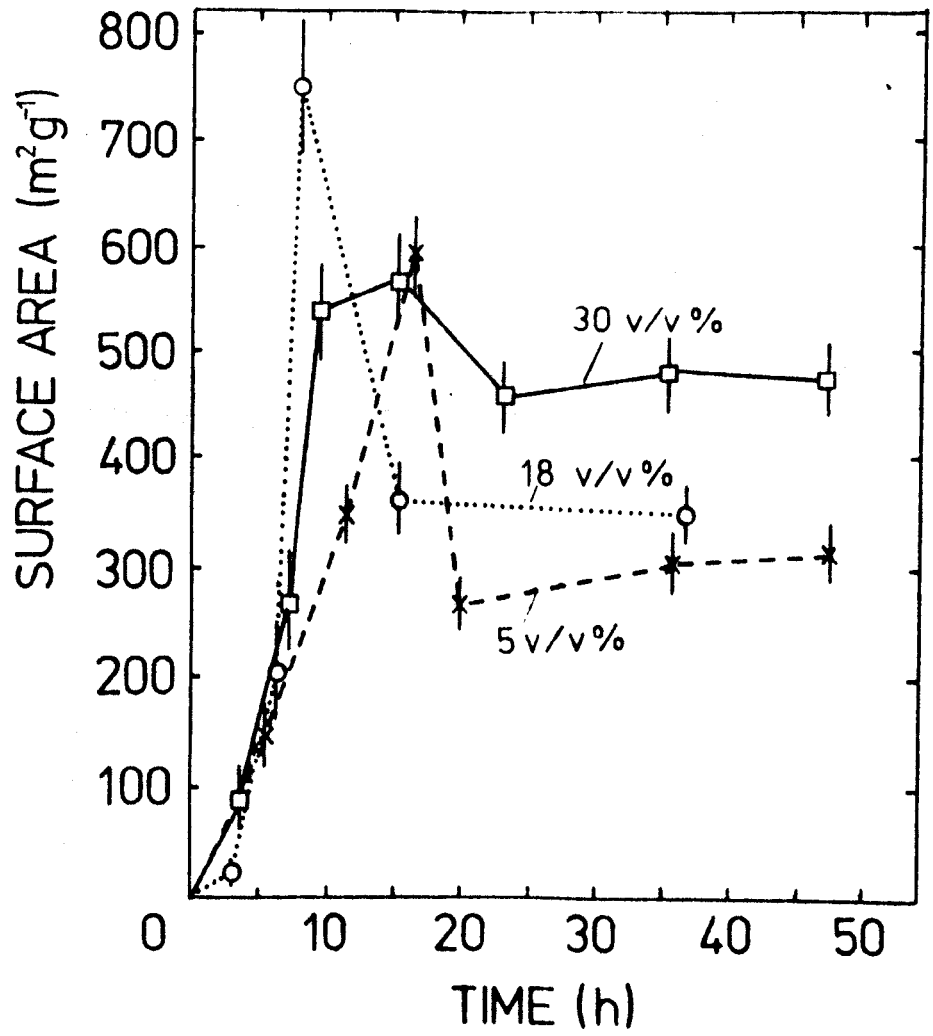

Figure 5.6 Surface area as a function of time in the leaching solution. 0.3mm dia. E-54 glass fibres in HCl solutions at 90°C

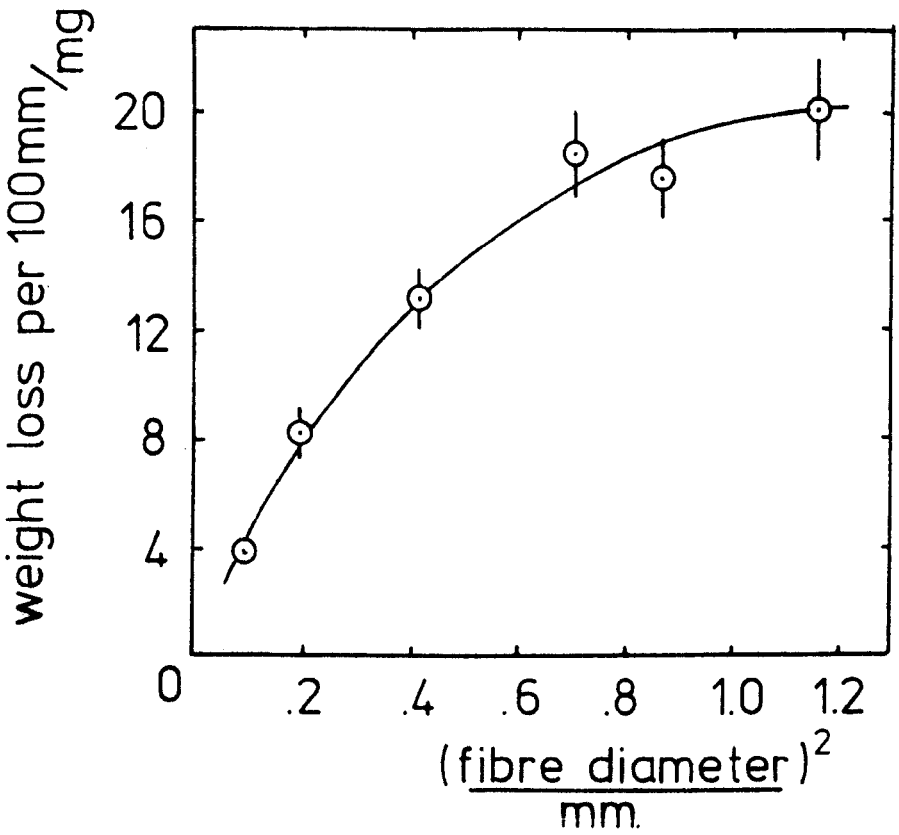

Figure 5.7 Weight loss as a function of (fibre-diameter)^2. E-54 glass fibres after 4 hours in 30v/v% HCl solutions at 90^{0}C

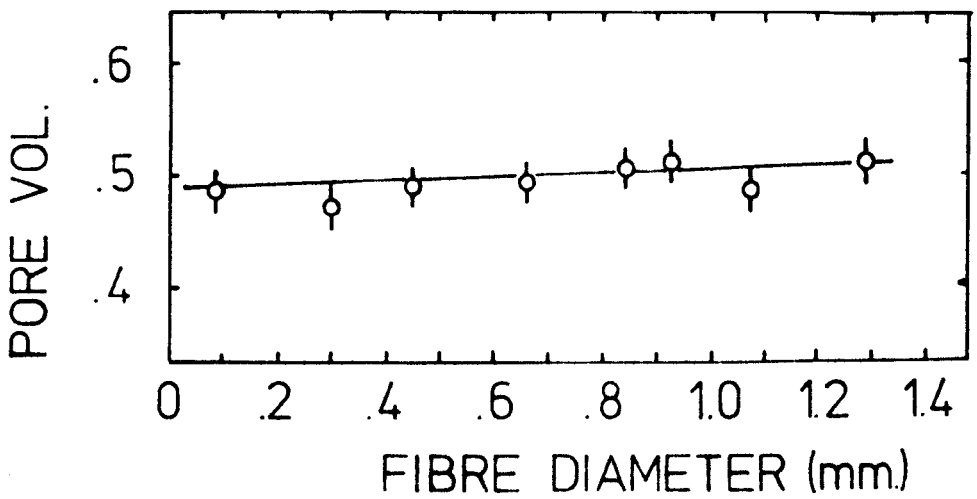

Figure 5.8 Pore volume as a function of fibre diameter. E-54 glass fully leached in 30v/v% HCl solutions at 90°C

The pore volume is essentially independent of fibre diameter over the range of diameters measured and is approximately 48% by volume. The specific surface areas of the fully leached glass fibres are shown as a function of fibre diameter in figure 5.9.

The increase in surface area with fibre diameter indicated in figure 5.9 is statistically valid to the 90% confidence level. As the pore volume is approximately constant, the average pore size of the leached glass must decrease with fibre diameter. The average pore size (calculated from equation 3.21) is shown as a function of fibre diameter in figure 5.10 and this apparently decreases from 1.5nm to 1.3nm in radius as the fibre diameter increases from 0.3mm to 1.3mm. This decrease is, however, significant only to the 70% confidence level owing to the additional uncertainty in the pore volume.

The pore size distributions calculated by a numerical analysis of the desorption isotherm confirm the decrease in pore size with increasing fibre diameter. Three distributions for fully leached glass E-54 are shown in figure 5.11. As the fibre diameter increases the peak in the pore size distribution of the leached glass decreases from 2.1nm to 1.8nm. The peak position in the distributions as a function of fibre diameter are shown in figure 5.12. The width of each distribution is also shown in figure 5.12.

This width is defined in figure 5.11 for the 0.3mm diameter fibre. The decrease in median pore size indicated in figure 5.12 is significant to the 95% confidence level.

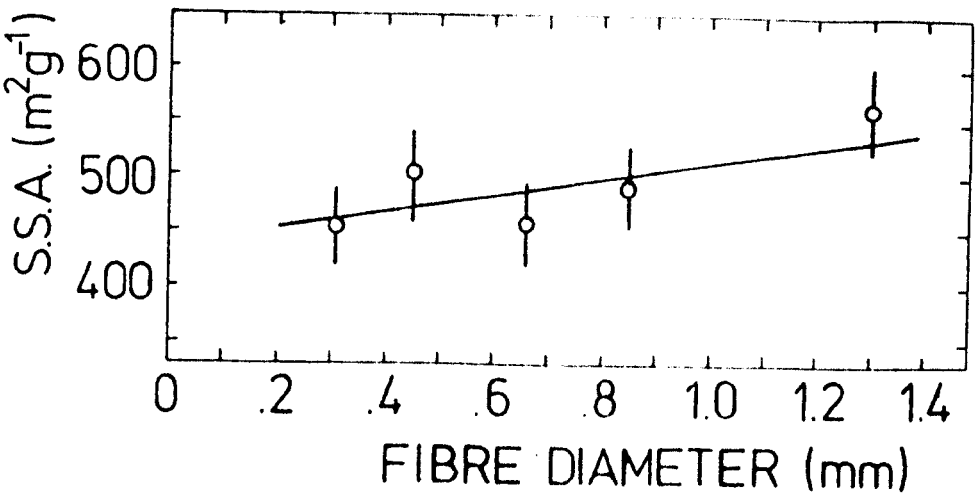

Figure 5.9 Specific surface area as a function of fibre diameter. E-54 glass, fully leached in 30v/v% HCl solutions at 90°C

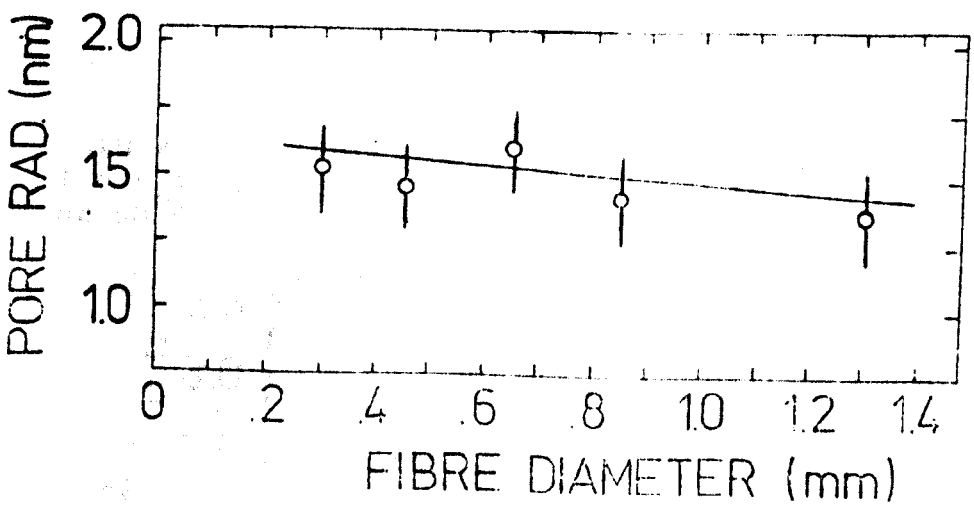

Figure 5.10 Mean pore size as a function of fibre diameter. E-54 glass, fully leached in 30v/v% HCl solutions at 90°C

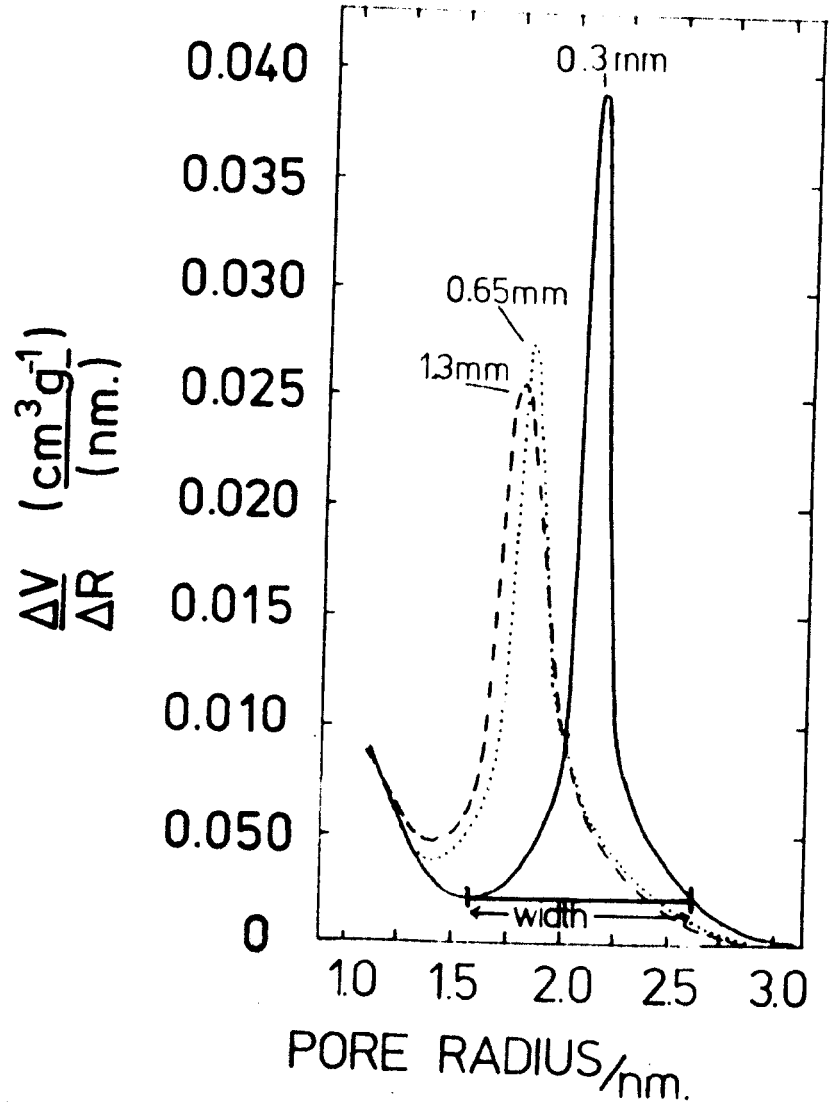

Figure 5.11 Three pore size distributions . E-54 glass fibres fully leached in 30v/v% HCl solutions at 90°C

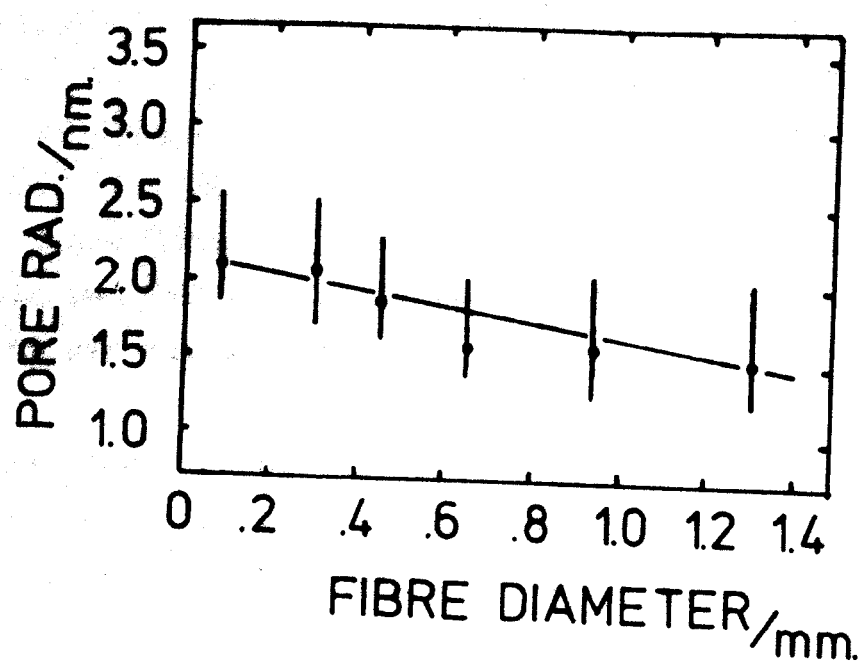

Figure 5.12 The most common pore size as a function of fibre diameter. E-54 glass, fully leached in 30v/v% HCl solutions at 90°C

Transmission electron micrographs of several of the fully leached E-54 glass fibres are shown in figure 5.13 The void volume fraction (calculated using equation 3.1) and the average distance between the phases (calculated using equation 3.3) are shown in figures 5.14 and 5.15 respectively. No other structure was resolved, over the range 0.5nm to several microns. As the structure detected was on the scale of a few nanometers the accuracy of the quantitative analysis of the micrographs is low. The mean distance between phases shows no significant correlation with the fibre diameter. Few conclusions can be drawn, therefore, from the microscopy data other than to observe that the distances are at least of the same order of magnitude as those indicated by the gas adsorption.

The pore size distribution analysis accounted for only 55±3% of the total pore volume of the leached glasses and for less than half of the total surface area. While the approximation to cylindrical pores made for the analysis may be responsible for some or all of the imbalance in surface area, this does not explain the volume unaccounted for in the analysis. There are two possible reasons for the volume imbalance: firstly, the porous volume of the glass may not be constant during the measurements or secondly, a significant number of pores exist which have dimensions less than 1nm and are therefore beyond the applicability of the Kelvin based analysis.

Dimensional changes in porous glass caused by the chemisorption of solvents have been reported by several investigators (e.g. Nordberg (1944), Amberg and McIntosh

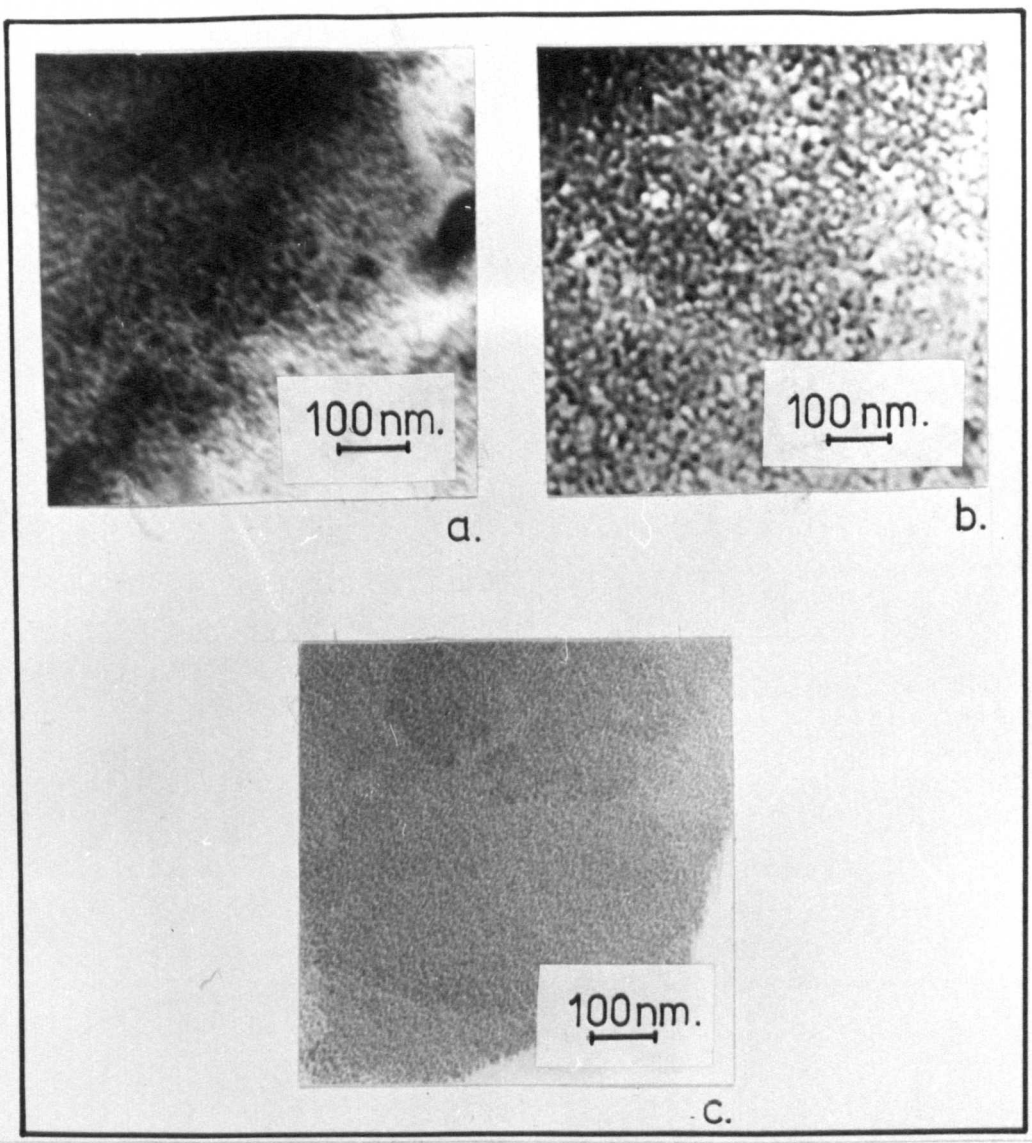

Figure 5.13 Transmission electron micrograph of E-54 glass fibres, fully leached in 30 v/v% HCl. solutions at 90°C. a: 0.1mm dia., b: 0.66mm dia., c: 0.34mm dia.

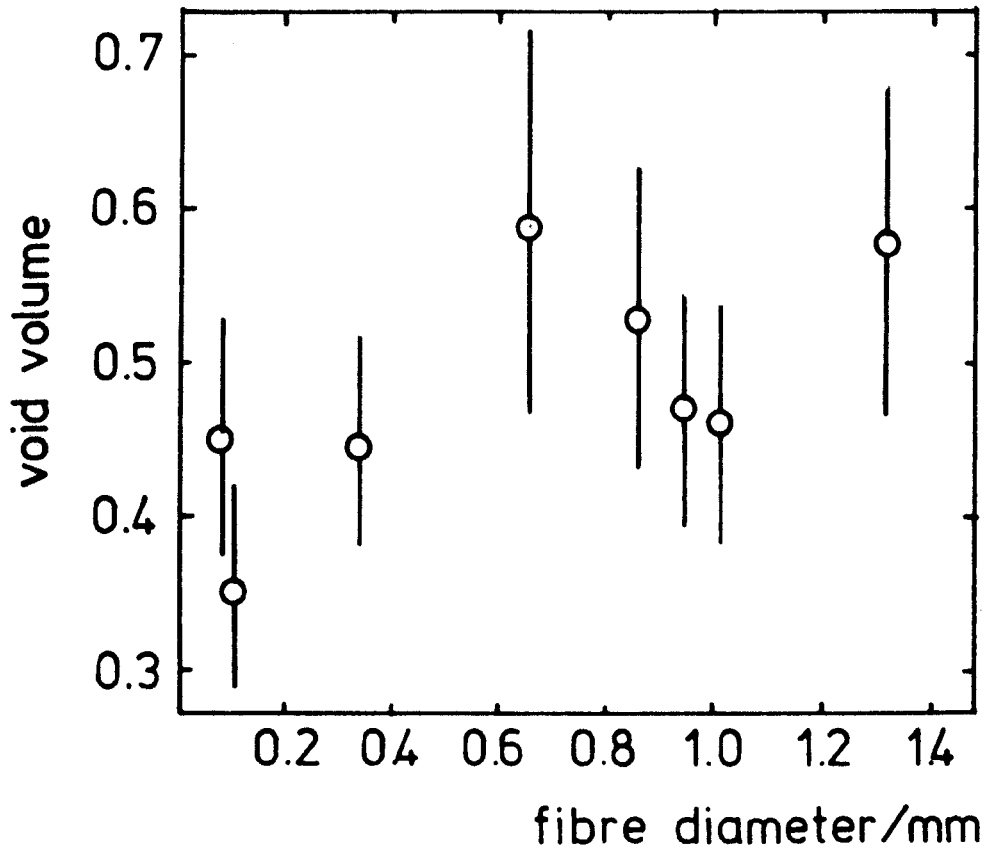

Figure 5.14 Void volume of E-54 glass fibres fully leached in 30v/v% HCl solutions at 90°C as a function of fibre diameter

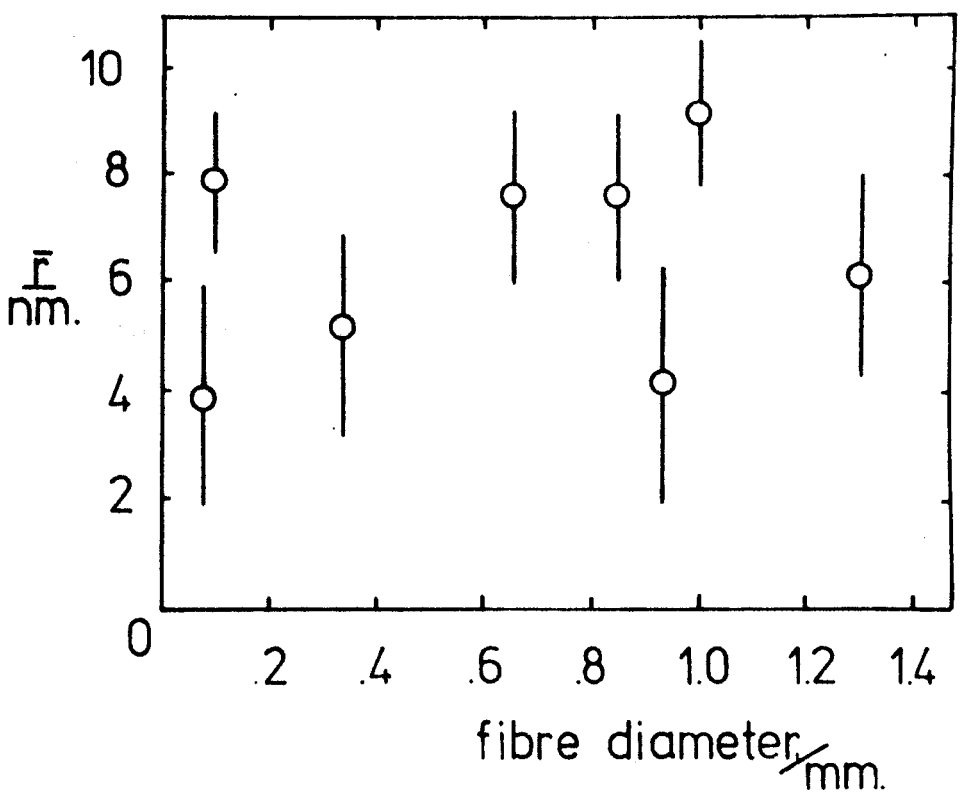

Figure 5.15 Average distance between phases of E-54 glass fibres fully leached in 30v/v% HCl solutions at 90°C, as a function of fibre diameter

(1952)) but no such changes have been reported as the result of the physical adsorption of inert gases. For that reason the most likely explanation is that there are a large number of smaller pores/cracks present in the leached material i.e. the full distribution is bimodal. All of the distributions show a rising shoulder at about 1nm, and in figure 5.16 this has been extrapolated to account for the extra pore volume and surface area measured. To do this it was necessary to assume that the smaller pores formed a Gaussian distribution (in volume) as well as smoothly fitting the measured distribution at 1.25nm radius.

As no data regarding the form of the distribution of the smaller pores were obtained, the assumption of a Gaussian distribution is entirely speculative and the particular bimodal distribution shown in figure 5.16 represents only one of an infinite series of bimodal distributions.

The bimodal pore size distribution explains the difference between the average pore size of 1.5nm (figure 5.10) and the 2.0nm (figure 5.11) of the distribution measurements. The mean pore size estimate assumes that the distribution is monomodal and so represents some average of the two actual peaks.

As the pore volume and surface area unaccounted for in the pore size distribution analysis is constant with changing fibre diameter, there is no evidence that the distribution of the smaller pores changes with fibre diameter. In particular, the decrease in the mean pore radius (calculated from the total pore volume and area) is due entirely to the change in larger pore distribution shown in figure 5.11.

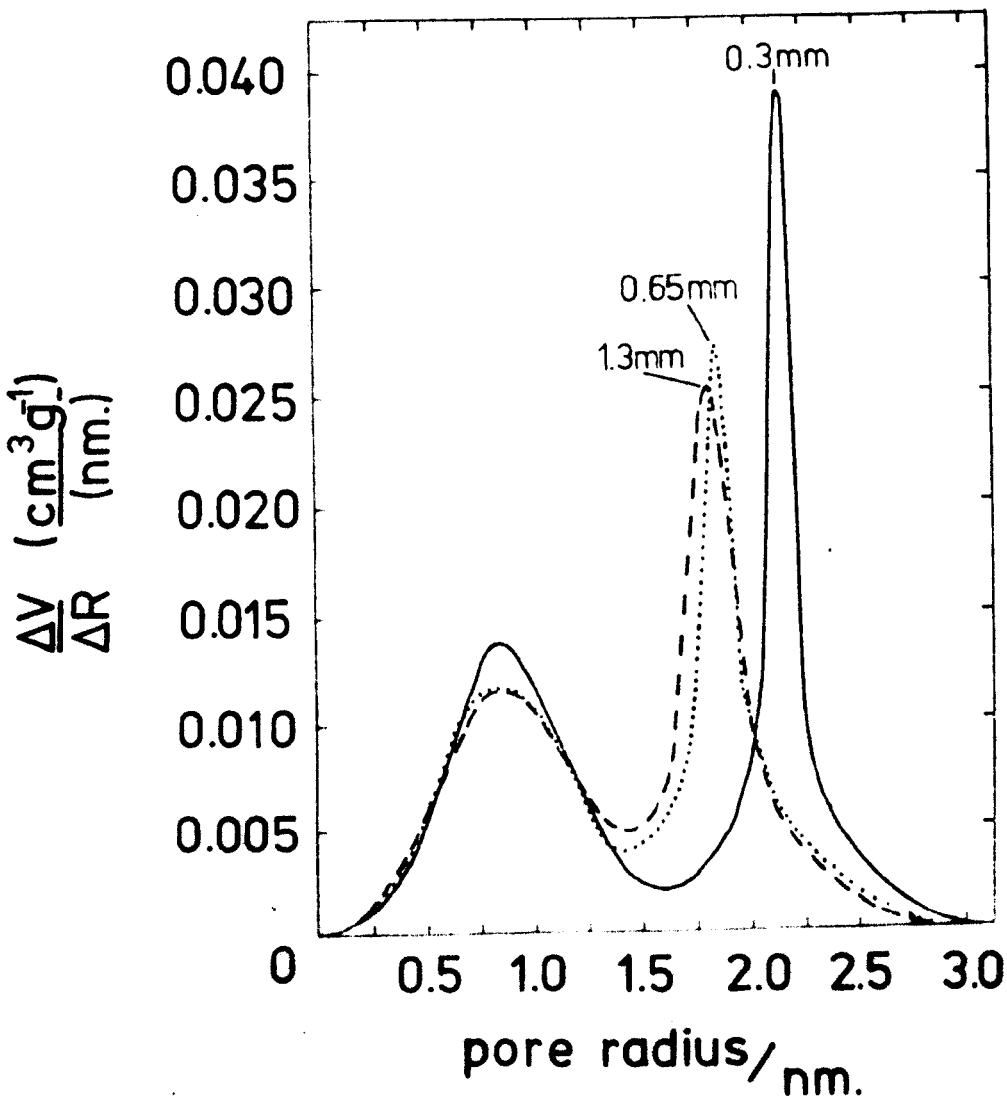

Figure 5.16 Extended pore size distributions of E-54 glass fibres fully leached in 30v/v% HCl solutions at 90°C

5.5 The effect of fibre composition

Porous skeletons could be obtained from all glasses having between 45 and 60% (by weight) SiO_2. Glasses with more than 60% SiO_2 exhibited almost negligible weight loss during leaching and those containing less than 45% SiO_2 dissolved leaving no visible reaction product. In figure 5.17 the weight losses of 0.3mm diameter fibres are shown after 4 and 8 hours as a function of the SiO_2 content for all the glasses investigated. The weight losses as a function of time are shown in more detail for glasses E-60, E-56.5 and E-0 in figure 5.18. These measurements could not be extended to the glasses containing less SiO_2 as these were extremely brittle and broke up during the measurements.

When fully leached, the pore volumes of glasses E-56.5 and E-60 were virtually independent of fibre diameter. The average pore volumes being 43% (by volume)for E-56.5 and 25% (by volume) for E-60. The surface areas of the leached fibres of both glasses apparently increased with fibre diameter. This increase was small, however, and not statistically significant. The average pore sizes of these two glasses as a function of fibre diameter are shown in figures 5.19 and 5.20.

The decreasing pore size with fibre diameter indicated in figures 5.19 and 5.20 refer to least squares data fits. These decreases were not, however, statistically significant. In figures 5.21 and 5.22, pore size distributions of examples of the two glasses are shown. Both show a peak in the distribution at pore radii of approximately 2nm. This is almost 20% higher than the mean

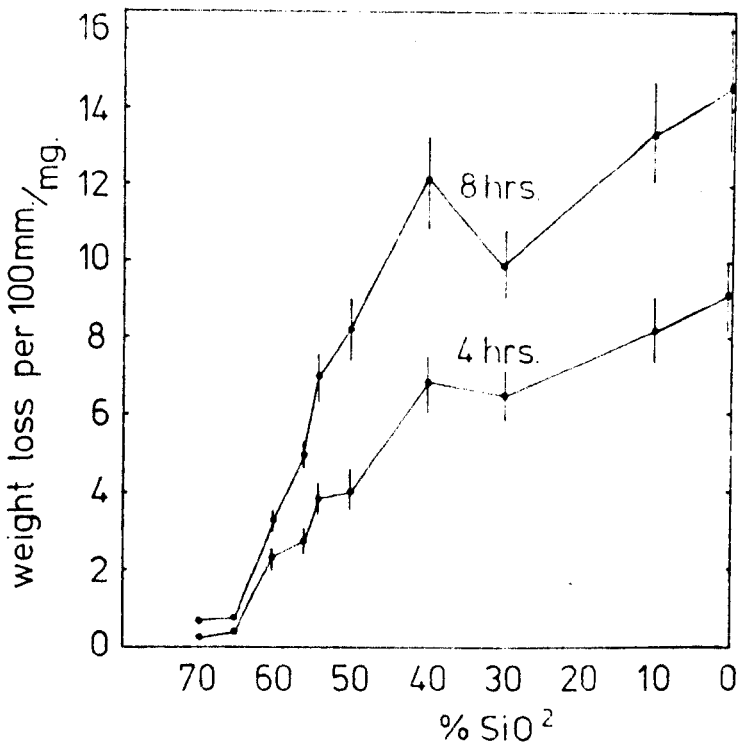

Figure 5.17 Weight loss of 0.3mm diameter glass fibres after 4 and 8 hours in leaching solutions of 30v/v% HCl at 90°C as a function of the SiO_2 content of the glass

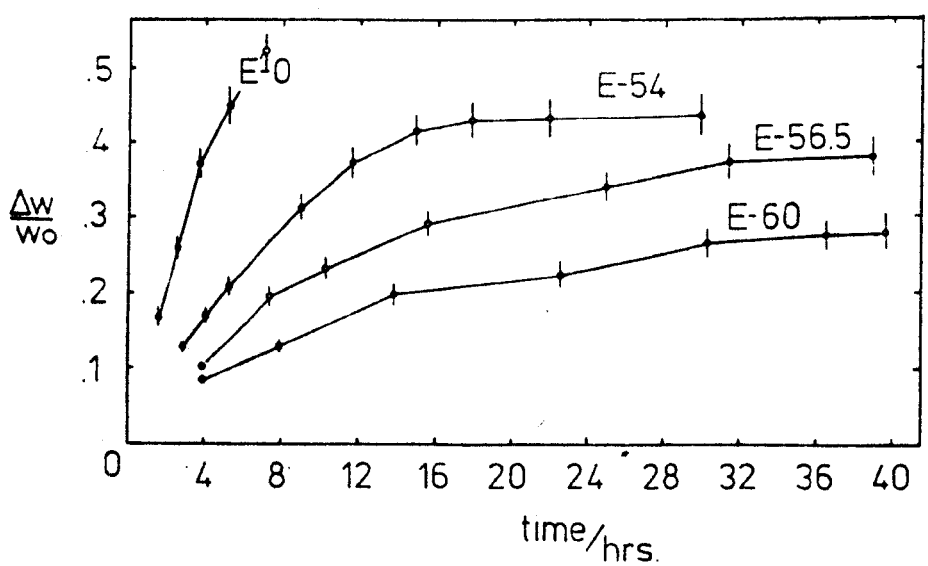

Figure 5.18 Weight loss of E-60, E-56.5 and E-0 glass fibres as a function of time in the leaching solutions of 30v/v% HCl at 90°C

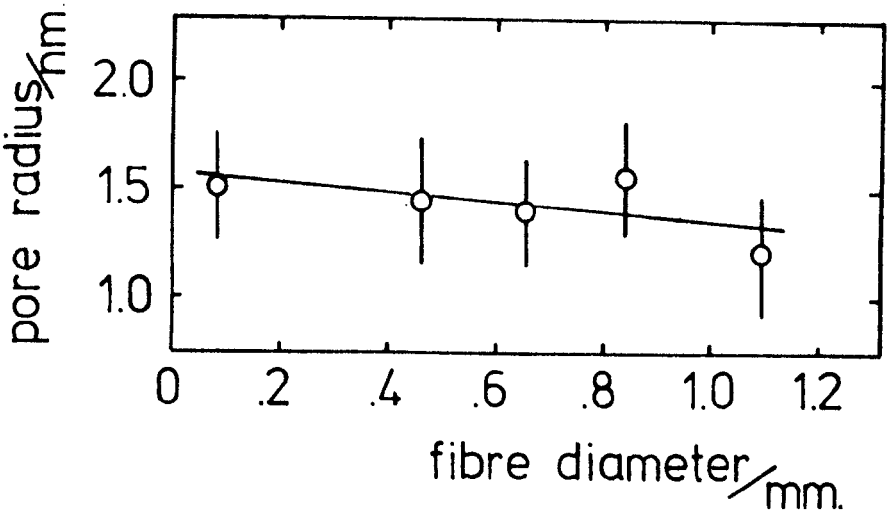

Figure 5.19 Mean pore size as a functionof fibre diameter for E-56.5 glass fibres fully leached in 30v/v% HCl solutions at 90°C

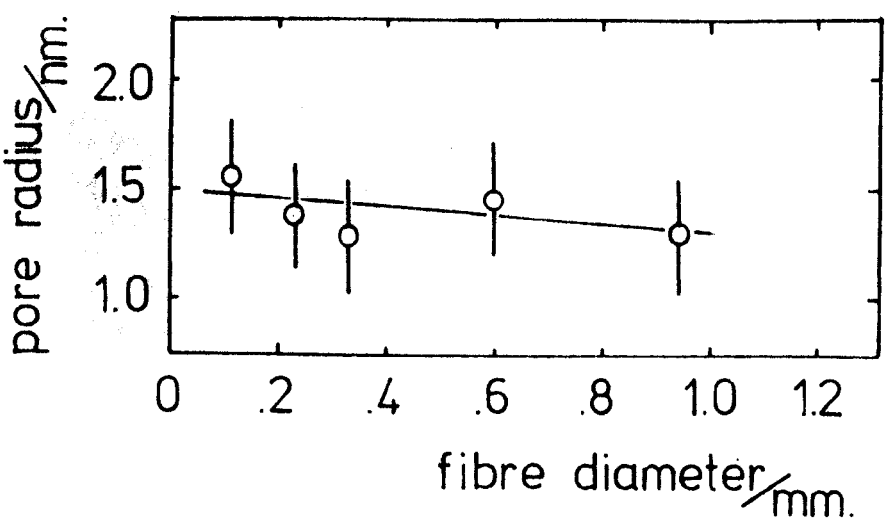

Figure 5.20 Mean pore size as a function of fibre diameter for E-60 glass fibres fully leached in 30v/v% HCl solutions at 90°C

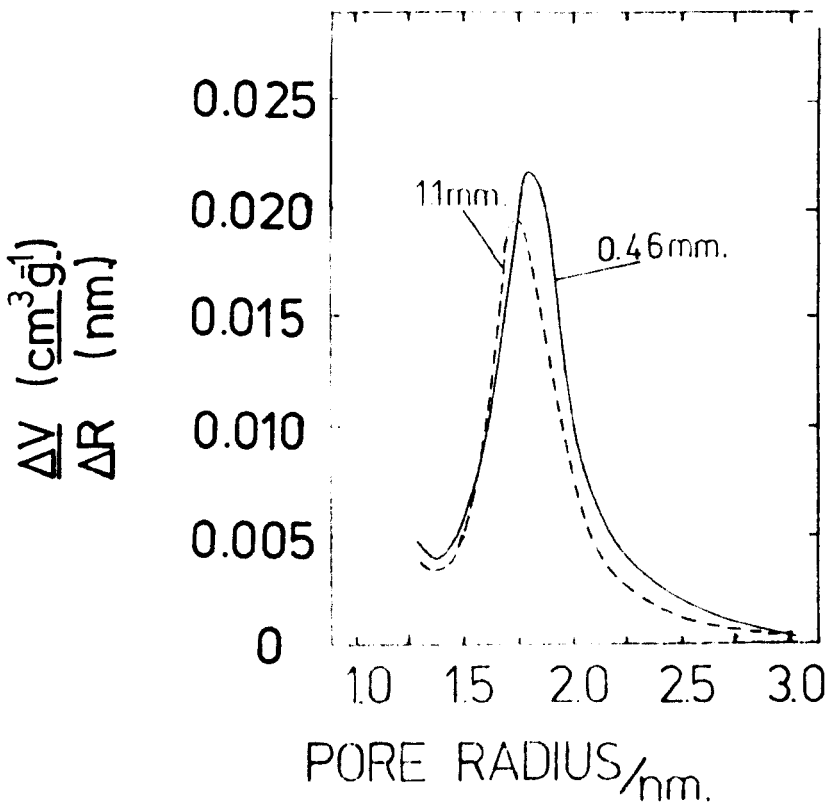

Figure 5.21 Two pore size distributions for E-56.5 glass fibres fully leached in 30v/v% HCl solutions at 90°C

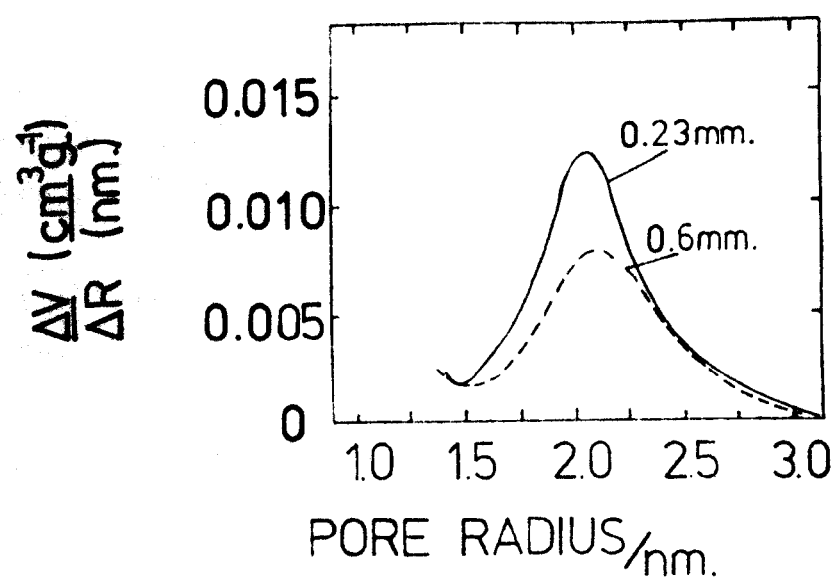

Figure 5.22 Two pore size distributions for E-60 glass fibres fully leached in 30v/v% HCl solutions at 90°C

pore size estimated from the total surface area and pore volume.

As with glass E-54, the pore volumes and surface areas accounted for in the pore size distribution analysis were less than the total pore volume and surface area. The differences were 45% in volume, 48% in surface area for glass E-56.5 and 40% in volume, 34% in surface area for glass E-60. As with glass E-54 this unaccounted for volume must relate to features of below 1nm in size and the measured distributions could be extrapolated to account for this.

Electron micrographs of the fully leached glass E-56.5 and E-45 are shown in figures 5.23 and 5.24 respectively. The average distances between the phases for these two glasses are shown in figures 5.25 and 5.26. As with glass E-54, the dimensions indicated by microscopy are in broad agreement with those of the gas adsorption measurements. The accuracy to which $\bar{r}$ (average distance between phases) could be measured was low and no correlation between the distance $\bar{r}$ and the fibre diameter was found.

5.6 The effect of leaching the porous glass in alkaline solutions

In alkali borosilicate based porous glasses there is much evidence of a silica based precipitate being present in the pores. If this is the case in these glasses under investigation, then a significant part of the measured surface area may be due to this precipitate. To investigate this some of the leached 0.3mm diameter glass was treated in 1n NaOH solutions at 20°C.

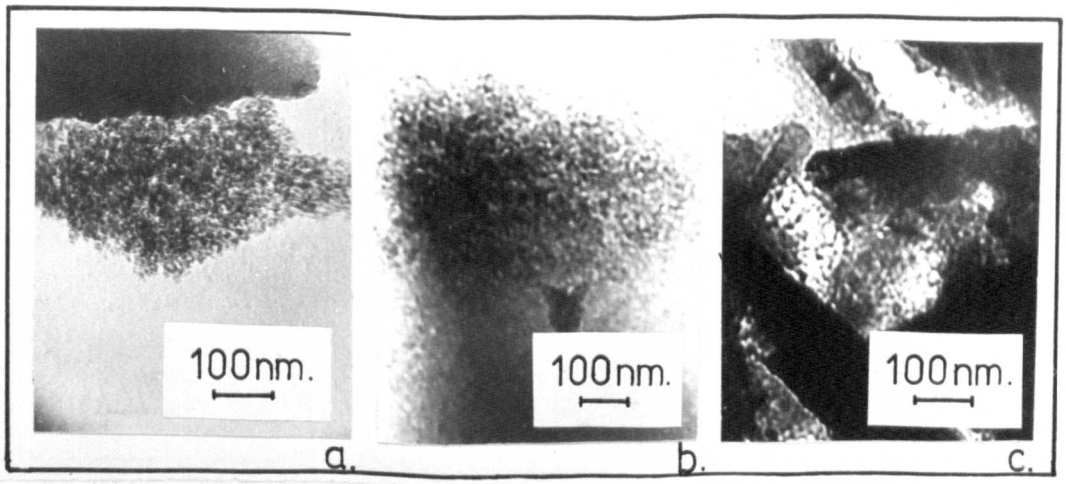

Figure 5.23 Transmission electron micrographs of E-56.5 glass fibres, fully leached in 30 v/v% HCl. solutions at 90°C. a: 0.19mm dia., b: 0.41mm dia., c: 0.70mm dia.

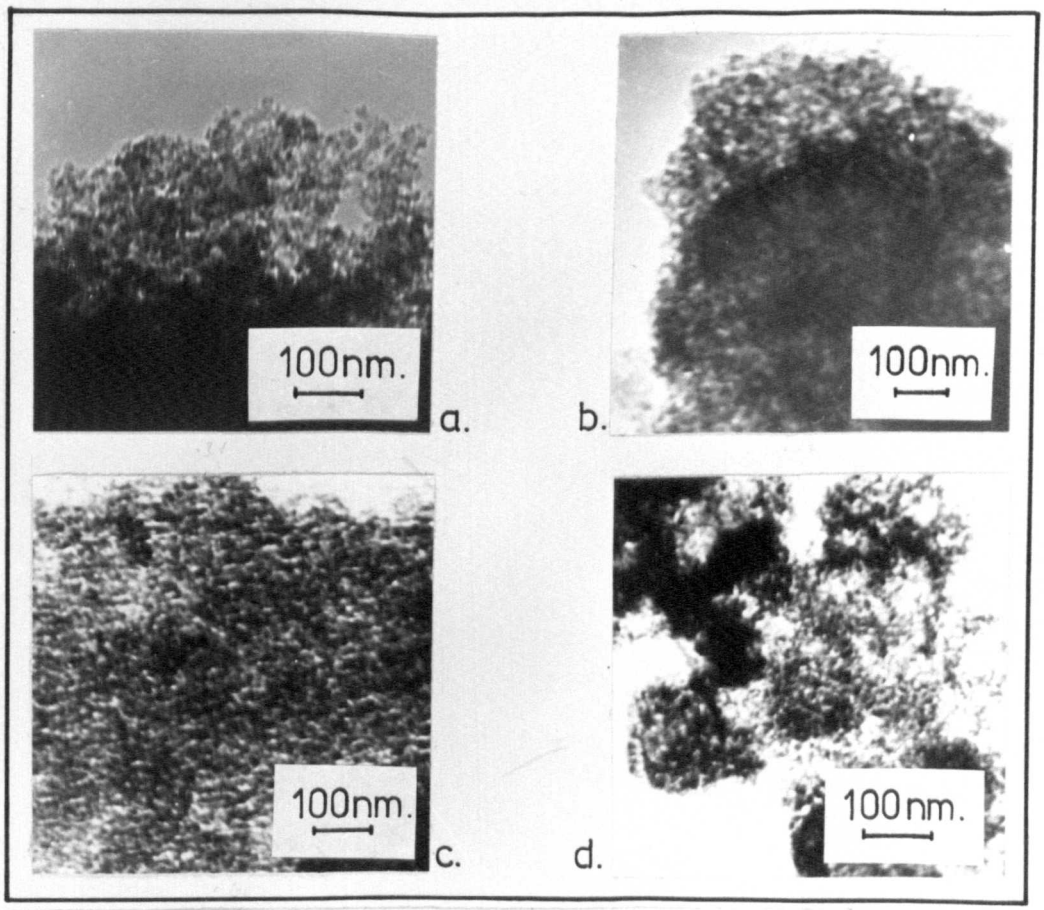

Figure 5.24 Transmission electron micrograph of E-45 glass fibres, fully leached in 30 v/v% HCl. solutions at 90°C. a: 0.31mm dia., b: 0.34mm dia., c: 0.66mm dia., d: 0.81mm d: 0.81mm dia.

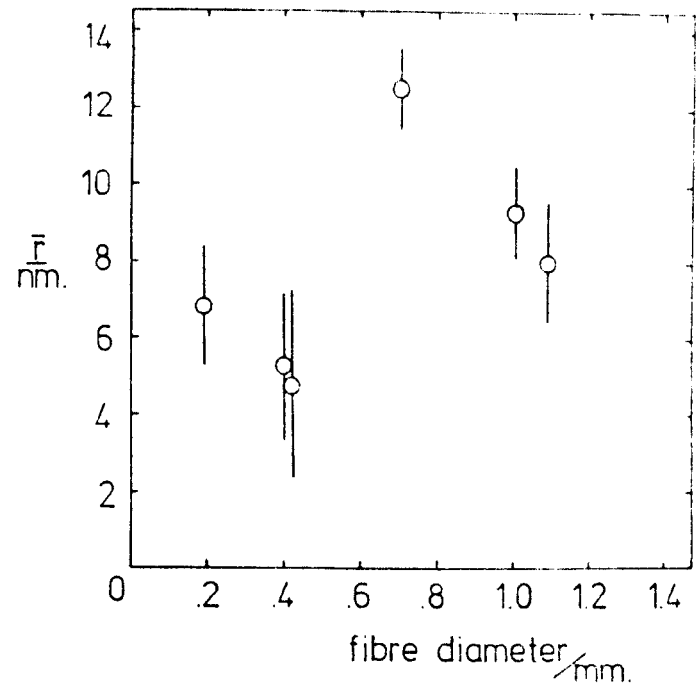

Figure 5.25 The average distance between phases as a function of fibre diameter for E-56.5 glass fibres fully leached in 30v/v% HCl solutions at 90°C

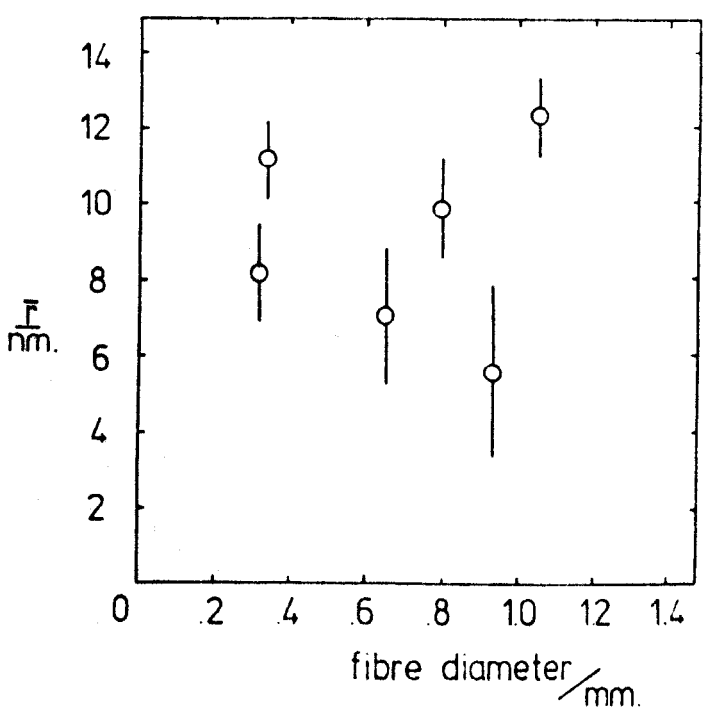

Figure 5.26 The average distance between phases as a function of fibre diameter for E-45 glass fibres fully leached in 30v/v% HCl solutions at 90°C

This treatment initially resulted in a decrease in the surface area and a small increase in the pore volume. The surface area as a function of treatment time in the alkaline solution is shown in figure 5.27. This is consistent with the finer features being fissures rather than particulate, as in the latter case, the void volume would initially increase rapidly. In figure 5.28 the pore size distributions before and after treatment for 2 hours are shown. The measured distributions have been extended to smaller pore size to account for the unmeasured volume and surface area. The unaccounted for surface area decreased with time in the alkaline solution, as can be seen in figure 5.27. The measured peak (~2nm radius) widened with treatment time, as would be expected if the alkaline solution was attacking the silica skeleton.

5.7 Summary of the leaching results

The leaching rate in all of the glasses investigated is strongly temperature dependent and only slightly dependent on the concentration of the acid solution. However, the concentration of the acid solution affected the final product and a strong acid solution was found desirable for the production of materials with an optimum surface area. Porous glass could be produced from parent glasses having between 45% and 60% SiO_2 (by weight), the pore volume of the porous glass being proportional to the SiO_2 content of the parent glass. The largest surface areas were produced by the leaching of thin (i.e. rapidly quenched) fibres which exhibited a narrow pore size distribution. Thicker fibres yielded a broader pore size distribution when leached, and the average pore size decreased as the

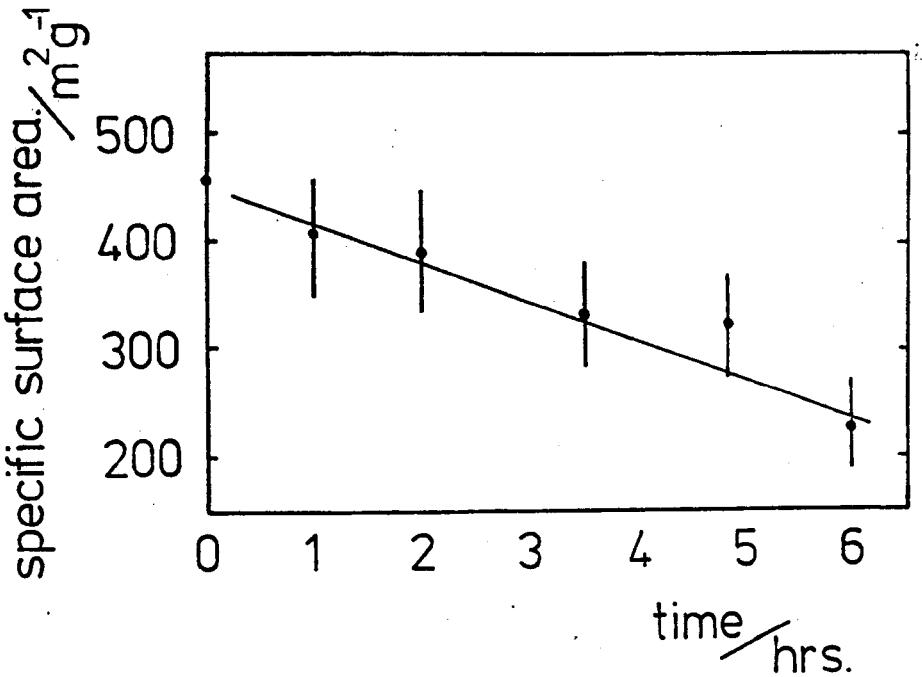

Figure 5.27 The surface area of fully leached 0.3mm diameter E-54 glass fibres as a function of time in 1n NaOH solutions at 20°C

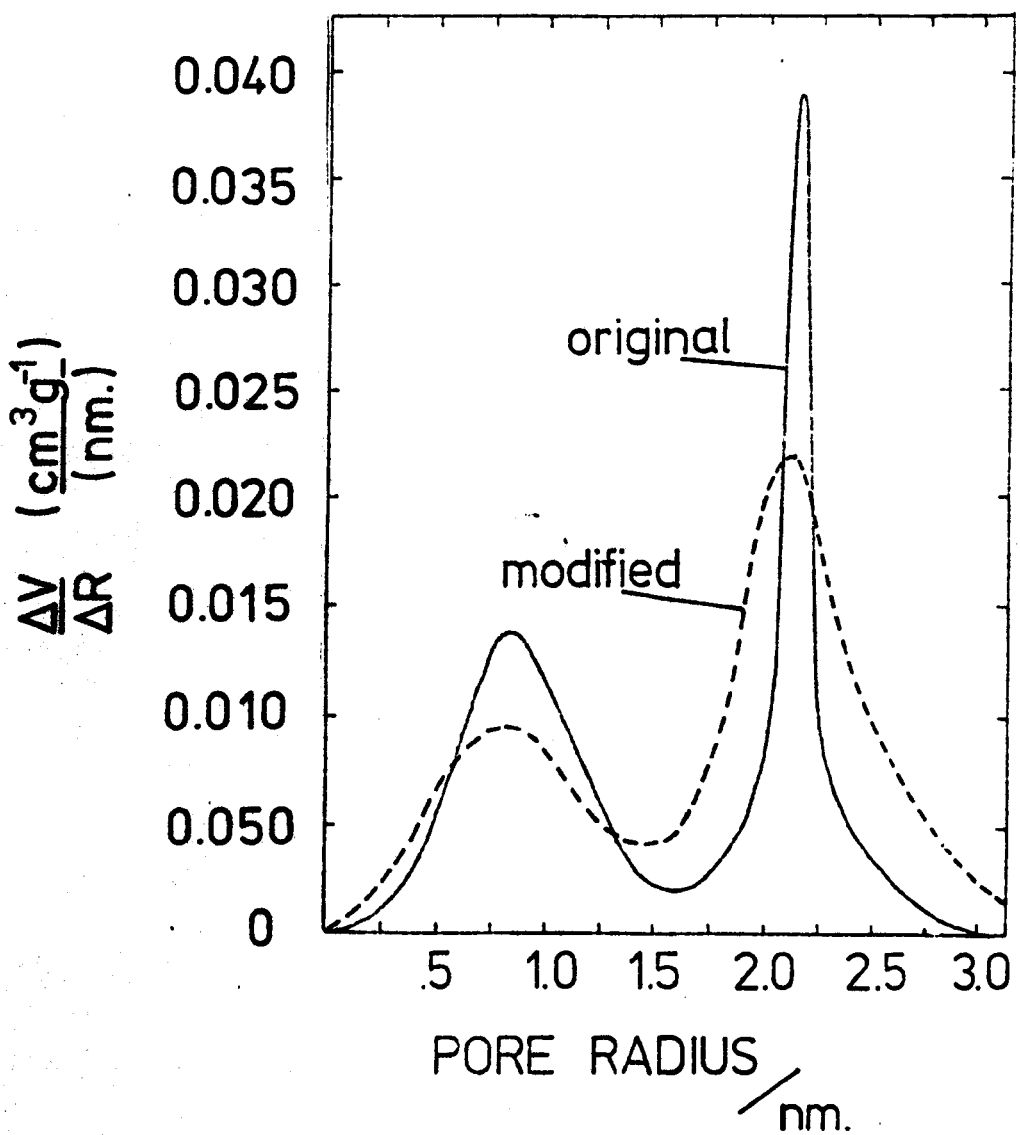

Figure 5.28 Extended pore size distributions of fully leached 0.3mm diameter E-54 glass fibres before and after treatment for 2 hours in 1n NaOH solution at 20°C

fibre diameter increased. There was evidence for the presence of features in the porous glass that were beyond the useful range of gas adsorption. These were not detected by electron microscopy, but the treatment of the leached glass in alkaline solutions indicated that these features were fine pores or cracks rather than a precipitate.

CHAPTER 6

Reverse osmosis measurements with porous glass membranes

6.1 Introduction

Most of the analysis techniques available to characterise fine structure can be applied to dry materials only, as is the case with the gas adsorption measurements and electron microscopy measurements used in this programme. The organic membranes used for reverse osmosis (r.o.) desalination undergo gross dimensional and chemical changes when dried, and, as a result of this, it is not possible to interpret their performance in terms of their structure. Porous glass is affected by the presence of water, but to a much smaller extent than are organic membranes. For that reason, it should be possible to relate desalination performance of porous glass membranes to the structure of the dry membranes. At the simplest level, the membrane might be expected to exhibit some salt rejection if the 'holes' are similar in size to the ions. This suggests a 'pore radius' of 0.1nm, but published work (section 1.5) indicates that membranes containing much larger pores reject salt. A hyperfiltration model of the salt rejection mechanism of porous glass membranes is described in this section.

The r.o. performance of several porous glass membranes was established, and these results are presented together with a detailed description of the experimental arrangement and conditions. Salt rejections as high as 55% were recorded at flux rates of $5 \times 10^{-4} m.h^{-1}$ with much higher fluxes at reduced salt rejections.

6.2 A hyperfiltration model of desalination with porous glass

A fresh silica surface is highly active and rapidly reacts with water to reduce its surface energy. This chemisorbed water layer is present on all aged silica surfaces and is responsible for a great many of the properties of this material. Chemisorbed water is also present on porous glass (Hair (1967)) and although the primary layer is far more strongly bound to the surface than subsequent water layers, these also show signs of a strong interaction with the glass. The properties of water in porous glass are, in general, slightly different to those of bulk water. The infra-red absorption spectrum of the water in porous glass has often been interpreted as indicating a modified water structure for some of the 'pore water' (e.g. Hair (1967)). The N.M.R. relaxation time of 'pore water' suggests that this is much more viscous than bulk water and the dielectric constant of 'pore water' is less than that of bulk water.

The extent of these effects is dependent on both the pore size and the amount of water present. This has resulted in the concept of bound water layers. These layers are considered to be present at the interface and, if the pore size is small, they make a significant contribution to the properties of the water/glass system. The extent of the modified water has been estimated to be larger than 10nm (Roberts and Northey (1972), but most of the available data suggest that bulk water properties are applicable at a distance of about 1nm from the interface.

The inclusion of this modified water into the porous-glass/saline-solution system makes it feasible to consider the desalination process of the membranes as an hyperfiltration action. This is illustrated in figure 6.1. Ions would be excluded from the bound water as its reduced dielectric constant makes it a less effective solvent. In figure 6.1, the interface between the bound water and the bulk water is shown to be clearly defined this is, of course, not the case and it is only intended to illustrate the situation schematically. From figure 6.1, the ions would be excluded from the membrane if the pore radius is of the order of (1nm+the effective radius of the ion).

In the crystalline state the anions and cations of NaCl are coordinated so as to minimise their electrostatic potentials. In aqueous solutions, water molecules will coordinate around the ions to effect a similar reduction in potential energy. Thus water is also bound to the ion and increases its size. The 'effective size' of the ion will, therefore, be its hydrated radius rather than its ionic radius. For one layer of water around the ion, the hydrated radius would be of the order of 0.3nm. The pore size required to exclude salt is, therefore, of the order of 1.5nm radius and significant rejection might be expected for pores of up to several nanometers in radius.

6.3 Experimental details

The reverse osmosis desalination performance of porous glass capillary membranes produced from three parent glasses was evaluated. The membranes were characterised by inert gas adsorption measurements, and

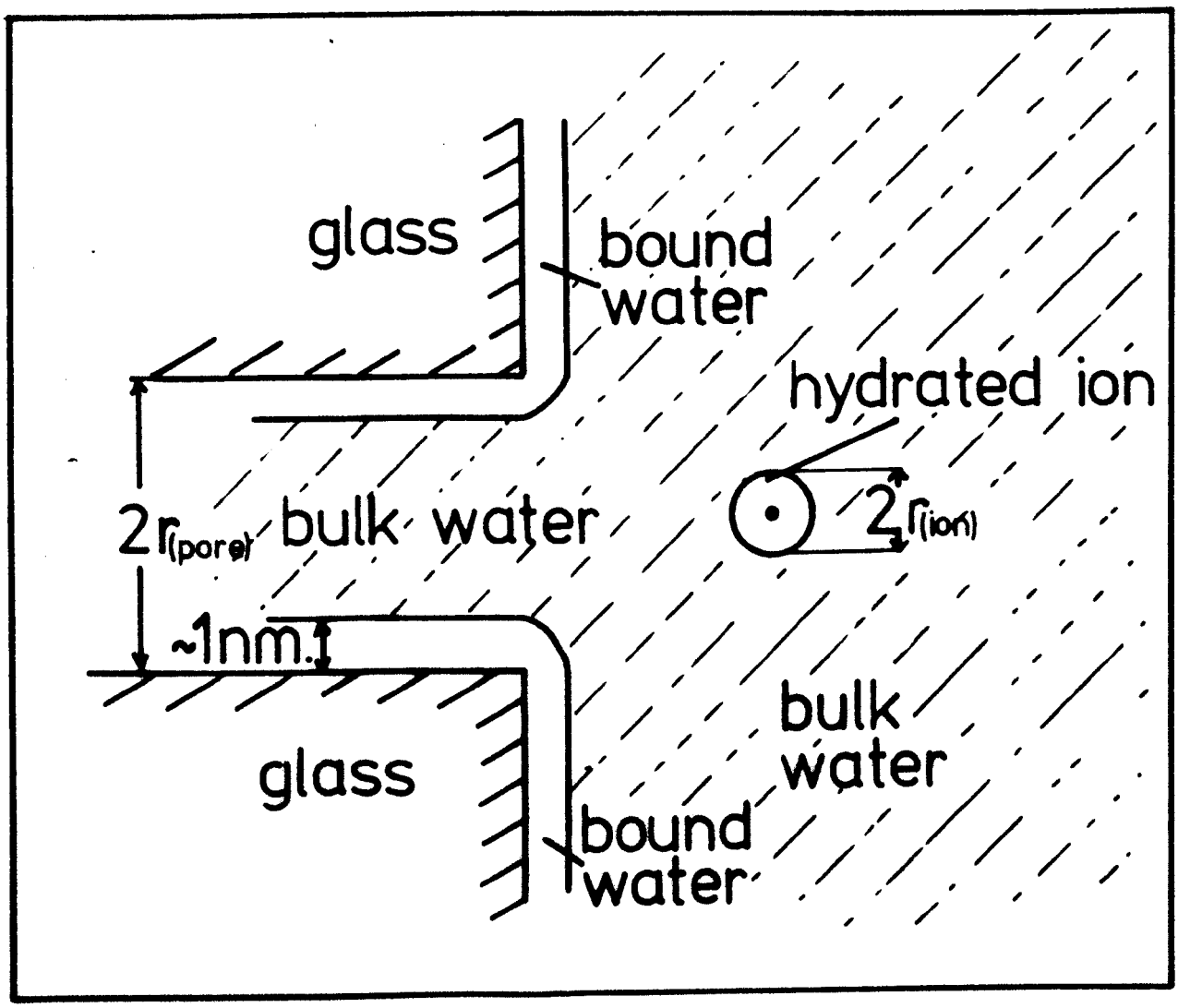

Figure 6.1 Schematic diagram, illustrating the importance of bound water in explaining the salt rejection of porous glass membranes

the r.o. performance evaluated using a single capillary membrane with the saline solution on the outside i.e. with the membrane under hydrostatic compression. The r.o. performance was characterised by establishing the salt rejection and the product flux rule.

6.3.1 Reverse osmosis test apparatus

This is shown schematically in figure 6.2 and consisted of the following items:

a. Metering pump:

This was a high pressure diaphragm pump system manufactured by Dia-Meter Limited of Liss, and consisted of an actuator pump and a metering head. The actuator pump (Model B60) supplied a reciprocating pressure to the metering head (Model MP3) which both circulated and pressurised the feed solution. The metering head was constructed of 316 stainless steel, employed a p.t.f.e. diaphragm and ceramic ball valves

b. Pressure gauge:

A Bourdon gauge manufactured by Gauges Bourdon of Blackpool was used to measure the system pressure. This was fitted with a p.t.f.e. isolation diaphragm and registered pressure via an intermediate hydraulic fluid. All parts in contact with the saline feed were of 316 stainless steel or p.t.f.e..

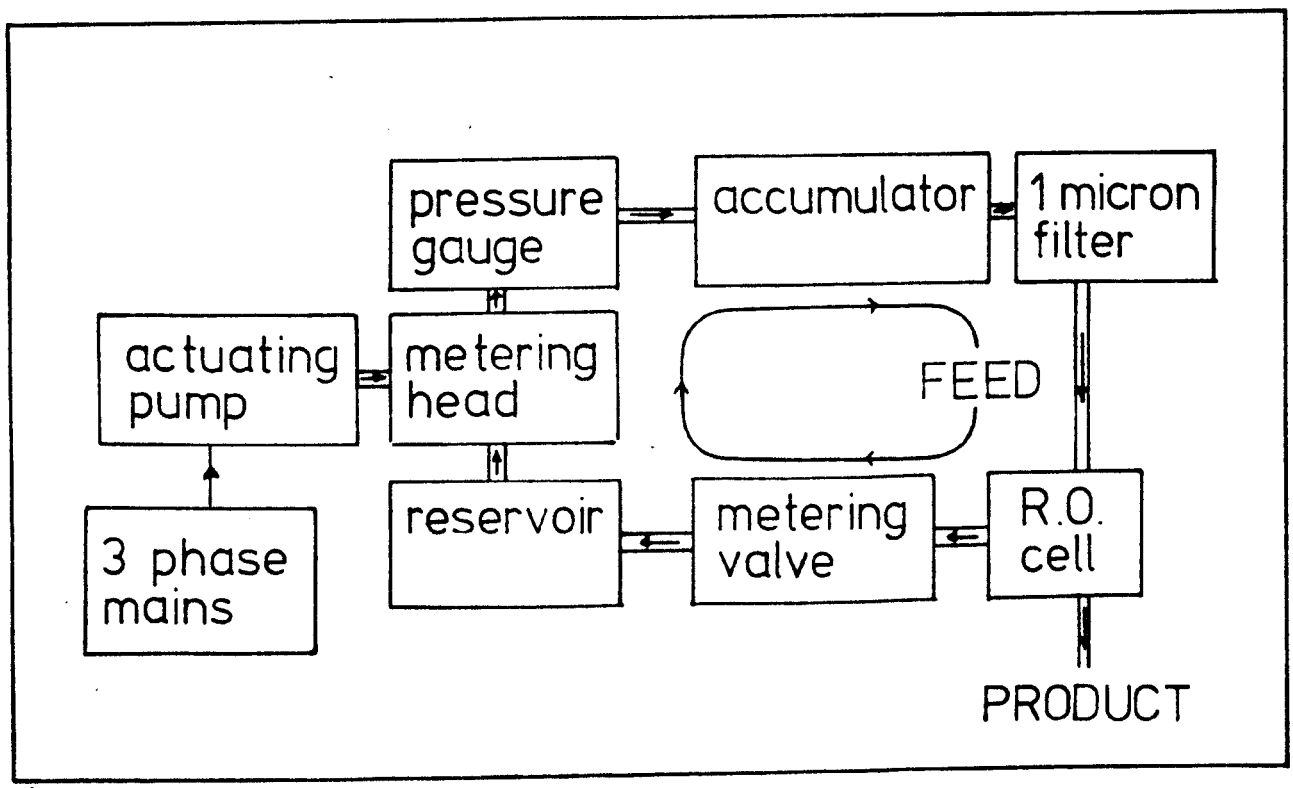

Figure 6.2 Schematic diagram of the reverse osmosis test rig

c. Accumulator:

A Greer-Mercier hydropneumatic accumulator was used to smooth the oscillating pressure supplied by the metering head. Unlike common hydraulic accumulators in the Greer-Mercier system, the gas cushion is contained in a neoprene isolation bag, making it suitable for fluids which show high gas solubilities e.g. aqueous solutions. The particular accumulator used was manufactured by Fawcett Engineering of Bromborough, and was supplied for use with corrosive fluids. The body of the accumulator was protected by a plastic coating and the majority of the inlet port fittings were of an unspecified stainless steel. A phosphor bronze spring was incorporated in the inlet port however, and this was suspected of being a source of the metal oxide contamination detected on the membranes after evaluation.

d. Filter:

To protect the porous glass membrane and the metering valve (item f) a sintered 316 stainless steel filter was included in the circuit. This was manufactured by Hoke Incorporated of New Jersey, and prevented the passage of particles greater than lum in diameter.

e. Reverse osmosis test cell:

This was constructed of 316 stainless steel in

the Physics Department and is shown in cross section in figure 6.3. The cell consisted of a main body, high pressure inlet and outlet ports and the membrane mounting assembly. All seals were by Viton 'O' rings or p.t.f.e. gaskets. The fluid entry port was arranged to encourage turbulent flow in the cell and so reduce concentration polarisation. The membranes were sealed into the mounting plug with epoxy resin as shown in figure 6.4. The exposed end of the hollow fibre membrane was also sealed with epoxy resin.

f. Micro-metering valve:

A needle valve was used to provide the resistance to flow necessary to obtain the high operating pressure. The valve used was manufactured by the Whitley Company of Cleveland, Ohio, and was supplied for use with corrosive fluids. Although the body of the valve was of 316 stainless steel, the needle was of 303 stainless steel and was another source of oxide contamination.

g. Reservoir:

This was a loosely covered Pyrex beaker of 2 litre capacity.

The individual components were connected with 316 stainless steel seamless tubing (¼" O.D., 1/10" wall thickness) and commercial (Swagelok and Gyrolok) 316

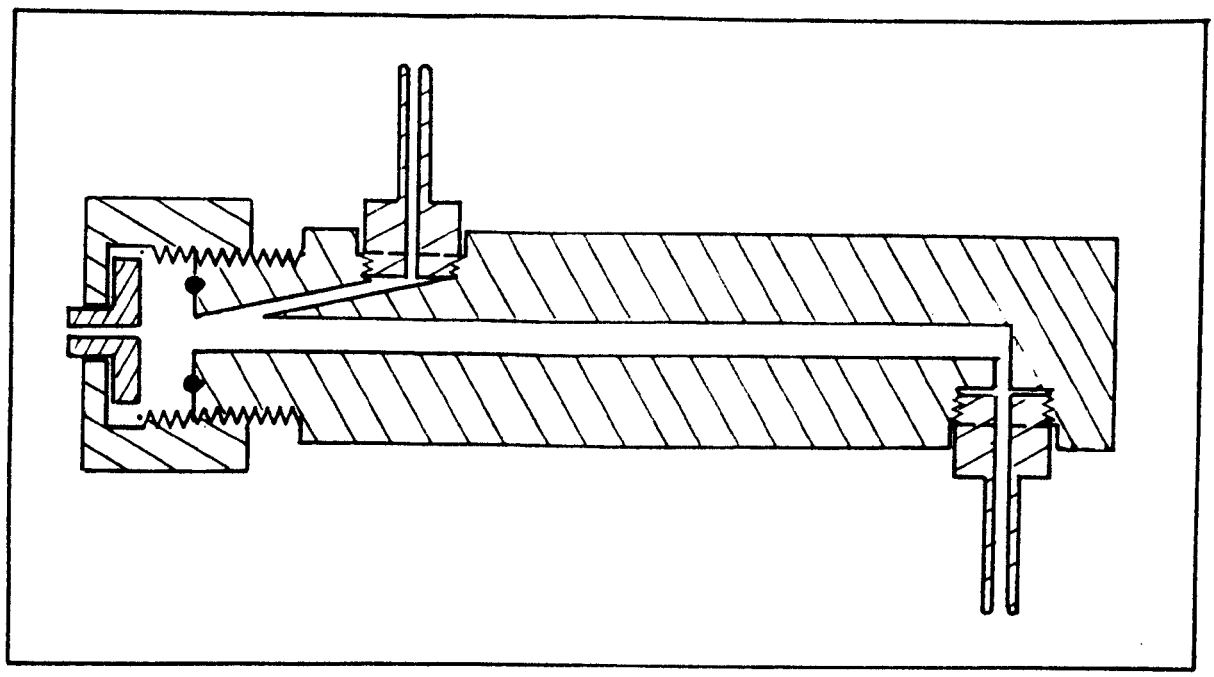

Figure 6.3 Sectional diagram of the reverse osmosis cell

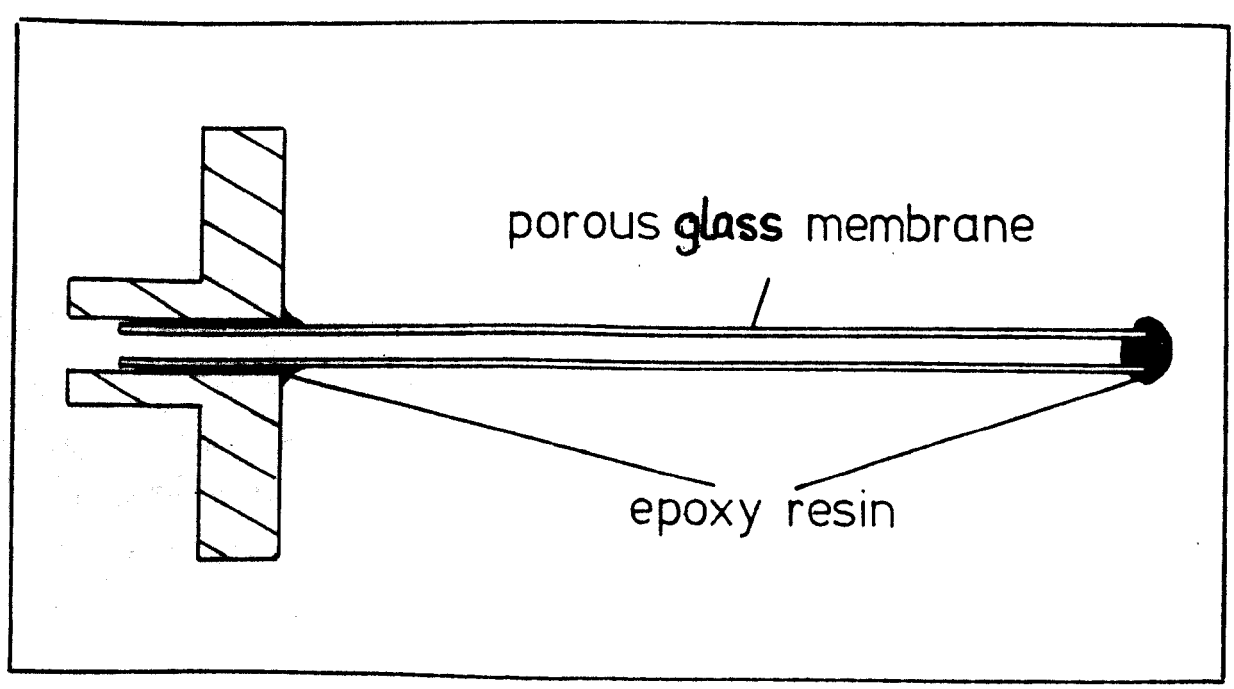

Figure 6.4 Schematic diagram illustrating the mounting and sealing of the porous glass membranes

stainless steel high pressure tube couplings.

6.3.2 Operating conditions

All measurements were undertaken using a 3.5wt. % (35,000p.p.m.) NaCl solution. This is the industry standard for the evaluation of seawater desalination processes. The operating pressure was maintained at 7.0 MPa to provide a positive driving pressure for reverse osmosis of 4.3 MPa. The maximum available feed rate of 3×10^{-3} l.s^{-1} was used for all measurements.

The temperature of the system fluid was observed to increase during operation. No attempt was made to control this and after about one hour the cell temperature stabilised at approximately 35°C

6.3.3 Analysis of the product

The two parameters of primary interest were the salt rejection and the product flux. The salt rejection is defined as

$$R(\%) = ((Cf-Cp)/Cp) \times 100 \qquad 6.1$$

where Cf is the feed salt concentration in weight % and Cp is the product concentration in weight %. The salt concentrations were determined from the direct measurement of the sodium ion concentration using a sodium sensitive electrode. The combination electrode used (Model 96-11) was manufactured by Orion Research Incorporated of Cambridge, Massachusetts. This electrode can operate on liquid volumes of 10µl (half a drop) and was selected for that reason. The electrode was operated with a Vibron electrometer (model 46-A)

The product flux was estimated by timing the filling of thin transparent plastic tubing. This method was used as evaporation losses are extremely small owing to the small exposed surface, and as high sensitivities are possible with thin tubing. With the tubing having the finest bore, 10ul represented over 10mm of filled tubing. The accuracy of the flux measurements was of the order of ±10% owing to non-uniformity of the tubing used and the presence of air bubbles in the filled sections.

6.3.4 Porous glass membranes

Hollow fibre porous glass membranes were used for all of the reverse osmosis desalination measurements. The membranes had outer diameters of between 500 and 1300μm, wall thicknesses of between 70 and 260μm and were typically of 120mm length. The parent hollow fibres from which the membranes were produced, were drawn directly from the glass melts and were not subjected to any further heat treatment prior to leaching.

On the basis of the results of the measurements on solid fibres, three glasses were selected as being potentially useful for reverse osmosis desalination. Although all of the glasses from which integral skeletons were obtained possessed pores of the correct size (~2nm radius), most were either mechanically very weak or did not have a large pore volume. The three parent glasses selected as being potentially suitable were E-56.5, E-58 and E-60. These were leached in HCl solutions at 85°C. For glasses E-56.5 and E-58 a 30 v/v% solution was used and these glasses were

fully leached (i.e. attained constant weight) in 36 hours. For glass E-60, 20v/v% HCl solutions were used and this glass was fully leached in 48 hours. The hollow fibres were leached in groups of about 10, corresponding to a single 'draw' of the parent glass. These were of similar dimensions and consequently, were all leached in similar times. Following leaching, the porous membranes were washed in several changes of doubly distilled water and stored under water until required.

During the reverse osmosis desalination measurements the membranes slowly became contaminated with organic and inorganic materials. Over a short term (~5 hours) this did not appear to significantly alter the r.o. properties of the membranes. This contamination, however, prevented the gas adsorption characterisation of the membranes used in the r.o. studies. In a few cases the pore size distribution of the membrane was estimated from the gas adsorption characterisation of a length of porous glass broken from the end of the membrane prior to the r.o. measurements. In most cases this was not possible, as the hollow fibres broke, too near the minimum practical length for r.o. characterisation, during the leaching and washing stages. In these instances, the gas adsorption measurements were performed on an externally identical section of membrane leached in the same operation. This was part of the same parent glass 'draw' and it was assumed that the pore size distribution in that section was similar to that of the section actually used as a membrane. The pore size distributions are included as appendix 3.

The majority of the reverse osmosis desalination measurements were undertaken with membranes produced from glass E-56.5. For the membranes produced from this

glass there was little correlation between the outside diameter of the fibre and the median pore size which was between 1.8 and 2.1nm for all of the membranes evaluated. The pore volume was dependent on the composition of the parent glass as was found for the solid fibres. The pore volume of the membranes produced from glass E-56.5 was 43±3v/v%, from glass E-58 this was 38±3v/v% and from glass E-60 the pore volume was 25±2v/v%.

6.4 Results of the reverse osmosis measurements

All of the membranes were discoloured as a result of the r.o. desalination experiments. This discolouration was considered to be due to metal oxide contamination although this was not conclusively established. Ferric ions can act as a dynamic membrane (i.e. a membrane that exists only when the conditions are suitable) and show salt rejection. The contribution that the metal oxide contamination may have made to the measured salt rejection was assumed to be negligible. This was considered reasonable as the salt rejection was approximately constant during the evaluation of a membrane, but the discolouration (and hence the amount of metal oxide present) increased steadily during the evaluation period.

The results of the r.o. desalination measurements are summarised in tables 6.1, 6.2 and 6.3. The highest salt rejections were of the order of 50%, and were shown by membranes of E-56.5 glass. The flux rate was generally inversely related to the rejection coefficient. This is illustrated in figure 6.5 for the data concerning membranes produced from E-56.5 parent glass.

Table 6.1 The r.o. performance of E-56.5 based membranes

No.	DIMENSIONS		flux m.hr^{-1}	rejection %
	O.D. mm.	wall thickness um		
1	1.25	170	25 ± 5	10
2	1.15	120	25 ± 5	15
3	1.10	150	12 ± 2	20
4	0.75	70	1 ± .5	40
5	1.20	100	30 ± 2	10
6	0.80	260	3 ± 1	35 ± 5
7	0.75	100	.5 ± .3	55 ± 5
8	0.75	70	2 ± .5	35 ± 5

Table 6.2 The r.o performance of E-58 based membranes

No.	DIMENSIONS		flux m.hr^{-1}	rejection %
	O.D. mm.	wall thickness um		
9	1.30	150	22 ± 2	7 ± 3
10	1.50	200	31 ± 1	8 ± 2
11	1.30	150	38 ± 2	10 ± 2
12	0.90	150	25 ± 1	10 ± 2
13	0.90	100	19 ± 1	10 ± 1

Table 6.3 The r.o. performance of E-60 based membranes

No.	DIMENSIONS		flux m.hr^{-1}	rejection %
	O.D. mm.	wall thickness um		
14	0.5	200	---	20 ±10
15	0.9	150	.2 ± .2	15 ± 5
16	0.9	150	1 ± .5	20 ± 5

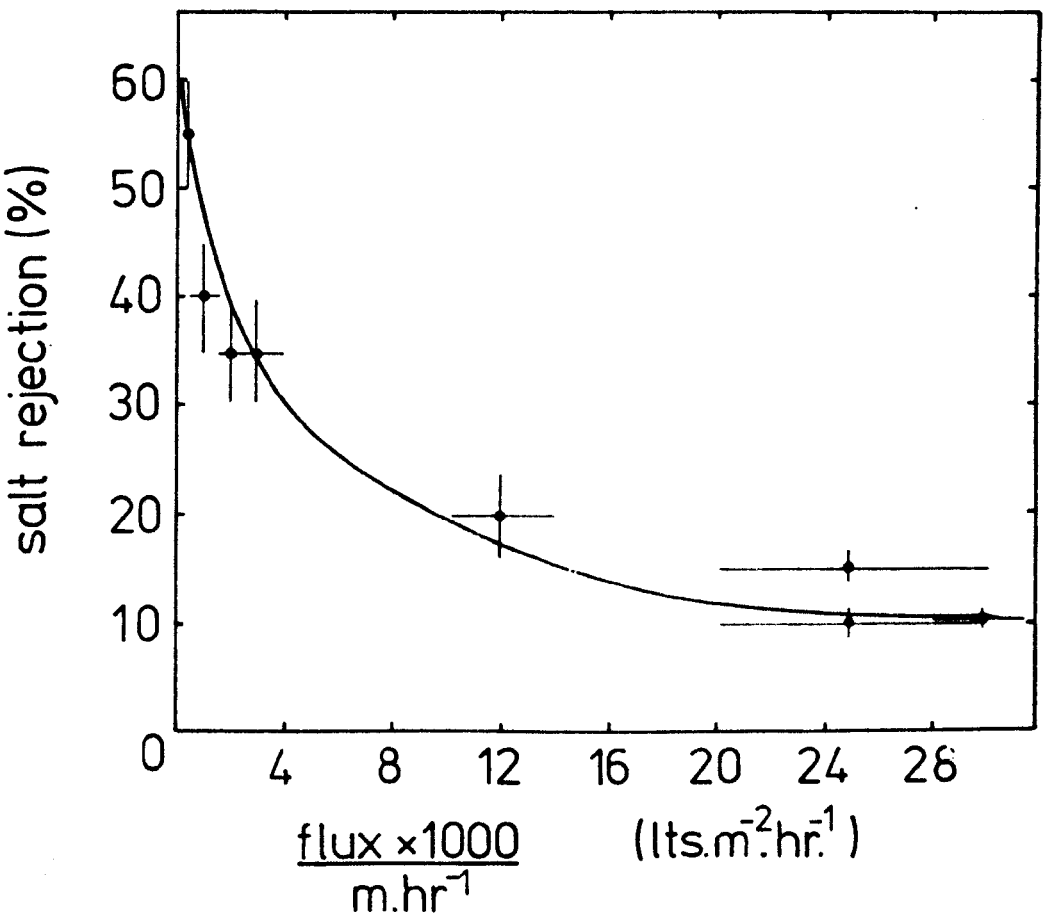

Figure 6.5 Salt rejection vs. flux rate for membranes produced from parent glass E-56.5

The pore size distributions of porous glass broken from the end of membranes 1 and 4 are shown in figure 6.6 The smaller median pore size of membrane 4 (1.85nm cf 2.05nm) is consistent with the higher salt rejection if a hyper filtration model is applicable. This was not the case for all of the membranes. In figure 6.7 the salt rejection is shown as a function of the median pore size for the E-56.5 based membranes. These two parameters show some correlation (a correlation coefficient of 0.86) but this is not strong.

6.5 Discussion of the r.o. measurements

As only a limited number of r.o. measurements were made, a rigorous statistical analysis is not possible. However, a few conclusions can be tentatively drawn from these results.

Although the salt rejection did not show a conclusive correlation with the median pore size (figure 6.7), the data obtained in this investigation are in broad agreement with the results of published work on the r.o. performance of porous glass membranes. This is illustrated in figure 6.8. In the few cases where the pore size was estimated from a section of the membrane rather than a similar membrane, the relationship between median pore size and salt rejection is much clearer. These points are shown circled in figure 6.8.

As most of the measurements concerned membranes produced from glass E-56.5, the effect of changing the glass composition is not clear. The one feature apparent is that membranes of glass E-60 exhibited a much lower flux than membranes produced from the other two parent glasses. As the median pore size was not very different in the E-60 membranes, this

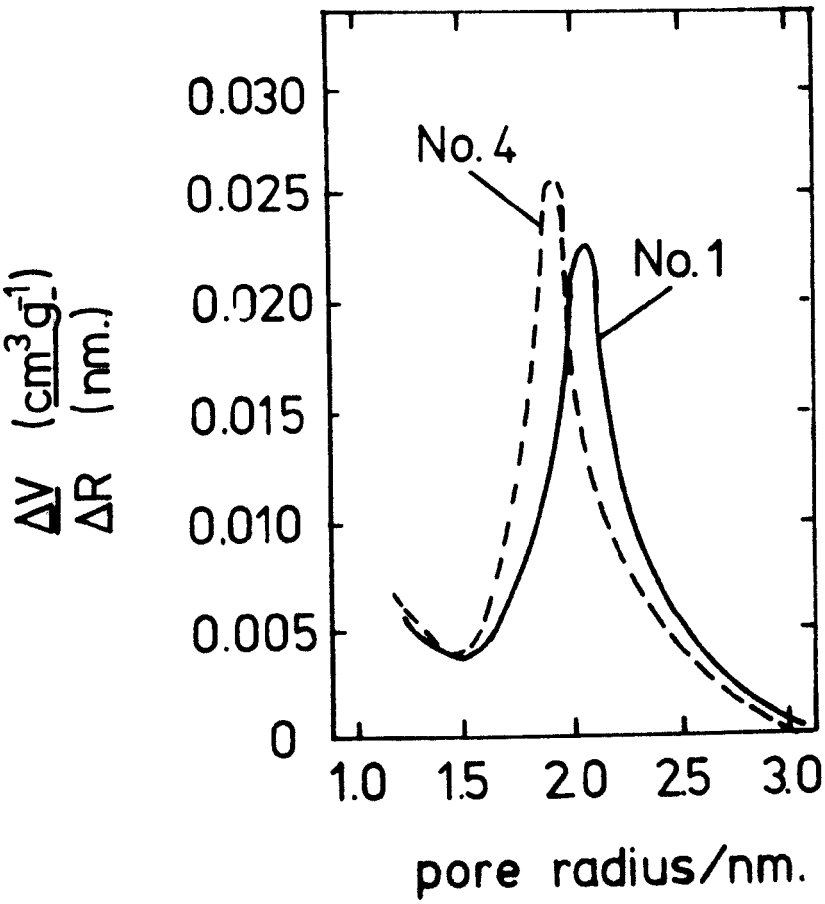

Figure 6.6 Pore size distributions for membranes nos. 1 and 4

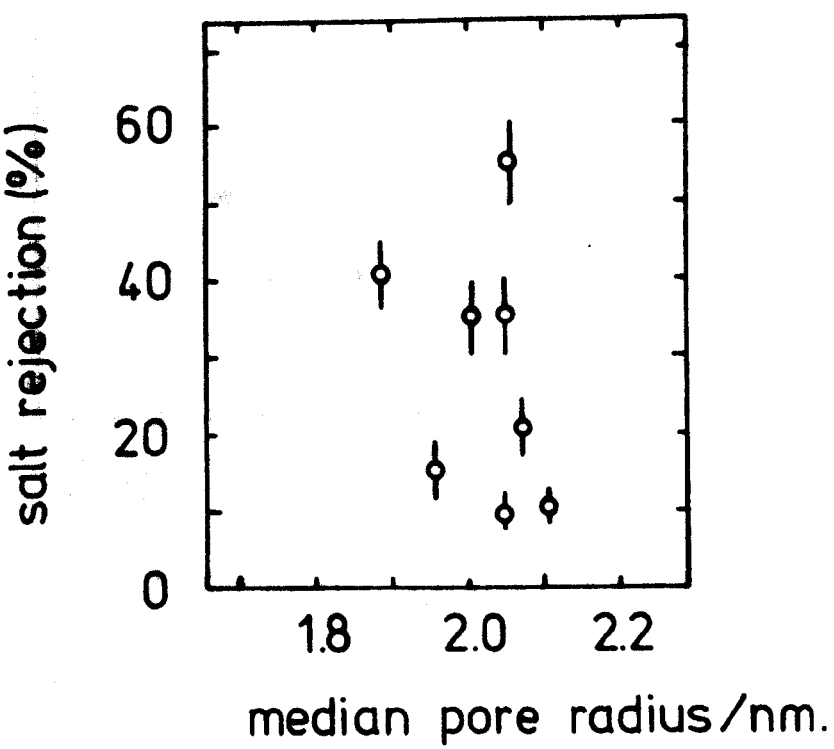

Figure 6.7 Salt rejection vs. median pore size for membranes produced from parent glass E-56.5

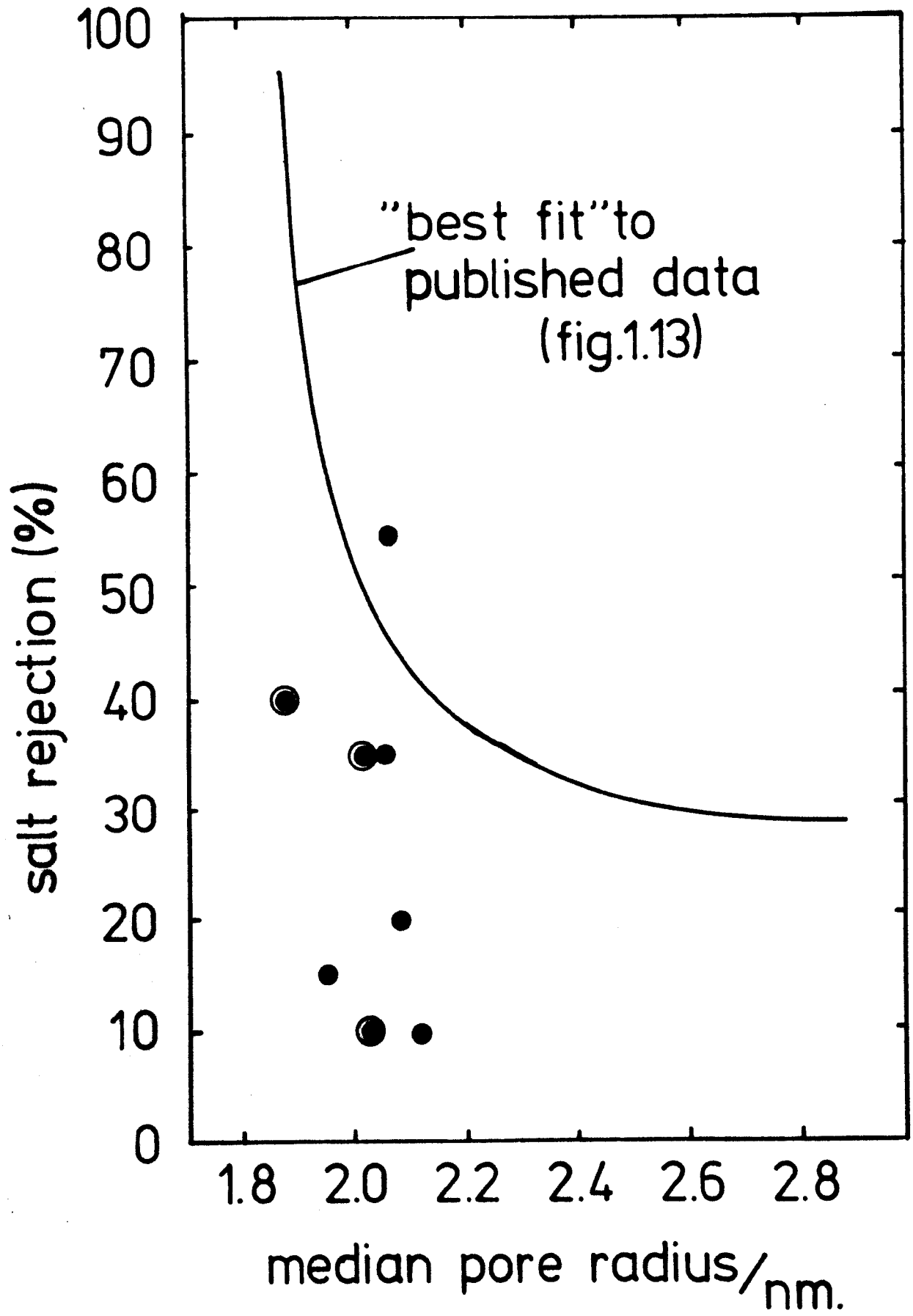

Figure 6.8 Salt rejection vs. median pore size (taken from figure 6.7 and published data referenced for figure 1.3)

reduced flux is probably related to the lower pore volume of E-60 membranes.

The clearest correlation determined was that between the product flux rate and the salt rejection coefficient (figure 6.5). This is as would be expected, and although it is predicted by the hyperfiltration model, it is compatible with all other models of reverse osmosis desalination.

In conclusion, it has been shown possible to manufacture porous glass membranes, showing some useful reverse osmosis properties from some of the glasses under investigation and these can be produced without the need for isothermally heat-treating the parent glass.

CHAPTER 7

Discussion of the results, conclusions and proposals for future work

7.1 Introduction

In this section the results of the investigation into the parent glasses, and the leaching of those glasses are discussed. The rapid development of the phase separated structure has prevented any information with regard to the exact decomposition mechanism being obtained. However, it is clear from the measurements made that the continuous cooling thermal history of these glasses has an effect on the morphology of the porous skeletons produced, and consequently, also affects the phase separated morphology of the parent glasses.

7.2 Physical properties of the parent glasses

The results of the cooling rate measurements made in this investigation (section 4.4) indicate that glass fibres quench at a rate inversely related to the diameter. As commercially manufactured E-glass fibres are typically of 10μm diameter, they cool very much more rapidly than the thicker fibres produced in this investigation. Commercially manufactured fibres can be leached to yield coherent porous silica skeletons and so must be phase separated into mutually interconnecting phases; one of acid insoluble silica and the other an acid soluble residue. As a phase separated melt would characteristically be separated on a coarse scale due to its fluidity, the fine scale of phase

separation obtained in commercial fibres must be the result of separation during cooling.

The cooling rates reported in section 4.4 show that thick glass fibres quench at a rate proportional to the fibre (diameter)$^{-1.5}$. This is similar to the result of Arridge and Priors (1964) measurements in which it was estimated that the rate was proportional to the fibre (diameter)$^{-1.8}$. Anderson (1958) predicted the rate to be proportional to the fibre (diameter)$^{-2.5}$, but as was pointed out by Glicksman(1968), Anderson used the thermal conductivity of glass rather than that of air in his calculations. As Newton's law of cooling is obeyed,the surface temperature of the fibre cannot be very different to the 'core' temperature, so it is the thermal conductivity of air that limits the process. The measured effect of drawing velocity however, is in closer agreement with Anderson's theory. He predicted that the quench rate should be proportional to the drawing (velocity)$^{0.5}$ and the measurements made here suggest a rate proportional to (velocity)$^{0.7}$.

In figure 7.1, the temperature of a 10μm diameter fibre as function of time is shown together with that of a 500μm diameter fibre. These data were obtained by extrapolation of the cooling rate measurements reported in section 4.4. As can be seen from figure 7.1, the time available for the thicker fibre to phase separate is of the order of 100 times that available to the commercial fibres. It is not suprising that the thick E-glass fibres produced in this investigation (glass E-54) could be leached to yield coherent porous skeletons and so were also phase separated.

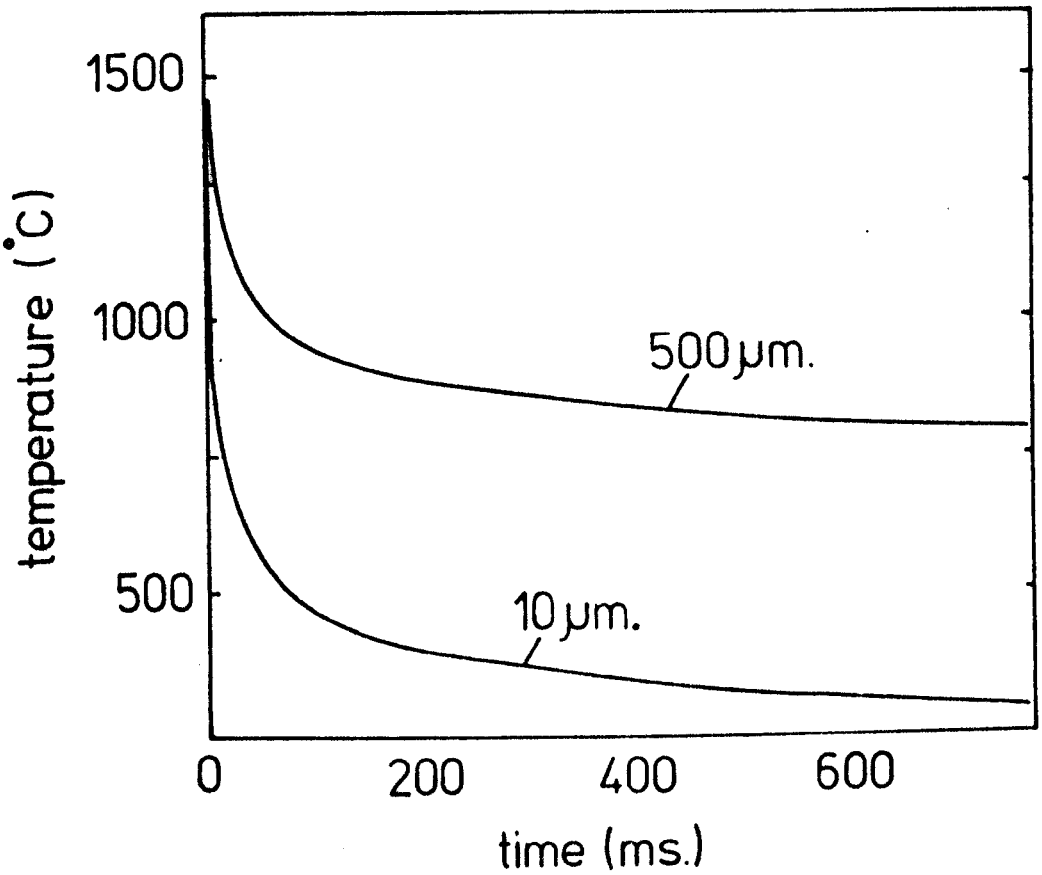

Figure 7.1 The cooling of 10μm and 500μm diameter fibres (by extrapolation of data on 90μm to 200μm fibres)

The critical (immiscibility) temperature for glass E-54 could not be established by opalesence measurements, but this glass exhibited an inflection in its electrical resistivity at (1040 $\pm$ 10)^{o}C (section 4.2). Similar inflections were found in all of the glasses for which resistivity measurements were made and in the two instances where opalescence measurements were successful, the inflection temperature was close to the critical temperature (section 4.5). As such an inflection is consistent with the effect of phase separation on the proposed conductivity mechanism (section 4.5), these inflections are considered to define the critical temperatures of the glasses.

In simple binary systems, the spinodal line can be estimated from the metastability line by using the 'root 3 rule' (Cook and Hilliard (1965)). This rule exploits the geometrical relationship between the two line and has the form

$$Cs - Cm = (C - Cm)/\sqrt{3} \qquad 7.1$$

where C is the equilibrium composition, Cs the spinodal composition and Cm the metastability limit composition. Although this rule has no theoretical basis it has proven to be as accurate as lengthy thermodynamic analysis on simple systems (Hilliard (1970)). As the family of glasses investigated in this programme is not binary, it is not possible to apply this analysis to the metastability limit estimated from the conductivity measurements. However, in other phase separating glass systems which are both binary and exhibit conductivity by oxygen ion diffusion, such measurements would be a convenient method of fully characterising the two phase region.

Figure 7.2 shows the estimated metastability limit for the glass compositions investigated, as a function of the SiO_2 content. Above the line, the glasses (or glass melts) are single phase, below it they are multiphase. The E-glass composition (E-54) lies near the peak in the metastability temperature and so has the most time available, of all the glasses investigated, to accomplish the separation. The absence of time dependent viscosity behaviour in glass E-54 is evidence of the advanced state of the decomposition of the glass occurring during the cooling from the molten state. The viscosity drift in other phase separating glasses occurs over several hours and an equilibrium viscosity is very slowly attained. The equilibrium viscosity of E-54 is established much more rapidly, before viscosity measurements are started.

This rapid decomposition also occurred in many of the other glasses investigated. All the glasses containing between 45 and 65% SiO_2 (by weight) could be leached to yield porous skeletons and so were phase separated, but exhibited no viscosity drift. During the cooling of these glasses a continuous silica skeleton was formed in all of these glasses and once present, this controlled the viscous properties of the glasses as it has a much higher viscosity than the residual (borate rich) phase. Increasing the SiO_2 content of the glass above 45% simply increases the volume fraction of the silica phase. This is shown in figure 7.3 which shows the volume fraction of the acid insoluble phase as a function of SiO_2 content (from data presented in section 5.5). Because of this, the viscosity of the glasses was not sensitive to the SiO_2 content over the compositional region where a porous silica skeleton could be obtained. This is

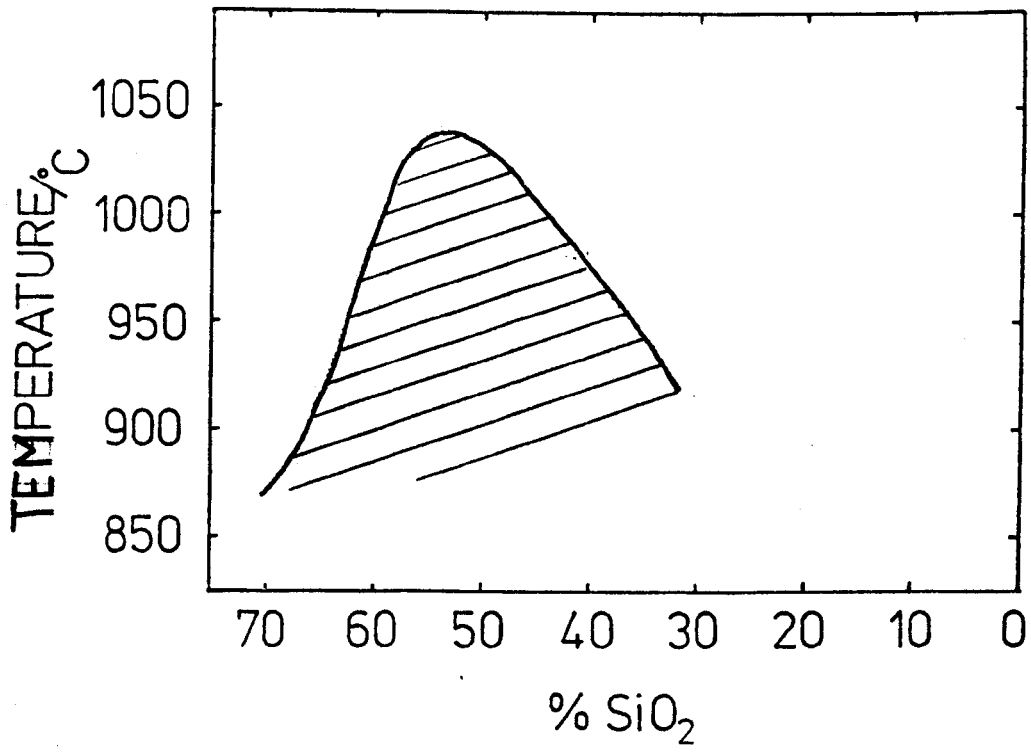

Figure 7.2 The meta-stability region of the 'E-glass system'

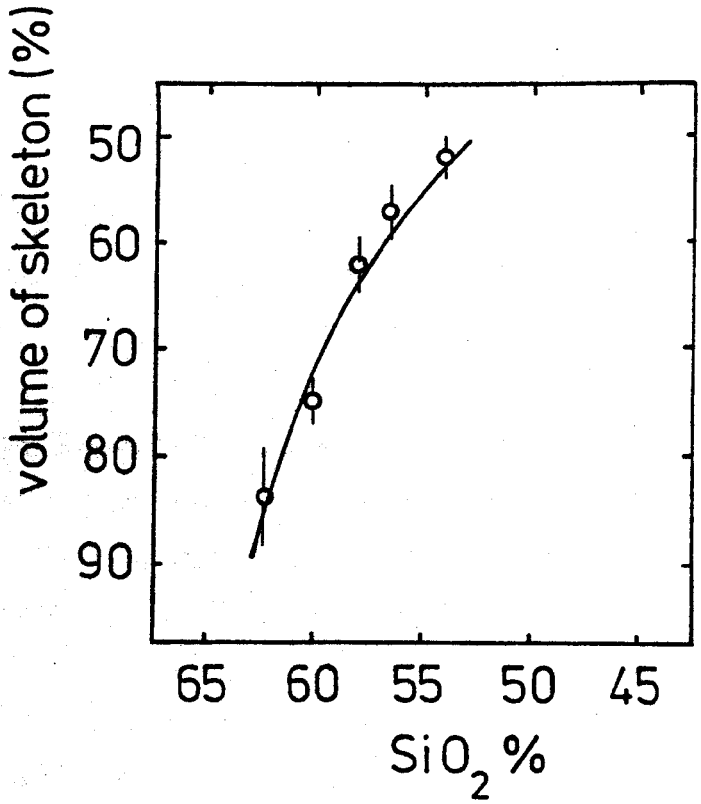

Figure 7.3 The volume fraction of the silica skeletons

illustrated in figure 7.4 (taken from figure 4.9). The activation energy of viscous flow was also insensitive to SiO_2 content over most of this region as would be expected if the stress bearing phase was of constant composition. This is shown in figure 7.5 together with the activation energy of electrical conductivity (taken from figure 4.17) which is also relatively insensitive to SiO_2 content.

Glass E-70 was the only glass investigated that exhibited any time dependent viscosity behaviour. Therefore, this glass must still have been undergoing the early stages of decomposition i.e. the compositional changes that cause the viscosity drift were still occuring. An equilibrium viscosity was not attained in this glass even after 50 hours thermal treatment, but after 30 hours at 800°C this glass started to devitrify and this may have prevented the establishment of an equilibrium viscosity. The viscosity drift of this glass was used to determine the critical temperature and this temperature was in agreement with that estimated by opalescence measurements.

The slow decomposition process in glass E-70 is consistent with the low metastability temperature in figure 7.2. This glass had a viscosity of 10^{11} poise at about 900°C (just above the critical temperature) and this is much greater than the estimated viscosities of the other glasses which had a lower SiO_2 content (table 4.5).

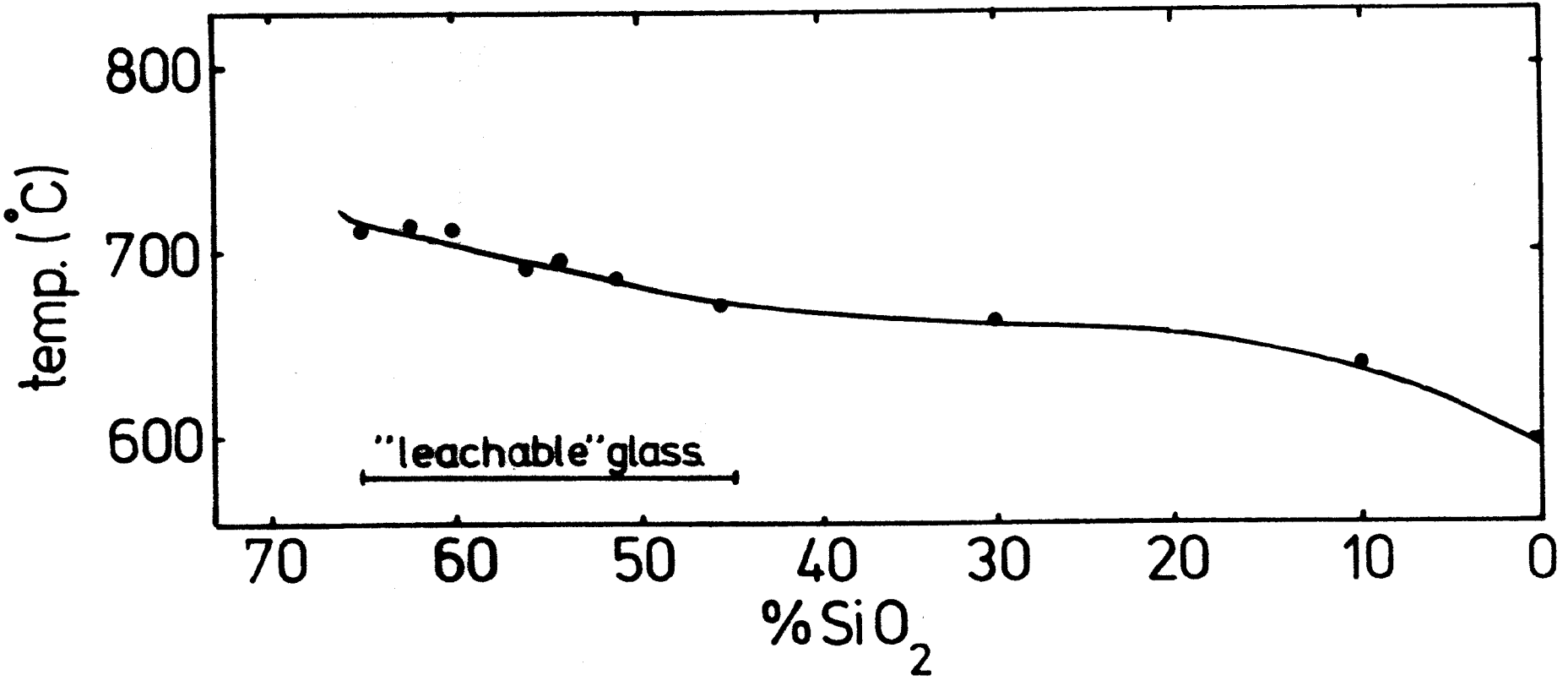

Figure 7.4 The temperature at which the glasses had a viscosity of 10^{13} poise

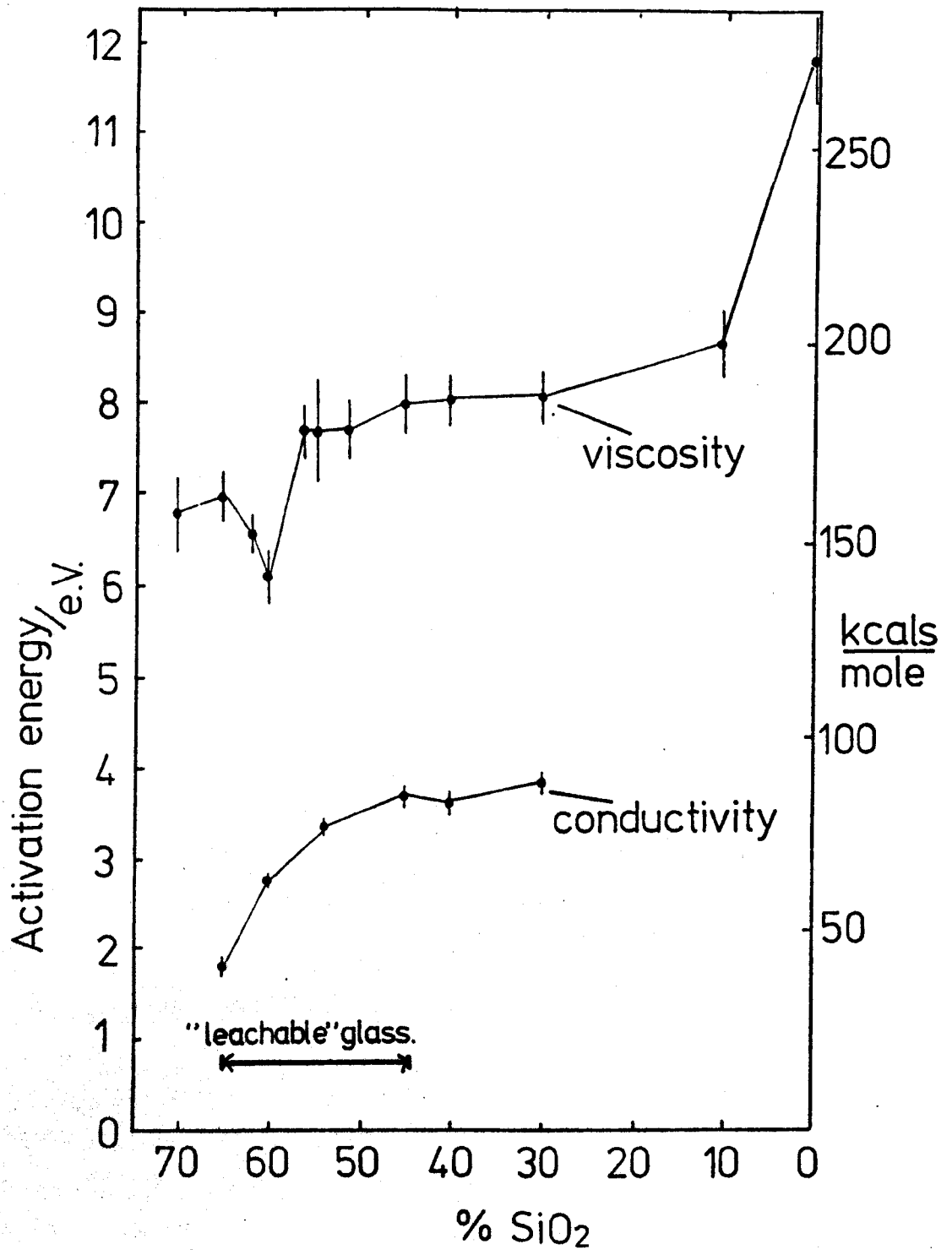

Figure 7.5 The activation energies of viscous flow and conductivity (below the inflection temp.)

7.3 The leaching of the glasses

Although it was dissolved in the leaching solution, the acid soluble phase in the glasses investigated here is more chemically durable than the acid soluble phase in phase separated alkali-borosilicate glasses. The leaching of a 1mm diameter phase separated sodium-borosilicate glass is complete after about one hour under the leaching conditions to which the glasses investigated here were subjected. It was the rate of dissolution of this phase that controlled the leaching in all of the glasses produced for this investigation. This is illustrated in figure 7.6 which shows the weight loss (as a fraction of the final weight loss) **versus** time in the leaching solution. This is a normalised version of figure 5.18. The fractional weight losses shown in figure 7.6 are similar for all four glasses shown and as one of these (E-0) was completely dissolved in the acid, diffusion through the porous layer present on the other glasses cannot be limiting the process.

7.4 The porous glass skeletons

As the fibre diameter determines the cooling rate of the fibre, the decrease in the pore size of the porous glass produced from parent glass E-54 (figure 5.12) can be related to the quench rate of the glass. For the case of spinodal decomposition, the maximum growth rate occurs at undercoolings (below the spinodal) of about 10% (section 1.2.2). As glass E-54 exhibited the highest metastability temperature, it is likely that the spinodal temperature is very close to the metastability temperature (figure 1.4). A 10%

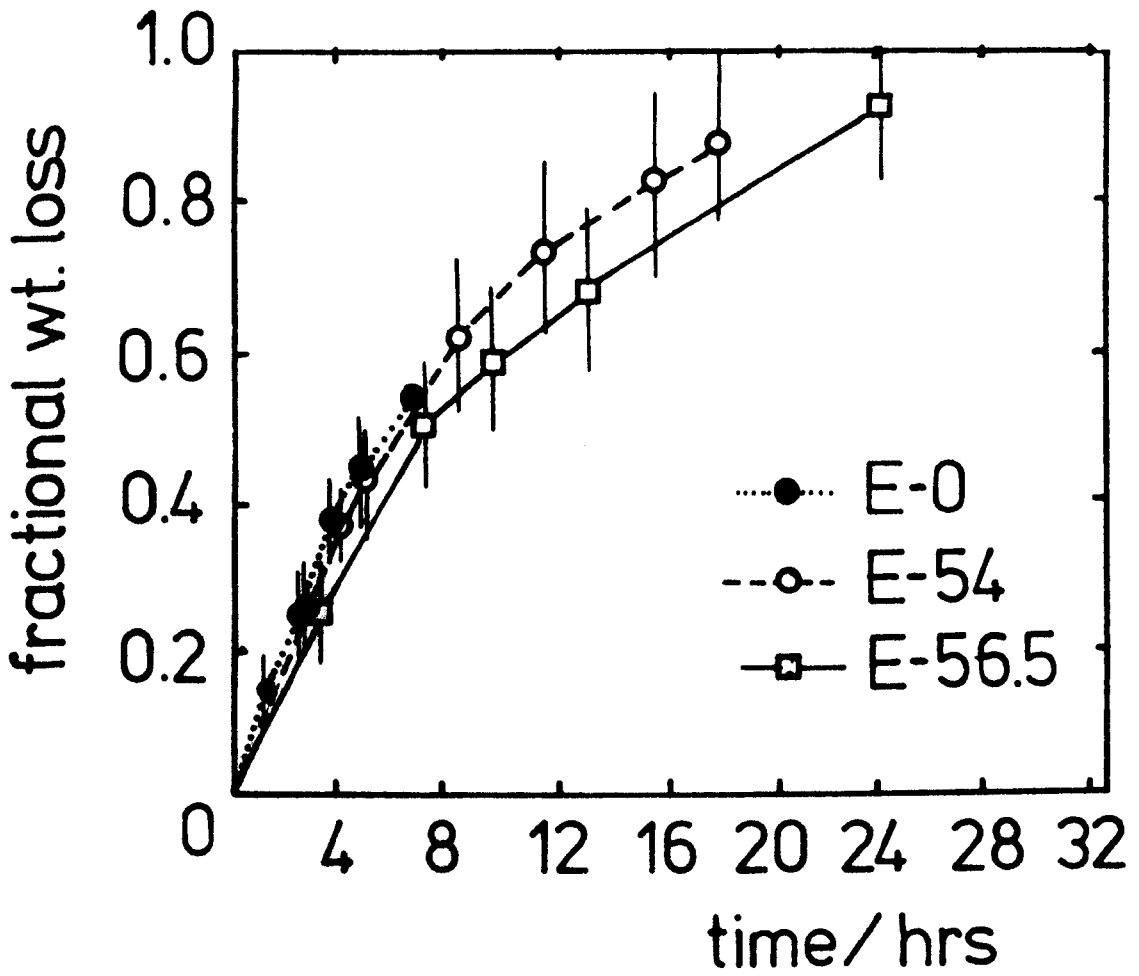

Figure 7.6 The weight loss as a function of time for three 0.3mm diameter fibres of different compositions.(30v/v% HCl solutions at 90^{o}C)

undercooling occurs at about 900°C for this glass and using the results of the cooling rate measurements (section 4.4) the quench rate at 900°C is shown as a function of the fibre diameter in figure 7.7. The pore size of leached E-54 glass fibres is shown as a function of the quench rates in figure 7.8.
It is clear from figure 7.8 that the pore size increases as the quench rate increases. This is the opposite trend to that predicted by Husten et al (section 1.2.2) for spinodal decomposition during continuous cooling Their theory, however, applies to the early stages of the decomposition which is known not to be the case for the E-54 glass fibres produced in this investigation. The fibres produced in this investigation have about 100 times the time available to commercial E-glass fibres to phase separate during cooling (figure 7.1). As commercial fibres are phase separated the thick fibres produced for this investigation would be more advanced in their decomposition. As excessive thermal treatment usually result in a coarsening of the structure (section 1.2) it is proposed that this is the case for the E-54 glass fibres produced here. The broadening of the peak in the measured pore size distribution with fibre diameter (and hence decreasing quench rate) is also consistent with the coarsening of the structure.

The decrease in pore size with increasing quench rate was less marked in the two other glasses evaluated (figures 5.19 and 5.20). This is consistent with the metastability line shown in figure 7.2. These two glasses (E-56.5 and E-60) start to phase separate at lower temperatures and are consequently more viscous during the phase separation. These glasses also contain more silica and are likely to be more viscous in the

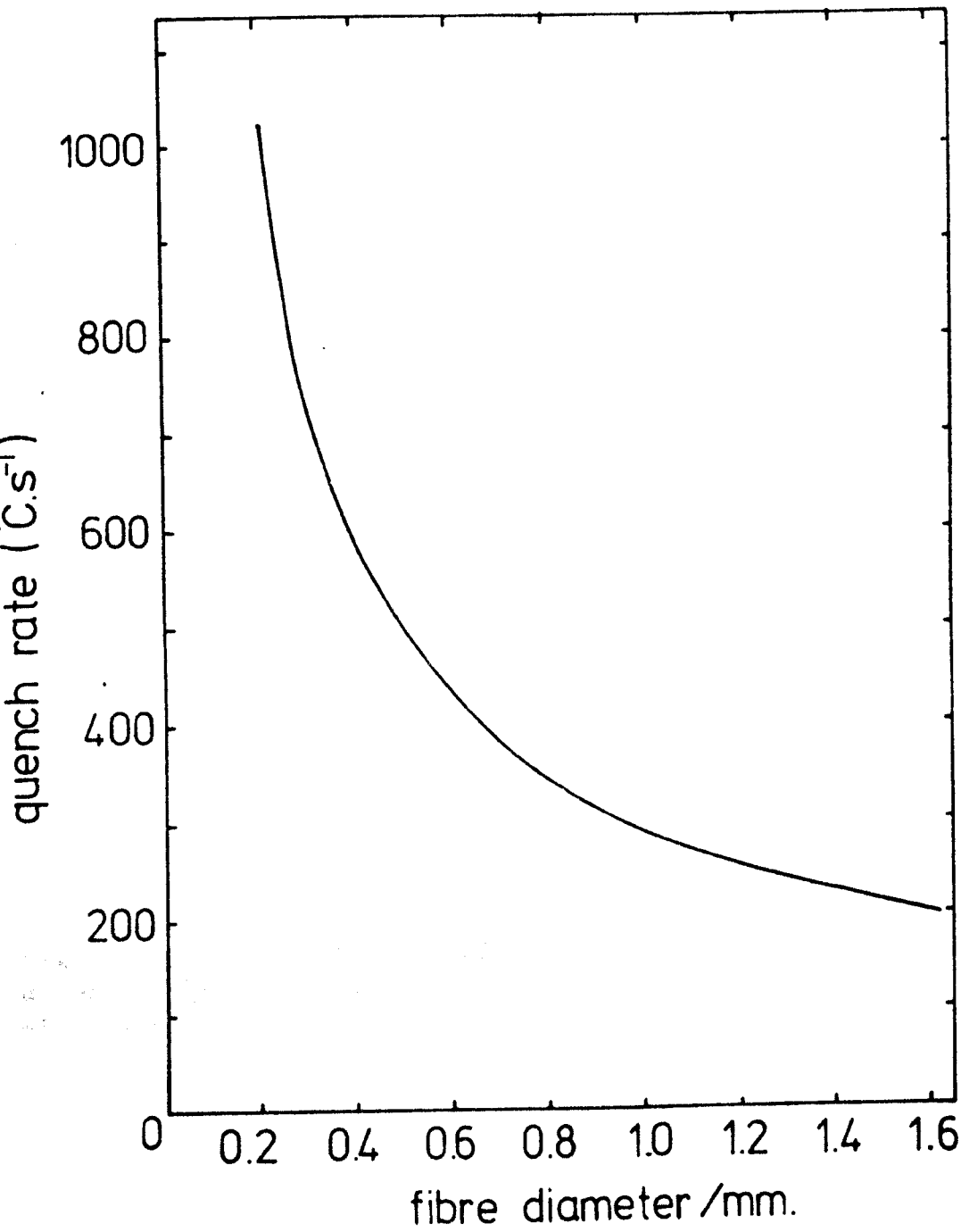

Figure 7.7 Quench rate at 900°C as a function of fibre diameter

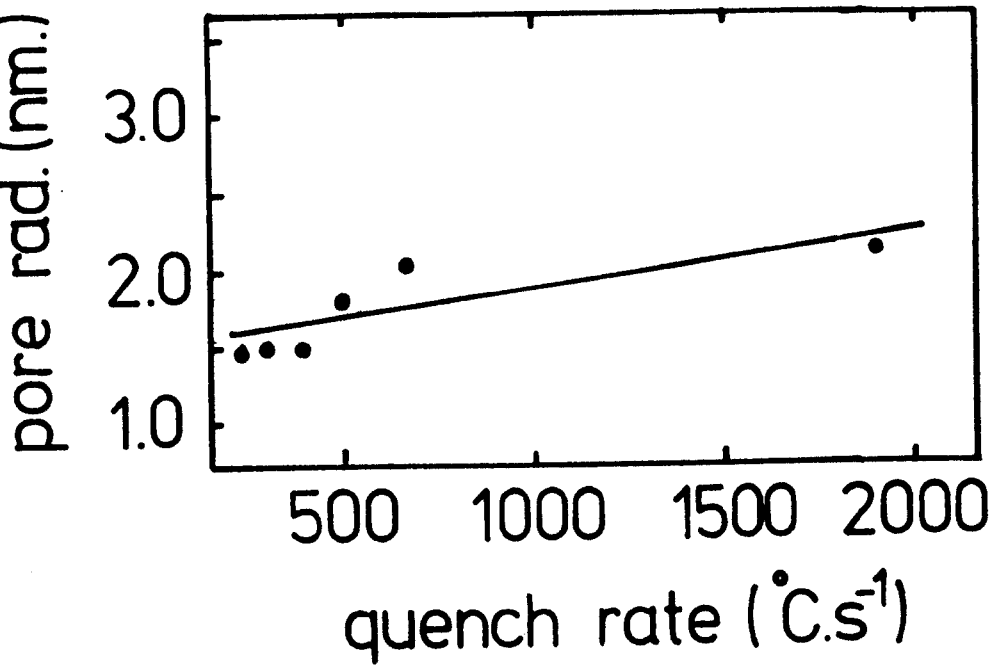

Figure 7.8 Pore size as a function of quench rate at 900°C for E-54 glass fibres (30v/v% HCl solution at 90°C)

in the homogeneous state for these reasons the development of the decomposition is likely to be less well advanced than in the case of glass E-54.

The pore size distributions measured by gas adsorption did not account for all of the measured porous volume and surface area in the leached glasses. In section 5.4 it was proposed that the "unaccounted for" surface area and pore volume was attributable to an extremely fine level of structure in or on the porous glass. The results of the treatment of the leached glass E-54 with dilute alkaline solutions suggested that this fine structure was not a precipitate and consequently must represent small pores or cracks in the porous skeleton.

As the contribution of the very fine structure, to the total pore volume and total surface area was unaffected by the cooling rate, it may be characteristic of the porous skeletons and may even represent some intrinsic feature of the parent glass. Other investigators (Huang et al (1972)) have reported evidence of 1.3nm radius pores in the surface of (unleached) E-glass fibres, and more recently, Akine et al (1979) have reported three levels of structure in (unleached) E-glass fibre; micro-pores (~0.7nm radius), meso-pores (1.8 to 4.5nm radius) and macro-pores (>10nm radius). The presence of small cracks of about 1nm has also been proposed to explain the mechanical properties of E-glass fibres (Bartenev (1969)).

The median pore size of the measured distributions were typically of the order of 2nm radius and the

total surface areas and pore volumes were typically $500 m^2 g^{-1}$ and $\lesssim 45$ v/v% . The highest surface areas were the result of the treatment of the parent glass in concentrated HCl solutions. Some of the porous skeletons were strong enough for use as semi-permeable membranes for reverse osmosis desalination (section 6.3). The membranes that were suitable were produced from parent glasses containing more than 54% SiO_2 (by weight) as those containing 54% or less SiO_2 were too weak for the process. Salt rejections of up to 50% were obtained with some of the membranes although too few results were obtained to apply any statistical analysis to the data.

7.5 Conclusions

1. The cooling rate of thick fibres is proportional to the fibre (diameter)$^{-1.5}$ and is only slightly dependent on drawing velocity

2. A mutually interconnecting phase microstructure develops in E-glass and similar glasses as they cool from the molten state. This multiphase morphology develops so rapidly that fibres quenched at rates similar to those used for the production of metallic glasses are phase separated and consequently homogeneous bulk glass of these compositions cannot be produced by melt cooling

3. The rapid development of the multiphase morphology is the result of the decomposition commencing when the glass forming material is fluid. The temperature at which this starts can be determined by conductivity measurements as the

as the conduction mechanism appears to be that of oxygen diffusion.

4. The viscosity of E-glass and similar glasses appears to be controlled by the silica skeleton forming one of the interconnecting phases. The rapid development of this phase precludes the observation of the time dependent viscosity behaviour exhibited by other phase separating glasses.

5. The leaching rate of E-glass and similar glasses is primarily limited by the rate of dissolution of the acid soluble phase and not by diffusion through the leached structure.

6. Porous glass skeletons can be prepared from parent glasses having SiO_2 contents between 45 and 65% (by weight). An excess of SiO_2 (above 65%) renders the glass unleachable and a deficiency (below 45%) either leads to a loss in the connectivity of the silica phase or to a tenuous (and therefore fragile) skeleton not suited to the production of porous glass.

7. Gas adsorption measurements are more suitable for the characterisation of porous glass skeletons than is electron microscopy. This is primarily because of the resolution limitations of electron microscopy, but gas adsorption measurements also have the advantage that a relatively large sample is used and statistical variations are consequently less important.

8. The porous glass skeletons had pore volumes ranging from 20% to 50% (by volume), depending on the SiO_2 content of the parent glass and surface areas of up to $500 m^2 g^{-1}$. The largest surface areas were the result of the treatment of the parent glass with concentrated acid solutions.

9. The pore size distribution in these porous glasses appears to be bimodal, peaked at approximately 2nm and about 1nm radius.

10. Parent glasses containing between 56.5 and 60% SiO_2 (by weight) were suitable for the production of porous glass membranes with reverse osmosis potential. These glasses yielded porous skeletons containing pores of 2nm radius and had sufficiently high mechanical strengths to withstand the large hydrostatic pressures applied in this desalination process.

7.6 Proposals for future work

Although it was possible to estimate the critical temperatures of the glasses investigated by electrical conductivity measurements, as these glasses were not binary, this information could not be used to determine the spinodal line. The application of this technique to binary systems would, therefore, be of even greater value than it was to this investigation.

At present, the metastability limit is either estimated by calorimetric measurements (applicable only below about 800°C) or by opalescence measurements. As opalescence measurements are lengthy, the measurement of electrical conductivity represents an attractive alternative to determine the metastability limit. This technique, however, may be only applicable to glass melts or glasses in which the conduction mechanism is primarily that of oxygen ion diffusion. This rules out glasses containing alkali ions but several separating systems may fulfil these requirements e.g. $MgO-SiO_2$, $B_2O_3-SiO_2$ and $Al_2O_3-SiO_2$.

It should also be possible to determine the metastability limit of these glasses by high temperature viscosity measurements. As the viscosity at low temperatures was controlled by the silica skeleton present in many of the glasses, the development of this phase would greatly effect the net viscosity of the glass or glass melt.

During the leaching of the glasses it was noted that the presence of inorganic salts in the leaching solution (e.g. ammonium chloride) reduced the amount of damage to the skeletons. This aspect was not investigated as the salt was not removed from the skeleton during the subsequent washing operations and its presence led to difficulties in the characterisation of the porous skeleton. As the reduction of damage to the skeleton is obviously of interest, the effect of dissolved salts in the solutions should be investigated. This would necessitate a more rigorous washing and flushing procedure than was used in this investigation.

The gas adsorption measurements indicated that an extremely fine level of structure was present in the leached glass. This was interpreted as cracks in the pore walls and these were apparently characteristic of the porous skeletons. These small cracks may act as strong 'stress raisers' and limit the strength of the membranes. For that reason, they are of interest and should be further investigated, but as other workers have found evidence of the presence of flaws of similar dimensions in unleached E-glass fibres these features may be of more fundamental interest and reflect an intrinsic feature of silica networks. The resolution of gas adsorption measurements can be improved by using an adsorbate of smaller dimensions than the N_2 used in this investigation e.g. He, but the published data concerning such measurements are limited and it may be more profitable to use other techniques such as small angle X-ray or neutron scattering , to study these features.

Further reverse osmosis desalination work using these membranes is clearly required. The limited amount of data collected on this aspect of the programme precluded any statistical analysis of the performance from being made. The results obtained did suggest that the membranes have some potential for this application, but much more work is required to establish their limitations and long term performance. Although the reverse osmosis test rig used in this investigation performed satisfactorily, a number of improvements are possible. The elimination of the few non-austenitic steel components would reduce the visible contamination to the membrane significantly, but a more satisfactory solution would be to use glass lined apparatus.

Work is also required to establish the actual mechanism of the salt rejection of glass membranes. This should include studies of the physical properties of the 'pore water' by infra-red absorption, nuclear magnetic resonance and dielectric constant measurements. These data may enable a more accurate interpretation of the reverse osmosis data to be made. The membranes themselves could be modified by partially collapsing the skeleton at elevated temperatures (reducing the pore size) or by treatment with H.F. solutions (increasing the pore size). The effect of these modifications on the properties of the pore water would provide further evidence as to the salt rejection mechanism.

REFERENCES

Akine,M.,Demirel,T. and Martin,D.M.(1979).Mater.Res. Bull.14,759.

Amberg,C.H. and MacIntosh,R.(1952).Can.J.Chem.30, 1012.

Anderson,O.L.(1958).J.Appl.Phys.29,9.

Arridge,R.G.C.and Prior,K.(1964).Nature.203,386.

A.S.T.M.(1945).Glass Ind.26,417.

Ballou,E.V. and Wydevan,T.(1972).J.Colloid Interface Sci.41,198.

Ballou,E.V.,Wydevan,T. and Leban,M.I.(1971).Envir. Sci.Tech.5,1032.

Barrett,E.P.,Joyner,L.G. and Halenda,P.P.(1951). J.Am.Chem.Soc.73,373.

Bartenev,G.M.(1969).Mater.Sci.Eng.4,22.

Bartenev,G.V. and Ismailova,L.K.(1962).Plastico,(4)62.

Belfort,G.(1972).PhD Thesis.University of California.

Blachere,J.R.(1974).J.Am.Ceram.Soc.57,268.

Brunauer,S.(1940).The Adsorption of Gases and Vapours. 1,Princeton University Press,New Jersey.

Brunauer,S.,Emmett,P.H. and Teller,E.(1935). J.Am.Chem.Soc.60,309.

Cahn,J.W.(1966).Acta.Metall.14,1685.

Cahn,J.W.(1968).Trans.A.I.M.E..242,166.

Cahn,J.W.(1965).J.Chem.Phys.42,93.

Cahn,J.W.and Charles,R.J.(1965).Phys.Chem.Glasses.6,181.

Cahn,J.W.and Hilliard,J.E.(1958).J.Chem.Phys.28,258.

Charles,R.J.(1964).J.Am.Ceram.Soc.47,559.

Charles,R.J.(1963).J.Am.Ceram.Soc.46,235.

Charles,R.J.(1969).Phys.Chem.Glasses.10,169.

Cook,M.E. and Hilliard,J.E.(1965).Trans.A.I.M.E.. 233,192.

Cranston,R.W. and Inkley,F.A.(1959).Advances in Catalysis. 9,143.Academic Press,New York.

Culpin,M.F. and Madoc-Jones,D.(1959).J.Scient.Instrum. 36,28.

Dalla Valle,J.M.,Orr,C. and Blocker,H.G.(1953). Final Rept.Project.181-119,Georgia Institute of Technology. Atlanta.

Diamant,R.M.E.(1974).The Prevention of Pollution.154. Pitman Press,Bath.

Eguchi,K.,Tasaka,K. and Tarumi,S.(1969).J.Ceram.Soc. Japan.77,301.

Elmer,T.M.(1978).Ceram.Bull.57,1051.

Elmer,T.H. and Nordberg,M.E.(1970).J.Am.Ceram.Soc. 53,171.

Everett,D.H.(1958).The Structure and Properties of Porous Materials.edited by D.H.Everett and F.S.Stone. Butterworths.London.

Fulcher,G.S.(1925).J.Am.Ceram.Soc.8,789.
Gladman,T.(1963).J.IronSteel Inst.(London).194,189.
Glicksman,L.R.(1968).Glass Technol.9,131.
Goldstein,M.(1968).J.Crystal.Growth.3,594.
Hagel,W.C. and MacKenzie,J.D.(1964).Phys.Chem.Glasses. 5,113.
Hair,M.L.(1967).Infra-red spectroscopy in surface chemistry.Marcell Dekker.New York.
Hakim,R.M. and Uhlmann,D.R.(1971).Phys.Chem.Glasses. 12,132.
Haller,W.(1965).J.Chem.Phys.42,686.
Haller,W. and Macedo,P.B.(1968).Phys.Chem.Glasses.9, 153.
Haller,W.,Simmons,J.M. and Napolitano,A.(1971). J.Am.Ceram.Soc.54,299.
Halsey,G.D.(1948).J.Chem.Phys.16,931.
Hammel,J.J. and Ohlberg,S.M.(1965).J.Appl.Phys. 36,1442.
Handbook of Chemistry and Physics.(1975).Ed.R.C. Weast.pD-81.C.R.C.Press,Ohio.
Hauser,E.A.(1940).Ind.Eng.Chem.32,659.
Hilliard,T.E.(1970).Phase Transformations.American Society for Metals.537.Chapman and Hall Ltd. London
Holloway,D.(1960).Contemporary Physics.1,230.
Hopper,R.W. and Uhlmann,D.R.(1970).Discuss.Faraday Soc.50,166.
Howe,E.D.(1966).Advances in Hydroscience.3,191. Edited by Ven Te Chow.Academic Press,London.
Huang,R.J.,Demirel,T. and McGee,T.D.(1972).J.Am.Ceram. Soc.55,399.
Huggins,M.L.(1954).J.Am.Ceram.Soc.35,284.
Husten,E.L.,Cahn,J.W. and Hilliard,J.E.(1966) Acta Metall.14,1053.
International Critical Tables.(1933).Compiled by J.West.3,297.McGraw Hill.London.
Joy,A.S.(1953).Vacuum.3,254.
Kraus,K.A.,Marcinkowsky,A.E.,Johnson,J.S. and Shor,A.J. (1966).151,194.
Kuznetsov,A.I.(1974).Glastech.Ber.47,79.
Langmuir,I.(1915).J.Am.Chem.Soc.37,1137.
Littman,F.E. and Gutter,G.A.(1968).Office of Saline Water,Report 379.
Littman,F.E.,Kleist,F.D. and Croopnick,G.A.(1971). Office of Saline Water,Report 720.
Lowrie,R.E.(1967).Modern Composite Materials.271. Edited by L.J.Broutmann and R.H. Krock.Addison Wesley Mass.U.S.A..
McMillan,P.W. and Matthews,C.E.(1976).J.Mater.Sci. 11,1184.
Mahoney,R.,Strinivason,G.R.,Macedo,P.B.,Napolitano,A. and Simmons,J.M.(1974).Phys.Chem.Glasses.15,24.

Mayhew,Y.R. and Roagers,G.F.C.(1972).Thermodynamic and Transport Properties of Fluids.2.Blackwell.Oxford.
Napolitano,A. and Hawkins,E.G.(1964). US Nat.Bur.Stands. 68A,439.
Nordberg,M.E.(1944)•J.Am.Ceram.Soc.27,299.
Nordberg,M.E. and Hood,H.P.(1938).U.S.Patent 2 106 744
Nordberg,M.E. and Hood,H.P.(1940).Borosilicate Glass, U.S. Patent 2 221 709.
Nordberg,M.E. and Hood,H.P.(1950). Making Glass Fibres of Special Compositions,U.S. Patent 2 494 259
Ohlberg,S.M.,Hammel,J.J. and Golob,H.R.(1965). J.Am.Ceram.Soc.48,178.
Orr,C. and Dalla Valle,J.M.(1959).Fine Partical Measurement. 271.The McMillan Co.,New York.
Orr,C.(1977).Treatise on Analytical Chemistry(3),4, 382.edited by I.M. Kolthoff,P.J. Elving and F.M. Stross. John Wiley and Sons, New York.
Owen,A.E.(1963).Progress in Ceramic Science.3, chapter 3 Edited by J.E. Burke. Pergammon Press, London.
Pickering,F.D.(1975).Basis of Quantative Metalography. Institute of Metallurgical Technicans. London.
Phillips,S.V.,Crozier,D.S.,McMillan,P.W.and Taylor,J.McC. (1974).Desalination.14,209
Porai-Koshits,E.A. and Averjanov,V.I.(1968).J.Non-Cryst. Solids.1,29.
Rawson,H.(1967).Inorganic Glass-forming Systems.152, Academic Press, London.
Redwine,R.H. and Field,M.B.(1969). J.Mater. Sci.4,713.
Roberts,N.K. and Northey,H.L.(1972).Nature.237.144.
Schnabel,R. and Vaulont,W.(1978).Desalination.24,249.
Scholze,H.(1959).Glass Ind.40,301.
Shimbo,Y.K.(1972).J.Ceram.Soc.Japan.80,69.
Spencer,D.H.T. and Faraday F.(1968).Chem.Ind.(6),847.
Stevels,A.G.(1954).Glass Ind.35,69.
Takamori,T. and Tomozawa,M.(1978).J.Am.Ceram.61,509.
Terai,R. and Hayama,R.(1975).J.Non-Cryst.Solids.18,217.
Thomas,W.(1960).Phys.Chem.Glasses.1,1.
Thomson,W.(1871),Phil.Mag.42,448.
Tomlinson,J.W.(1956).J.Soc.Glass Technol.40,25.
Tomozawa,M.(1978).J.Am.Ceram.Soc.61,444.
Tran,S.M.(1976),Microporous glass for reverse osmosis. Interim report RO2/3 Central Dockyard Laboratory, Portsm.
U.K.E.A.(1967).Desalination and its role in water supply. 38.Central Office of Information,London.
Veltri,R.D.(1963).Phys.Chem.Glasses.4,221.
Vogel,W.(1966).Structure of Glass.6.Edited by E.A. Porai-Koshits.114-20. Consultants Bureau, New York.
Weyl,W.A. and Marboe,E.C.(1964a).The Constitution of Glasses.2,(1).658.

Weyl,W.A.. and Marboe,E.C.(1964b).The Constitution of Glasses.2,661.John Wiley and Sons, London.
Wolf,M.B.(1961a).Technical Glasses.Chapter 10. Pitman and Sons Limited, London.
Wolf,M.B.(1961b).Technical Glasses.181.Pitman and Sons Limited, London.
Wolf,M.B.(1961c).Technical Glasses.424.Pitman and Sons Limited, London.
Wolf,M.B.(1961d).Technical Glasses.Chapter 8.Pitman and Sons Limited, London.
Wolf,M.D.(1961e).Technical Glasses.24.Pitman and Sons Limited, London.
Young,G.J.(1958).J.Colloid Sci.13,67.

The cooling rate of glass fibres

R. Maddison & P. W. McMillan

Department of Physics, University of Warwick, Coventry

The cooling rates of glass fibres of diameter 0·1 to 0·2 mm have been measured during continuous drawing from the melt. Cooling times typically of the order of seconds were measured and Newton's law of cooling was found to be obeyed. The cooling time was found to be proportional to drawing (velocity)$^{-0.7}$ and (radius)$^{1.5}$. These results are compared with previous estimates of the cooling rate.

There have been two previous estimates of the cooling rates of glass fibres. Anderson[1] made theoretical predictions for thin fibres (10–50 μm diameter) and Arridge & Prior[2] measured the rates for fibres of similar dimensions, pulled down from a rod. Anderson's cooling times were of the order of a few milliseconds from 1700 C to near room temperature. Arridge & Prior however measured rates some 30 times slower than his predictions and also found a different relationship between cooling rate and fibre diameter.

The purpose of this investigation was to measure the cooling times of thicker glass fibres (100–200 μm) and to determine the relationship between the fibre diameter and cooling rate.

Experimental

Fibres were drawn from a glass melt of the wt% composition 53·5 SiO_2, 19 BaO, 8 Na_2O, 7·5 B_2O_3, 5 Al_2O_3, 3 CaO, 2 MgO, 2 ZnO. This composition has previously been exploited for commercial continuous filament production.[3] A fibre was drawn from a melt in an electric furnace and wound onto a drum mounted approximately 1 m above it. The drum was driven by an electric motor and was marked so that velocity could be measured with a stroboscopic lamp; the velocity of the drum could be maintained to within 1% of that required during the experimental measurements.

To start the drawing, a weighted wire was connected to the drum and the weight 'dipped' into the glass melt. The motor was started and the wire was wound onto the drum drawing a glass filament with it.

The temperature was measured by an adaption of that first suggested by Culpin & Madoc-Jones[4] and used by Arridge & Prior in their measurements. The original technique was to mount a thermocouple in thermal contact with a heating element and then to touch this thermocouple onto the glass filament. If the thermocouple temperature changes, then either heat is flowing to or from the fibre. Using a sensitive meter and varying the thermocouple temperature (via the heating element) or by moving the point of contact with the fibre, the temperature of any position on the moving fibre may be determined. This procedure is repeated to obtain a series of temperature/position measurements and as the drawing velocity is known these data can be converted directly to temperature/time information.

The same technique was used here but was modified by heating the measuring thermocouple directly using a hot stage microscope power supply. The heating current is supplied at mains frequency through half wave silicon rectifiers. During alternate half cycles when the current is off, the generated emf is registered by means of a phased synchronous chopper. This cycle is repeated sufficiently rapidly to sustain the thermocouple at a constant temperature which can be continuously measured. The experimental apparatus used in these measurements is shown in Figure 1.

A T_1/T_2 thermocouple was used to obtain high sensitivity in the region 400–800°C and by using wires of different gauges for the arms a symmetrical hot junction could be obtained despite the differing conductivities of the thermocouple alloys. Measurements on cold threads indicated that the effect of frictional heating on the thermocouple was negligible.

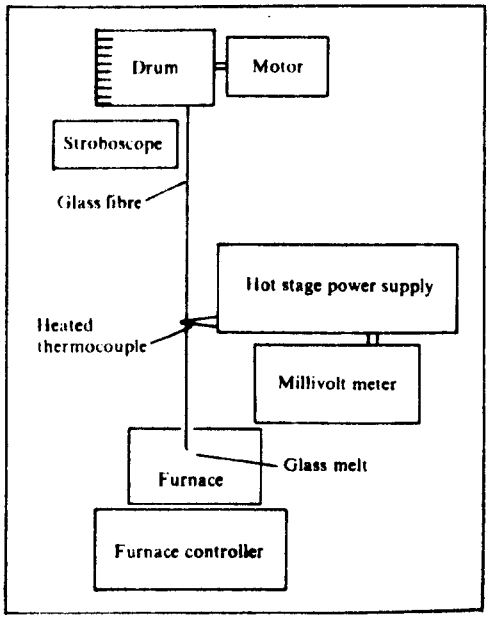

Figure 1. *Schematic diagram of the apparatus used*

Results

The cooling time data for fibres having four different diameters drawn at 100 cm/s and two diameters drawn at 150 cm/s are shown on a log temperature–time basis in Figures 2–7. Within experimental error these are straight lines, confirming that over the measured temperature range, Newton's law of cooling is obeyed, i.e. the rate of heat loss is proportional to excess temperature.

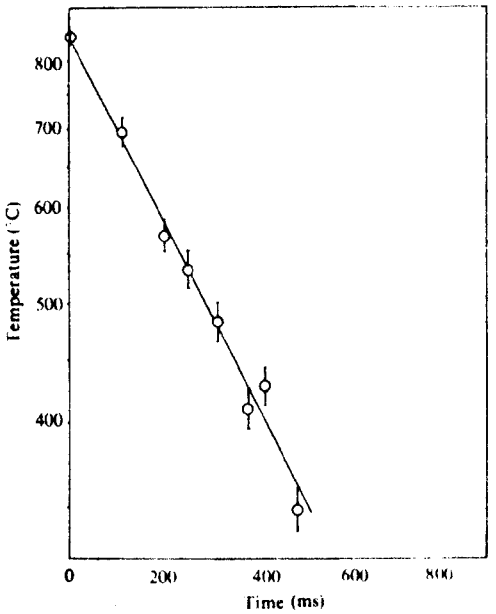

Figure 2. *The cooling rate of a 0·09 mm diameter fibre drawn at 100 cm/s*

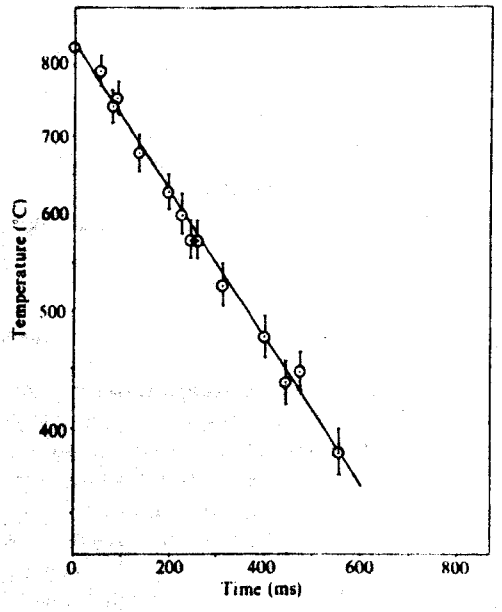

Figure 3. *The cooling rate of a 0·12 mm diameter fibre drawn at 100 cm/s*

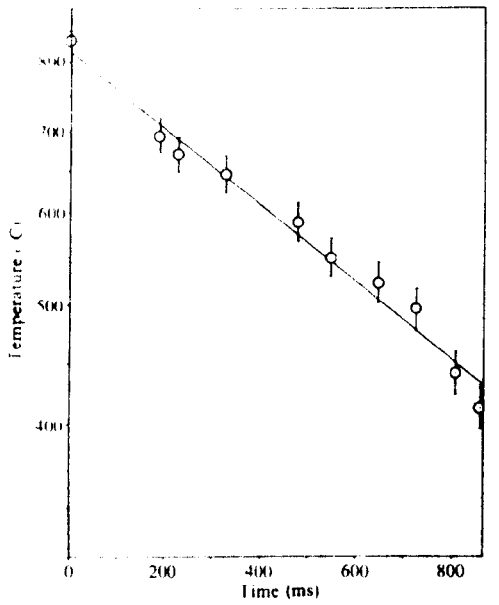

Figure 4. *The cooling rate of 0·18 mm diameter fibre drawn at 100 cm/s*

Figure 8 shows the measured times for the fibres to cool from 800 to 400 °C as a function of fibre diameter using a log–log plot. For the drawing velocity of 100 cm/s this plot has a gradient of 1·5 ± 0·2. Thus the time required for a fibre to cool through a given temperature range is proportional to the fibre (radius)$^{1·5}$. From Figure 8 it may also be seen that fibres drawn at 150 cm/s cool more rapidly than those drawn at 100 cm/s. Although only two fibre diameters drawn at that speed were investigated, the cooling time appears to be proportional to (velocity)$^{-0·7}$.

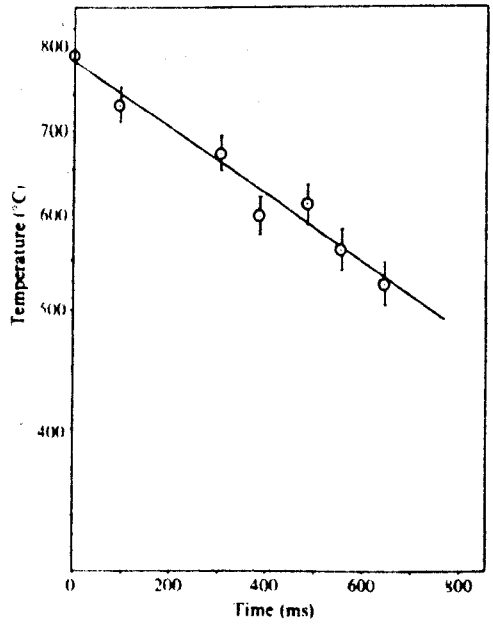

Figure 5. *The cooling rate of a 0·2 mm diameter fibre drawn at 100 cm/s*

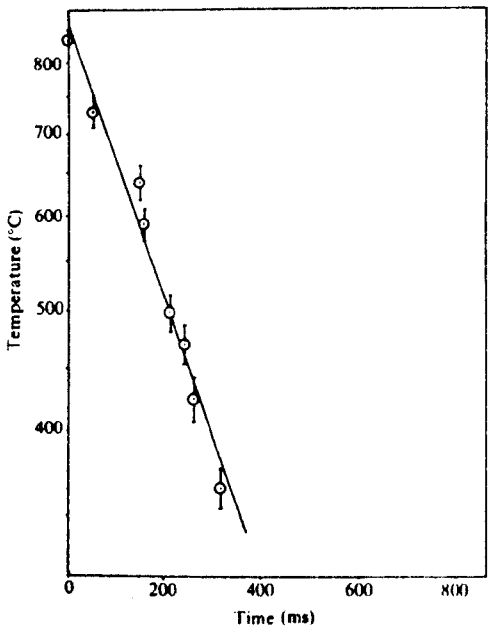

Figure 6. *The cooling rate of a 0·09 mm diameter fibre drawn at 150 cm/s*

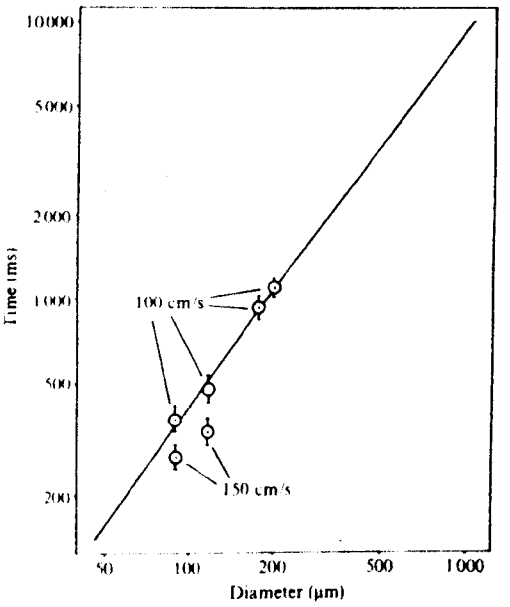

Figure 8. *The relationship between cooling time from 800 to 400 °C and fibre diameter*

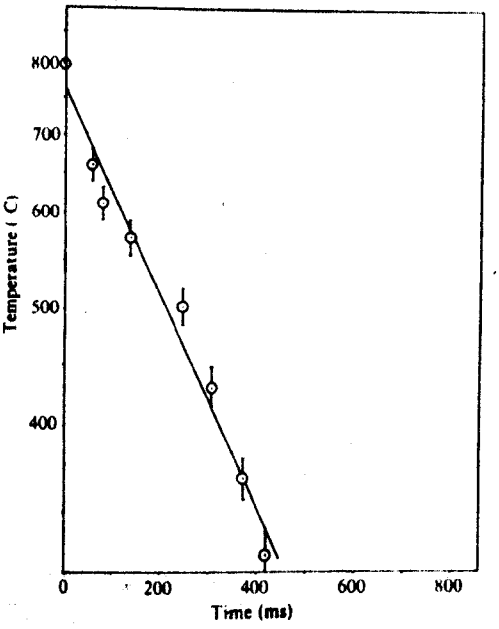

Figure 7. *The cooling rate of a 0·12 mm diameter fibre drawn at 150 cm/s*

Discussion

The cooling time for glass fibres measured here have been found to be proportional to (fibre radius)$^{1·5}$. This is close to the value determined by Arridge & Prior of (radius)$^{1·8}$ and is considerably different from Anderson's predicted (radius)$^{2·5}$. The cooling time however, was also found to be proportional to (drawing velocity)$^{-0·7}$, which is near Anderson's (velocity)$^{-0·5}$ and disagrees with Arridge & Prior's evidence that cooling time increases as the drawing velocity increases. The actual time to cool for a fibre has been found to be of the order of seconds, in agreement with Arridge & Prior's work and some 30 to 40 times slower than Anderson's predicted times.

The cooling rates measured here have been found to be proportional to the excess temperature; Arridge & Prior found this to be true until temperatures ~150 °C were reached. As Newton's law is obeyed, it is clear that the cooling rate is controlled only by the 'surface resistance' of the fibre, i.e. the thermal conductivity of the fibre is large in comparison with the rate of heat transfer from the glass surface.

Conclusions

It has been found that the cooling rate of thick glass fibres is similar to that expected by extrapolation of the evidence of Arridge & Prior. The only exception to this is in the effect of velocity, where the cooling time has been found to be proportional to (velocity)$^{-0·7}$ which is near the value predicted by Anderson. The cooling time was also found to be proportional to (radius)$^{1·5}$ and to be typically of the order of seconds.

The rate of heat loss is given by Newton's law of cooling and because of this, one would not expect to find any radial anisotropy, e.g. a surface compressive layer for fibres of these diameters.

Acknowledgement

This investigation has been sponsored by the Procurement Executive, Ministry of Defence.

References

1. Anderson, O. L. (1958). *J. Appl. Phys.* **29**, 9.
2. Arridge, R. G. C. & Prior, K. (1964). *Nature, Lond.* **203**, (4943), 386.
3. Volf, M. B. (1961). *Technical glasses*. Pitman, p. 424.
4. Culpin, M. F. & Madoc-Jones, D. (1959). *J. scient. Instrum.* **36**, 28.

APPENDIX 2 THE COMPUTER PROGRAM USED FOR THE ANALYSIS OF THE GAS ADSORPTION DATA. Written primarily by S.M. Tran, with minor modifications by R. Maddison.

```
BEGIN
  INTEGER NOP, ITV, C;
                % NOP IS THE NO. OF PTS
    NOP:=READN;
      ITV:=READN;
    C:=(NOP-1)*ITV+1;
                % C IS THE NO. OF PTS AFTER INTERPOLATION
  BEGIN
  INTEGER I, K, IMAX;

                % IMAX IS PT WHEN PORE VOL=SAT VOL
  REAL THN2, SUMV;
                % THN2 IS THICKNESSOF N2
                % SUMV IS SUM OF VOL
  REAL SLMAX, VRMAX, LRMAX;
  LABEL LB;
  REAL ARRAY T[1:C,1:14], X,Y1,Y2,Y3,Y4[0:C];
                % T IS ARRAY TABLE 2 DIMENTIONAL
                % THE DATA IS READ IN
  FOR I:=1 STEP ITV UNTIL C DO
  T[I,1]:=READN;
  FOR I:=1 STEP ITV UNTIL C DO
  T[I,2]:=READN*0.001244;
  I:=1;
                % LINEAR INTERPOLATION OF DATA
LP: FOR K:=1 STEP 1 UNTIL ITV-1 DO
  BEGIN
  T[(I-1)*ITV+K+1,1]:=T[(I-1)*ITV+1,1]-
      (T[(I-1)*ITV+1,1]-T[I*ITV+1,1])*K/ITV;
  T[(I-1)*ITV+K+1,2]:=T[(I-1)*ITV+1,2]-
      (T[(I-1)*ITV+1,2]-T[I*ITV+1,2])*K/ITV;
  END;
  IF I<NOP-1 THEN
  BEGIN
  I:=I+1;  GO TO LB;
  END;
                % END OF INTERPOLATION
  FOR I:=1 STEP 1 UNTIL C DO
  BEGIN
  T[I,3]:=3.54*((-5)/LN(T[I,1]))**(1/3);
                % HAUSERS EQATION IS DEFINDE
  T[I,4]:=-9.53/LN(T[I,1]);
```

```
                % KELVINS EQUATION IS DEFINED
  T[I,5]:=T[I,3]+T[I,4];
                % RK+T IS CALCULATED
  END;
                % PREPARING FOR THE CALCULATION
  FOR K:=6 STEP 1 UNTIL 14 DO
  T[1,K]:=0;
  IMAX:=0;
  VRMAX:=0;     LRMAX:=0;
  FOR I:= 2 STEP 1 UNTIL C DO
  BEGIN
                % DELTA V IS CALCULATED
  T[I,6]:=T[I-1,2]-T[I,2];
                % RK+T IS CALCULATED

X[I-2]:=T[I,13]:=(T[I-1,5]+T[I,5])/2;
                %DELTA VP IS CALCULATED (PORE VOL INCREMENT)
  T[I,7]:=(T[I,6]-(T[I-1,3]-T[I,3])*(T[I-1,10]-(T[I-1,3]+T[I,3])
      *0.5*T[I-1,12])*1.03-4)*(T[I,13]/((T[I-1,4]+T[I,4])*0.5
      +(T[I-1,3]-T[I,3])))**2;
                % SIGMA DELTA VP IS CALC.(CUMULATIVE PORE VOL)
Y3[I-2]:=T[I,8]:=T[I-1,8]+T[I,7];
                %DELTA SP IS CALC.(SURFACE AREA INCREMENT)
  T[I,9]:=2*T[I,7]/T[I,13]*1.034;
                % SIGMA DELTA SP IS CALC.
  T[I,10]:=T[I-1,10]+T[I,9];
                % 2 PI DELTA LP IS CALC.
  T[I,11]:=T[I,9]/T[I,13];
                % LP IS CALC.(PORE LENGTH)
Y2[I-2]:=T[I,11]/2/3.14159265 35/(T[I-1,5]-T[I,5]);
                % 2 PI SIGMA DELTA LP IS CALC.
  T[I,12]:=T[I-1,12]+T[I,11];
                % SIGMA DELTA LP IS CALC.
Y4[I-2]:=T[I,12]/2/3.14159265 35;
                % DELTA VP / DELTA R IS CALC.
Y1[I-2]:=T[I,14]:=T[I,7]/(T[I-1,5]-T[I,5]);
  IF T[I,14]>VRMAX THEN
  VRMAX:=T[I,14];
  IF Y2[I-2]>LRMAX THEN
  LRMAX:=Y2[I-2];
  IF T[I,7]<0 THEN
  BEGIN
                %THE DATA IS INTERIGATED FOR -VE DELTA VP'S
      WRITES("I=");
      WRITEI(I,4);
      SPACE(3);
  END;
                % IMAX WHEN PORE VOL = SAT VOL IS FOUND
  IF IMAX=0 THEN
  BEGIN
                % THE CORRESPONDING THICKNESS IS SRORED
  IF T[I,8]>=T[1,2] THEN
  BEGIN
  IMAX:=I;
  THN2:=T[I,3];
  END
  ELSE
  BEGIN
  IMAX:=C;
  THN2:=T[C,3];
  END;
  END;
  END;
  SUMV:=0;
```

```
                    % THE VOL. AT THICKNESS ABOVE IS CALC.
      FOR I:=2 STEP 1 UNTIL IMAX DO
      SUMV:=SUMV+THN2*(2*T[I,13]-THN2)*T[I,11]/2*1.0#-4;
      NEWLINE(2);
                    % THE SAT. VOL. IS PRINTED
      WRITES("SATV=");
      WRITEN(T[1,2]);
      SPACE(5);
      WRITES("IMAX=");
                    % IMAX IS PRINTED
      WRITEI(IMAX,4);
      SPACE(5);
      WRITES("SUMV=");
                    % CUMMULATIVE VOL. IS PRINTED
      WRITEN(SUMV);
      SPACE(5);

      WRITES("RV=");
                    % REMAINING VOL. IS PRINTED
      WRITEN(T[IMAX,2]);
      NEWLINE(2);
WRITES("    P/PS    N2VOL      T       RK      RK+T      DELV    DELVP    ");
WRITES("SUMVP   DELSP   SUMSP   2PISP  2PISUMLP  RK+T");
WRITES("  DEL(V/R) DEL(L/R)");
      NEWLINE(1);
      FOR I:=1 STEP ITV UNTIL C DO
      BEGIN
                    % THE DATA TABLE IS REDUCED FOR PRINTING
      FOR K:=1 STEP 1 UNTIL 14 DO
      WRITEF(T[I,K],4,2);
      IF I>=2 THEN
                    % THE DATA TABLE IS PRINTED
      WRITEF(Y2[I-2],4,2);
      NEWLINE(1);
      END;
      SLMAX:=Y4[C-2];
      GHOST;
                    % THE GRAPH PLOTTER IS CALLED
      PSPACE(1.0,9.0,0.5,6.5);
                    % THE PLOTTIG SPACE IS DEFINED --A4
      MSPACE(5,T[2,13]*1.1,C,0.32);
      AXES;
                    % PLOT OF CUMMULATIVE PORE VOL.
      GRAPHN(X,Y3,1,C-1);
      FRAME;
      MSPACE(5,T[2,13]*1.1,0,SLMAX*1.1);
      AXES;
                    % PLOT OF CUMMULATIVE PORE LENGTH
      GRAPHN(X,Y4,1,C-1);
      FRAME;
MSPACE(5,T[2,13]*1.1,0,VRMAX*1.1);
      AXES;
                    % PLOT OF DELTA V/ DELTA R
      GRAPHN(X,Y1,1,C-1);
      FRAME;
      MSPACE(5,T[2,13]*1.1,0,LRMAX*1.1);
      AXES;
                    % PLOT OF DELTA L/ DELTA R
      GRAPHN(X,Y2,1,C-1);
      FRAME;
      GREND;
                    % THE GRAPH PLOTTER IS LEFT

      END;

    END.
```

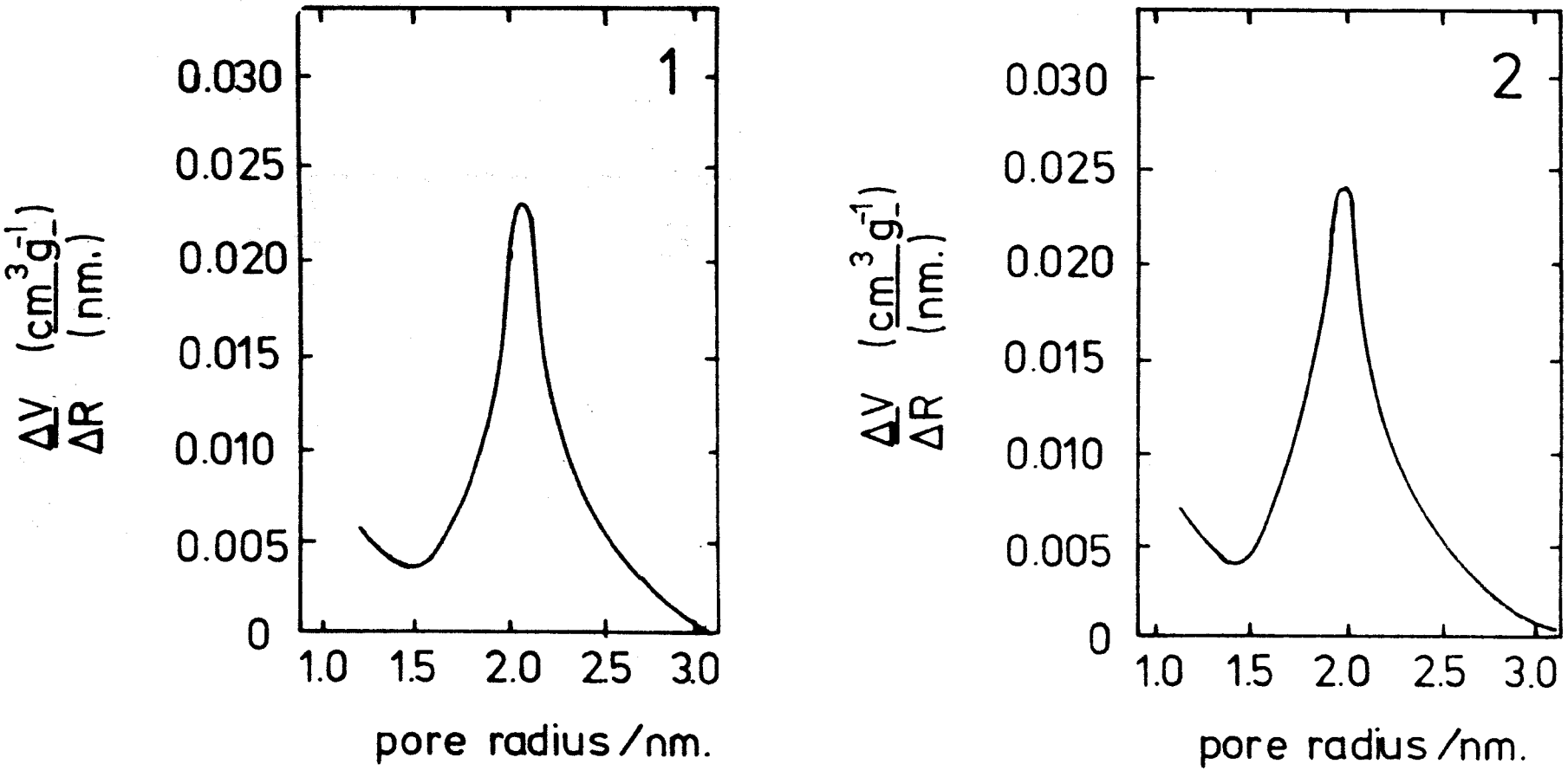

APPENDIX 3 PORE SIZE DISTRIBUTIONS OF THE MEMBRANES USED IN THE REVERSE OSMOSIS MEASURENTS. NUMBERED AS IN TABLES 6.1, 6.2, 6.3.

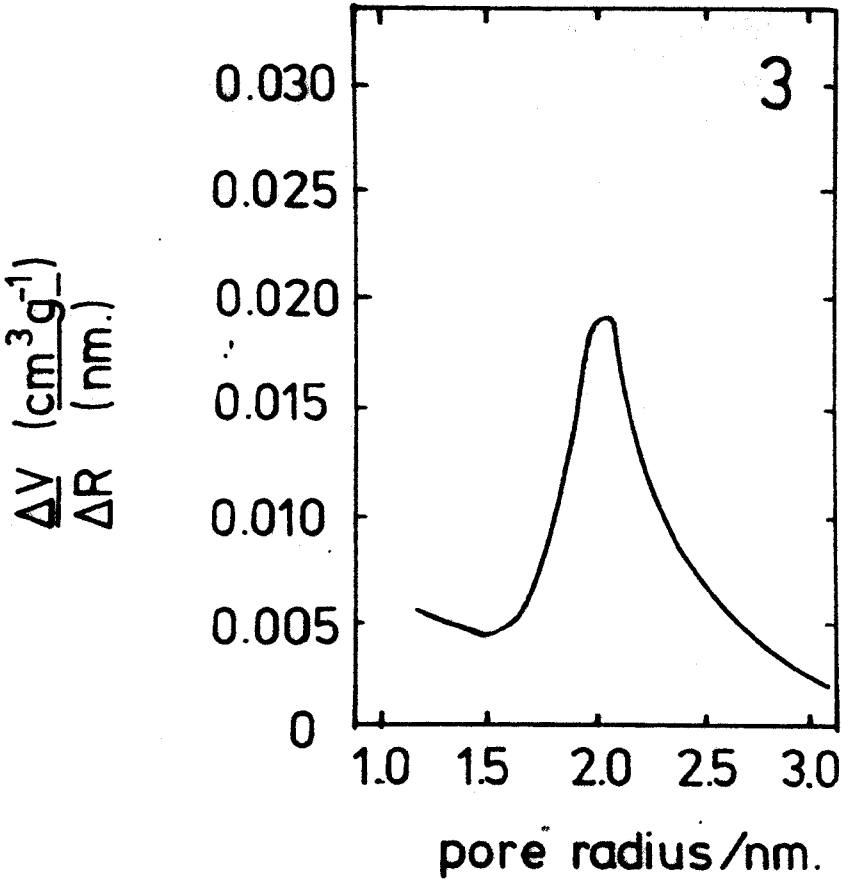
3
0.030
0.025
0.020
0.015
0.010
0.005
0
1.0
1.5
2.0
2.5
3.0
pore radius/nm.
ΔV/ΔR (cm³g⁻¹) (nm.)

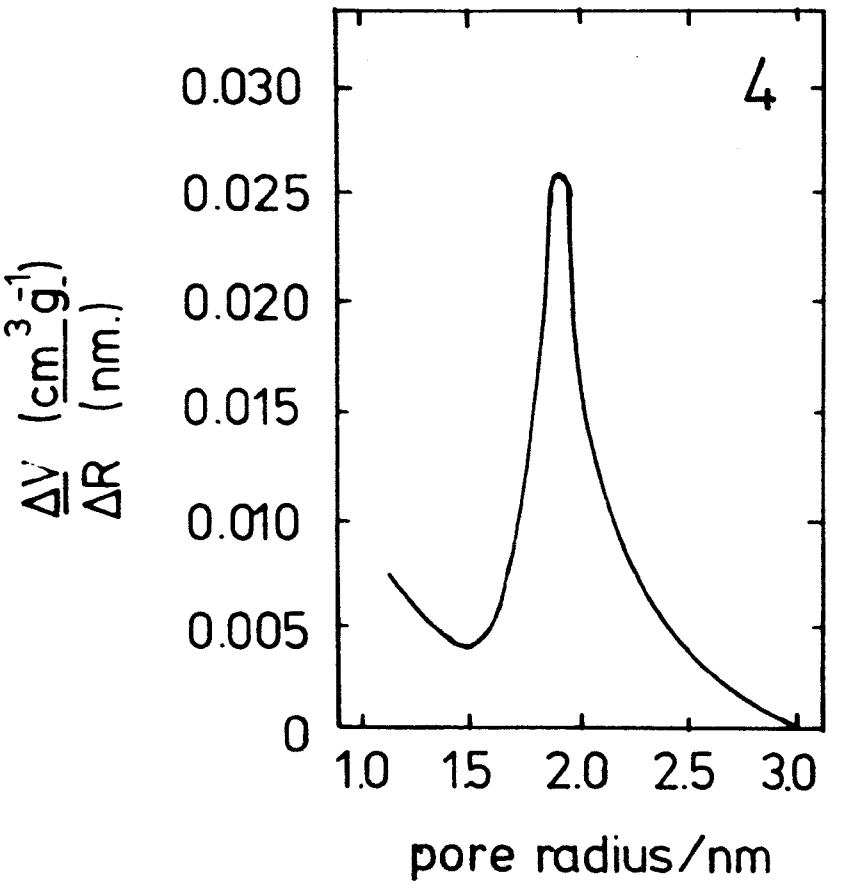
4
0.030
0.025
0.020
0.015
0.010
0.005
0
1.0
1.5
2.0
2.5
3.0
pore radius/nm
ΔV/ΔR (cm³g⁻¹) (nm.)

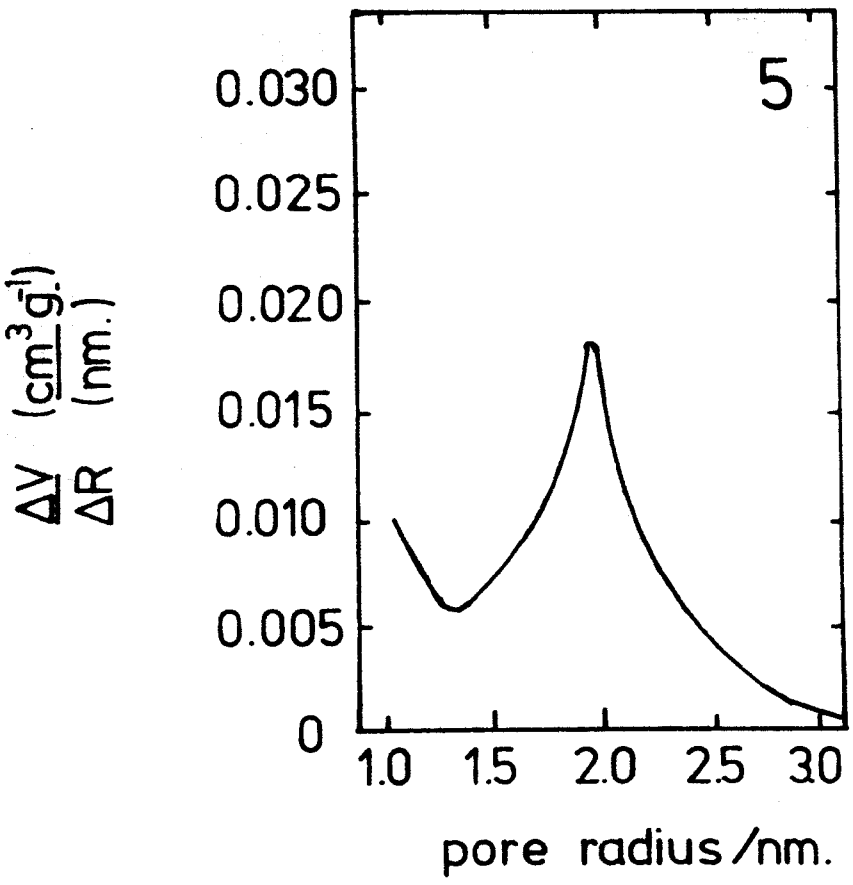
5
0.030
0.025
0.020
0.015
0.010
0.005
0
1.0
1.5
2.0
2.5
3.0
ΔV/ΔR (cm³g⁻¹/(nm.))
pore radius /nm.

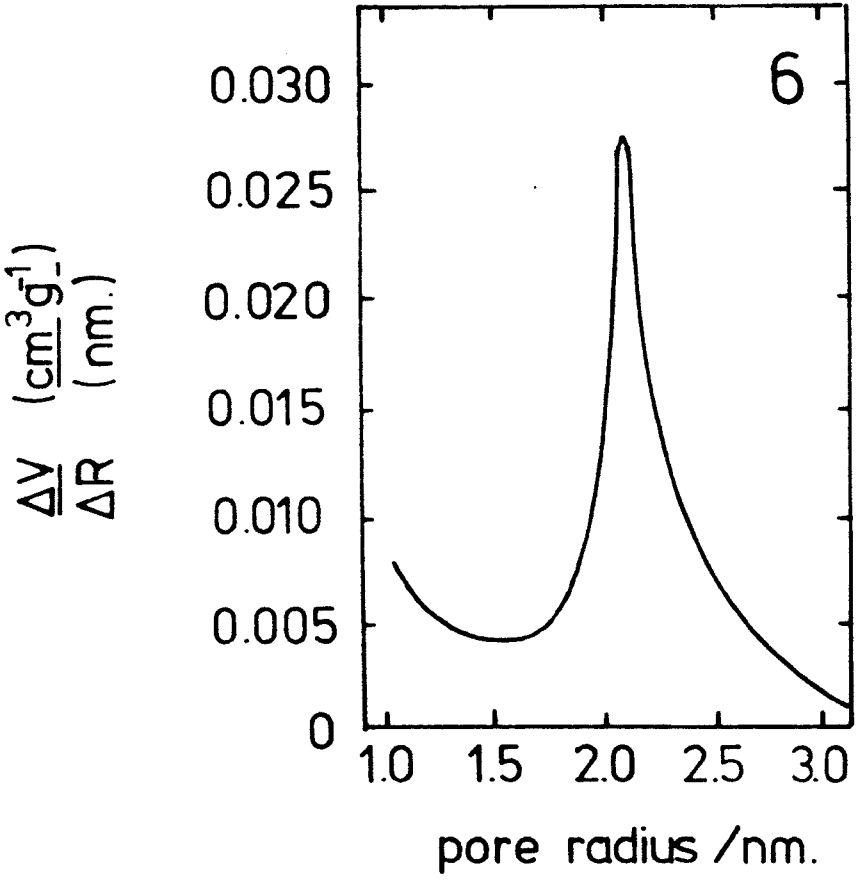
6
0.030
0.025
0.020
0.015
0.010
0.005
0
1.0
1.5
2.0
2.5
3.0
ΔV/ΔR (cm³g⁻¹/(nm.))
pore radius /nm.

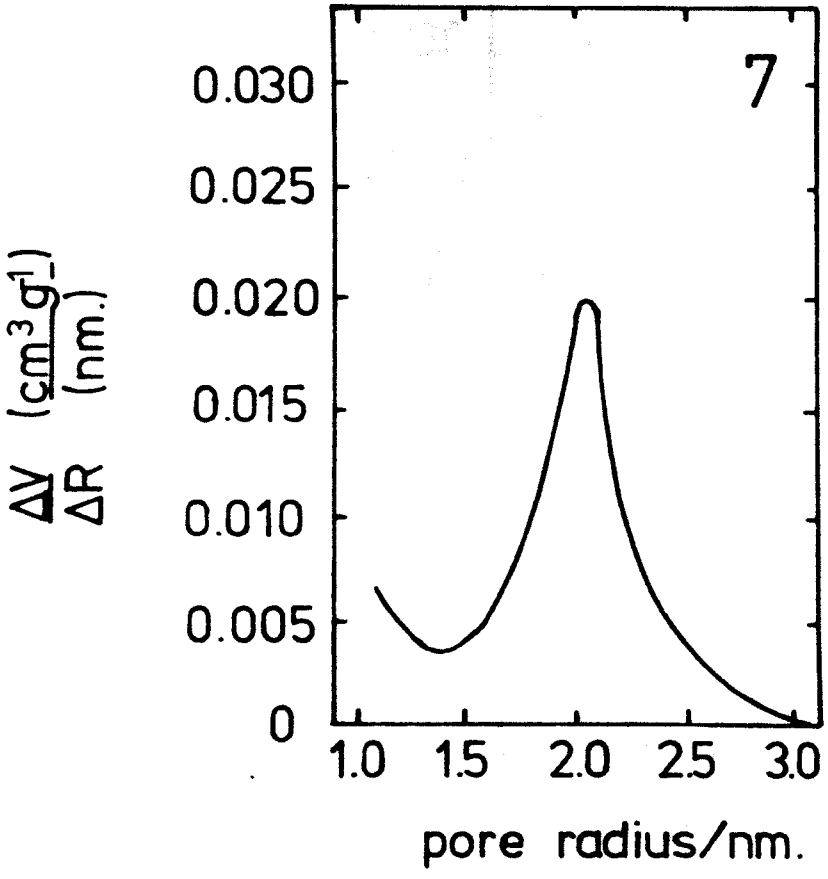
7
0.030
0.025
0.020
0.015
0.010
0.005
0
1.0
1.5
2.0
2.5
3.0
ΔV/ΔR (cm³g⁻¹/(nm.))
pore radius/nm.

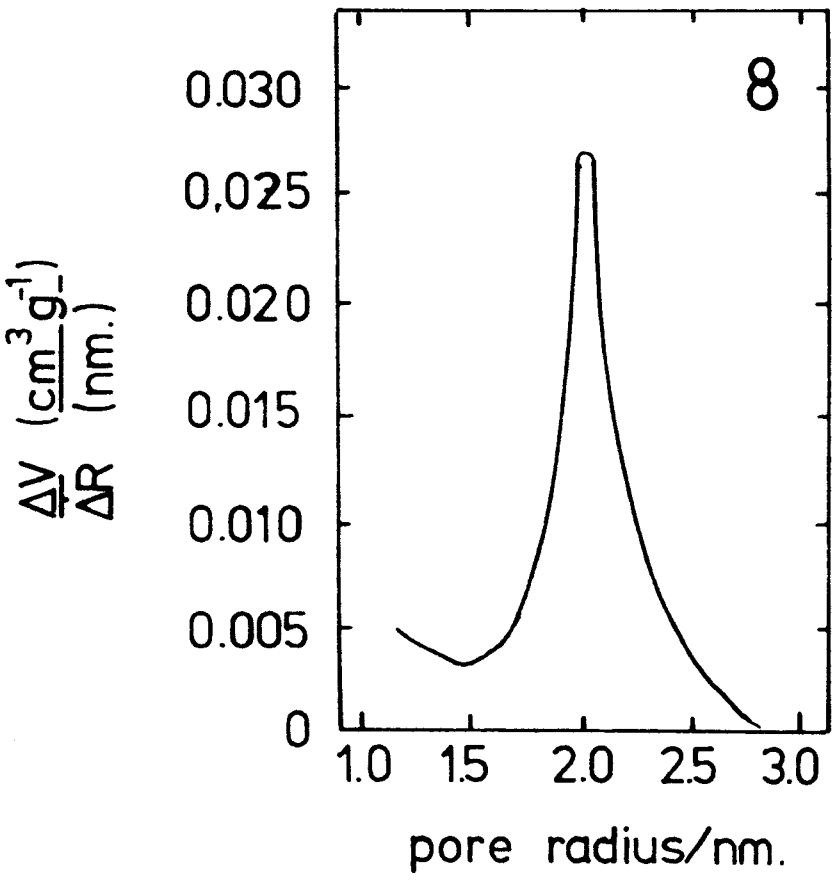
8
0.030
0,025
0.020
0.015
0.010
0.005
0
1.0
1.5
2.0
2.5
3.0
ΔV/ΔR (cm³g⁻¹/(nm.))
pore radius/nm.

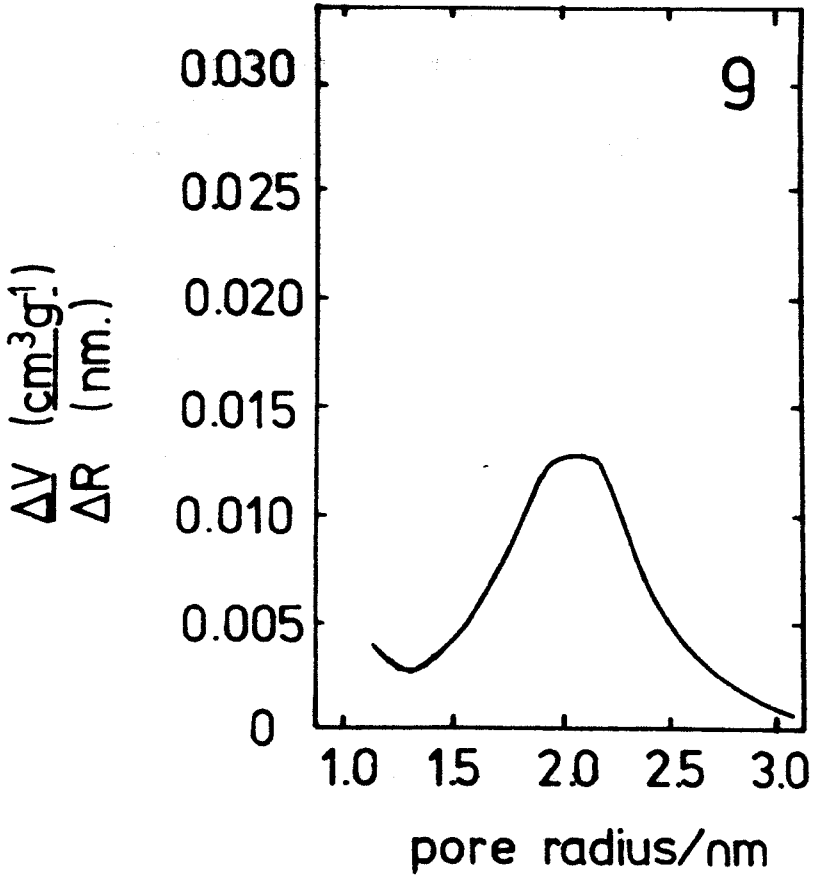
9
0.030
0.025
0.020
0.015
0.010
0.005
0
1.0
1.5
2.0
2.5
3.0
ΔV (cm³g⁻¹)
ΔR (nm.)
pore radius/nm

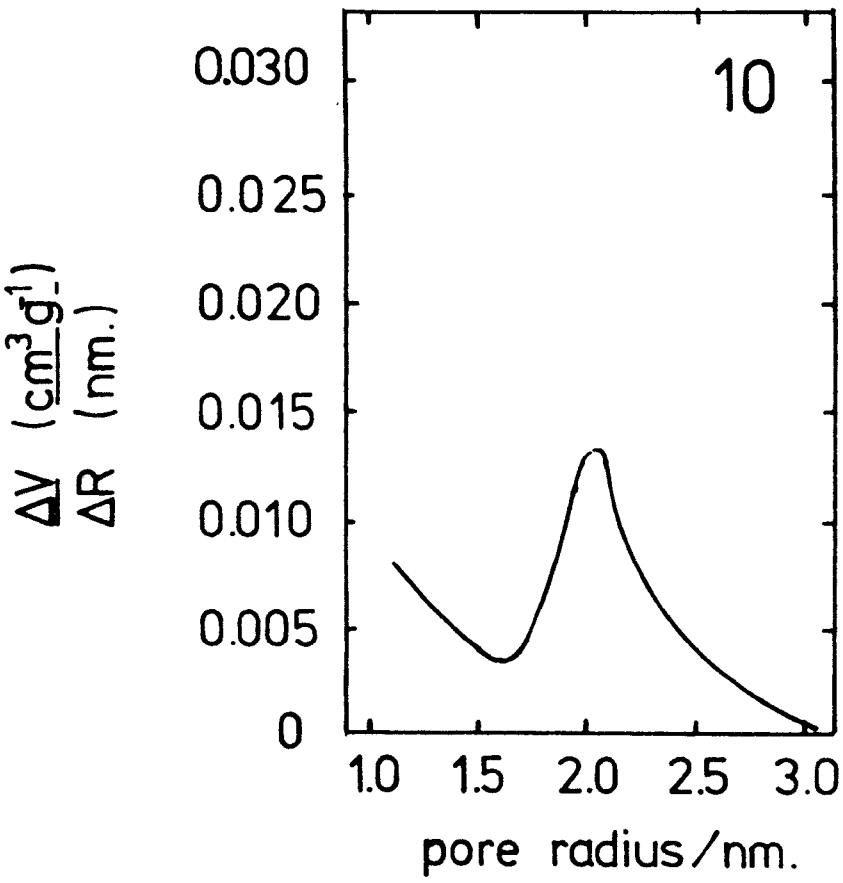
10
0.030
0.025
0.020
0.015
0.010
0.005
0
1.0
1.5
2.0
2.5
3.0
ΔV (cm³g⁻¹)
ΔR (nm.)
pore radius/nm.

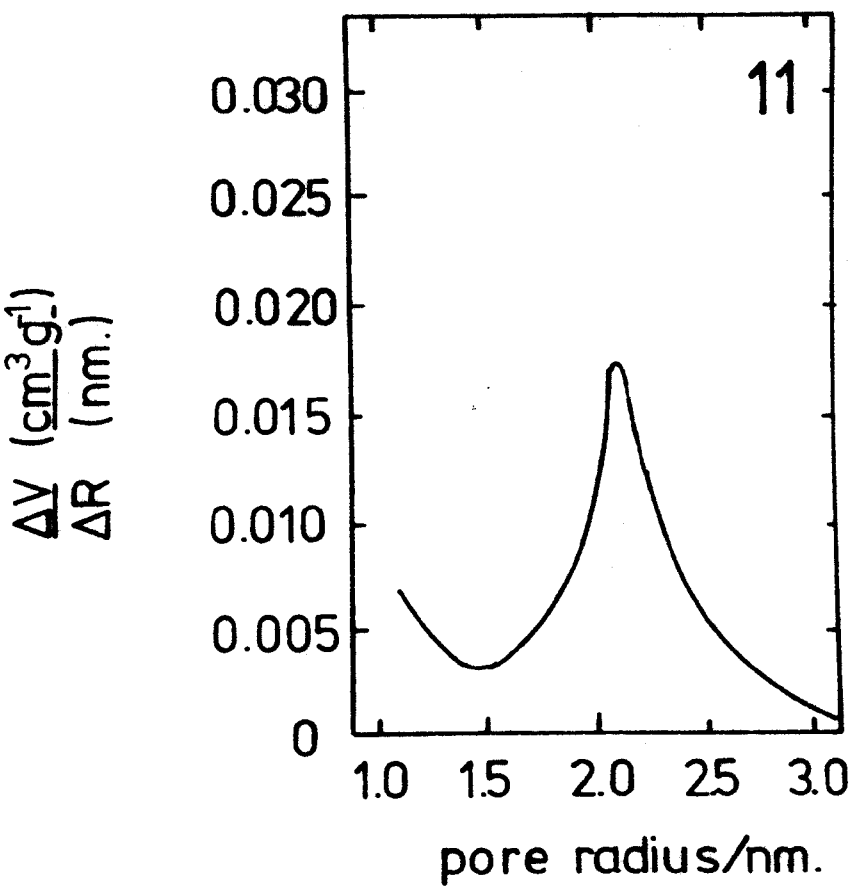
11
0.030
0.025
0.020
0.015
0.010
0.005
0
1.0
1.5
2.0
25
3.0
ΔV (cm³g⁻¹)
ΔR (nm.)
pore radius/nm.

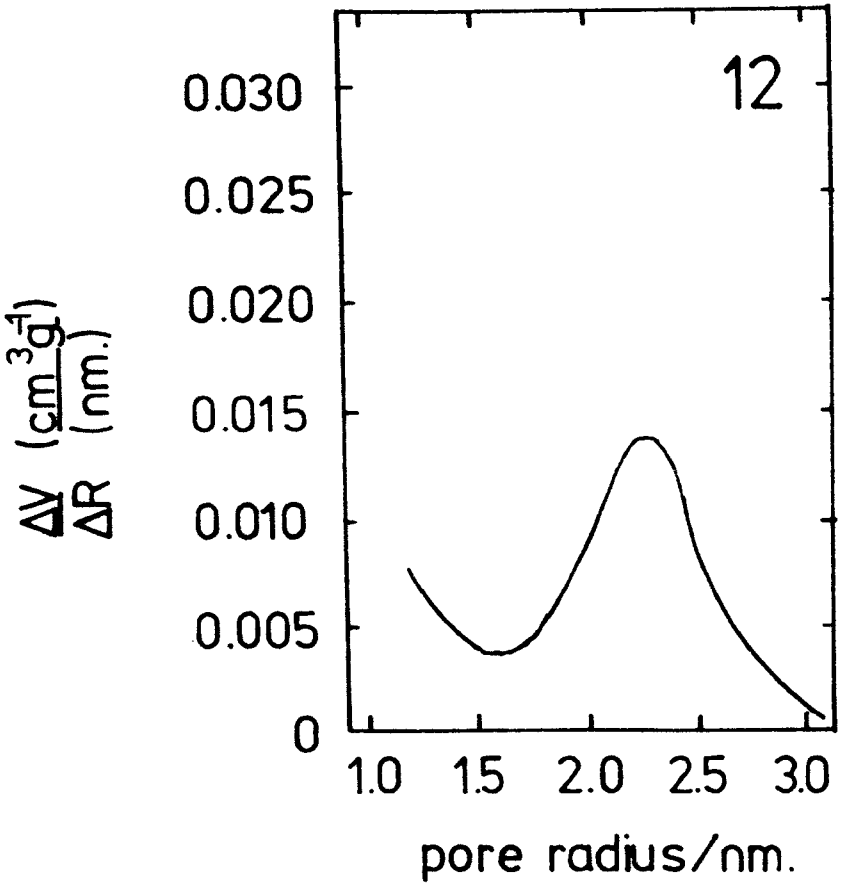
12
0.030
0.025
0.020
0.015
0.010
0.005
0
1.0
1.5
2.0
2.5
3.0
ΔV (cm³g⁻¹)
ΔR (nm.)
pore radius/nm.

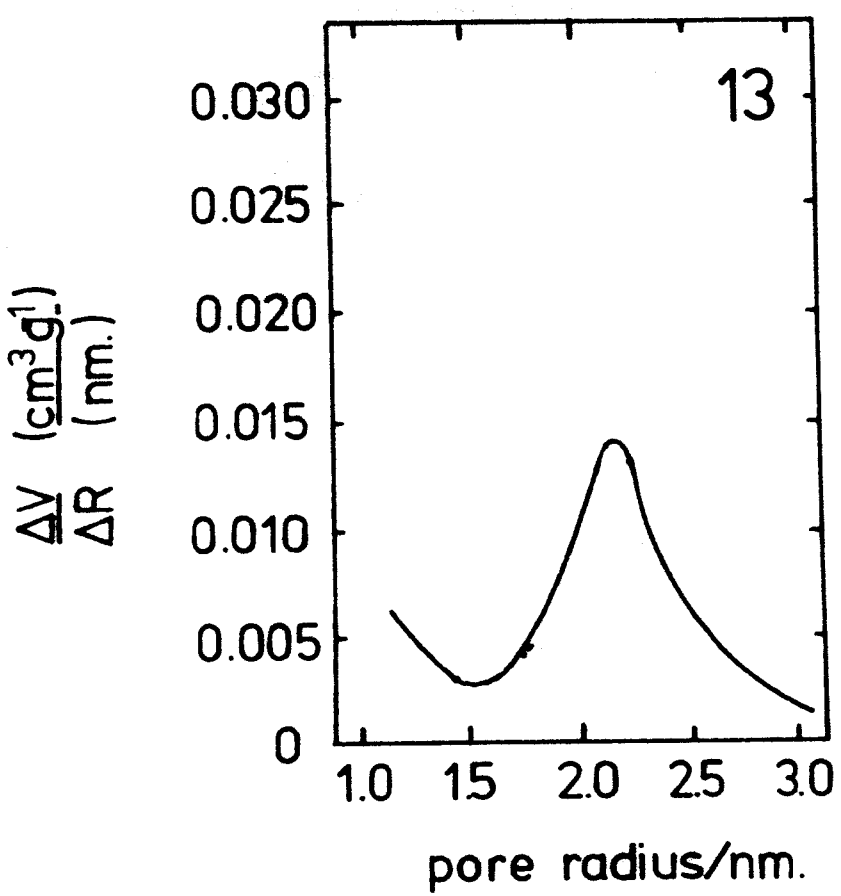
13
0.030
0.025
0.020
0.015
0.010
0.005
0
1.0
1.5
2.0
2.5
3.0
ΔV/ΔR (cm³g⁻¹ (nm.)
pore radius/nm.

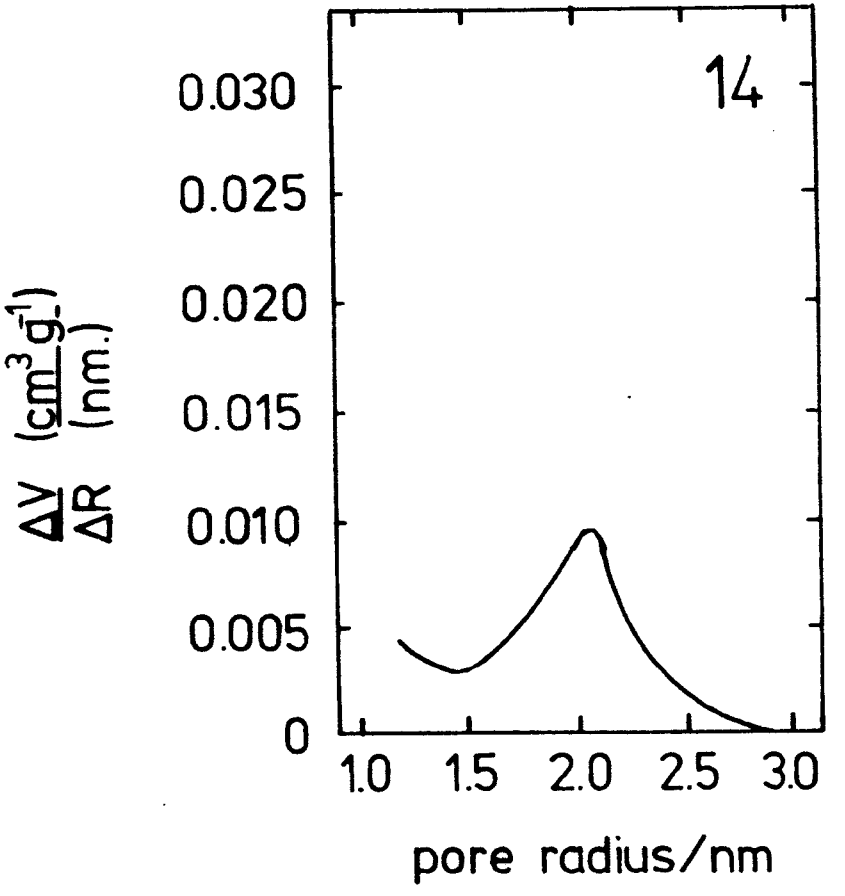
14
0.030
0.025
0.020
0.015
0.010
0.005
0
1.0
1.5
2.0
2.5
3.0
ΔV/ΔR (cm³g⁻¹ (nm.)
pore radius/nm

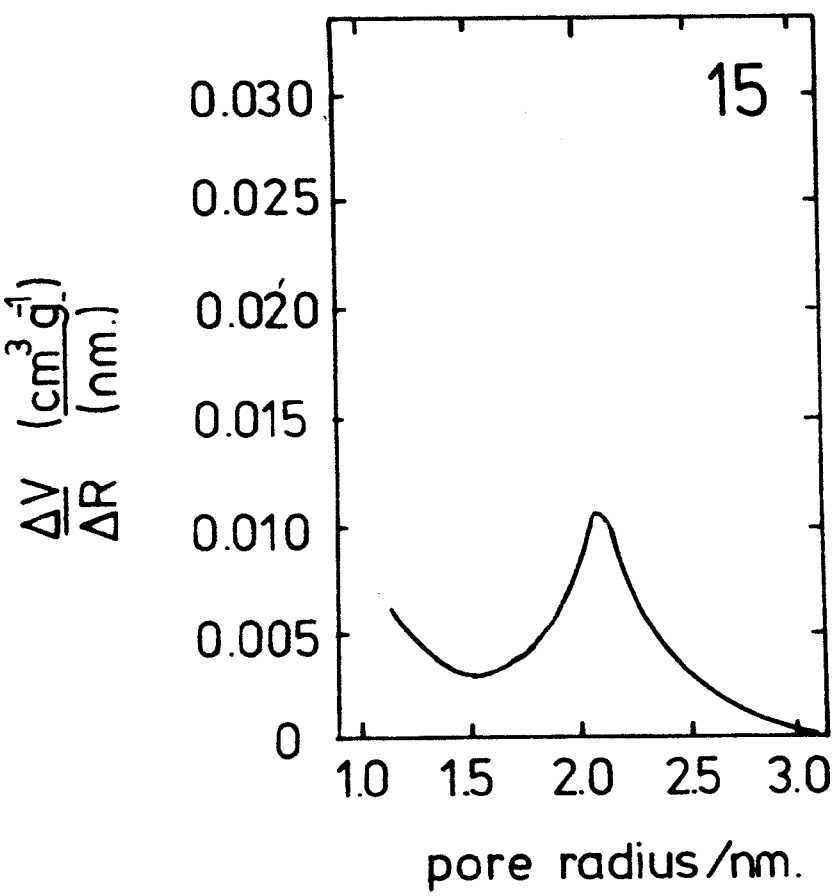
15
0.030
0.025
0.020
0.015
0.010
0.005
0
1.0
1.5
2.0
2.5
3.0
ΔV/ΔR (cm³g⁻¹/(nm.))
pore radius/nm.

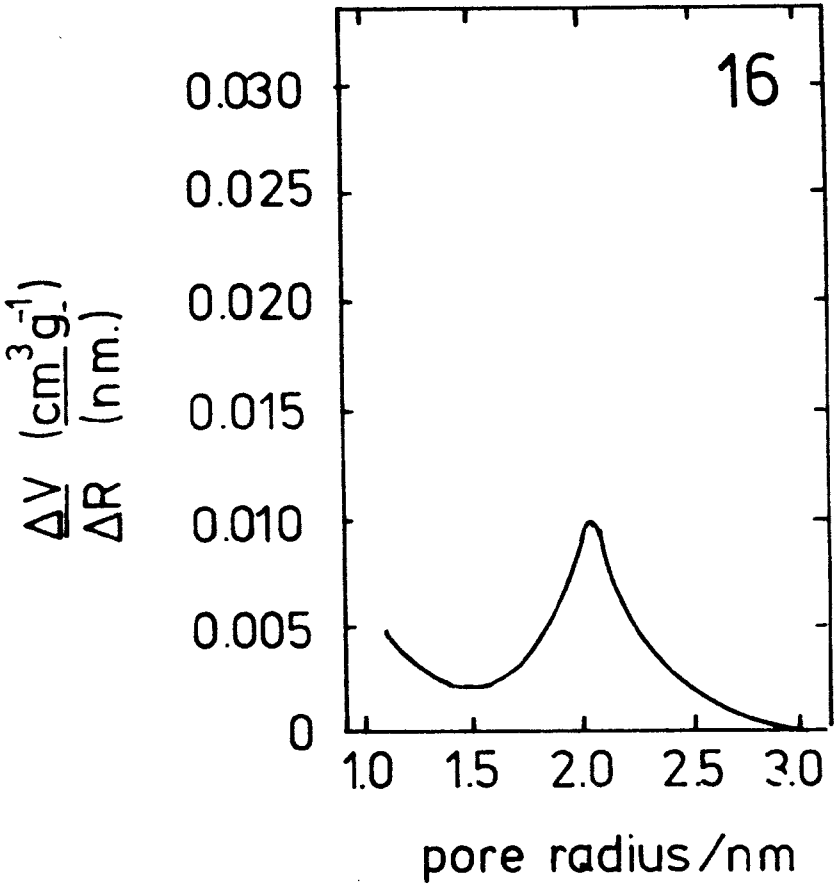
16
0.030
0.025
0.020
0.015
0.010
0.005
0
1.0
1.5
2.0
2.5
3.0
ΔV/ΔR (cm³g⁻¹/(nm.))
pore radius/nm